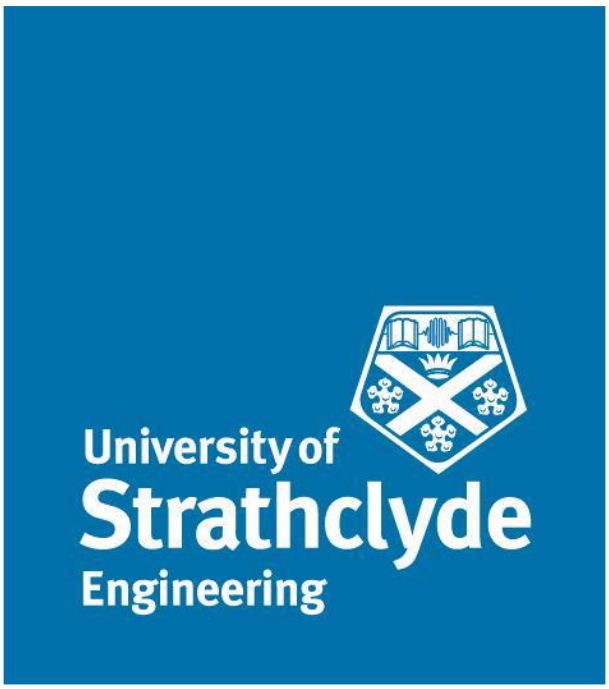

Optimisation of generators for direct drive offshore wind turbines

Nurul Azim Bhuiyan

A thesis submitted for the degree of

Doctor of Philosophy (PhD)

Department of Electronic and Electrical Engineering

University of Strathclyde

2019

This thesis is the result of the author's original research. It has been composed by the author and has not been previously submitted for examination which has led to the award of a degree. The copyright of this thesis belongs to the author under the terms of the United Kingdom Copyright Acts as qualified by the University of Strathclyde Regulation 3.50. Due acknowledgement must always be made of the use of any material contained in, or derived from, this thesis.

Nurul Azim Bhuiyan

November 2019

Abstract

A large proportion of offshore wind turbine designs are now based on directly driven permanent magnet synchronous generators using rare earth materials. The objective of this study is to optimise permanent magnet synchronous generators for offshore direct drive wind turbines in order to reduce the cost of energy, reduce the use of rare earth materials and increase the machine efficiency. A 6MW wind turbine design is assumed and parametric electromagnetic and structural generator models are introduced for a surface-mounted magnet generator topology (using magnets with high BH_{max}) and a flux-concentrating variant (using magnets with both higher and lower BH_{max}). Finite element method models are used to check key dependent variables calculated by the analytical models. These are optimised using a hybrid Genetic Algorithm and Pattern Search process with four different objective functions.

Further steps to improve the quality of the model include the effect of generator mass on the design, cost of the turbine tower and foundation and the impact of generator diameter limits have on the choice of optimum independent variables. Further optimizations are carried out for different power ratings (6 MW, 8 MW and 10 MW), choice of magnet grades, BH_{max} and working temperature. The effect of variable power factor and sensitivity to magnet specific cost, availability, operation and maintenance cost, wind conditions and rest of the turbine cost are also investigated in this study.

A detailed thermal model is used to estimate the effect of temperature due to power losses, calculate the cooling airflow requirements to bring the magnet operating temperature from 120°C to 80°C and controlling the cooling air flow for variable losses. Allowing the use of cheaper temperature grades of magnets, the additional cooling reduces winding losses and improves the effective BH_{max} of the magnets.

Discussions and conclusions highlights the impact of different investigations on the optimal generator design and find out the possible best way to optimise the generator for offshore wind energy application.

Acknowledgements

I would like to thank my first supervisor Dr Alasdair McDonald, who gave me opportunity, support, guidance and freedom to carry out the research. This thesis would not have been possible without his moral and technical contributions. I am also grateful to him and the University of Strathclyde for the research funding and the financial assistance for the journal and conference publications. I am extremely lucky and thankful to have had him as my supervisor and mentor during my PhD.

I would also like to thank Professor Lie Xu, Professor David Infield, my second supervisor Professor Olimpo Anaya-Lara and administrative staff (Drew Smith and Elaine Black) from Department of Electronic and Electrical engineering for their assistance over the past 4 years.

My gratitude goes to friends and colleagues at the Department of Electronic and Electrical Engineering, University of Strathclyde for their help and diversion. Special thanks to Kerri Hart, James Carroll, Pablo Jaen Sola, Godwin Jimmy, Chandra Pun and Md Habibur Rahman. I would also like to thank my friends and relatives outside the university, who supported me throughout my PhD research and writing this thesis. Particularly, little Manha for taking my mind off my PhD whenever I needed it.

Finally, but most importantly, I would like to thank my parents Nurjahan Begum and Abdur Rahim Bhuiyan and my sister Rownak Jahan for their encouragement and unlimited support for me.

Table of Contents

List of Figures

List of Tables

Nomenclature

Roman letters

Symbol	Description
A_{cu}	Cross-section area of the conductor
A_f	Flow section area
A_p	Area of magnetic pole at air-gap
A_s	Rotor swept area
A_{slot}	Area of a slot
b	Average beam width (circumferential)
B_g	Amplitude of the quasi square air-gap flux density
BH_{max}	Maximum energy product
B_r	Magnet’s remanence
B_{sy}	Stator yoke flux density
B_t	Stator teeth flux density
C	Scale parameter
C_{Cu}	Copper cost
C_E	Revenue corresponding to 1 kWh of electrical energy
C_{fan}	Total cost of fan
C_{Fe}	Active iron cost
C_{fen}	Cost of electricity consumed by fans
C_{fmn}	Manufacturing cost of the total number fan
C_{gact}	Generator active materials cost
C_{gstr}	Generator structural materials cost

C_{hex}	Cost of heat exchanger
C_P	Power coefficient
C_{PM}	Magnet cost
C_{rt}	Rest of the turbine cost
C_{sf}	Substructure and foundation cost
C_{tower}	Tower cost
d	Average beam width (axial)
d_w	Water depth
D	Generator air-gap diameter
D_r	Rotor diameter
E	Induced no-load voltage
E_y	Annual energy production
f_e	Frequency of the field in the iron
F_1	First objective function
F_2	Second objective function
F_3	Third objective function
F_4	Fourth objective function
F_p	Number of fan in parallel
F_s	Number of fan in series
g	Mechanical air-gap
g_{add}	Additional air-gap
g_{eff}	Effective air-gap
$g_{eff,d}$	Effective air-gap in the direct axis
$g_{eff,q}$	Effective air-gap in the quadrature axis

h_{FEMM}	Chosen height in FEMM
h_{al}	Aluminium ring height
h_{hub}	Hub height
h_{m}	Height of the magnet
h_{p}	Height of the pole shoe
h_{y}	Height of the yoke
h_{ry}	Height of the rotor yoke
h_{s}	Height of the tooth/slot
h_{sy}	Height of the stator yoke
h_{y0}	Extra yoke height due to deflection
H_{c}	Coercivity of the magnet
H_{cJ}	Intrinsic Coercivity
I	Current
I_{r}	Second moment of area of the cross-section of yoke
I_{d}	Direct axis current
I_{y}	Second moment of area of the structural arms in the axial direction
I_{z}	Second moment of area of the structural arms in the circumferential direction
k	Shape parameter
k_{c}	Carter factor of the stator slot
$k_{c,q}$	Carter factor from the rotor side in the quadrature axis
k_{f}	Coefficient of related fluid resistance
k_{sfil}	Slot filling factor
k_{thc}	Specific heat capacity of the cooling air

k_w	Winding factor
K_{th}	Thermal conductance
l_{ar}	Radial length of the arms
l_b	Radial length of the beam
l_{cu}	Length of conductor in phase
l_s	Stack length in axial direction
L	Total inductance
L_{air}	Air-gap leakage inductance
L_d	Direct axis inductance
L_{end}	End winding leakage inductance
$L_{leakage}$	Leakage inductance
L_m	Magnetizing inductance
$L_{m,d}$	Direct axis magnetizing inductance
$L_{m,q}$	Quadrature axis magnetizing inductance
$L_{m,u}$	Mutual inductance
L_q	Quadrature axis inductance
L_{slot}	Slot leakage inductance
L_{skew}	Skew leakage inductance
L_{tooth}	Tooth tip leakage inductance
m_{act}	Generator active material mass
m_{PM}	Magnet mass
m_{mp}	Mono-pile mass
m_{rot}	Active material masses in the rotor
m_{rtop}	Rest of the turbine top head mass excluding the generator mass

m_{sf}	Substructure and foundation mass
m_{stat}	Active material masses in the stator
m_{str}	Generator structural mass
m_{top}	Top head mass of the turbine
m_{tower}	Tower mass
m_{tpos}	Mass of monopole transition piece
n_{ar}	Number of arms
N_s	Number of turns of the phase winding
N_{slot}	Number of conductor per slot
p	Pole pair
p_r	Probability of a given range of wind speeds
P	Power output
P_{cu}	Copper losses
P_d	Pressure drop
P_{Fe}	Total iron losses in the stator
P_{Fe0e}	Eddy current loss per unit mass
P_{Fe0h}	Hysteresis loss per unit mass
P_{Fest}	Iron losses for the stator teeth
P_{Fesy}	Iron losses for the stator yoke
P_{loss}	Power loss
q	Number of slot per pole per phase
q_r	Mean normal radial stress
q_{vc}	Cooling air flow
Q_s	Number of slots

r_s	Stator radius
$r_{s,out}$	Outer radius of the stator
R_s	Phase resistance
R_{st}	Radius of the structure
R_{sto}	Outer radius of the structure
R_{sys}	System flow resistance
R_{th}	Thermal resistance
$R_{th,cool}$	Thermal resistance in cooling duct
t_a	Wall thickness of beam
T	Rated generator torque
T_r	Turbine rating
T_{max}	Maximum torque of generator
u	Radial deflection
v	Wind speed
V	Voltage
w	Weight component of the arms
w_m	Magnet width
$w_{m,i}$	Magnet width at the inner radius
w_p	Width of the pole shoe
w_s	Width of the stator slot
w_t	Width of the stator tooth
W	Weight component of the back iron
X_s	Phase reactance
X_d	Direct axis reactance

X_q	Quadrature axis reactance
Y_{st}	Young's Modulus of the structural material
y	Axial deflection
z	Deflection in tangential or circumferential direction

Greek letters

Symbol	Description
α	Function of the number of arms and the dimensions of the rotor or stator structure
α_i	Effective pole arc coefficient
α_t	Temperature coefficient
δ	Load angle
ΔT	Difference of the temperature
η	Generator efficiency
θ	Angle between terminal voltage and current
θ_p	Angle in pole piece
λ_{cool}	Equivalent conductivity for cooling channel
μ_0	Permeability of air
$\mu_{r,iron}$	Relative permeability of the iron
$\mu_{r,m}$	Relative permeability of the magnet
$\mu_{r,steel}$	Relative permeability of the steel
ρ	Density of air
ρ_{20}	Resistivity of copper at 20^{o}C
ρ_{cu}	Resistivity of copper

ρ_m	Density of magnet
ρ_{st}	Density of the material
τ_p	Pole pitch
τ_s	Slot pitch
φ	Flux
φ_g	Flux of the air-gap
φ_L	Leakage flux
φ_m	Flux of the magnet
φ_{ry}	Flux of the rotor yoke.
φ_{sy}	Flux of the stator yoke
ω	Mechanical angular speed of the rotor

Abbreviations

Letters	**Description**
AC	Alternating current
AEP	Annual energy production
AOM	Annual operation and maintenance cost
CoE	Cost of energy
DC	Direct current
DDPMG	Direct-drive permanent-magnet generator
DDSG	Direct-drive synchronous generator with electrical excitation
DFIG	Doubly-fed induction generator
DFIG1G	Doubly-fed induction generator with single-stage gearbox
DFIG3G	Doubly-fed induction generator with three-stage gearbox

EMF	Electromotive force
EV	Electric vehicle
FC	Flux-concentrating
FCR	Fixed charge rate
FFT	Fast Fourier Transform
FE	Finite element
FEMM	Finite element method magnetics
GA	Genetic algorithm
HAWT	Horizontal-axis wind turbine
HVG	High voltage generator
ICC	Initial capital cost of the turbine
IGBT	Insulated-gate bipolar transistor
LB	Lower boundaries of independent variables
MMF	Magnetomotive force
MRI	Magnetic resonance imaging
NREL	National renewable energy laboratory
OSIG	OptiSlip induction generator
PSO	Particle swarm optimization
PM	Permanent magnet
PMG1G	Permanent-magnet generator with single stage gearbox
PMSG	Permanent magnet synchronous generator
PS	Pattern search algorithm
rpm	revolutions per minute
SCIG	Squirrel cage induction generator

SM	Surface-mounted
SRG	Switched reluctance generator
SynRG	Synchronous reluctance generator
SynRM	Synchronous reluctance machine
TFG	Transverse-flux generator
UB	Upper boundaries of independent variables
VAWT	Vertical-axis wind turbine
WRIG	Wound rotor induction generator
WRSG	Wound rotor synchronous generator

Chapter 1

Introduction

1.1 Research overview

Offshore wind turbines are increasingly using synchronous generators with permanent magnets manufactured using rare earth materials. These generators – whether they are high or low speed – tend to be more efficient than competing generator technologies such as the doubly fed induction or the field-wound synchronous generator. The lack of rotor copper losses means that these generators have flat, relatively high efficiency curves. This leads to higher energy yields, albeit at usually a higher cost. The onshore cost of energy calculation tends to push wind turbine designers to choose a cheaper induction machine. Offshore – where the non-turbine costs are so high – the cost of energy calculation puts a greater emphasis on maximising annual energy yield through maximising efficiency and availability. For something like the generator, which makes up only part of the capital cost but which involves all of the power output, it makes sense to choose highly efficient, reliable generators such as those using permanent magnets.

A number of researchers have started to explore alternative synchronous generator types, included structural materials along with active materials, different cooling method, different objective function to optimise, to achieve highly efficient, reliable and cost effective generators for offshore wind turbine. Eriksson and Bernhoff presented an interchangeable rotor design where two generators are designed with the same stator but interchangeable rotors with different PM material (Nd-Fe-B and ferrite) [1]. Polinder et al. show a comparison of different types of generator in terms of annual energy yield per cost, which is analogous to payback period [2]. Grauers optimized low speed permanent magnet machines using generator costs and losses, including an estimation of generator structural cost and also shows a method where the generator outer surface of the stator core is cooled by air forced through circumferential cooling channels [3]. Bazzo et al. outlined some objective functions to

minimize costs and maximize efficiency which included minimizing active and structural materials cost and minimizing cost of losses to get maximum return of investment [4]. Zavvos *et al.* offered an analytical tool that minimises the generators mass or cost by optimising both the electromagnetic and structural design at the same time [5]. McDonald showed the structural models with different types of rotor and stator structures for direct drive generators [6]. Polinder shows an objective function that minimises the cost of generator active materials (i.e. magnet, copper and iron) and the generator losses as well [7]. The generator system cost is minimized in [8].

Although different researchers have used different methods, topologies and objective functions to optimise their machine, it is worth to know the best approach to optimise a generator for an offshore wind turbine. This study looks for the best approach to optimise a generator for an offshore wind turbine by using different generator topologies, objective functions and other factors that interest a typical machine designer.

1.2 Research question

What is the 'best' approach to optimise a generator for an offshore wind turbine?

To answer this primary research question, a number of other smaller secondary research questions must be answered first. These secondary research questions are answered throughout each chapter of this thesis. The beginning of each chapter will set out the secondary research question to be answered in that chapter. The conclusion of each chapter will answer the secondary research questions and contribute towards answering the primary research question stated above.

1.3 Secondary research questions

Different designers optimise in different ways and come to different conclusions. They include different models, topologies, algorithm, objective functions to find the best possible solutions. The following secondary research questions will help to choose the best possible ways to optimise a generator for offshore wind turbines, hence answer the primary question.

Q1) Can different magnet materials and rotor topologies be used to reduce Nd-Fe-B content in offshore wind turbines?

The most common material used in permanent magnet electrical machines is Neodymium - Iron - Boron (Nd-Fe-B). This class of material has a high maximum energy product (BH_{max} = 30-50MGOe) leading to compact machines with light generator rotors. The remanent flux density of these magnets can lead to air gap flux densities of the order of ~1T when the magnets are mounted onto the rotor surface.

While alternative technologies are under investigation or already exist, rare earth magnets (i.e., Nd-Fe-B) are unlikely to be replaced as an essential input for clean technologies and high efficiency consumer goods. The combination of rapid increase in the use of rare earth minerals, along with supply shortages caused rapid price increases and the threat of non-delivery [9].

Wind turbines increasingly use permanent magnets in the electrical generators. The price level fluctuation and availability of these rare earth materials can contribute to a high cost of energy. Largely as a result of the instability (price and availability) of the rare earth materials market, research into alternate materials and technologies has become very essential.

This study investigates different generator rotor topologies using Nd-Fe-B magnet and ferrite magnet to reduce the use of rare earth permanent magnet for offshore wind turbine.

Q2) Should the generators structural model, tower, substructure and foundation be included with active materials in optimisation of generators for offshore direct drive wind turbines?

In order to design lightweight and cost effective direct drive generators, the designer could include a structural model of the generator along with the active material model. McDonald showed that the structural mass of a 5 MW permanent magnet direct drive generator can be more than 80% of its total mass [6]. The generator mass, which is part of turbine top head mass can affect the tower, substructure and foundation cost that goes into turbine capital cost and effect on cost of energy [10]. According to a NREL technical report, the substructure and foundation cost is 9% of the total offshore wind turbine cost [11]. It is a significant part of the total turbine cost.

In this study, models and results include generator active and structural materials and the effect of generator mass on turbine tower and foundations.

Q3) Are these findings dependent on turbine power ratings? If so, to what degree?

Wind turbines are getting larger. Their rated power capacities are moving from the 6 MW range to 10 MW and beyond. As a result, their size and mass, which grow rapidly with power capacity, is becoming a problem in terms of capital cost, logistics and assembly. Moreover, there is a move to offshore installations. A large proportion of offshore wind turbine designs are now based on directly driven permanent magnet (PM) synchronous generators. It is particularly attractive to use direct-drive systems as they promise lower maintenance cost, high efficiency and longer life as gearboxes are considered to be less reliable and incur mechanical losses [12], [13]. However, the large size (due to the high torque rating), mass, the massive generator structures needed to maintain the small air-gap clearance against the large attraction forces between the rotor and the stator and the large quantities of rare earth permanent magnet materials are the main challenges for designers of direct drive permanent magnet generators [14].

A number of different direct drive generator topologies with different rated power (6, 8 and 10 MW) are used in this study to compare the differences in results for power ratings in terms of turbine cost of energy, capital cost, annual energy production, efficiency and other variables.

Q4) How does the choice of magnet grade affect the resulting optimal design?

Choosing magnet grade for Nd-Fe-B magnet is also important for generator design. Neodymium magnets are available in a variety of grades, typically extends from 35 MGOe to 52 MGOe. The higher the grade number, the higher the energy density. Usually the higher the energy density the stronger the magnet, but this is very much dependent upon the magnet's operational environment. Cost of magnet also increases with higher grade magnets [15].

This study estimates and compares the cost of energy, magnet mass, annual energy production and other variables for different magnet grades.

Q5) How does the thermal model, cooling circuit and machine temperature affect the optimal design?

Nd-Fe-B is temperature sensitive and typically it operates best at lower temperature. So cooling the magnets improves the effective remanent flux density. The heat propagation from the stator windings and iron cores to the permanent magnets mounted in the rotor should be minimized because of the temperature sensitive properties of the magnets [16], [17]. In most direct drive generators, I^2R losses dominate. As the electrical resistivity of most conductors is generally temperature dependent, cooling also helps machines operate at higher electrical loading or with smaller losses.

A detailed thermal model is developed in this study to estimate the effect of temperature due to power losses and a cooling system is introduced to reduce the magnet temperature from 120^{o}C to 80^{o}C.

Q6) How does the choice of objective function affect the resulting optimal design?

The generator designer needs to deliver a number of performance characteristics including high efficiency, low power losses at part load, high availability, low machine mass, reduced volume and lower material and manufacturing costs. Normally the designers employ some element of optimisation to achieve the best balance of these aspects [18].

This study optimises the generators with different objective functions to find the best objective function to optimise a generator for offshore direct drive wind turbine.

1.4 Approach taken

Figure 1.1 shows the steps taken in this thesis in order to answer the primary research question outlined in the previous Section 1.2. The following step numbers also match with each chapter number of this thesis. Each step also shows the secondary research questions that relates with the step. Further details on the methodology for each step can be found in each chapter.

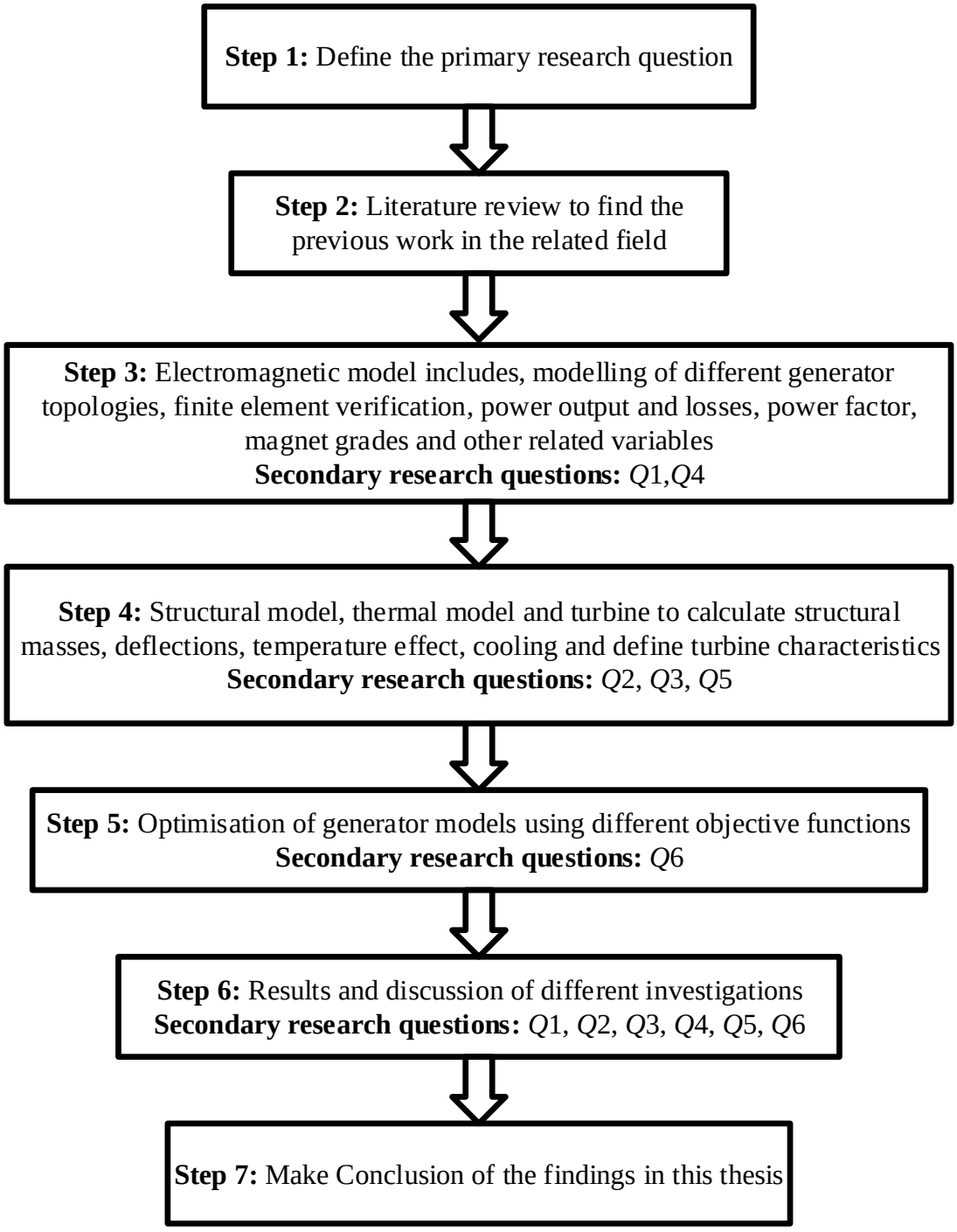

Figure 1.1: Step taken to complete this thesis and related secondary question in each step

1.5 Chapter structure

Each of the chapters consists of a short introduction/background, section to the work carried out in that chapter and the purpose of that chapter to answer the research questions at the very beginning. Then an overview of the methodology used to obtain the results shown in that chapter and a results section. The end of each chapter will

have a discussion and conclusion sub-section. The references for each chapter are provided at the end of that chapter.

The next chapter will introduce the reader about wind energy, different types of generator, magnet materials and previous work related to this research area. Chapter 3 describes the electromagnetic model of different generator topologies, finite element verification, power output and losses, magnet materials and other related variables. In Chapter 4, structural model, thermal model and turbine is defined to calculate structural masses, deflections, temperature effects, required cooling and turbine characteristics. Chapter 5 shows the optimisation of generator models using different objective functions. There will be a detailed investigation results and overall discussion in chapter 6 and conclusion at the end of the thesis.

1.6 Novelty of the research

The novelty of this study is the process of optimising large, low speed generators for offshore direct drive wind turbines, exploring the different objective functions that a machine designer could use. This is done for different generator topologies to test whether the recommendation of objective functions is independent of the machine type. The study also investigates the effect on the optimisation of a number of factors that interest a typical designer: the inclusion of structural generator material in the objective function, the inclusion of the impact of generator mass on the cost of the turbine tower and foundation, the bounds of generator diameter, variable power factor, energy consumption due to high inertia, different rated power, the inclusion of different magnet materials and magnet grades in the generator rotor, the inclusion of a generator thermal model and the cooling system and controlling the cooling air flow for variable losses. The sensitivity to magnet specific cost, availability, operation and maintenance cost, wind conditions and rest of the turbine cost are also investigated.

1.7 Research output

Peer Reviewed Journals published or submitted:

[1] A. McDonald and **N. A. Bhuiyan**, “On the Optimization of Generators for Offshore Direct Drive Wind Turbines,” IEEE Trans. Energy Convers., vol. 32, no. 1, pp. 348-358, Mar. 2017.

[2] **N. A. Bhuiyan** and A. McDonald, "Optimization of offshore direct drive wind turbine generators with consideration of permanent magnet grade and temperature," IEEE Trans. Energy Convers., vol. 34, no. 2, pp. 1105-1114, Nov. 2018.

Peer Reviewed Conferences:

[1] **N. A. Bhuiyan** and A. McDonald, "Assessment of the Suitability of Ferrite Magnet Excited Synchronous Generators for Offshore Wind Turbines," at Eur. Wind Energy Assoc. Offshore Conf., Copenhagen, Denmark, Mar. 10-12, 2015.

[2] **N. A. Bhuiyan** and A. McDonald, "Optimisation and comparison of generators with different magnet materials for a 6MW offshore direct drive wind turbine," in Proc. 8th IET Int. Conf. Power Electron., Mach. Drives (PEMD), Glasgow, UK, 2016, pp. 1-6.

[3] **N. A. Bhuiyan** and A. McDonald, "Optimisation and comparison of flux-concentrating Nd-Fe-B generator considering variable power factor and wind conditions for a 6MW offshore wind turbine," at 53rd Int. Universities Power Engineering Conf. (UPEC), Glasgow, UK, Sept. 4-7, 2018.

Chapter 2

Literature review

2.1 Introduction

Windmills have been used largely for grinding grain or pumping water for over 3000 years. The wind has been an important source of power for even longer in sailing ships. Horizontal axis windmills were a vital part of the rural economy from medieval times and only fell into disuse with the initiation of low-cost fossil-fuelled static machines and the spread of electrification. The electricity generation from wind turbine can be found back to the late nineteenth century. However, for much of the 20^{th} century the battery charging for remote dwellings was the main interest which was replaced once the electricity grid access became available [19], [20].

The motivation behind the development of wind energy in 1973 was the increasing price of oil and concern over limited fossil-fuel resources. A significant number of government-funded programmes of research, development and demonstration were initiated. Now obviously, the main driver of using wind turbine is to generate electrical power with a very low CO_2 emission (over the entire life cycle of manufacture, installation, operation and de-commissioning) and the potential of wind energy to help limit climate change [19], [21].

The development of wind energy is not similar in all countries. Some countries are flourishing while some others couldn't not fulfil the expected potential of the wind resource, the reasons are complex. Some significant factors include the financial-support mechanisms for wind-generated electricity, the process of local authority's permission to construct the wind farms, and the perception of the general population particularly with respect to visual impact. In order to overcome the concerns of the rural population over the environmental impact of wind farms, the interest of developing offshore wind farms are increasing [19], [22].

Although the non-turbine costs are so high for the offshore wind turbine, maximising annual energy yield through maximising efficiency and availability puts a greater

emphasis on turbine cost of energy. The generator, which makes up only part of the capital cost but involves all of the power output should be highly efficient and reliable to achieve best possible power output with lowest cost of energy.

The main purpose of this chapter is to investigate previous works related to research questions given in section 1.2 and 1.3 includes wind power resources and turbine, drive train, generator type, magnet materials, optimisation process through literature review.

2.2 Wind resource

The available energy from the wind varies as the cube of the wind speed as shown in equation (2.1). So it is critical to understand the characteristics of the wind resource to all aspects of wind energy exploitation, from the identification of suitable sites and predictions of the economic viability of wind farm projects through to the design of wind turbines themselves and understanding their effect on electricity distribution networks and consumers [19], [23].

From the point of view of wind energy, variability is the most striking characteristic of the wind resource. Both geographically and temporally the wind is highly variable and persists over a very wide range of scales, both in space and time. The importance of this is amplified by the cubic relationship to available energy [19], [24].

The winds are driven almost entirely by the sun's energy, causing differential surface heating. The heating is most intense on land masses closer to the equator, and obviously the greatest heating occurs in the daytime, which means that the region of greatest heating moves around the earth's surface as it spins on its axis. Warm air rises and circulates in the atmosphere to sink back to the surface in cooler areas [19].

Different climatic regions can be described by the spatial variability, some much windier than others. The latitude is largely dictating these regions, which affects the amount of insulation. In a climatic region, the variation on a smaller scale, largely dictated by physical geography – the proportion of land and sea, the size of land masses, and the presence of mountains or plains for example. The type of vegetation may also have a significant influence through its effects on the absorption or reflection of solar radiation, affecting surface temperatures, and on humidity. The wind climate is greatly affected by the topography. The tops of the hills and mountains experience more wind than in the lee of high ground or in sheltered valleys, for instance. The wind velocities are significantly reduced by obstacles such as trees or buildings [19].

2.3 Wind energy

The kinetic energy of the wind is converted into mechanical power by using a wind turbine that drives an alternating current (AC) induction generator to produce electricity. Wind turbines produce electricity by using the power of the wind to drive an electrical generator. Wind passes over the blades, generating lift and exerting a turning force. Further rotation affects the direction and magnitude of the lift and drag which can be resolved into thrust (not useful for power generation) and torque (which is useful for power production). The rotating blades turn a shaft inside the nacelle, which typically goes into a gearbox. The gear box increases the rotational speed and steps down the torque to that which is appropriate for the generator. The generator converts the rotational power into electrical power by using magnetic fields. The power output goes to a transformer, which converts the electricity from the generator at around 690V to the suitable voltage for the power collection system, typically 33kV [25]. The power output P, from a wind turbine is given as,

$$P = \frac{1}{2} C_{\mathrm{P}} \rho A_{\mathrm{s}} v^3 \tag{2.1}$$

where C_{P} is the power coefficient, ρ is the density of air, A_{s} is the rotor swept area and v is the wind speed. The density of air is 800 times lower than water which powers hydro plants and tidal turbines, and this leads directly to the large size of a wind turbine rotor. The rotor of a1.5 MW wind turbine can be more than 60 m in diameter depending on the design wind speed chosen. The power coefficient describes that fraction of the power in the wind that may be converted by the turbine into mechanical work. It has a theoretical maximum value of 0.593 (the Betz limit) and rather lower peak values are achieved in practice. The power coefficient of a rotor varies with the tip speed ratio (the ratio of rotor tip speed to free wind speed) and is only a maximum for a unique tip speed ratio. Incremental developments in the power coefficient are continually being sought by detailed design changes of the rotor and, by operating at variable speed; it is possible to maintain the maximum power coefficient over a range of wind speeds. However, these measures will give only a modest increase in the power output. By increasing the swept area of the rotor or by locating the wind turbines at higher wind speeds, a major increase in the power output can be achieved [19], [26]. The power output increases four-times when doubling the rotor diameter. Hence over the last 10 years there has been a continuous increase in the rotor diameter of commercially

available wind turbines from around 40 m to more than 170 m. The impact of the wind speed is more noticeable with a doubling of wind speed leading to an eight-fold increase in power. Thus, there have been significant efforts to make sure that wind farms are developed in areas of the highest wind speeds and the turbines optimally located within wind farms. In certain countries very high towers are being used (more than 160–180 m) to take advantage of the increase of wind speed with height [19], [27].

In the past, a number of studies were undertaken to determine the optimum size of a wind turbine by balancing the complete costs of manufacture, installation and operation of various sizes of wind turbines against the revenue generated. The results indicated a minimum cost of energy would be obtained with wind turbine diameters in the range of 35–60 m, depending on the assumptions made [19]. However, these estimates would now appear to be rather low and there is no obvious limit for rotor diameters, and hence output power, particularly for offshore wind turbines.

2.4 Types of wind turbine

Modern wind turbines are classified into two configurations: horizontal-axis wind turbines (HAWT) and vertical-axis wind turbines (VAWT), depending on rotor operating principles. There are two other types based on rotor facing: Upwind or Downwind Turbine.

2.4.1 Horizontal axis wind turbine (HAWT)

HAWT turbines are widely used for commercial applications where the rotor blades are connected to a horizontal shaft. A horizontal-axis wind turbine may have a rotor with upwind design to face the wind or a rotor with downwind design to enable the wind to pass the tower and nacelle before it hits the rotor.

Most modern wind turbines have upwind design configurations and range from 20 kW to 9 MW nominal power output capacities. Most of the design efforts are directed toward the major components such as rotor diameter, number and twist angle of rotor blades, tower height, rated electrical power, and control strategy [29]. Figure 2.1(left) shows a horizontal-axis wind turbine.

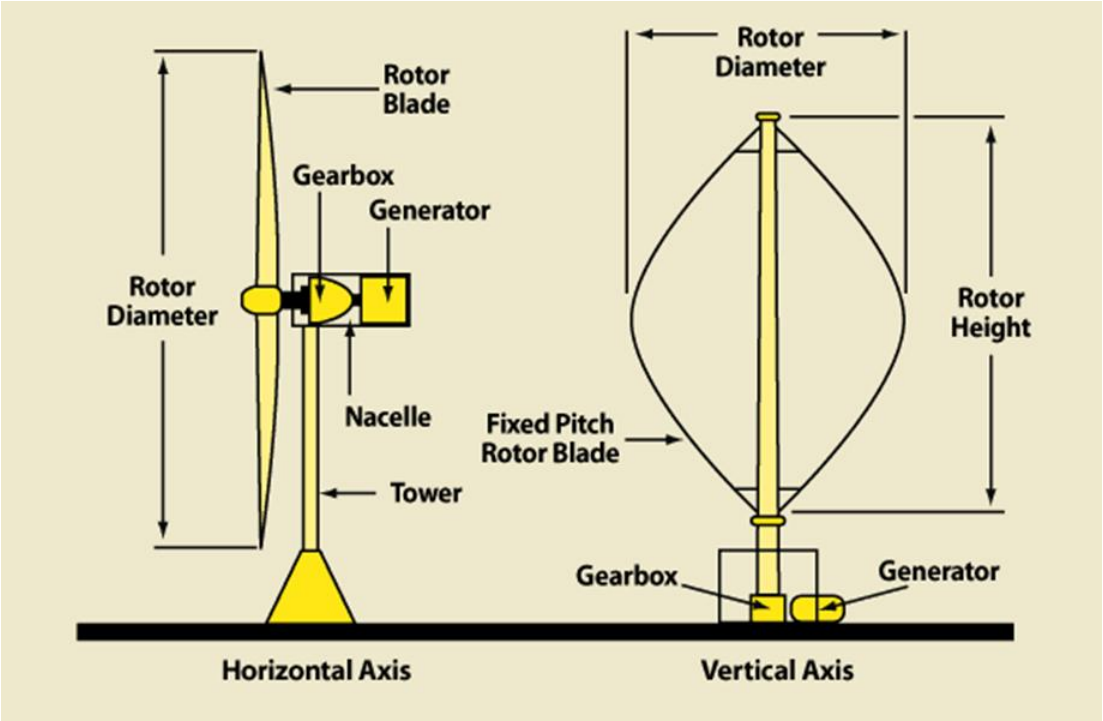

Figure 2.1: Horizontal-axis and vertical-axis wind turbine [28]

The wind speed increases with the height above the ground, so the tower height for a HAWT is particularly important. Rotor diameter is equally important because it determines the area required to meet specific output power level. HAWT systems are best suited for electrical power generation and micro-turbines composed of two to six rotor blades are most attractive for battery charging applications. Since the 1980s, some versions employ grid-connected wind turbines consisting of two or three rotor blades, some with the downwind rotor and others with the upwind rotor configurations [29].

The most common wind turbine is HAWT with two or three blades. Wind blowing over the blades causes the blades to lift and rotate at low speeds. The three bladed wind turbines are operated upwind with rotor blades facing into the wind. The tapering of rotor blades is selected to maximise the kinetic energy from the wind. Optimum wind turbine performance is strictly dependent on blade taper angle and the installation height of the turbine on the tower. Some of the wind turbine manufacturing company initiated the development of wind turbine technology by exploiting its unique capabilities such as improved performance under variable wind environments, variable speed control under reduced load conditions, and cost-effective electronics for local grids [29].

2.4.2 Vertical axis wind turbine (VAWT)

The main advantage of a VAWT is that it doesn't need the yawing mechanisms, thereby easy to service and repair. However, VAWTs in general, have lower tip speed ratios, hence they have lower rotor speeds and hence more challenging from the powertrain perspective. These turbines have small output capacities and hence are widely used for low-power applications such as battery charging in areas where power grids are not available, telecommunication masts and remote lighthouses [29]. Figure 2.1 (right) shows a vertical-axis wind turbine.

2.5 Drive train

The drive train consists of all the elements from the rotor up to and including the generator. This section of the turbine is where the mechanical energy extracted from the wind is transferred, torque up as necessary for the generator, and then converted into electrical energy. The most important parts of a drive train are:

1. Main shaft
2. Couplings
3. Gearbox
4. Generator
5. Brakes [30]

The mechanical transmission that helps to transmit the rotational motion of the turbine rotor to the electrical generator is called drive train. Depending on the technology it has various types of structure. For example, a turbine using a directly driven synchronous generator doesn't need a gearbox. The turbine using an induction machine generally requires gearbox to multiply speed for the generator. Therefore, an increased rotational speed of the electrical machine reduces electromagnetic torque [31]. The main advantage of the geared concept is that the generator has a smaller torque rating and as the volume and mass are generally proportional to torque, these generators are cheaper. Direct drive concept is often thought to be more reliable as it avoids a gearbox and lower losses in low wind speed [32]. A wind turbine drive train with gearbox is shown in Figure 2.2.

Until the late 1990s, the fixed speed wind turbines of below 1.5MW was built by most of the wind turbine manufacturers that using multistage gearbox and squirrel-cage induction generator directly connected to the grid. Since the late 1990s, 1.5 MW wind turbines with variable speed was the popular option for wind turbine manufacturer.

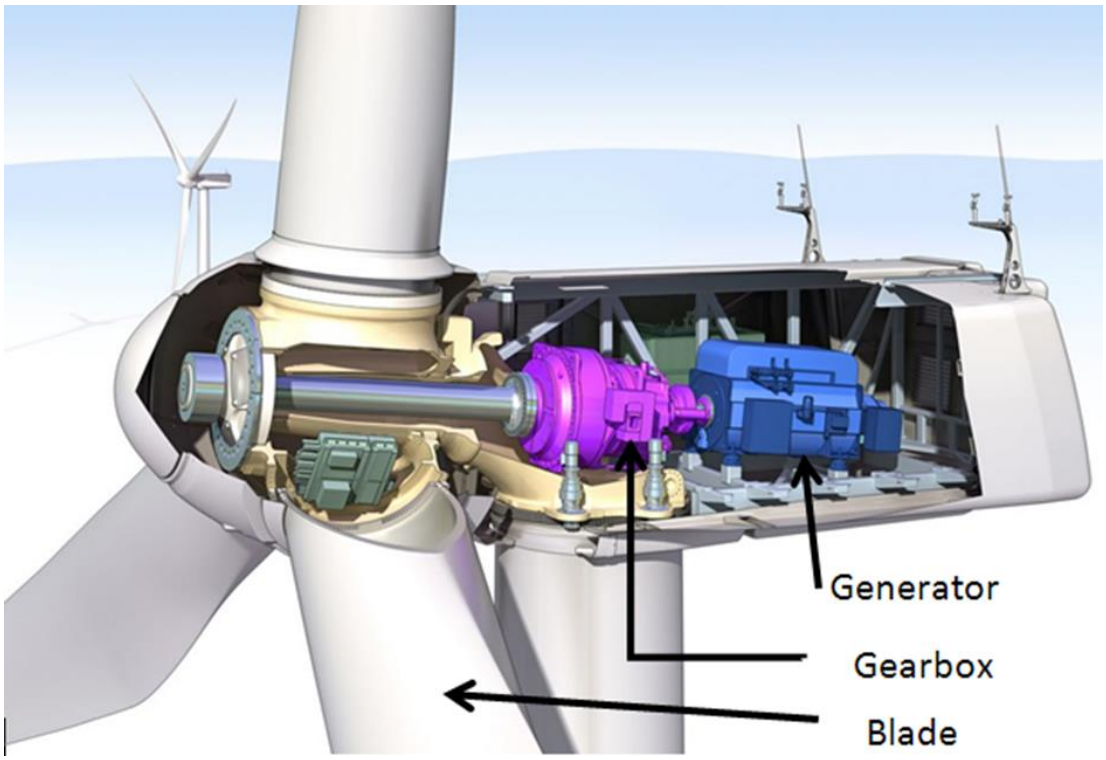

Figure 2.2: Typical wind turbine drivetrain with gearbox [33]

DFIG with multistage gearbox and partial rated power converter have used for this type of wind turbines. Since 1991, direct-drive generators have been proposed for gearless wind turbine generator to reduce failure rate and maintenance cost. A full-rated power converter is required for the grid connection. Figure 2.3 shows different types of drivetrain choice for some large wind turbines. Some of the most commonly used wind turbines are:

1. DFIG3G (Doubly-fed induction generator with three-stage gearbox)

2. DDSG (Direct-drive synchronous generator with electrical excitation)

3. DDPMG (Direct-drive permanent-magnet generator)

4. PMG1G (Permanent-magnet generator with single stage gearbox)

5. DFIG1G (Doubly-fed induction generator with single-stage gearbox) [2]

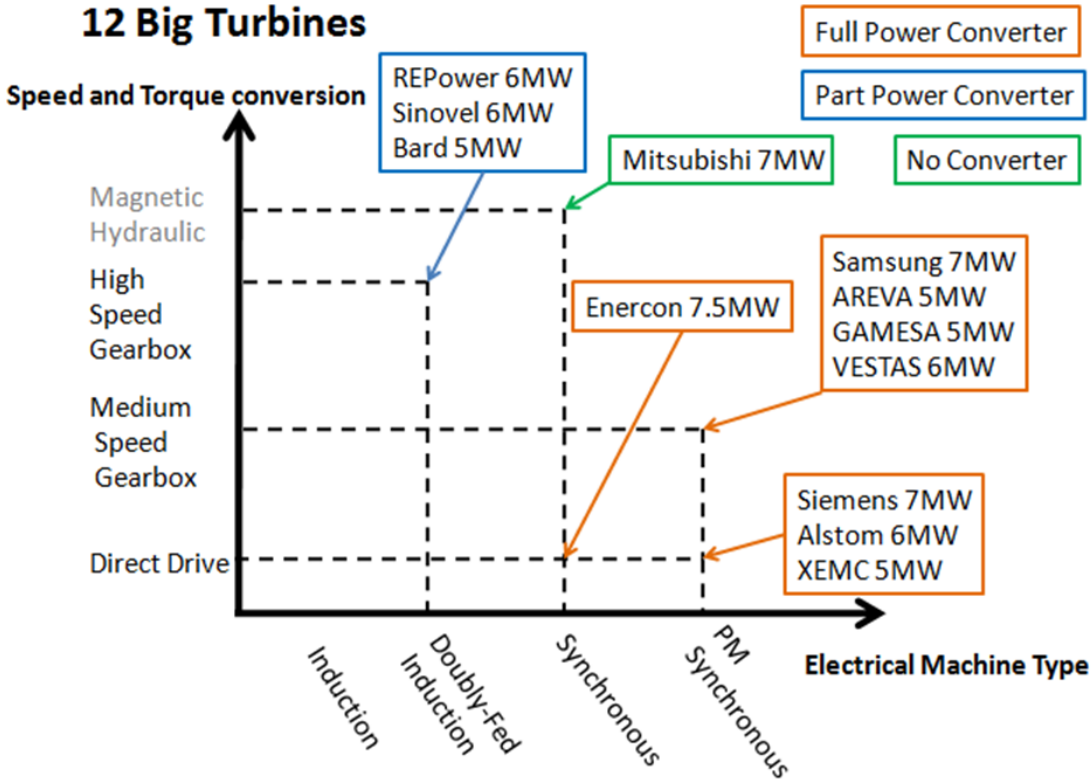

Figure 2.3: Different types of drivetrain choice for some large wind turbines

2.6 Gearbox

The gearbox changes the shaft speed up to a generator required operating speed in terms of revolutions per minute (rpm). The gearbox is one of the heaviest, most expensive parts of a turbine and usually made by a specialized gearbox manufacturer. All gearboxes contain some common parts for transmitting energy, like shafts and gears, bearings and seals, and casing. Most gearboxes have one input shaft (low-speed) and one output shaft (high speed). Gears can be made of many different materials, but the most common ones are made of extremely hard and strong steel, so the steel is usually carburized or heat-treated in some way [30].

There are different types of gearbox stages. The two most common ones in wind turbines are parallel-shaft and planetary gearboxes. Bearings in parallel-shaft gearboxes support two or more parallel shafts with gears on them. Single-stage models contain one low-speed shaft connected to the rotor. They also contain one high-speed shaft connected to the generator. The low-speed shaft has a large gear that connects with the high-speed shaft's smaller gear. The gear's pitch diameter ratio is inversely proportional to the rotational speed ratio [30].

Planetary gearboxes are different from parallel-shaft gearboxes in two main ways. First, the input and output shafts are coaxial. Second, they contain many gears meshing together at the same time, so the mechanical load on each gear is less than parallel-shaft gearboxes. Thus, they are relatively small and light as well.

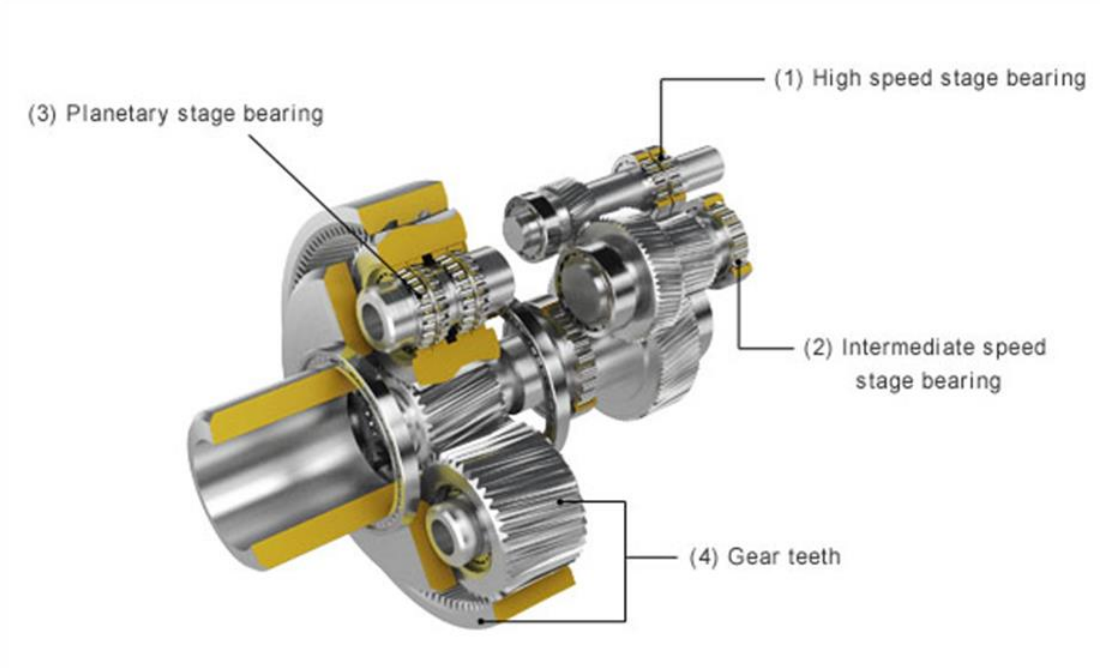

Figure 2.4: Wind turbine gearbox [34]

The low-speed (input) shaft enters the gearbox supported by bearings and is connected to a planetary carrier. The planetary carrier can rotate and carries three small identical gears called “planetary gears” which are able to rotate about their own axes. They are free to run, and they mesh with a large-diameter ring gear and a small “Sun” gear. When the low-speed shaft and carrier rotate, the meshing with the ring gear rotates the planet gears at a higher speed. They then rotate the sun gear at an even higher speed, and that drives the high-speed (output) shaft [30].

One of the most troublesome parts of a wind turbine – from a reliability perspective – is the gearbox as the downtime for a failure of a gearbox is very high. The statistical analysis from the wind industry says that, the contribution of gearbox to the overall offshore failure rates is about 7.6% and it share about 20% of total downtime in wind turbines which is a large proportion among all the components [35] [36]. The failure of the gearbox takes a long time to repair or replacement which reduces the wind turbine availability. The cost of replacing gearboxes, especially offshore, can be very expensive. So, it is very important to detect gearbox faults at an early stage and repair

on time to reduce downtime and avoid damage of the wind turbines [35]. To avoid the gearbox failure, many offshore turbines are now designed without gearboxes, i.e., direct drive.

2.7 Generator

Generators are used in conversion of mechanical power to electrical power. Synchronous and asynchronous generators are both used but need different power conversion steps depending on electrical machine type and whether the turbine is fixed or variable speed [37]. Generally, generator designers and wind turbine designers are not same. They either specify the requirements of the generator to be specially designed or select commercially available generator with some minor change. The key considerations of the wind turbine designer to choose a generator are given below:

- High efficiency
- High availability
- Low stable cost
- Low mass
- Compactness
- Method of starting
- Operating speed
- Type of insulation
- Operation with high electrical noise on conductors
- Efficiency at full load and part load
- Protection from environment
- Heat removal
- Ability to withstand fluctuating torques
- Feasibility of using multiple generators [38]

2.7.1 AC Generators

The three-phase AC (alternating current) system supplies electricity at a sinusoidal waveform with a fixed frequency and amplitude. Most industrial and many domestic loads use sinusoidal AC voltage and current. As most existing generator technologies supply AC, it is convenient for wind turbine to produce AC voltage. AC generators are mainly two types in wind power system [39].

1. Asynchronous or Induction Generator
    - Squirrel cage induction generator (SCIG)
    - Wound rotor induction generator (WRIG)
        - OptiSlip induction generator (OSIG)
        - Doubly-fed induction generator (DFIG)
2. Synchronous Generator
    - Wound rotor synchronous generator (WRSG)
    - Permanent magnet synchronous generator (PMSG)

2.7.2 Asynchronous or Induction Generator

Induction generators are still the most popular in wind energy systems. The initial reasons of popularity are the simple, rugged structure and low cost of the squirrel cage induction machine and the ability to connect directly to the grid (for fixed speed turbines). The operating speed of an Induction machine is slightly greater than synchronous speed in generator mode and slightly less than synchronous speed in motor mode. This difference in speed is described as "slip" and gives the rise to the name asynchronous machine [40], [41].

The main drawback of the induction machine is the reactive magnetising current needed by stator. As the induction generator has no permanent magnet or separate excitation, its need excitation current from other sources and thus reactive power consumed. This reactive power can be delivered by the grid or by a power electronic system. After connecting to the grid, the generator's magnetic field is produced. Squirrel cage and wound rotor are the types of rotors for an induction generator [42]. Figure 2.5 shows the image of these two types of rotor is an induction generator.

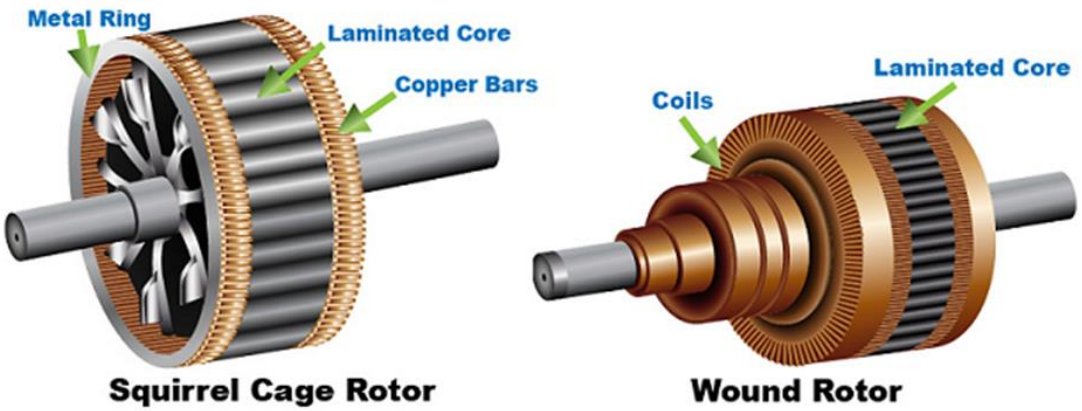

Figure 2.5: Squirrel cage rotor and wound rotor for induction generator [43]

2.7.2.1 Squirrel cage induction generator (SCIG)

The squirrel cage induction generator (SCIG) are widely used because of its mechanical simplicity, high efficiency and low maintenance requirements. The SCIG speed changes by only a few percent. The copper losses are proportional to the generator slip and machines designed to have higher slip could become very hot. Therefore, this generator is used for fixed-speed wind turbines. The generator and the wind turbine rotor are coupled through a gearbox, as the optimal rotor and generator speed ranges are different. It also used for full variable speed wind turbines where the variable frequency power of the machine is converted to fixed-frequency power by using a bidirectional full-load back to-back power converter [41], [44].

SCIGs have a steep torque speed characteristic and therefore fluctuations in wind power are transmitted directly to the grid. These fluctuations are especially critical during the grid connection of the wind turbine, where the in-rush current can be up to 7–8 times the rated current. In a weak grid, this high in-rush current can cause severe voltage disturbances. Therefore, the connection of the SCIG to the grid should be made gradually in order to limit the in-rush current [42].

During normal operation and direct connection to a stiff AC grid, the SCIG is very robust and stable. The slip varies and increases with increasing load. The major problem is that, because of the magnetising current supplied from the grid to the stator winding, the full load power factor is relatively low. This has to be put in relation to the fact that most power distribution utilities penalise industrial customers that load with low power factors. Clearly, generation at a low power factor cannot be permitted here either. Too low a power factor is compensated by connecting capacitors in parallel to the generator. There is a unique relation between active power, reactive power, terminal voltage and rotor speed in SCIGs. This means that in high winds the wind turbine can produce more active power only if the generator draws more reactive power. For a SCIG, the amount of consumed reactive power is uncontrollable because it varies with wind conditions. Without any electrical components to supply the reactive power, the reactive power for the generator must be taken directly from the grid. Reactive power supplied by the grid causes additional transmission losses and in certain situations, can make the grid unstable. Capacitor banks or modern power electronic converters can be used to reduce the reactive power consumption [41].

2.7.2.2 Wound rotor induction generator (WRIG)

In the case of a WRIG, the electrical characteristics of the rotor can be controlled from the outside, and thereby a rotor voltage can be controlled. The windings of the wound rotor can be externally connected through slip rings and brushes or by means of power electronic equipment, which may or may not require slip rings and brushes. By using power electronics, the power can be extracted or impressed to the rotor circuit and the generator can be magnetised from either the stator circuit or the rotor circuit. It is thus also possible to recover slip energy from the rotor circuit and feed it into the output of the stator. The disadvantage of the WRIG is that it is more expensive and not as robust as the SCIG [41].

The most commonly used WRIGs in wind turbine industry are:

- OptiSlip induction generator (OSIG) and
- Doubly-fed induction generator (DFIG) concept

2.7.2.3 OptiSlip induction generator (OSIG)

The Danish manufacturer Vestas introduced the OptiSlip feature to minimise the load on the wind turbine during gusts. The OptiSlip feature allows the generator to have a variable slip (narrow range) and to choose the optimum slip, resulting in smaller fluctuations in the drive train torque and in the power output. The variable slip is a very simple, reliable and cost-effective way to achieve load reductions compared with more complex solutions such as full variable-speed wind turbines using full-scale converters. The slip of the generator is changed by modifying the total rotor resistance by means of a converter, mounted on the rotor shaft. No slip rings are necessary as the converter is optically controlled. The stator of the generator is connected directly to the grid [41].

The advantages of this generator concept are a simple circuit topology, no need for slip rings and an improved operating speed range compared with the SCIG. This concept can reduce the mechanical loads and power fluctuations caused by gusts to a certain extent. However, it still requires a reactive power compensation system. The disadvantages are:

- The speed range is typically limited to 0–10 %, as it is dependent on the size of the variable rotor resistance
- Only poor control of active and reactive power is achieved

- The slip power is dissipated in the variable resistance as losses and hence heat

2.7.2.4 Doubly-fed induction generator (DFIG)

The concept of the DFIG is the default option for onshore turbines today. The DFIG consists of a WRIG with the stator windings directly connected to the constant-frequency three-phase grid and with the rotor windings mounted to a bidirectional back-to-back IGBT voltage source converter. The term 'doubly fed' refers to the fact that the voltage on the stator is applied from the grid and the voltage on the rotor is induced by the power converter. This system allows a variable-speed operation over a large but restricted range. The converter compensates the difference between the mechanical and electrical frequency by injecting a rotor current with a variable frequency. The behaviour of the generator is thus governed by the power converter and its controllers during both normal operation and faults. The power converter consists of two converters, the rotor-side converter and grid-side converter, which are controlled independently of each other [41], [45].

The main idea is that the active and reactive power is controlled by the rotor-side converter by controlling the rotor current components, while the line-side converter controls the DC-link voltage and ensures a converter operation at unity power factor (i.e. zero reactive power).

Power is fed into or out of the rotor depending on the operating condition of the drive. It flows from the rotor via the converter to the grid in super-synchronous situation, whereas in a sub-synchronous situation, it flows in the opposite direction. The stator feeds energy into the grid in both cases. The DFIG has several advantages. It has the ability to control reactive power and to decouple active and reactive power control by independently controlling the rotor excitation current. It is not necessary to magnetise the DFIG from the power grid, it can also be magnetised from the rotor circuit. It is also able to generate reactive power that can be delivered to the stator by the grid-side converter. However, the grid-side converter is not involved in the reactive power exchange between the turbine and the grid as it normally operates at unity power factor. In the case of a weak grid, where the voltage may fluctuate, the DFIG may be ordered to produce or absorb an amount of reactive power to or from the grid, with the purpose of voltage control [41].

The size of the converter is not related to the total generator power but to the selected speed range and hence to the slip power. Thus, the cost of the converter increases when the speed range around the synchronous speed becomes wider. The selection of the speed range is therefore based on the economic optimisation of investment costs and on increased efficiency. A drawback of the conventional DFIG is the inevitable need for slip rings which wear out and need replacing [41]. Some authors have proposed brushless DFIGs which essentially use a secondary stator winding as a rotating transformer to manipulate the rotor currents.

2.7.3 Synchronous generator

Synchronous generators are used in large central station power plant. The synchronous generator is generally more expensive and mechanically more complicated than an induction generator of a similar size. However, it has one clear advantage over the induction generator, it does not need a reactive magnetising current [41].

The magnetic field in the synchronous generator can be created by using permanent magnets or with a conventional field winding. If the synchronous generator has a suitable number of poles (a multi pole WRSG or a multi pole PMSG), it can be used for direct-drive applications without any gearbox [41], [46].

As a synchronous machine, it is probably most suited for full power control as it is connected to the grid through a power electronic converter. The primary goals of the converter are: (1) to act as an energy buffer for the power fluctuations caused by an inherently gusting wind energy and for the transients coming from the net side, (2) to control the magnetisation and to avoid problems by remaining synchronous with the grid frequency and (3) to control the generator torque and speed. Applying such a generator allows a variable-speed operation of wind turbines [41], [46].

2.7.3.1 Wound rotor synchronous generator (WRSG)

The WRSG is the workhorse of the electrical power industry. The rotational speed is strictly fixed by the frequency of the supply grid as the stator windings of WRSGs are directly connected to the grid. Slip rings and brushes or brushless exciter with a rotating rectifier is used for excitation in the rotor winding with direct current. Additional reactive power compensation system does not require for the synchronous generator. The rotor winding rotates with synchronous speed, generates the excitation field due to current in the field winding. The number of pole pairs of the rotor and the

frequency of the rotating field determine the speed of the synchronous generator. Enercon and Lagerwey are the top wind turbine manufacturers who use low speed multi-pole WRSG with no gearbox. The advantage of this machine is that it does not need a gearbox which can increase the reliability, but the generator is very costly as a large and heavy generator with full-scale power converter is required [41].

2.7.3.2 Permanent magnet synchronous generator (PMSG)

The PMSGs in wind turbines allows an operation at high power factor and high efficiency because of its self-excitation property. The efficiency of the permanent magnet machine is higher than induction machine as the excitation requires no external energy supply. However, it is costly to produce permanent magnets and tough to work with them in a manufacturing time. The additional cost of this PM excitation is the requirement of full-scale power converter to adjust the frequency and voltage of generation with transmission system. However, the advantage is the generation of power at any speed to fit the current conditions. The stator of the PMSG is wound and the rotor may have salient poles or cylindrical with permanent magnet pole system. The salient poles are a good option for low-speed wind turbine generator. Actually, most machines are surface mounted – with no magnetic saliency [41], [42].

2.7.3.3 Direct-drive generator

The drive connecting the main rotor shaft to the generators can either be routed through a gearbox system (to increase the rotor speed) or a direct-drive (gearless) system. Direct-drives do not have the mechanical noise associated with a gearbox. Direct-drive generators (using magnet in rotors) rotating at lower speeds can still produce the same required ‘grid compatible’ electric output as the generators with gearbox if the length or the diameter of the generator is increased. This is because the power output is not only proportional to the strength of the magnetic field and the rotor speed, but also to the length of the generators and the square of its diameter. As the diameter has more effect than the length it is the diameter that is usually increased. Direct-drive turbines are often seen to have wide nacelles.

As lower rotor speeds require larger generators, they use more material and so are more expensive and heavier. However, the lower-speed designs increase simplicity and reliabilities, reduce the need for maintenance and extend the life of machine [47]. Figure 2.6 shows a typical direct-drive wind turbine.

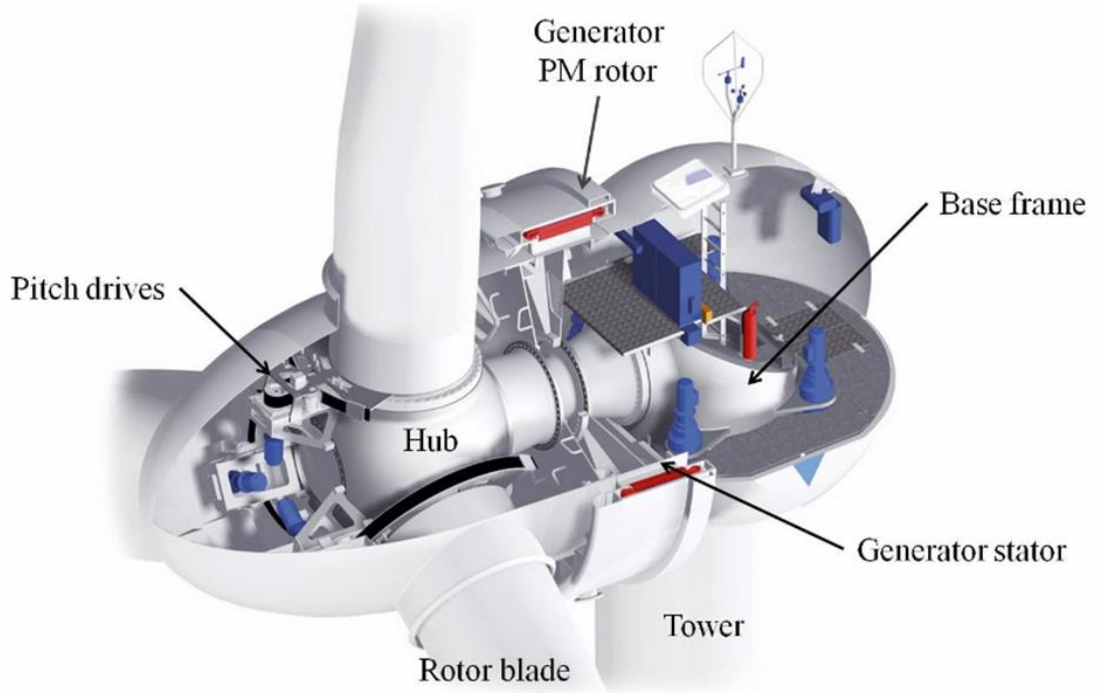

Figure 2.6: Goldwind direct-drive permanent magnet wind turbine [48]

2.7.4 Flux orientation

2.7.4.1 Radial-flux machine

The magnetic field can be given a radial direction by placing the stator around the rotor. A machine construction like this is called a radial-flux machine. Constructing a stator and rotor out of laminated steel is easier and cheaper for a radial-flux topology since laminations can be stacked.

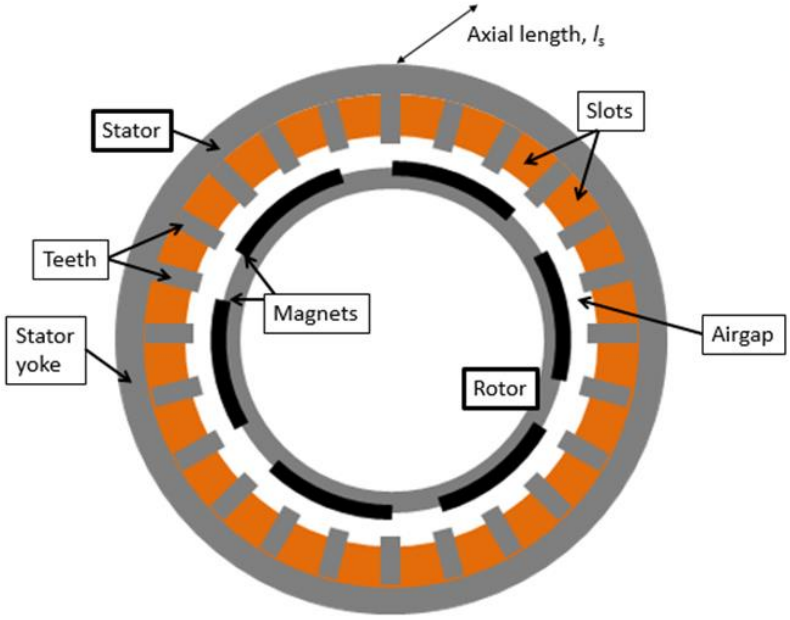

Figure 2.7: Radial-flux inner-rotor machine

A radial-flux machine can be outer-rotor or inner-rotor (Figure 2.7). An advantage of radial-flux outer-rotor permanent-magnet synchronous generator compared to inner-rotor PMSG is that the magnets are more easily attached to the rotor surface [46].

2.7.4.2 Axial-flux machine

The axial-flux PM machine is an alternative of the radial-flux machine. The main difference of this machine with radial-flux machine is the magnetic flux that passes axially rather than radially across the air gap. These machines are suitable for electrical vehicles, pumps, valve control, centrifuges, fans, machine tools, robots and industrial equipment. Axial-flux PM machines also named as disk type generator can be designed as single sided or double sided, slotted or slotless windings, with internal or external PM rotor (Figure: 2.8), iron-cored or ironless stator with surface mounted or interior type PM machine [6]. The contact surface between the rotor and shaft becomes shorter as output power of the axial-flux generator increases. A major cause of failure of axial-flux machine is the design of the rotor-shaft mechanical joint which must be given careful attention [46].

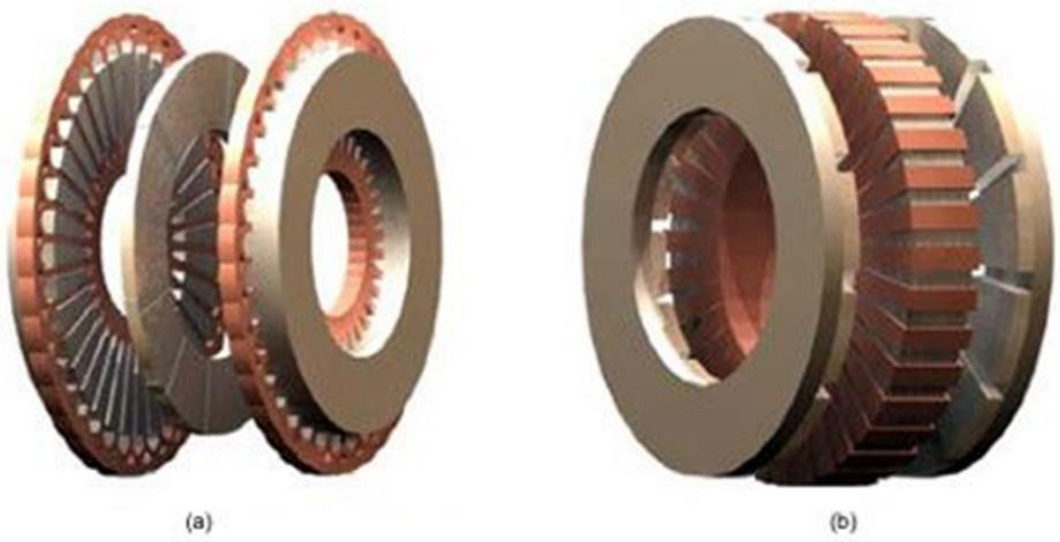

Figure 2.8: (a) Internal rotor axial-flux machine, (b) Torus axial-flux machine [49]

2.7.4.3 Transverse- flux generator

The transverse-flux generator (TFG) is a fairly new topology. However, to use for a wind turbine generator, more research on TFG machine is required. The transverse-flux topology can be applied to a range of machine types. It could be used both in

permanent magnet and in reluctance machines, for instance. The high ratio of torque per kilogram of active material seems to be very attractive [42], [46].

A TFG utilises a magnetic circuit that is in a direction perpendicular (transverse) to the direction of motion and that of current flow. The geometrical layout of TFG have a homo polar flux in the stator cores. This allows an increase in the VA rating of the machine with an increase in the pole number for given geometrical dimensions (same external diameter and length), raw material and current loading [46], [50].

The advantage of independently setting the current and magnetic loading in the machine is another attracting aspect of a TFG over the radial-flux machine. In a TFG the peripheral length (air gap diameter) sets the magnetic loading whereas the axial length of the machine sets the current loading. As these are the most critical factors during a machine design phase, an absence of competition between the two is favourable for the designer. On the other hand, in a radial-flux machine both, the current as well as the magnetic loading is dependent upon the peripheral length of the machine, i.e. the air gap diameter. Hence, they compete for the same space, and cause design limitations [46], [50].

The nature of operation is same as a synchronous machine, and it will function in a way that is similar to any other PM machines. It can comprise a very large number of poles, which may make it suitable for direct gearless applications [46].

A disadvantage of the TFG is the large number of individual parts is required and a lamination technology has to be used. It can be improved with the advance of powder technology. The high amount of flux leakage is another drawback of a TFG, which increases with the pole number and results in a poor power factor. This practically sets the limit upon the pole width, as otherwise one could go down to an infinite number of poles and obtain an infinite power from the machine. The power factor can be improved, but at the cost of decreasing the torque density of the machine [46].

Kumar *et al.* shows TFG for wind power applications with different topologies, their advantages and limitations [51]. Husain *et al.* presented a double-sided TFG for direct-drive wind turbine applications. The proposed TFG has a modular structure with quasi U-core stators and toroidal ring windings. A flux-concentrating ferrite magnets setup in the rotor to achieve high air gap flux density [52]. Nasiri-Zarandi *et al.* proposed a

TFG using Halbach-array permanent magnet for direct-drive wind turbine applications to reduce cogging torque [53].

2.7.5 Properties of permanent magnets

There are three classes of PMs currently used for electric generator:

- Alnicos (Al, Ni, CO, Fe)
- Ceramics (ferrites), e.g., barium ferrite BaO×6Fez03 and strontiumferrite SrO×6Fez03
- Rare-earth materials, i.e., samarium-cobalt SmCo and neodymium-iron-boron Nd-Fe-B

2.7.5.1 Alnico

Alinco has an advantage of high magnetic remanent flux density and low temperature coefficients. The temperature coefficient of *B*, is -0.02%/^{o}C and maximum service temperature is 520^{o}C. These advantages allow a high air gap magnetic flux density at high magnet temperature. Unfortunately, coercive force is very low, and the demagnetization curve is extremely non-linear. Therefore, it is very easy not only to magnetize but also to demagnetize Alnico. Alnico has been used in PM DC commutator generator of disk type with relatively large air-gaps. This results in a negligible armature reaction magnetic flux acting on the PMs. Sometimes, Alnico PMs are protected from the armature flux, and consequently from demagnetization, using additional mild steel pole shoes. Alnicos dominated the PM generator market in the range from a few watts to 150 kW between the mid-1940s and the late 1960s when ferrites became the most widely used materials [46].

2.7.5.2 Ferrites

In the 1950s Barium and strontium ferrite were developed. A ferrite has a higher coercive force than Alnico, but at the same time has a lower remanent magnetic flux density. Temperature coefficients are relatively high, i.e. the coefficient of *B*, is -0.2%/^{O}C and the coefficient of *H*, is -0.27%/^{o}C. The maximum operating temperature is 400^{o}C. Low cost and very high electric resistance are the major advantages of ferrites, which means no eddy-current losses in the PM volume. Ferrite magnets are most cost-effective in fractional horsepower generator and may show a financial advantage over Alnico up to about 7.5 kW [46]. Barium ferrite PMs are commonly used in small DC commutator motors for automobiles (blowers, fans, windscreen

wipers, pumps, etc.) and electric toys. Ferrites are produced by powder metallurgy. Their chemical formulation may be expressed as MO×G(Fe203), where M is Ba, Sr, or Pb. Strontium ferrite has a higher coercive force than barium ferrite. Lead ferrite has a production disadvantage from an environmental point of view. Ferrite magnets are available in isotropic and anisotropic grades [46].

2.7.5.3 Rare-earth permanent magnets

In terms of energy density BH_{max}, there has been great progress in development of rare-earth PMs during the last three decades. The rare-earth elements are in general not rare at all, but their natural minerals are widely mixed compounds. To produce one specific rare-earth metal, several others have to be refined, which has no commercial application. This limits the availability of these metals. The first generation of these new alloys based on the composition $SmCo_5$ and developed in the 1960s has been commercially produced since the early 1970s. Now it is a well-established hard magnetic material. $SmCo_5$ has the advantage of high remanent flux density, high coercive force, high energy product, linear demagnetization curve and low temperature coefficient. The temperature coefficient of B_r is 0.03 to 0.045%/°C and the temperature coefficient of H_c is 0.14 to 0.40%/°C. Maximum operating temperature is 300 to 350°C. It is suitable for generator with low volume, high power density and class of insulation F or H. The only disadvantage is, it is expensive due to supply restrictions of both Sm and Co [46].

A significant progress in terms of low raw material costs has been achieved after developing a second generation of rare earth magnets on the basis of cheap neodymium (Nd). The Nd is a much more abundant rare-earth element than Sm. Nd-Fe-B magnets give better magnetic properties than SmCo, which arc now produced in increasing quantities. Nd-Fe-B magnets have great potential of improving the performance-to-cost ratio for many applications. Because of this, they will have a major impact on the development and application of PM apparatus in the future [46].

2.7.6 Magnet Mounting

2.7.6.1 Surface PM generators

In a surface mounted generator (Figure 2.9), the magnet can be magnetized radially or sometimes circumferentially. To protect the PMs against demagnetisation and centrifugal forces, an external non-ferromagnetic cylinder is used. It can act as a

damper and provides an asynchronous starting torque. The synchronous reactance in the direct axis and quadrature axis are same in terms of rare earth permanent magnet [46].

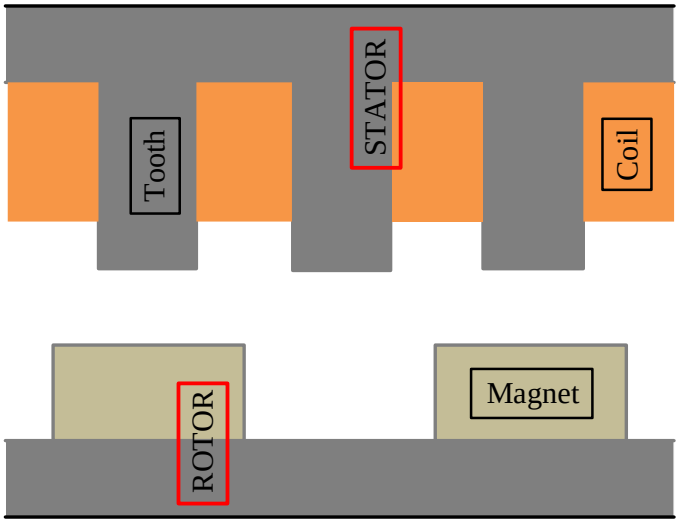

Figure 2.9: Typical diagram of a surface mounted PM generator

2.7.6.2 Buried PM generators

In a buried magnet generator (Figure 2.10), the rotor is magnetized circumferentially and the PMs are embedded in between pole shoes. The height of the PM is in tangential direction, i.e., along the pole pitch due to circumferential magnetization. The effective pole arc coefficient α_i is dependent on the slot width. The synchronous reactance in the quadrature axis is greater than the direct axis.

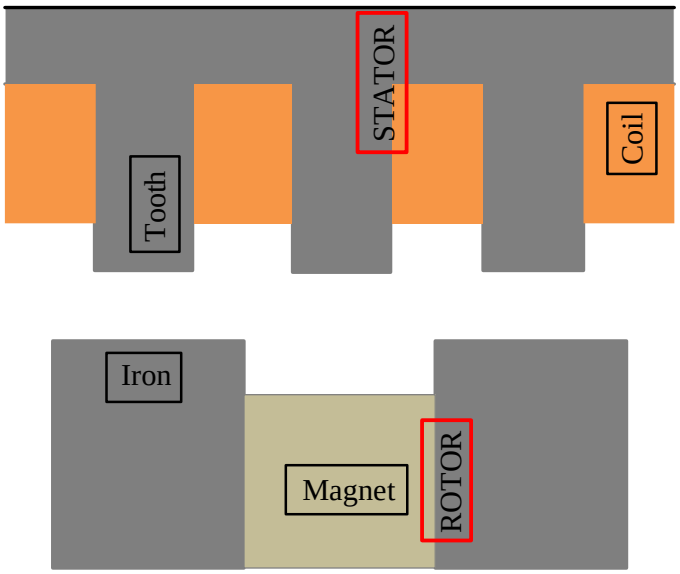

Figure 2.10: Typical diagram of a buried PM generator

A starting asynchronous torque is produced with the help of both a cage winding integrated in slots in the rotor pole shoes (laminated core) and solid salient pole shoes made of mild steel. A non-ferromagnetic shaft is required in order to increase the air gap flux linkage. Including ferromagnetic shaft, a large portion of produced magnetic flux goes through the shaft [46]. To increase the air gap flux linkage, another process is to equip a non-ferromagnetic sleeve between the ferromagnetic shaft and the rotor core.

2.7.6.3 Shaping PMs

Permanent magnets can show different characteristics depending on their shape. The cogging and commutation torque ripple can be reduced by shaping the PMs thinner at the edges than in the centre. A multilateral cross section of the rotor core is needed for magnet shapes. Decentred PMs together with split stator slots can suppress the cogging torque as effectively as skewed slots with much less reduction of the *EMF* [46]. By selecting proper magnet shape and dimension, it is possible to reduce the induced voltage harmonic.

2.7.6.4 Halbach Arrays

A Halbach array (Figure 2.11) is named for its inventor Klaus Halbach, which is a special arrangement to concentrate magnetic field of permanent magnet on one side of the array while cancelling the field to zero on the other side. This is achieved by having a spatially rotating pattern of magnetisation [54].

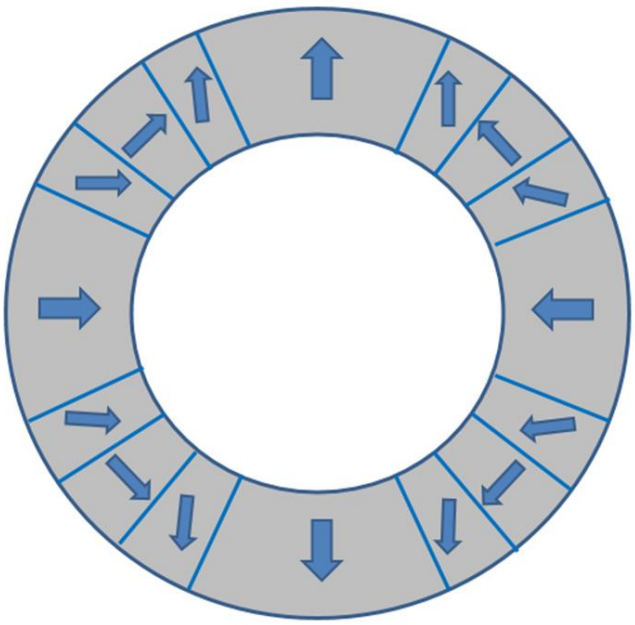

Figure 2.11: Typical diagram of a Halbach Array machine

This type of electrical machine can be constructed using multipole fields. Therefore, for the high speed electrical machine manufacturer, dipole field has some advantages as it can be manufactured with only permanent magnets. No other magnetic materials, laminations or back iron needed. The main advantages of this concept are the conventional core loss and eddy current loss in the lamination or back iron does not exist. Another advantage is the lightweight of the machine because of no back iron or laminations required. It can extract a very high peak power over short time scales because of the field uniformity [55].

2.7.7 Stator/winding Design

2.7.7.1 Slotted PM generators

In a slotted stator, the core is carbon steel sheet or a lamination of silicon steel sheet. The armature winding is located in the stator slots. The conductors torque secured in the slots and reinforced by the slot insulation and epoxy resin. Therefore, a slotted stator is long-lasting and consistent than a slotless-stator. A core with large number of slots has less electromagnetic noise and cogging torque. To make the production easy, the generators manufactured by an automated mass production process must use even number of slots in the core. In terms of quality, odd number of slots are preferred with ferromagnetic cores due to low cogging torque [46]. The diagram of the slotted-stator and slotless-stator is shown in figure 2.12.

2.7.7.2 Slotless PM generators

It is possible to remove the cogging effect by designing PM generators without stator slots, i.e. the windings are fixed with the inner surface of the laminated stator yoke. Sometimes, coils wound around the cylindrical stator core are more convenient for small generator. Making zero cogging torque, slotless PM generator have some other advantages over slotted generators that given below:

- Higher efficiency in the higher speed range
- Lower winding cost in small sizes
- Higher winding-to-frame thermal conductivity
- Lower acoustic noise

There are some disadvantages including the use of more PM material, lower efficiency in the lower speed range, lower torque density and higher armature current. The air gap flux density and electromagnetic torque decreases with the increase of total air gap

(mechanical clearance plus winding radial thickness). To keep the torque close to the equivalent slotted motor, then the height of PMs must significantly increase [46].

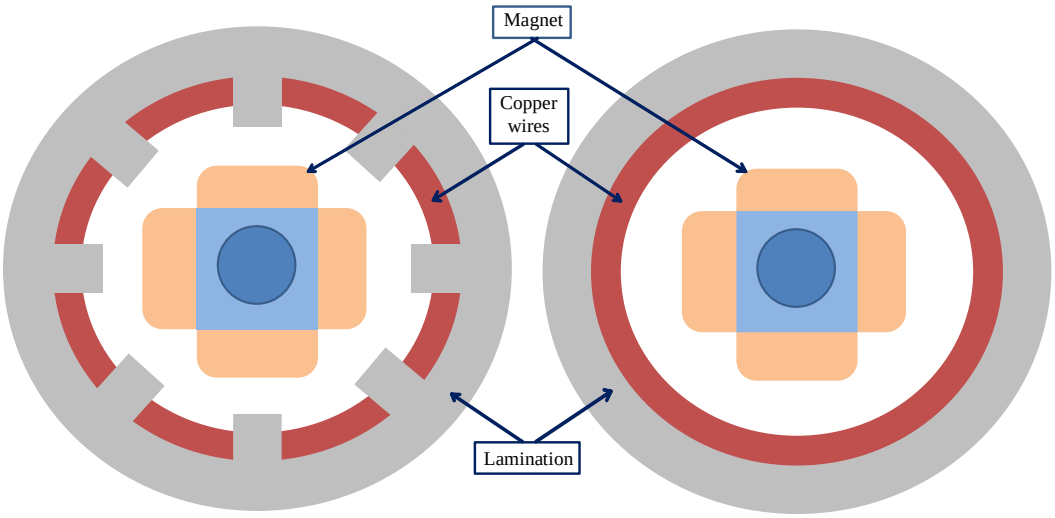

Figure 2.12: Slotted-stator (left) and slotless-stator (right) PM generator

2.7.8 Applications

There are various types of application for rare earth permanent magnets. Hard disk drives, CD's and DVD's are the largest sector of permanent magnet application. Motors are another largest sector as the conversion from induction to permanent magnet motor is growing for efficiency gain.

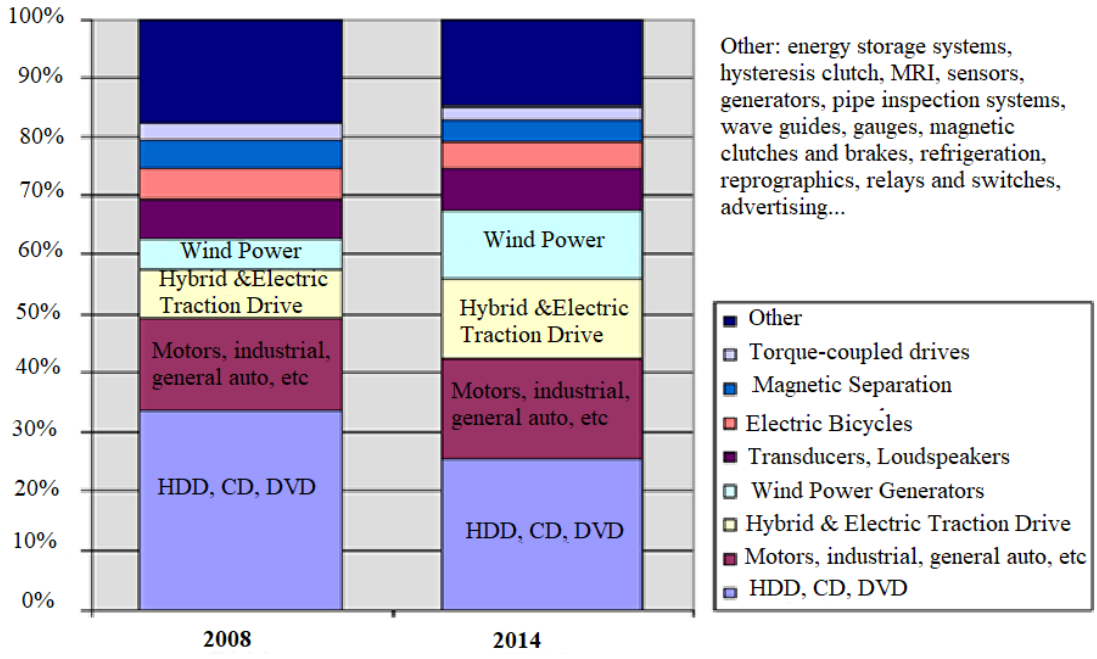

Figure 2.13: Applications of rare earth permanent magnets [56]

Wind power generation and hybrid (and EV) drive system are in newest growth categories. In addition to wind power, other environmental friendly generators are being designed and installed such as tidal turbine, some using PM generators. Some other applications of permanent magnets are electric bicycle, transducer, loudspeakers, torque-coupled drives, energy storage systems, hysteresis clutch, MRI, sensors, refrigeration, brushless DC machine, transport and many more.

2.7.9 Magnetic grades

The strength of a magnetic material is defined as its magnetic grade. It doesn't depend on the physical properties of the magnet, but the maximum energy product BH_{max}. The higher grade denotes that the magnet is stronger. A grade forty (N40) means that the magnetic material has a maximum energy product of 40 MGOe [57].

Table 2.1: Characteristics of some regular Neodymium-Iron-Boron magnet grades [58]

Properties	**Residual Induction, B_r**	**Coercivity, H_{cB}**	**Intrinsic Coercivity, H_{cJ}**	**Maximum Energy Product, BH_{max}**	**Temperature**
Grade	Typical mT	min kA/m	min kA/m	Typical MGOe	Max ^oC
N30	1105	796	955	30	80
N33	1150	836	955	33	80
N35	1210	860	955	35	80
N38	1260	860	955	38	80
N40	1285	923	955	40	80
N42	1315	860	955	42	80
N45	1350	860	955	44	80
N48	1400	836	875	47	80
N50	1425	836	875	49	80
N52	1450	836	875	51	60
N55	1490	716	876	54	60

The characteristics of regular Nd-Fe-B magnet are given in Table 2.1, the demagnetisation curve of Nd-Fe-B (N40) magnet also shown in figure 2.14.

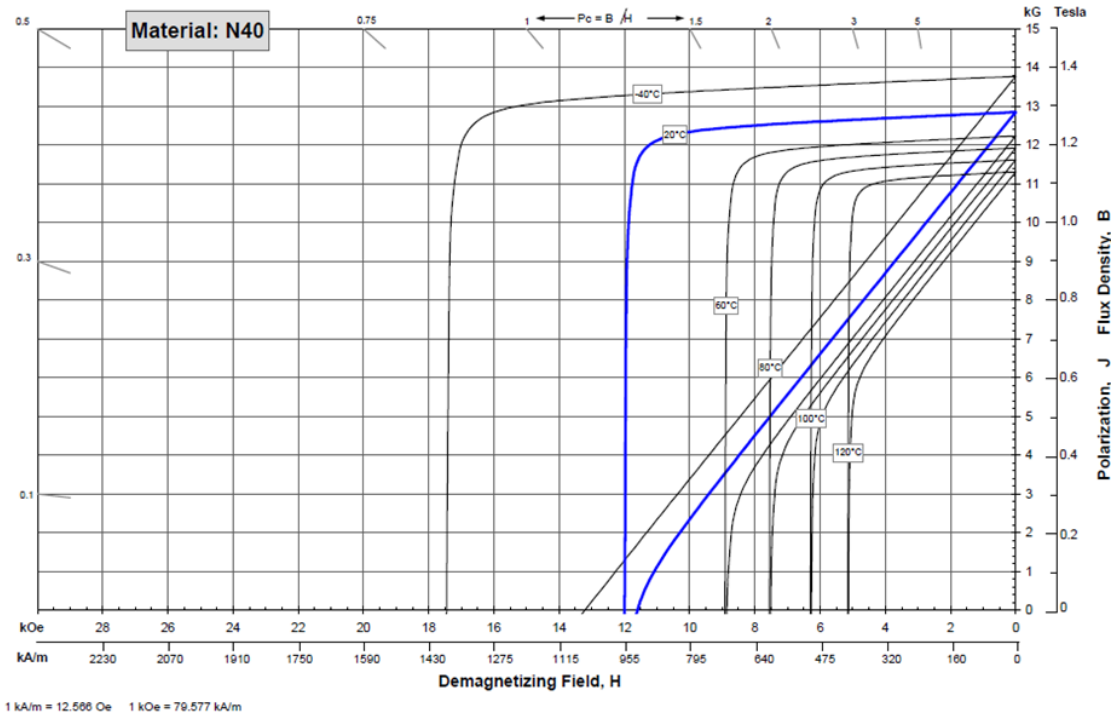

Figure 2.14: Demagnetisation curve of Neodymium-iron-Boron (N40) magnet [58]

2.7.10 Other types of generators

2.7.10.1 High voltage generator

Wind turbine generators can be operated at high voltage by using transformer. The main objective of increasing the voltage of the generator is to reduce the current which reduces losses. This can help to increase the efficiency of wind turbine at higher load and reduce the size of the generator. The use of a transformer is not required, if the voltage of the machine and the grid voltage are same. HVGs are manufactured both as synchronous generators and as asynchronous generators [42].

For large wind turbines exceeding 3MW, HVGs are a potentially interesting alternative. The major drawbacks are the uncertainty regarding its long-term performance, the high cost of the entire system and the safety requirements, which are more complex than those for low-voltage machines. The cost of the HVG including, the power electronics and the auxiliary equipment, such as switchgears, increases significantly with the size of the generator. If the number of wind turbines with HVGs increases significantly, the price could decrease in the future [42].

2.7.10.2 The switched reluctance generator

The switched reluctance generator (SRG) has a robust and simple mechanical structure with reduced costs and the opportunity to eliminate the gearbox. For the aerospace applications, it is more interesting because of its ability to continue operating at reduced output in the presence of faults in the generator itself. In the case of wind turbines, the literature on SRGs is not substantial, and much research is required before adapting for wind turbine application [41], [42].

The SRG is a synchronous generator with a doubly salient construction, with salient poles on both the stator and the rotor. Excitation of the magnetic field is provided by the stator current in the same way as the induction generator. The SRG is considered inferior to the PMSG machine because of its lower power density. The SRG requires a full-scale power converter in order to operate as a grid-connected generator. Moreover, the SRG has a lower efficiency than a PMSG and a lower power factor than asynchronous generators [42], [59].

2.7.10.3 Synchronous reluctance generator

The first SynRM was introduced by Kostko in 1923. The synchronous reluctance motor was developed particularly in the 1960's as a line-start synchronous AC motor. A significant amount of work and research on the design and control of synchronous reluctance motors have been done during the 1990's. Recently, the SynRM have been further improved [60]. Figure 2.15 shows the cross-section of a synchronous reluctance generator.

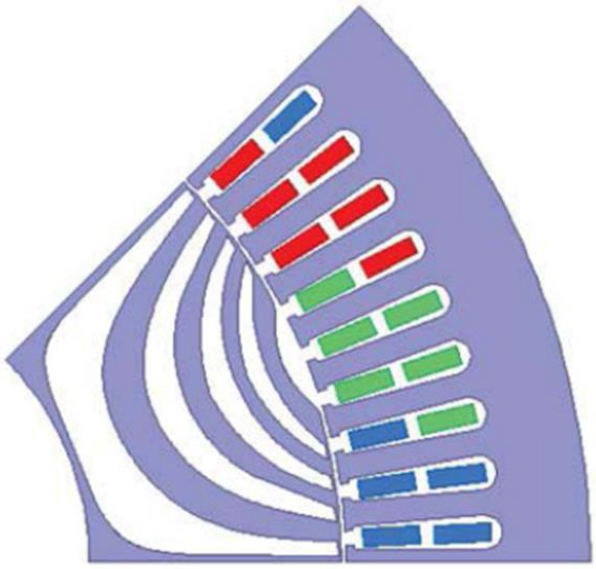

Figure 2.15: Cross-section of the synchronous reluctance generator [60]

Even though most of the researchers have explored the application of the reluctance machine as a motor, the field of the synchronous reluctance generator (SynRG) has also been brought to attention. One of the interesting applications of the SynRG is for wind turbine generation systems, since SynRGs are robust, inexpensive and they have a simple rotor construction. Moreover, SynRGs have low noise emission and are suitable for variable speed operation. Although synchronous permanent magnet generators often are a very good choice for many variable-speed drive applications, the advantages of using synchronous reluctance generators is that, the very expensive permanent magnets are not needed [60].

2.8 Power converter

Power converters are used to convert electrical power from one form to another, such as AC to DC, DC to AC, one voltage to another, or one frequency to another. There are various types of applications for power converter in wind energy system. Generator starters, variable speed wind turbines and isolated network are some example of the use of power converters. Power converters are also capable of adjusting the generator frequency and voltage to the grid [61, 62]. The penetration of power electronics in wind turbine systems has been continuously growing since the 1980's, when it consisted of a thyristor-based soft-starter just for initially interconnecting the wind turbine and after that being bypassed. In the 1990's, it was mainly the use of rotor resistance control with a diode bridge and a power electronic switch; finally, the back-to-back power converter emerged, first in reduced power for DFIG, then in full power. The most adopted solution in power converters for wind turbine systems in the best seller range 1.5-3 MW is the use of two two-level voltage source converters in a back-to-back configuration. At lower and higher powers, it is possible to find other solutions such as a diode-bridge for the generator in the case of a synchronous generator and the use of multilevel converters to enter medium voltage [63].

2.8.1 Full power converter

Full power converter in wind energy system increases the efficiency of wind power conversion compared to other converter types (partially rated converters) and improves the grid compatibility for high power wind turbines [63]. Permanent magnet synchronous generator using full scale converter in wind energy system needs less maintenance than other configuration. In a variable speed with full-scale power

converter wind turbine, the generator is connected to the grid through a power converter and it is fully variable speed controlled.

For the whole speed range, the frequency converter performs a smooth grid connection and reactive power compensation. The generator types that can be used with full power converter are electrically excited (wound rotor synchronous generator WRSG), a permanent magnet excited (permanent magnet synchronous generator PMSG) or induction generator. The full-scale power converter is connected in between the stator windings and the grid. In the cases of gearless variable speed wind turbine system, a heavier direct drive multi-pole generator is used. Major wind turbine manufacturer who are using direct drive generator are Enercon and Siemens Wind Power [63]. Figure 2.16 is the diagram of variable speed wind turbine with full scale power converter.

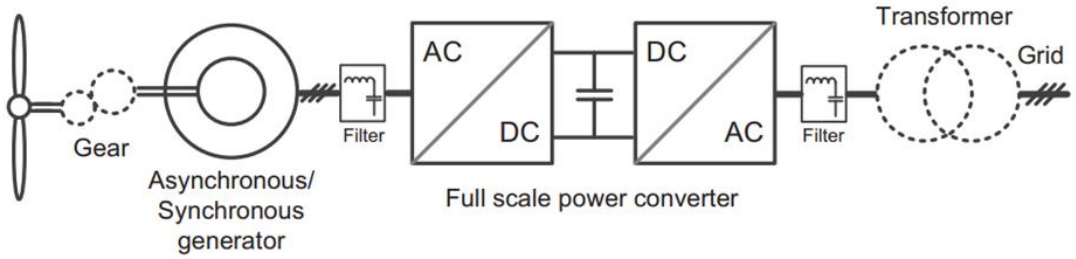

Figure 2.16: Variable speed wind turbine with full scale power converter

2.8.2 Partial rated power converter

The concept of partial scale-power converter (rated to approx. 30% of generator nominal power) used on the rotor circuit with a variable speed wind turbine with a wound rotor induction generator (WRIG) is known as Doubly-Fed Induction Generator (DFIG). The rotor speed and the rotor frequency are controlled by partial-scale power converter and the stator is directly connected to the grid. The speed range (usually ±30% around synchronous speed) is defined by the power rating of this partial-scale frequency converter. The smooth grid interconnection and the reactive power compensation also performed by this converter. It is economically cheaper as the frequency converter is smaller. The wind turbine is acting as a dynamic power source to the grid in this case. However, the use of slip-rings and the protection schemes/controllability in grid fault time is the major disadvantages of this concept [63]. The variable speed wind turbine with partial-scale power converter is shown in Figure 2.17.

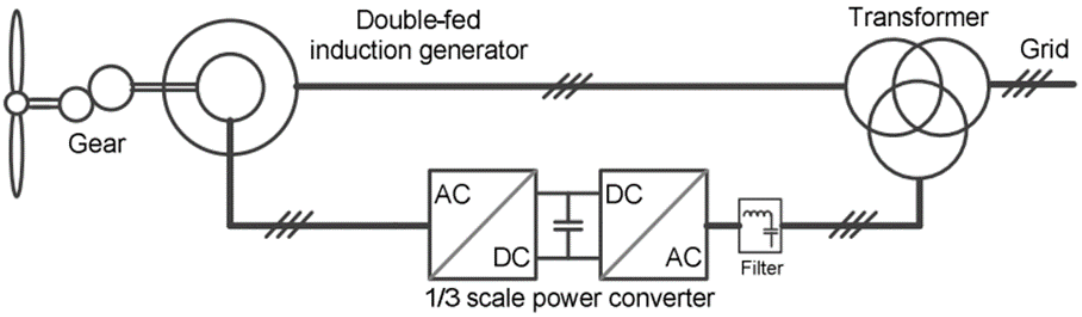

Figure 2.17: Variable speed wind turbine with partial scale power converter

2.9 State of the art drivetrains

The newest addition in Siemens Gamesa range is 8 MW turbine SG-8.0-167 DD which is the upgraded version of Siemens 7 MW turbine SWT-7.0-154 for offshore application. This is gearless direct drive technology with variable speed pitch regulated wind turbine. They also have onshore wind turbine from 2 MW to 4 MW range and offshore wind turbine from 6 MW to 8 MW range [64]. General Electric wind turbines feature rated capacities from 1.7 MW to 4.8 MW (Onshore) and 6 MW to 12 MW (Offshore), where Haliade-X 12 MW is their recently introduced turbine, which is the most powerful offshore wind turbine to date, featuring a 12 MW capacity with 220-meter rotor for offshore operation [65]. The latest addition of Enercon is 3.5 MW EP 3 series, which is a direct drive wind turbine. They also have gearless generator in kW and MW range [66]. It can be seen that, in terms of big turbines, most of the leading companies are using medium speed or direct drive technology.

2.10 Drivetrains in this thesis

In this study, direct drive permanent magnet generators with surface-mounted and flux-concentrating rotor configuration are chosen to perform optimisation. Two different magnet materials: Nd-Fe-B and ferrite are used in the generator rotor. The increased popularity of permanent magnet direct drive wind turbine in recent years as shown in section 2.9 encourages to work on this. The surface-mounted machine is one of the most popular rotor configuration in recent years. An alternative configuration using flux-concentrating topology with different magnet materials are used to compare the machine performance in terms of cost of energy, use of rare earth magnet, annual energy production, efficiency and other related variables. Radial-flux inner rotor topology is used for all the generators in this study with different power ratings (6, 8 and 10 MW). Because of economic factors, radial-flux is the predominant machine

topology utilised in direct drive multi-megawatt wind turbines and the majority of them have conventional inner rotor. This technology has reached maturity in terms of its manufacturing processes. The Nd-Fe-B magnet was varied from N35 to N52 to estimate the effect of different magnet grade on turbine cost of energy.

2.11 Previous research works in related area

There is no established / recognised "best way" to optimise generators for offshore wind turbines. People optimise including different aspect of the machine and comes to different conclusion. Some of the previous research works related to research questions given in section 1.3 are as follow:

Q1) Use of different magnet materials and rotor topologies

A number of researchers have started to explore alternative synchronous generator types that can deliver most of the benefits of the rare earth based permanent magnets. Eriksson and Bernhoff presented an interchangeable rotor design where two suggested generators are designed with the same stator but interchangeable rotors with different PM material (Nd-Fe-B and ferrite) [1]. Polinder et al. show a comparison of different types of generator in terms of annual energy yield per cost, which is analogous to payback period [2]. Although these papers show the comparison of different generator topologies, these are not optimised. This study optimises the generator topologies and introduces new topology to compare with them.

Q2) Generators structural model, tower, substructure and foundation for offshore wind turbine

Grauers optimised low speed permanent magnet machines using generator costs and losses, including an estimation of generator structural cost in [3]. Bazzo *et al.* included active and structural materials for the machine optimisation [4]. Zavvos *et al.* offered an analytical tool that minimises the generators mass or cost by optimising both the electromagnetic and structural design at the same time [5]. Wu *et al.* also outlined the optimization of generator rotor structure for minimum generator mass where deflections were constrained [67]. McDonald showed the structural models with different types of rotor and stator structures for direct drive generators [6]. L. Fingersh et al. shows the turbine top head mass can affect the tower and foundation cost that goes into turbine capital cost and effect on cost of energy [10]. According to a NREL technical report, the substructure and foundation cost is 9% of the total offshore wind

turbine cost [11]. In all these papers, authors successfully achieved their aim for some specific area and other areas are simplified. This thesis includes all of them together in details to see the overall performance and how they change with different objective functions in optimisation.

Q3) Turbine power ratings

Duan and Ionel optimised permanent magnet synchronous machine for a wide range of power ratings from 1 kW to 1 MW [68]. Carroll et al. estimated cost of energy for different wind turbine ratings [69]. H. Li et at. compared one direct drive permanent magnet generator topology with different geared generator and power ratings [8]. Others have worked for one specific power rating, not for a range of power ratings. This study used the power rating up to 10 MW for different direct drive permanent magnet generator topologies to compare them.

Q4) Choice of magnet grade

Fasolo et al. shows some effect of different magnet grade on machine performance [70]. Galioto proposed some permanent magnet machine designs with various grades of expensive dysprosium (Dy)-free magnets to compare the machine performance with different magnet grade and to reduce the use of rare earth magnet [71]. Gutfleisch et al. shows the importance of choosing improved magnetic materials for high energy efficiency [72]. Although some of the researchers showed the performance using different magnet grades, they did not include the cost of different magnet grades. This thesis includes the cost of different magnet grades to find the cost effective machine with better performance.

Q5) Thermal model, cooling circuit and machine temperature

Grauers shows a method where the generator outer surface of the stator core is cooled by air forced through circumferential cooling channels [3]. Alexandrova et al. show internal direct liquid cooling of the stator winding to manage joule heating losses [73]. Others have looked at different cooling methods and coolants [17], [74,75]. This study optimised different generator topologies to find the lowest cooling cost with better performance.

Q6) Objective function

Different authors have approached the problem of formulating the objective function of such optimizations in different ways. Polinder shows an objective function that minimizes the cost of generator active materials (i.e. magnet, copper and iron) and the generator losses as well [7]. The generator system cost is minimized in [8]. Bazzo et al. outlined some objective functions to minimize costs and maximize efficiency which included minimizing active and structural materials cost and minimizing cost of losses to get maximum return of investment [4]. Others have looked at different optimization methods with different objectives [3], [5], [67]. This study compares four different objective functions to find the best approach of optimising generator for offshore wind turbine.

2.12 Discussions and conclusions

This chapter shows the previous works related to research area/ research questions given in chapter 1. There are various types of wind turbine with high speed, medium speed and direct drive. In terms of failure rate, efficiency, operation and maintenance the direct drive option may become more popular in future. Permanent magnet excitation is the most popular option for wind turbine generator and increasing the use significantly. To achieve the best performance machine, designers need to look for alternative designs, magnetic materials, structural design, effective cooling and optimisation. Following chapter will describe the methodology, results and discussion to answer the research questions.

Chapter 3

Electromagnetic Modelling

3.1 Introduction

In order to optimise a generator for a wind turbine, it is necessary to produce an electromagnetic model that links independent variables such as dimensions and machine parameters to output performance. Elements of this output performance can be used in the objective function. The main purposes of this chapter are:

- To model electromagnetic design of different generator topologies analytically
- To verify electromagnetic model using finite element software
- To calculate power output, losses, masses and other variables for different generator topologies
- To minimise the use of rare earth magnet
- To estimate the effect of variable power factor
- To estimate the effect of different magnet grades

The baseline designs and related results are given in this chapter. The electromagnetic models of three different direct drive generator topologies for offshore wind turbine are described after that. The generator topologies studied are: (a) Surface mounted Nd-Fe-B generator (SM Nd-Fe-B), (b) Flux-concentrating Nd-Fe-B generator (FC Nd-Fe-B) and (c) Flux-concentrating ferrite generator (FC ferrite). SM Nd-Fe-B is one of the most cost effective, reliable, well performed generator found in previous researches and other topologies are used here as good alternative. These generator topologies are modelled analytically in MATLAB and verified with Finite element method magnetics (FEMM) software. The calculation of flux density, induced *EMF*, inductance, terminal voltage, power output and losses are also described in this chapter. The calculation of active materials masses, effect of variable power factor and different magnet grades comes after that.

This chapter is important step to answer secondary research questions *Q1 and Q4*, also supports answering *Q2*, *Q3*, *Q5* and *Q6* partially, that includes: electromagnetic modelling of different generator topology, different strategies to reduce rare earth permanent magnet, magnet grades, power factor, losses and active material mass for different generator topologies. The next chapter will describe the mechanical, thermal, turbine and cost modelling that helps to answer some of the secondary research questions, hence the primary research questions for overall optimisation.

3.2 Baseline designs

The generators with 6 MW power ratings are chosen as the base line design for all the generator types in this study. The magnet grade for Nd-Fe-B is 40H and ferrite is Y30. The properties of these baseline magnet materials are given in Table 3.1. Generator materials properties and cost modelling for the baseline design are given in Table 3.2. The distributed winding type is used for all the generator topologies. It is assumed that the machines are running at unity power factor at all the wind speeds.

Table 3.1: Baseline magnet properties for rare earth Nd-Fe-B and ferrite magnet materials [76]

Magnetic Materials		
Magnet material	Nd-Fe-B	Ferrite
Grade	N40H	Y30
Remanence, min (T)	1.25	0.4
Normal Coercivity, min (kA/m)	923	240
Intrinsic Coercivity, min (kA/m)	1355	245
Density (kg/m^3)	7600	5000

Table 3.2: Generator materials and cost modelling [2]

Generator Material Characteristics	
Slot filling factor	0.6
Resistivity of copper at 120^{o}C (μΩ·m)	0.024
Eddy-current losses in laminations at 1.5 T, 50 Hz (W/kg)	0.5
Hysteresis losses in laminations at 1.5 T, 50 Hz (W/kg)	2

Results from baseline electromagnetic designs of different 6 MW generator topology are given in Table 3.3.

Table 3.3: Some results from baseline electromagnetic designs of different 6 MW generator topology

	SM Nd-Fe-B	**FC Nd-Fe-B**	**FC ferrite**
	Generator Dimensions		
Stator radius, r_s (m)	3.5	3.5	4
Stack length, l_s	1.53	1.5	1.5
Number of pole pairs, p	100	100	100
Air-gap g (mm)	7	7	8
Stator slot width w_s (mm)	18.3	18.3	20.8
Stator tooth width w_t (mm)	18.3	18.3	20.8
Stator slot height h_s (mm)	80	80	80
Stator yoke height h_{sy} (mm)	23.4	24.9	25.9
Rotor yoke height h_{ry} (mm)	23.4	-	-
Magnet width/pole pitch, w_m/τ_p	0.75	0.65	0.75
Magnet height h_m (mm)	20	50	400
Al ring height h_{al} (mm)	-	50	50
	Generator Parameters		
Direct axis inductance per phase L_d (mH)	19.7	23	22.6
Quadrature axis inductance per phase L_q (mH)	19.7	30.9	25.3
Stator resistance per phase R_s (mΩ)	152.8	150	134.3
	Generator Material Mass (tonne)		
Iron	23.2	26.2	51.1
Copper	8.3	8.1	9.4
Magnet	3.84	4.4	42.7
Total	35.34	38.7	103.2
	Generator losses (MWh)		
Copper losses	1812.4	958.5	1541.1
Iron losses	231	310.2	255.8

For the baseline design, contour plots were used to reduce magnet mass and increase the air-gap flux density. Figure 3.1 and Figure 3.2 shows the contour plot of a 6 MW SM Nd-Fe-B and FC ferrite generator. It shows the effect of magnet height and magnet width on the air-gap flux density and magnet mass for the both generators.

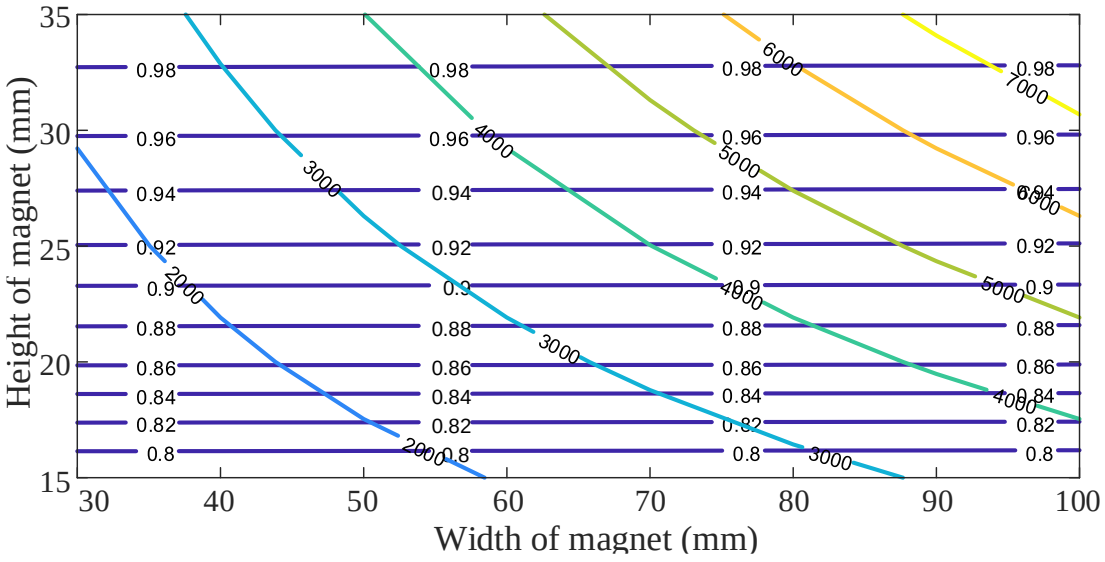

Figure 3.1: Contour plot of fundamental air-gap flux density for a 6 MW SM Nd-Fe-B rotor(purple, labelled in T) and magnet mass (multi-coloured, labelled in kg)

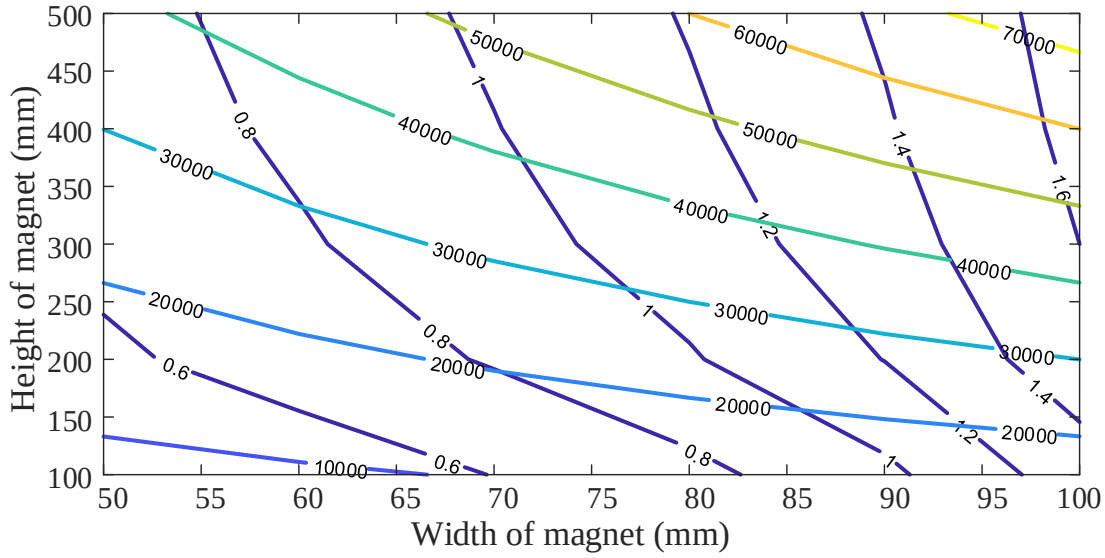

Figure 3.2: Contour plot of fundamental air-gap flux density for a 6 MW FC ferrite rotor (purple, labelled in T) and magnet mass (multi-coloured, labelled in kg)

As shown in Section 3.5, the flux concentrating buried magnet rotor can be further optimised by increasing the magnet width at inner radius and altering the magnet height to increase the air-gap flux density. Figure 3.3 shows that for a constant magnet mass (37,600kg in this example), higher air-gap flux densities can be achieved as the angle increases. The maximum value of the angle is $\theta_{\mathrm{p,max}}$=6.2° which occurs when $w_{\mathrm{m,i}} = \tau_{\mathrm{p}}$.

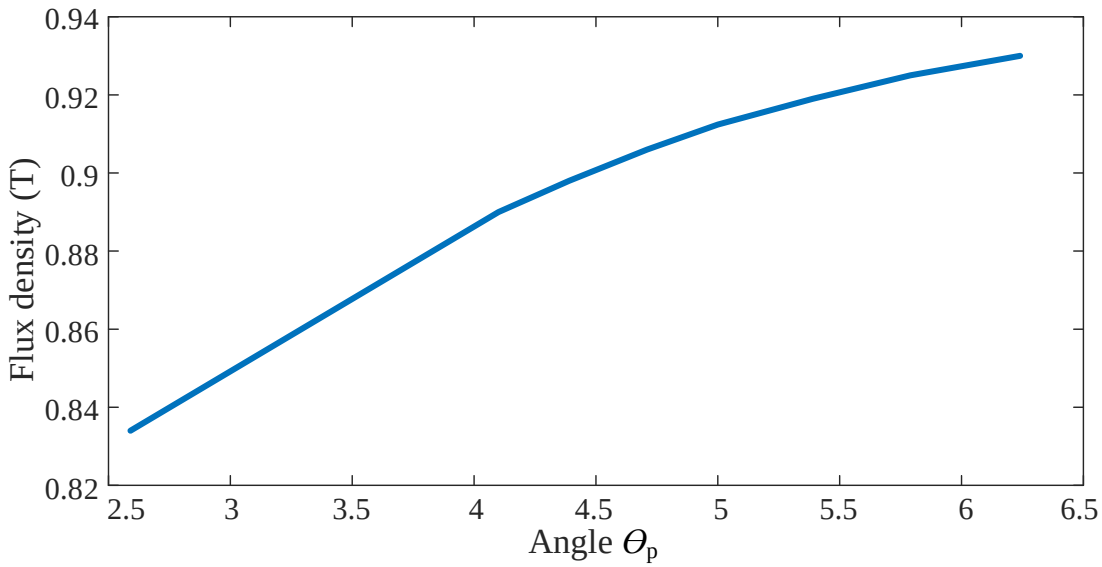

Figure 3.3: Flux vs. θ_p for a ferrite magnet rotor with angular pole

It also possible to keep same air-gap flux density at reduced mass by increasing the angle θ_p and decreasing magnet height. Figure 3.4 shows a line of constant air-gap flux density ($\widehat{B_g}$=0.91T in this example) and how the magnet mass can be minimized.

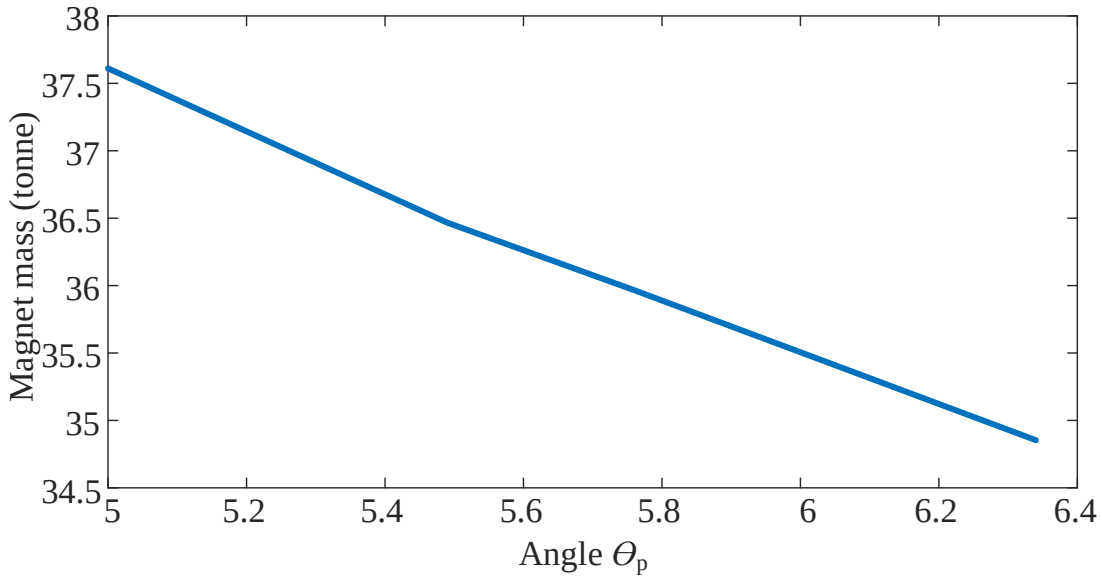

Figure 3.4: Magnet mass vs. angle θ_p. All points on the curve give the same fundamental air-gap flux density

3.3 Magnetic circuit

A magnetic circuit represents the flow of magnetic flux from a magnetic source that returns through a magnetic conducting path. It is a lumped parameter approximate method to find magnetic flux. The permanent magnet or electromagnet produces magnetomotive force which generates the flux that confined to the path by high permeability materials like iron, although there may be air gaps or other materials in

the path with low permeability. A magnetic circuit can be drawn as the equivalent of electric circuit where magnetomotive force $\mathscr{F}$, flux φ and reluctance $\mathscr{R}$ is the analogous to voltage *V*, current *I* and resistance *R* as shown in Figure 3.5.

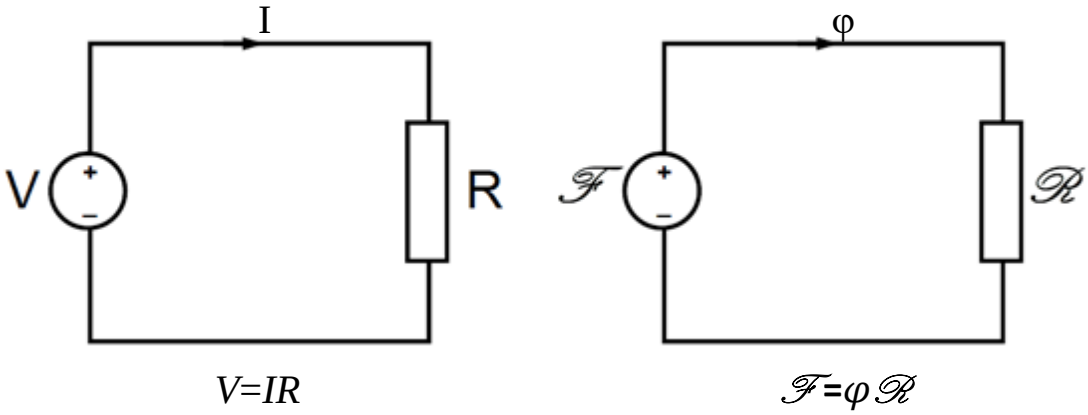

Figure 3.5: Equivalent electric (left) and magnetic (right) circuit

In this study, the magnetic circuit for different generator topologies are drawn to calculate magnetomotive force, reluctance, flux and flux density described in the following section 3.4.

3.4 Generator electromagnetic models

A radial flux inner rotor and outer stator permanent magnet direct drive generator type is chosen in this study. The generators are modelled analytically in the steady state. Lumped parameter magnetic circuit models are used to calculate flux per pole. The magnetic properties of the chosen magnet materials are given in Table 3.1. Flux density in the various parts of the system and the induced *EMF* can be calculated from these magnetic circuits. The magnetic circuit design variables, calculation of reluctances, *MMF*, air-gap flux, inductance, air-gap flux density and induced *EMF* for specific generator topology is described in the following sub-sections. The distributed winding type is used for all the generator topologies. In the initial case, it is assumed that the machines run at unity power factor at all wind speeds. This simplification is applied to all the generator types and reduces the complexity of the optimisation.

3.4.1 Surface mounted Nd-Fe-B generator

3.4.1.1 Magnetic circuit and reluctances

In a SM Nd-Fe-B generator, the Nd-Fe-B magnets are mounted in the rotor surface of the generator. The simplified (linearized) section of the SM Nd-Fe-B generators magnetic circuit models for one pole pair is shown in Figure 3.6.

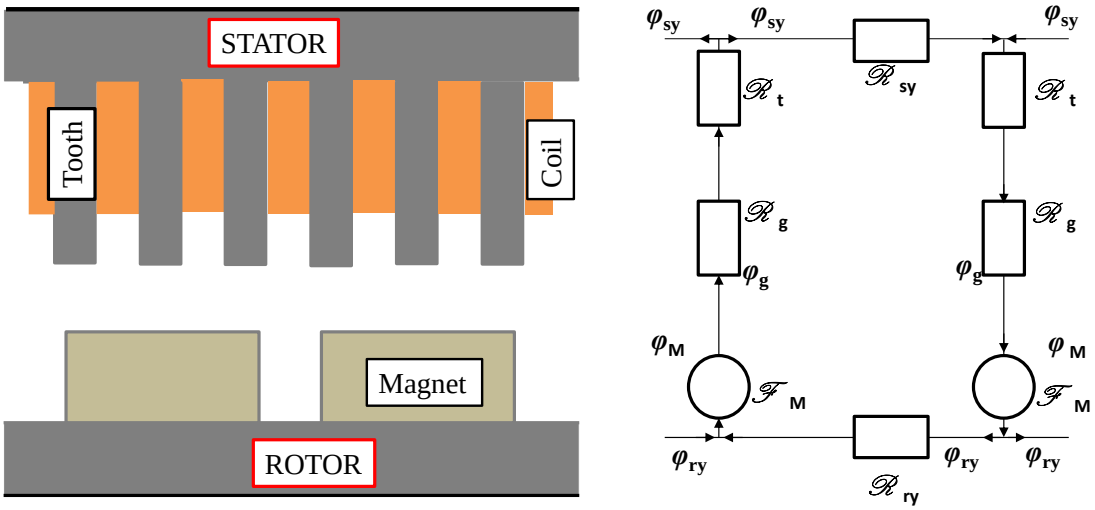

Figure 3.6: Magnetic circuit for modelling air-gap flux per pole for the SM Nd-Fe-B generators

Assuming the leakage flux φ_L=0, the flux of the air-gap can be calculated from Ampere's law,

$$2\mathscr{F}_m - 2\mathscr{R}_g\varphi_g - 2\mathscr{R}_t\varphi_g - \mathscr{R}_{sy}\varphi_{sy} - \mathscr{R}_{ry}\varphi_{ry} = 0 \qquad (3.1)$$

where $\mathscr{F}_m$ is the *MMF* of the magnet, $\mathscr{R}_g$ is the reluctance of air-gap, φ_g is the flux of the air-gap, $\mathscr{R}_t$ is the reluctance of the stator tooth, $\mathscr{R}_{sy}$ is the reluctance of stator yoke, φ_{sy} is the flux of the stator yoke, $\mathscr{R}_{ry}$ is the reluctance of rotor yoke and φ_{ry} is the flux of the rotor yoke.

From Gauss's law,

$$\varphi_g = \varphi_m = 2\varphi_{ry} = 2\varphi_{sy} \qquad (3.2)$$

where φ_m is the flux of the magnet, From the equation (3.1) and equation (3.2), it can be found that,

$$\varphi_g = \frac{4\mathscr{F}_m}{4\mathscr{R}_t + 4\mathscr{R}_g + \mathscr{R}_{ry} + \mathscr{R}_{sy}} \qquad (3.3)$$

The magnetomotive force can be calculated as,

$$\mathscr{F}_m = \frac{B_r}{\mu_0\mu_{r,m}} h_m = H_c h_m \qquad (3.4)$$

where B_r is the remanence, μ_0 is the permeability of air, $\mu_{r,m}$ is the relative permeability of the magnet, H_c is the coercivity of the magnet and h_m is the height of the magnet in the direction of magnetization.

The reluctance of the stator tooth can be given as,

$$\mathscr{R}_t = \frac{h_s}{0.5\mu_0\mu_{r,steel}l_s w_m} \tag{3.5}$$

where h_s is the height of the tooth/slot, $\mu_{r,steel}$ is the relative permeability of the steel, l_s is the stack length in axial direction and w_m is the magnet width.

The reluctance of the rotor yoke can be calculated as,

$$\mathscr{R}_{ry} = \frac{\tau_\rho}{\mu_0\mu_{r,steel}l_s h_{ry}} \tag{3.6}$$

where τ_p is the pole pitch and h_{ry} is the height of the rotor yoke. The pole pitch can be given as,

$$\tau_p = \frac{\pi D}{2p} \tag{3.7}$$

where D is the generator diameter and p is the pole pair.

The reluctance of stator yoke can be calculated as,

$$\mathscr{R}_{sy} = \frac{\tau_\rho}{\mu_0\mu_{r,steel}l_s h_{sy}} \tag{3.8}$$

where h_{sy} is the height of the stator yoke.

The reluctance of air gap can be found as,

$$\mathscr{R}_g = \frac{g_{eff}}{\mu_0 w_m l_s} \tag{3.9}$$

where g_{eff} is the effective air-gap for a surface mounted machine including extra length for flux to cross air-gap due to slotting and magnet. The effective air-gap for a surface mounted machine can be given as,

$$g_{eff} = k_c\left(g + \frac{h_m}{\mu_{r,m}}\right) \tag{3.10}$$

where k_c is the Carter factor of the stator slot and g is the mechanical air-gap. The mechanical air-gap is always kept as a fixed proportion of the air-gap diameter D, so that $g = D / 1000$. The Carter factor can be found as,

$$k_c = \frac{\tau_s}{\tau_s - g_1 \gamma} \tag{3.11}$$

$$g_1 = g + \frac{h_m}{\mu_{r,m}} \tag{3.12}$$

$$\gamma = \frac{4}{\pi}\left(\frac{w_s}{2g_1}\arctan\left(\frac{w_s}{2g_1}\right) - ln\sqrt{1+\left(\frac{w_s}{2g_1}\right)^2}\right) \tag{3.13}$$

where τ_s is the slot pitch and w_s is the width of the stator slot.

$$w_s = w_t = \frac{\tau_p}{6} \tag{3.14}$$

where w_t is the width of the stator tooth.

3.4.1.2 Air-gap flux density and induced EMF

The flux density of the air-gap can be calculated as,

$$B_g = \frac{\varphi_g}{A_p} = \frac{\varphi_g}{w_m l_s} \tag{3.15}$$

where A_p is the area of magnetic pole at the air-gap.

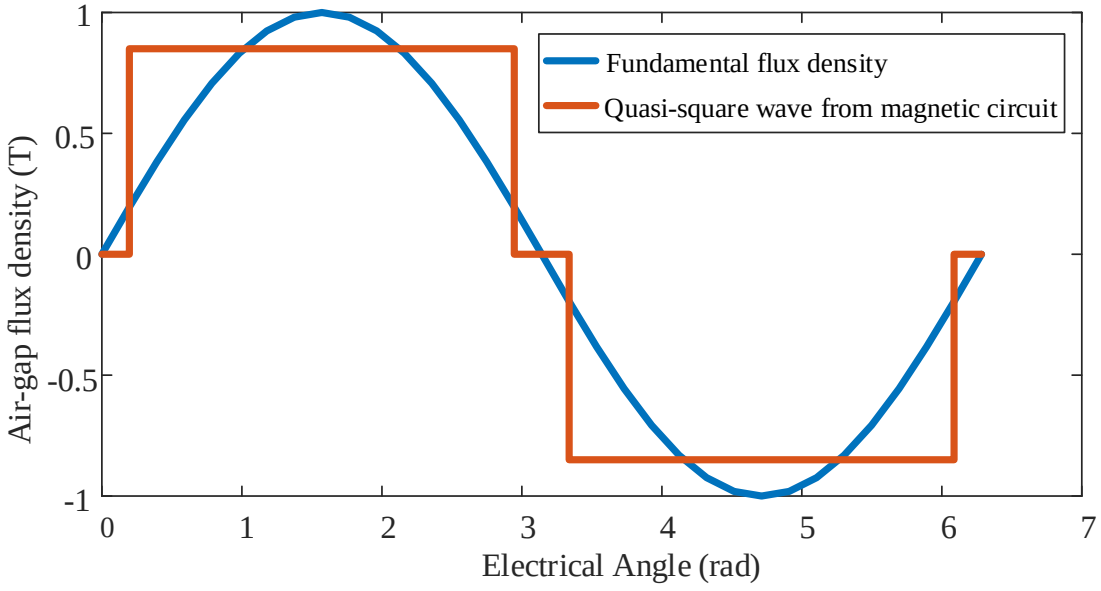

Figure 3.7: An example of the fundamental and quasi-square wave of air-gap flux density

The fundamental flux density can be given as,

$$\widehat{B_g} = B_g \frac{4}{\pi}\sin\left(\frac{\pi}{2}\frac{w_m}{\tau_\rho}\right) \tag{3.16}$$

where B_g is the amplitude of the quasi square air-gap flux density. Figure 3.7 shows an example of the quasi-square wave from magnetic circuit and the fundamental used in *EMF* calculation for air-gap flux density.

The no-load voltage induced by the flux density in a stator winding can be given as,

$$E = \sqrt{2} k_{\mathrm{w}} N_{\mathrm{s}} \omega r_{\mathrm{s}} l_{\mathrm{s}} \widehat{B_{\mathrm{g}}} \tag{3.17}$$

Where k_{w} is the winding factor, ω is the mechanical angular speed of the rotor, r_{s} is the stator radius and N_{s} is the number of turns of the phase winding that can be given as,

$$N_{\mathrm{s}} = N_{\mathrm{slot}}\, pq \tag{3.18}$$

where N_{slot} is the number of conductor per slot and q is the number of slot per pole per phase which is one in this study.

3.4.1.3 Inductance calculation

The magnetizing inductance can be calculated as [77],

$$L_{\mathrm{m}} = \frac{4\mu_0 \tau_{\mathrm{p}} l_{\mathrm{s}} (k_{\mathrm{w}} N_{\mathrm{s}})^2}{p g_{\mathrm{eff}} \pi^2} \tag{3.19}$$

The leakage inductance of the machine can be calculated as [77],

$$L_{\mathrm{leakage}} = L_{\mathrm{slot}} + L_{\mathrm{tooth}} + L_{\mathrm{air}} + L_{\mathrm{skew}} + L_{\mathrm{end}} \tag{3.20}$$

where L_{slot} is the slot leakage inductance, L_{tooth} is the tooth tip leakage inductance, L_{air} is the air-gap leakage inductance, L_{skew} is the skew leakage inductance and L_{end} is the end winding leakage inductance.

The total inductance can be given as,

$$L = L_{\mathrm{m}} + L_{\mathrm{m,u}} + L_{\mathrm{leakage}} \tag{3.21}$$

where $L_{\mathrm{m,u}}$ is the mutual inductance which is one-third of the magnetizing inductance.

3.4.1.4 Phasor diagrams and terminal voltage

Assuming that the machines run at unity power factor at all the wind speeds. In the case of a machine having permanent magnets mounted on the rotor surface, the direct axis and quadrature axis inductance are equal, $L_{\mathrm{d}} = L_{\mathrm{q}}$ and hence $X_{\mathrm{d}} = X_{\mathrm{q}}$. If stator resistance is neglected, the following phasor diagrams can be used. Figure 3.8 (a) shows the generator operating at low wind speed and current. At higher wind speeds (e.g. Figure 3.8 (b)) the induced *EMF*, *E* increases until pitch regulation starts and keeps the rotation speed constant. The current, *I*, is varied as shown in Figure 3.8, so

that the correct power is produced at each wind speed. This implies that the load angle, δ, varies with wind speed up to rated wind speed.

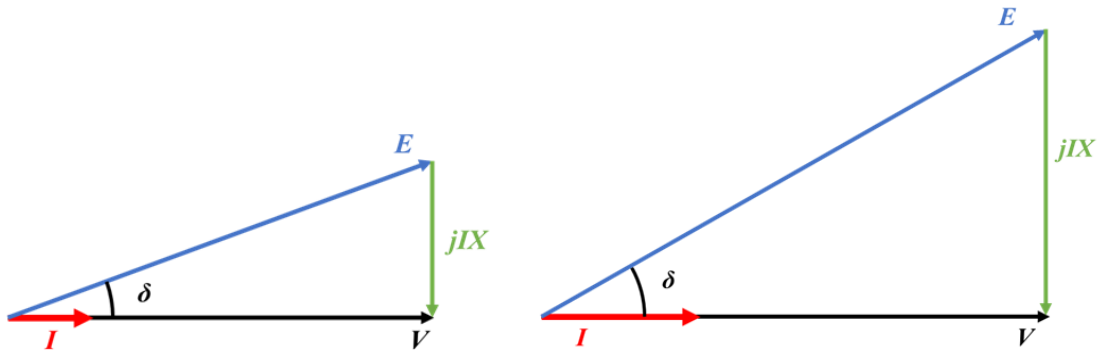

Figure 3.8: Phasor diagram, when the generator operating at:(a,left) low wind speed and (b,right) high wind speeds

The terminal voltage for a machine having PM mounted on the rotor surface can be calculated as [78],

$$V = \sqrt{E^2 - (IX_s)^2} = E\cos\delta \tag{3.22}$$

where X_s is the reactance.

3.4.1.5 Verification using finite element software

The analytical results of electromagnetic model are verified using Finite element method magnetics (FEMM) software [79]. FEMM is a set of programs for solving low frequency electromagnetic on two-dimensional planar and axisymmetric domains. The Lua scripting language is integrated into the interactive shell of FEMM. Lua is a complete, open-source scripting language. Because the scripting files are text, they can be edited with any text editor. Lua scripts facilitate the build and analysis of the electromagnetic model and evaluate the post-processing results in FEMM software without interacting with the model manually. In this research, Lua scripts are used to run the electromagnetic model from Excel directly to FEMM. With the help of Excel VBA, it can automate tasks in Excel by creating macros, which can be executed after clicking on a command button[80]. This process can simplify producing and analysing of 2D Finite element model and save time.

Figure 3.9 shows the magnetostatic finite element analysis results for two poles of a 6 MW SM Nd-Fe-B generator. The analytical results of direct axis and quadrature axis inductance are also verified which shows agreement within about 1% difference in both axes. Table 3.4 shows some key dependent variables verified using FEMM for the baseline generator design. In the case of the inductance calculations the 2D results

do not include the end winding leakage inductance – these are calculated using analytical equation. For the sake of comparison, the analytical results presented in Table 3.4 also exclude the end winding leakage inductances. All the SM Nd-Fe-B generators used in this study are verified using same method.

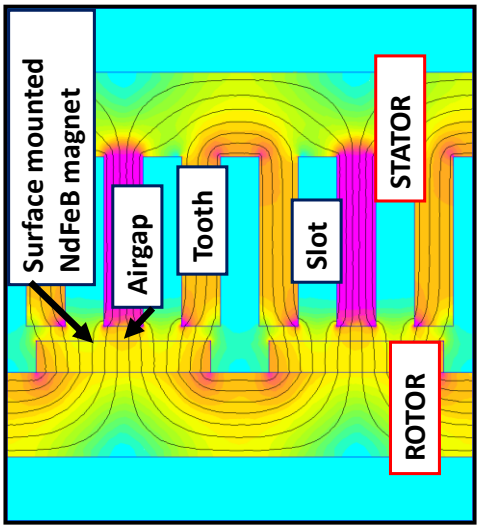

Figure 3.9: Magnetostatic finite element analysis of SM Nd-Fe-B generator, ■0T→■1.5T. Software is FEMM [79]

Table 3.4: Analytical results vs FEMM analysis results for a 6 MW SM Nd-Fe-B generator

Variables	**SM Nd-Fe-B generator**	
	Analytical	**FEMM**
Fundamental air-gap flux density, $\widehat{B_g}$ (T)	1	0.99
Direct axis inductance, L_d (mH)	19.7	19.5
Quadrature axis inductance, L_q (mH)	19.7	19.5

The fundamental flux density from FEMM analysis result can be found by using Fast Fourier Transform (FFT) analysis and verified with analytical result as shown in Table 3.4. Figure 3.10 shows the spatial FFT analysis of the air-gap flux density for a 6MW SM Nd-Fe-B generator.

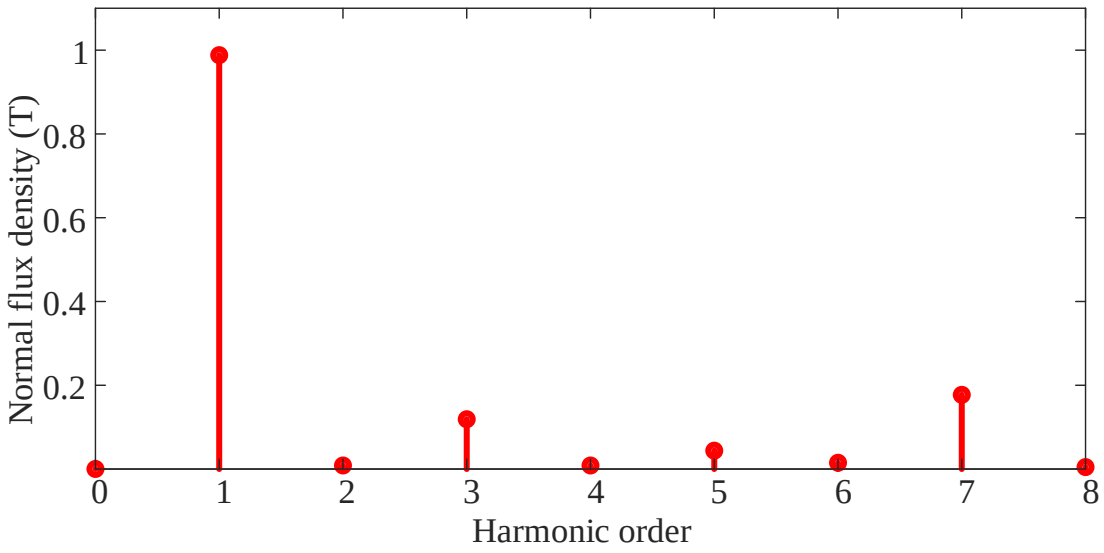

Figure 3.10: FFT analysis of the air-gap flux density for a 6 MW SM Nd-Fe-B generator

3.4.2 Flux-concentrating Nd-Fe-B generator

3.4.2.1 Magnetic circuit and reluctances

A more complicated rotor is required for flux concentration than for surface mounted magnets where magnets are placed between magnetically conducting pole shoes in order to reinforce the air-gap flux. As a result, the rotor of these machines would normally be heavier. Tangentially magnetized magnets are placed between pole shoes with every other magnet magnetized in the opposite direction, i.e. two north poles will face each other forcing the flux to travel through the pole shoe to the stator. The pole shoes are made of solid iron. Pole shoes and magnets are mounted on a solid ring made of nonmagnetic aluminium, in order to force the flux to travel through the stator. The aluminium ring is then mounted on a supporting structural steel ring connected to the shaft [1]. The simplified section of the FC Nd-Fe-B generators magnetic circuit models for one pole pair is shown in Figure 3.11.

Assuming the leakage flux φ_L=0, The flux of the air-gap can be calculated from the Ampere's law,

$$\mathscr{F}_m - 2\mathscr{R}_p\varphi_g - 2\mathscr{R}_g\varphi_g - 2\mathscr{R}_t\varphi_g - \mathscr{R}_{sy}\varphi_{sy} - \mathscr{R}_m\varphi_m = 0 \tag{3.23}$$

where $\mathscr{R}_p$ is the reluctance of the pole shoe. From the Gauss's law,

$$\varphi_g = 2\varphi_m = 2\varphi_{sy} \tag{3.24}$$

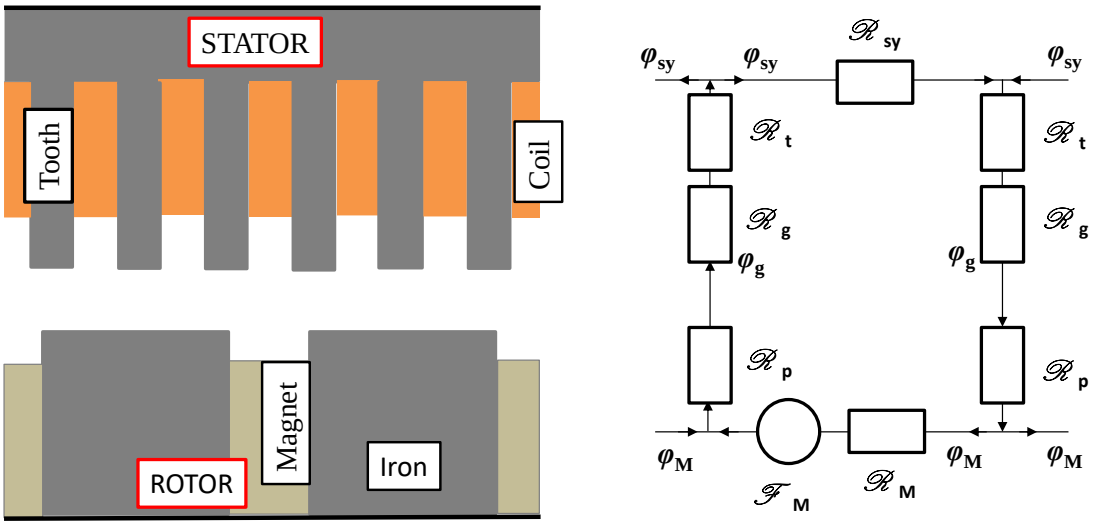

Figure 3.11: Magnetic circuit for modelling air-gap flux per pole for the FC Nd-Fe-B generators

The flux of the air-gap can be found from the equation (3.23) and equation (3.24),

$$\varphi_g = \frac{2\mathscr{F}_m}{\mathscr{R}_m + \mathscr{R}_{sy} + 4(\mathscr{R}_t + \mathscr{R}_g + \mathscr{R}_p)} \tag{3.25}$$

where $\mathscr{R}_m$ is the reluctance of the magnet.

The magnetomotive force can be calculated as,

$$\mathscr{F}_m = \frac{B_r}{\mu_0 \mu_{r,m}} w_m \tag{3.26}$$

The reluctance of the stator tooth can be given as,

$$\mathscr{R}_t = \frac{h_s}{0.5\mu_0 \mu_{r,steel} l_s w_p} \tag{3.27}$$

where w_p is the width of the pole shoe.

The reluctance of the magnet can be calculated as,

$$\mathscr{R}_m = \frac{w_m}{\mu_0 \mu_{r,m} h_m l_s} \tag{3.28}$$

The reluctance of the pole shoe can be given as,

$$\mathscr{R}_p = \frac{h_p}{\mu_0 \mu_{r,iron} l_s w_p} \tag{3.29}$$

where h_p is the height of the pole shoe and $\mu_{r,iron}$ is the relative permeability of the iron.

The reluctance of stator yoke can be calculated as equation 3.8. The reluctance of the air-gap can be given as,

$$\mathscr{R}_{\mathrm{g}} = \frac{g_{\mathrm{eff}}}{\mu_0 w_{\mathrm{p}} l_{\mathrm{s}}} \tag{3.30}$$

where the effective air-gap of the FC Nd-Fe-B generator can be given as,

$$g_{\mathrm{eff}} = k_{\mathrm{c}} g \tag{3.31}$$

Carter factor, k_{c} can be found as equation 3.11.

3.4.2.2 Air-gap flux density and induced EMF

The flux density of the air-gap for a flux-concentrating generator can be calculated as,

$$B_{\mathrm{g}} = \frac{\varphi_{\mathrm{g}}}{A_{\mathrm{p}}} = \frac{\varphi_{\mathrm{g}}}{w_{\mathrm{p}} l_{\mathrm{s}}} \tag{3.32}$$

The fundamental flux density can be given as,

$$\widehat{B_{\mathrm{g}}} = B_{\mathrm{g}} \frac{4}{\pi} \sin\left(\frac{\pi}{2} \frac{w_{\mathrm{p}}}{\tau_{\rho}}\right) \tag{3.33}$$

The induced *EMF* can be calculated by using the equation 3.17.

3.4.2.3 Inductance calculation

The FC Nd-Fe-B generator is a type of salient-pole machine and has different inductance on the pole (direct axis inductance, L_{d}) and between two poles (quadrature axis inductance, L_{q}). The direct axis and the quadrature axis inductance for a flux-concentrating machine can be calculated from the magnetizing inductance (Equation 3.19) where the effective air-gap is different.

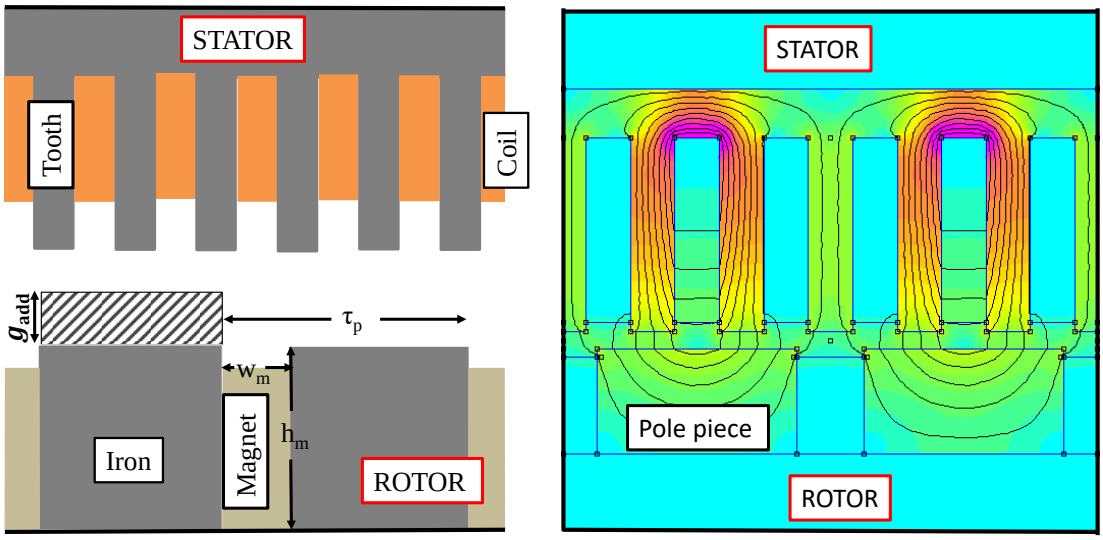

Figure 3.12: Flux-concentrating Nd-Fe-B generator (a) additional air-gap height used in direct axis magnetizing inductance formulation (b) stator field lines in the quadrature axis

The effective air-gap in the direct axis, $g_{\mathrm{eff,d}}$ can be found by adding an additional air-gap, g_{add} shown in Figure 3.12 (a), where the magnet reluctance $\mathscr{R}_{\mathrm{m}}$ is expressed in terms of air-gap reluctance.

$$\mathscr{R}_{\mathrm{m}} = \frac{w_{\mathrm{m}}}{\mu_0 \mu_{\mathrm{r,m}} h_{\mathrm{m}} l_{\mathrm{s}}} = \frac{g_{\mathrm{add}}}{\mu_0 \tau_{\mathrm{p}} l_{\mathrm{s}}} \tag{3.34}$$

$$g_{\mathrm{add}} = \frac{w_{\mathrm{m}} \tau_{\mathrm{p}}}{h_{\mathrm{m}} \mu_{\mathrm{r,m}}} \tag{3.35}$$

$$g_{\mathrm{eff,d}} = g_{\mathrm{eff}} + g_{\mathrm{add}} \tag{3.36}$$

For the quadrature axis, the majority of the flux found by using finite element software crosses only pole (for the both FC Nd-Fe-B and FC ferrite generator) as shown in Figure 3.12 (b). The magnetic pole resembles a tooth surrounded by slots, and so the Carter factor can be applied to calculate the effective air-gap,

$$g_{\mathrm{eff,q}} = k_{\mathrm{c,q}} g_{\mathrm{eff}} \tag{3.37}$$

where $k_{\mathrm{c,q}}$ is the Carter factor from the rotor side in the quadrature axis,

$$k_{\mathrm{c,q}} = \frac{\tau_{\mathrm{p}}}{\tau_{\mathrm{p}} - g\gamma_{\mathrm{q}}} \tag{3.38}$$

$$\gamma_{\mathrm{q}} = \frac{4}{\pi}\left(\frac{w_{\mathrm{m}}}{2g}\arctan\left(\frac{w_{\mathrm{m}}}{2g}\right) - \ln\sqrt{1+\left(\frac{w_{\mathrm{m}}}{2g}\right)^2}\right) \tag{3.39}$$

The direct axis and quadrature axis inductances can be found as

$$L_{\mathrm{d}} = L_{\mathrm{m,d}} + L_{\mathrm{m,u}} + L_{\mathrm{leakage}} \tag{3.40}$$

$$L_{\mathrm{q}} = L_{\mathrm{m,q}} + L_{\mathrm{m,u}} + L_{\mathrm{leakage}} \tag{3.41}$$

where $L_{\mathrm{m,d}}$ is the d-axis magnetizing inductance, $L_{\mathrm{m,q}}$ is the q-axis magnetizing inductance, $L_{\mathrm{m,u}}$ is the mutual inductance which is one-third of the magnetizing inductance and L_{leakage} is the leakage inductance which can be calculated as [77].

3.4.2.4 Phasor diagrams and terminal voltage

In the case of the machines with buried magnets, there is significant saliency, i.e. $L_{\mathrm{d}} \neq L_{\mathrm{q}}$. In this case, the phasor diagram of a flux-concentrating machine with unity power factor is shown in Figure 3.13 and the terminal voltage can be found as [78],

$$V = \sqrt{(E - I_{\mathrm{d}}(X_{\mathrm{d}} - X_{\mathrm{q}}))^2 - \left(IX_{\mathrm{q}}\right)^2} = E\cos\delta - I_{\mathrm{d}}\left(X_{\mathrm{d}} - X_{\mathrm{q}}\right)\cos\delta \tag{3.42}$$

where I_{d} is the direct axis current.

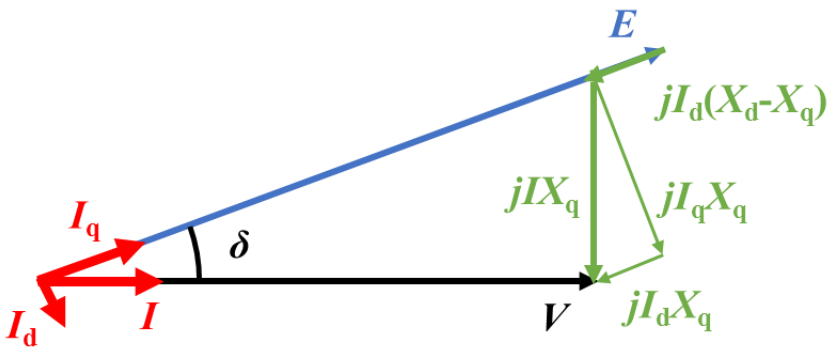

Figure 3.13: Phasor diagram of a flux-concentrating machine

These equations can be solved iteratively to find the load angle for every wind speed if the relationship between wind speed and rotor speed and between wind speed and current are known.

3.4.2.5 Verification using finite element software

Figure 3.14 shows the magnetostatic finite element analysis results for two poles of a 6 MW FC Nd-Fe-B generator. The analytical results of direct axis and quadrature axis inductance for FC Nd-Fe-B are also verified which shows agreement within about 1% difference in both axes. Table 3.5 shows some key dependent variables verified for the baseline generator design. The analytical results presented in Table 3.5 also exclude the end winding leakage inductances as the 2D FE results do not include the end winding leakage inductance. All the FC Nd-Fe-B generators used in this study are verified using same method.

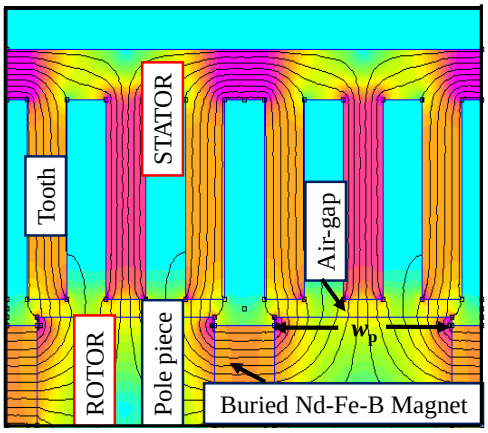

Figure 3.14: Magnetostatic finite element analysis of FC Nd-Fe-B generator, ■0T→■1.5T. Software is FEMM [79]

Table 3.5: Analytical results vs FEMM analysis results for a 6 MW FC Nd-Fe-B generator

Variables	**FC Nd-Fe-B generator**	
	Analytical	**FEMM**
Fundamental air-gap flux density, $\widehat{B_g}$ (T)	1.04	1.02
Direct axis inductance, L_d (mH)	23.0	22.8
Quadrature axis inductance, L_q (mH)	30.9	30.6

The fundamental flux density can be found by using Fast Fourier Transform (FFT) analysis. Figure 3.15 shows the FFT analysis of the air-gap flux density for a 6MW FC Nd-Fe-B generator.

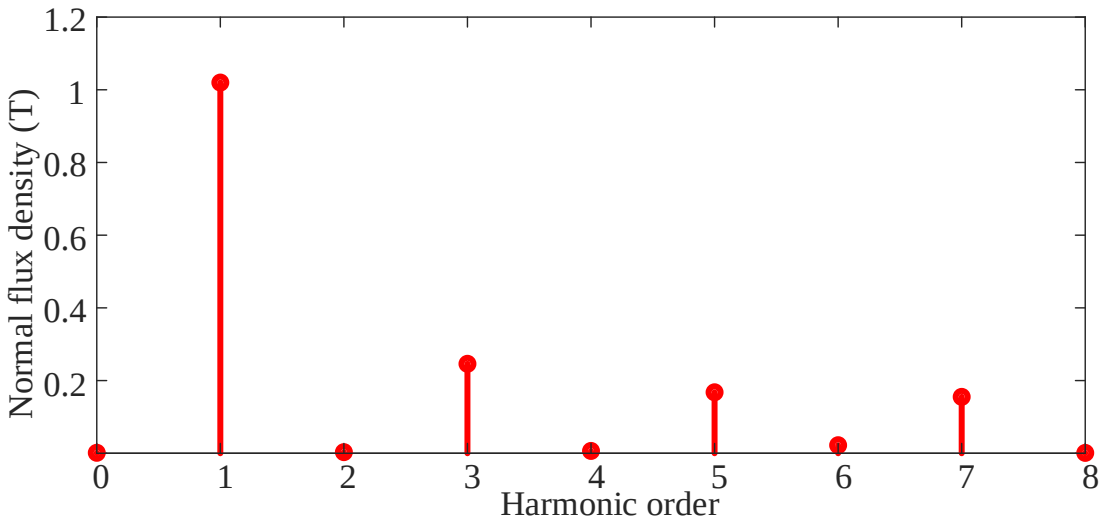

Figure 3.15: FFT analysis of the air-gap flux density for a 6MW FC Nd-Fe-B generator

3.4.3 Flux-concentrating ferrite generator

3.4.3.1 Electromagnetic model

Flux concentration can be used to utilize cheap low-energy magnets and still obtain a high air-gap flux density. A common low-energy magnet material is ferrite which has a remanent flux density of about 0.4 T [3]. The required mass for ferrite magnets is much higher than that for Nd-Fe-B magnets. However, the cost for the PMs, when substituting Nd-Fe-B with ferrite, is only one fourth to one fifth; that is, if the larger mass can be accepted a large cost reduction can be expected [78]. The rotor of the FC ferrite generator has ferrite magnets buried between pole shoes in order to reinforce the air-gap flux. The simplified section of the FC ferrite generators magnetic circuit models for one pole pair is shown in Figure 3.16.

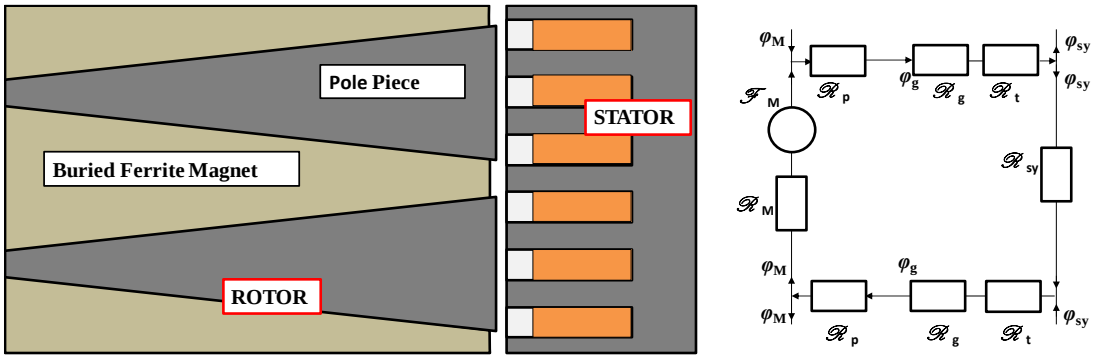

Figure 3.16: Magnetic circuit for modelling air-gap flux per pole for the FC ferrite generator

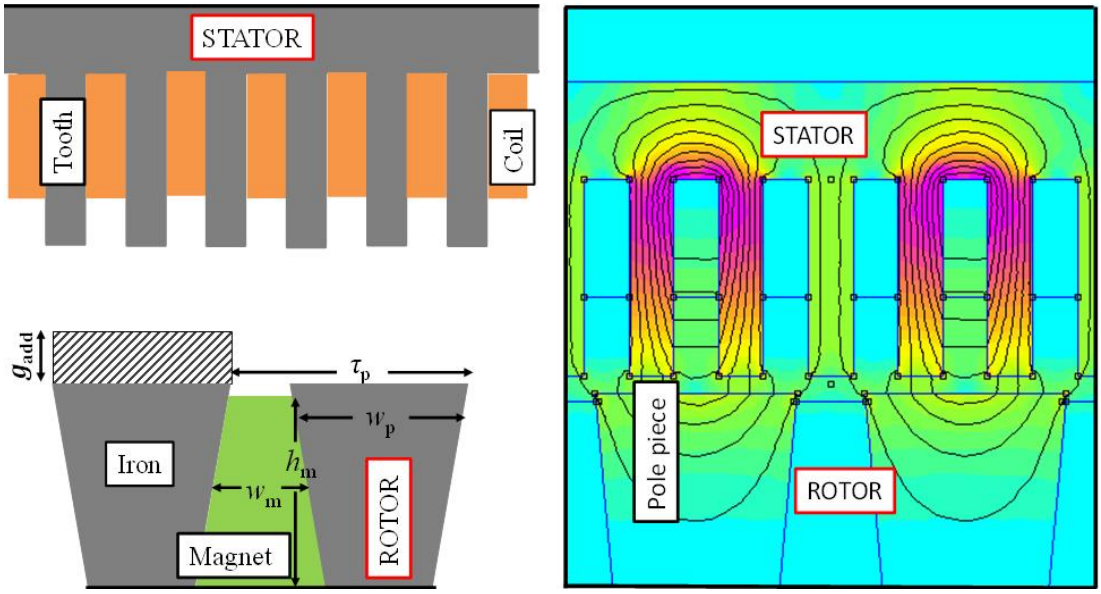

Figure 3.17: Flux-concentrating ferrite magnet generator (a) additional air-gap height used in direct axis magnetizing inductance formulation (b) stator field lines in the quadrature axis

Figure 3.17 shows that, in quadrature axis the majority of the flux found by using finite element software crosses only pole. The magnetic pole resembles a tooth surrounded by slots, and so the Carter factor can be applied to calculate the effective air-gap as shown in section 3.4.2.3.

The reluctances, air-gap flux density, induced *EMF*, resistance, inductance, phasor diagram and terminal voltage of the FC ferrite generator can be found by using same procedure given for FC Nd-Fe-B generator in section 3.4.2.

3.4.3.2 Verification using finite element software

Figure 3.18 shows the magnetostatic finite element analysis results for two poles of a 6 MW FC ferrite generator. The analytical results of direct axis and quadrature axis inductance for FC ferrite are also verified which shows agreement within about 1% difference in both axes. Table 3.6 shows some key dependent variables verified for the baseline generator design. The analytical results presented in Table 3.6 also exclude

the end winding leakage inductances as the 2D FE results do not include the end winding leakage inductance. All the FC ferrite generators used in this study are verified using same method.

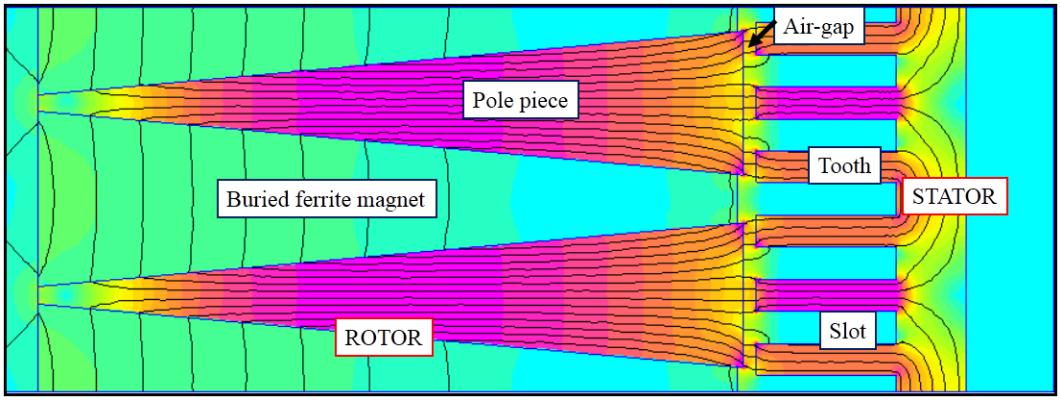

Figure 3.18: Magnetostatic finite element analysis of FC ferrite generator, ■0T→■1.5T. Software is FEMM [79]

Table 3.6: Analytical results vs FEMM analysis results for a 6 MW FC ferrite generator

Variables	**FC ferrite generator**	
	Analytical	**FEMM**
Fundamental air-gap flux density, $\widehat{B_g}$ (T)	0.98	0.96
Direct axis inductance, L_d (mH)	22.6	22.5
Quadrature axis inductance, L_q (mH)	25.3	25.1

The fundamental flux density can be found by using Fast Fourier Transform (FFT) analysis. Figure 3.19 shows the FFT analysis of the air-gap flux density for a 6MW FC ferrite generator.

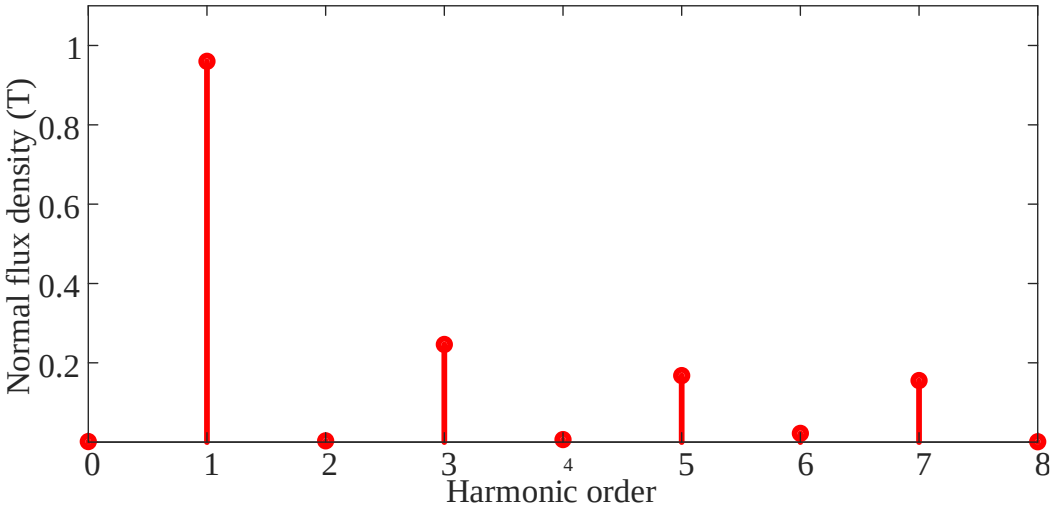

Figure 3.19: FFT analysis of the air-gap flux density for a 6 MW FC ferrite generator

3.5 Magnet mass minimisation

With a fixed pole width and number of pole pairs, the flux-concentrating magnet geometry can be optimised to minimise magnet mass while achieving the same fundamental flux density as the surface mounted magnet machine. Increasing the magnet width at the inner radius, $w_{m,i}$ leads to the angle, θ_p increasing (Figure 3.20). This variation, accompanied with changing in the magnet height, h_m allows the magnet mass to be minimised.

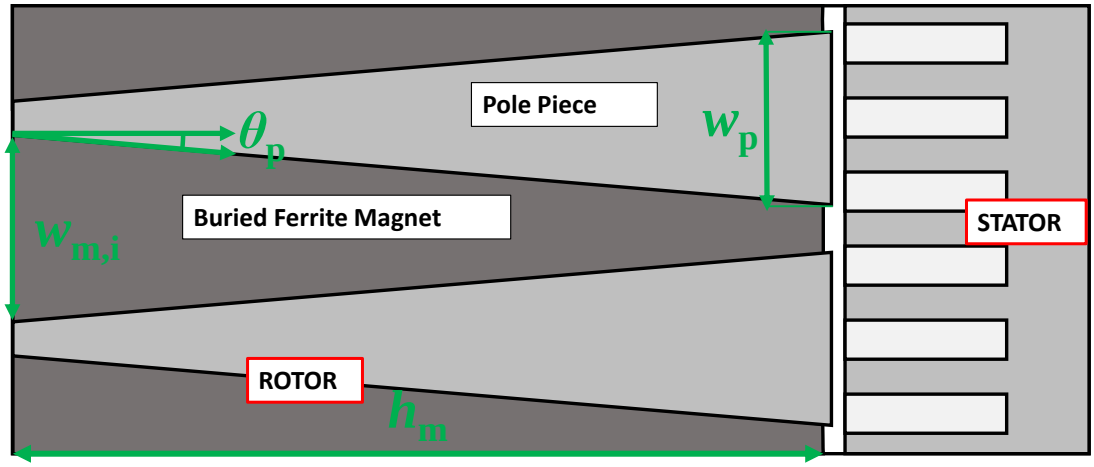

Figure 3.20: Schematic diagram of ferrite magnet rotor with angular pole

To further minimise the magnet mass, contour plots of magnet mass and air-gap flux density from SM Nd-Fe-B and FC ferrite rotors are plotted against different magnet widths and heights.

3.6 Masses and inertia

The Mass of materials within a generator can be calculated by multiplying the density of the material with its volume. Magnet mass can be calculated as,

$$m_{PM} = 2p\rho_m w_m h_m l_s \tag{3.43}$$

where ρ_m is the density of magnet. To calculate the cost of the generator, the masses of iron and copper are also calculated and multiplied by the assumed cost per kilogram of the materials given later in Table 4.4.

The total mass of active materials in the generator can be given as,

$$m_{act} = m_{stat} + m_{rot} \tag{3.44}$$

where m_{stat} is the total active material masses in the stator and m_{rot} is the total active material masses in the rotor.

Moment of inertia of rotating components with mass, m at radius, r on the rotor can be given as,

$$J = \Sigma_i^{\frac{1}{2}} m_i r_i^2 \tag{3.45}$$

Equation (3.45) can be used for the magnet, rotor iron and rotor structure (with correct masses and radii). The inertia of the rotating parts of the generator are used in Bladed model to compare the energy capture of generator with different inertia, as described in Section 4.4.3.

3.7 Power output, losses and efficiency

The electrical power output can be calculated as,

$$P_{\text{electrical}} = 3IV\cos\theta \tag{3.46}$$

where θ is the angle between terminal voltage and current The copper losses can be calculated from currents and resistances as,

$$P_{\text{cu}} = 3I^2 R_{\text{s}} \tag{3.47}$$

Phase resistance can be calculated as,

$$R_{\text{s}} = \rho_{\text{cu}} \frac{l_{\text{cu}}}{A_{\text{cu}}} \tag{3.48}$$

where ρ_{cu} is the resistivity of copper, l_{cu} is the length of conductor in phase and A_{cu} is the cross-section area of the conductor.

The resistivity of the copper can be found as,

$$\rho_{\text{cu}} = \rho_{20}(1 + \alpha_{\text{t}}\Delta T) \tag{3.49}$$

where ρ_{20} is the resistivity of copper at 20°C which is the ambient temperature, α_{t} is the temperature coefficient and ΔT is the difference of the temperature.

The cross-section area of conductor can be given as,

$$A_{\text{cu}} = \frac{k_{\text{sfil}} A_{\text{slot}}}{N_{\text{slot}}} \tag{3.50}$$

where k_{sfil} is the slot filling factor and A_{slot} is the area of a slot.

$$A_{\text{slot}} = w_{\text{s}} h_{\text{s}} \tag{3.51}$$

The length of conductor in phase can be given as,

$$l_{\mathrm{cu}} = N_{\mathrm{s}}(2l_{\mathrm{s}} + 4\tau_{\mathrm{p}}) \tag{3.52}$$

The specific iron losses (the iron losses per unit mass) for the stator yoke can be calculated as [2], [81],

$$P_{\mathrm{Fesy}} = 2P_{\mathrm{Fe0h}}\left(\frac{f_{\mathrm{e}}}{f_0}\right)\left(\frac{\hat{B}_{\mathrm{sy}}}{\hat{B}_0}\right)^2 + 2P_{\mathrm{Fe0e}}\left(\frac{f_{\mathrm{e}}}{f_0}\right)^2\left(\frac{\hat{B}_{\mathrm{sy}}}{\hat{B}_0}\right)^2 \tag{3.53}$$

Where f_{e} is the frequency of the field in the iron, P_{Fe0h} is the hysteresis loss per unit mass at the given angular frequency, f_0 and flux density B_0, P_{Fe0e} is the eddy current loss per unit mass and B_{sy} is the stator yoke flux density.

The stator yoke flux density can be given as,

$$B_{\mathrm{sy}} = \frac{\emptyset_{\mathrm{sy}}}{h_{\mathrm{sy}}l_{\mathrm{s}}} \tag{3.54}$$

The specific iron losses for the stator teeth can be calculated as,

$$P_{\mathrm{Fest}} = 2P_{\mathrm{Fe0h}}\left(\frac{f_{\mathrm{e}}}{f_0}\right)\left(\frac{\hat{B}_{\mathrm{t}}}{\hat{B}_0}\right)^2 + 2P_{\mathrm{Fe0e}}\left(\frac{f_{\mathrm{e}}}{f_0}\right)^2\left(\frac{\hat{B}_{t}}{\hat{B}_0}\right)^2 \tag{3.55}$$

where B_{t} is the stator teeth flux density that can be given as,

$$B_{\mathrm{t}} = \frac{\emptyset_{\mathrm{g}}}{\frac{1}{2}wl_{\mathrm{s}}} \tag{3.56}$$

where $w = w_{\mathrm{m}}$ for the SM Nd-Fe-B generator and $w = w_{\mathrm{p}}$ for the flux-concentrating generators (where $w_{\mathrm{s}} = w_{\mathrm{t}}$).

To calculate the total iron losses, the iron losses in teeth and yokes are evaluated and added. The total iron losses in the stator can be given as,

$$P_{\mathrm{Fe}} = P_{\mathrm{Fesy}} + P_{\mathrm{Fest}} \tag{3.57}$$

The generator efficiency can be given as,

$$\eta = \frac{P_{\mathrm{electrical}}}{P_{\mathrm{mechanical}}} \times 100\% \tag{3.58}$$

where $P_{\mathrm{mechanical}}$ is the mechanical power from the wind turbine rotor.

3.8 Variable power factor

It is assumed that the generators in this study run at unity power factor at all wind speeds. This simplification is applied to all the generator types and reduces the complexity of the optimization. This assumption tends to overestimate the generator losses and material costs and underestimate the power converter rating and cost than

for example varying the load angle so that the phase current is between the induced emf and terminal voltage [2].

To see the effect of variable power factor on turbine cost of energy, generator losses, materials cost, converter cost and other variables, the current is placed in the middle between the terminal voltage and induced *EMF* and the phasor diagram is shown in Figure 3.21.

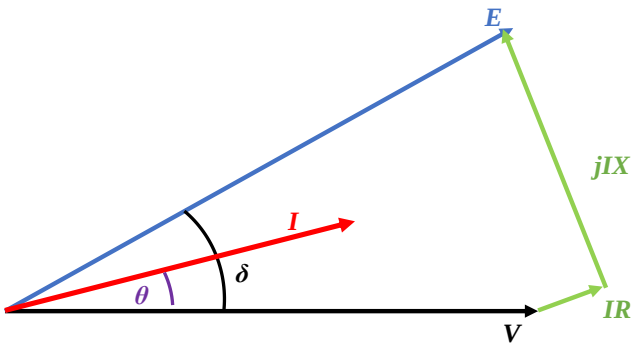

Figure 3.21: Phasor diagram of a surface-mounted machine with variable power factor ($\theta = 0.5\delta$) [82]

Terminal voltage can be given as,

$$V = \sqrt{E^2 - (IX_s \cos\theta)^2} + IX_s \sin\theta \tag{3.59}$$

where power factor angle Θ is half of the load angle δ,

Load angle can be calculated as,

$$\delta = \sin^{-1} \frac{IX_s \cos\theta}{E} \tag{3.60}$$

3.9 Magnet grades

When choosing the type of Nd-Fe-B magnet, a generator designer can pick from a number of magnet grades. These grades are often expressed as N*XY* where 'N' indicates that this is an Nd-Fe-B magnet, *X* is the maximum energy product (BH_{max}) in MGOe and *Y* indicates the maximum working temperature. The maximum energy product of the magnet material is the product of magnet's flux density and field ($B_m H_m$) which is maximum. BH_{max} is a volume independent magnetic characteristic, meaning a small and large magnet made from the same Nd-Fe-B magnet alloy will have the same BH_{max}, although they result in different magnetic fields or flux. Although the actual *BH* of a magnet depends on the magnetic circuit design in which it is placed, BH_{max} is a good figure of merit and a higher number indicates a stronger magnet.

Table 3.7: Magnet properties for different magnet grades [58]

Magnet grade	**Remanent flux density (T)**		
	Regular	**"H" grade**	
Operating Temperature	**80˚C**	**80˚C**	**120˚C**
N35	1.12	1.12	1.06
N38	1.17	1.17	1.11
N40	1.20	1.20	1.13
N42	1.21	1.21	1.15
N45	1.25	1.25	1.19
N48	1.30	1.30	1.23
N50	1.32	1.32	1.25
N52	1.34	1.34	1.27

The production of rare earth permanent magnets is based on the combination of intermetallic compounds of rare earth elements and the transition metals Fe or Co. The development in the last few decades has led to significant improvements in energy product BH_{max} and higher Curie temperatures (the temperature at which the magnet will become completely demagnetized) [83-84].

Gutfleisch [83] shows different manufacturing routes of magnets for high BH_{max} and high operating temperatures. Based on the proportion of intermetallic compounds of rare earths, transition metals, other impurities, structure, heat treatment and processing route, BH_{max} and the maximum operating temperature and the cost of a magnet will be different. Generally speaking, the higher BH_{max} and temperatures need progressively more substitution of Dysprosium for the Neodymium. For this to be effectively used, there are also additions of Cobalt and Gallium in the manufacturing process. Commercial magnetic characteristics are advertised with tolerance; this is why there is an effective range for the maximum energy product.

A number of different Neodymium magnet grades (N35 to N52) are used in this study for a 6 MW SM Nd-Fe-B generator. The baseline neodymium magnet grade in this study is N40H. The optimization process is repeated for other magnet grades and the optimal designers are compared. Table 3.7 shows the magnetic properties, the maximum operating temperature of different Neodymium magnet grades and their actual operating temperatures. The cost of magnets is collected from [85] and [86]. After that collected data are normalised so that the magnet size is not so much an issue. The normalised current specific per unit cost of different magnet grades are shown in Fig. 3.22. The cost of different magnet grades, C(X) can be found from the baseline

magnet cost C(40H) given in Table 4.4, multiplied with unit price, *U* given in Figure 3.18.

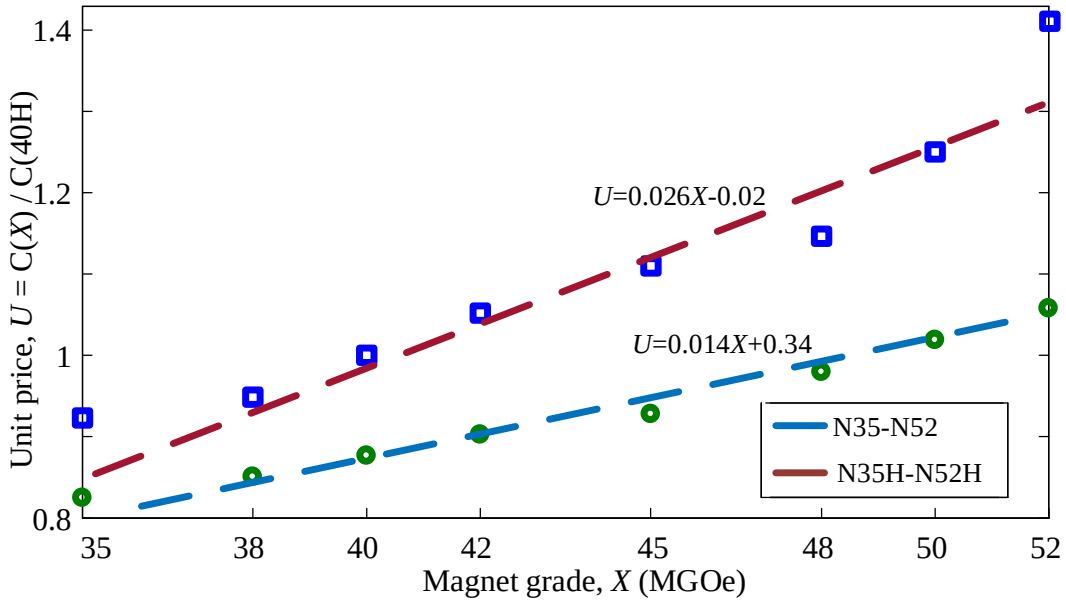

Figure 3.22: Fitted trend lines of the per unit specific cost of Nd-Fe-B magnet grades (relative to N40H). X represents the maximum energy product and the graph shows 'regular' and high temperature magnets. [85-86]

3.10 Discussions and Conclusions

This chapter describes the method of electromagnetic modelling for different generator topologies. The generator designs are also optimised using contour plots. Analytical models are partially verified using finite element software. Baseline electromagnetic designs of different generator topologies are also shown in this chapter. Essentially this is a methodology chapter, but if someone wish to look at the baseline designs and where the designer might improve the design and what the relative pros and cons of each are. The air-gap flux density, generator dimensions and power losses are linked with mechanical and thermal models. The overall optimisation will be performed including electromagnetic design, mechanical and thermal design (given in next chapter), which will help to answer the primary research question.

Chapter 4

Mechanical, Thermal Modelling and Turbine

4.1 Introduction

In order to have a full understanding of a generator design, it is important to be able to include structural and thermal elements alongside the magnetic and electrical circuits shown in Chapter 3. It is also important to include a representation of the wind turbine and how the generator design will affect the cost and performance of the turbine. The structural and thermal model in this Chapter are the extension of the electromagnetic model in Chapter 3, which will be optimised all together in Chapter 5.

The main purposes of this chapter are:

- To include the structural model of the generators along with the electromagnetic model given in chapter 3
- To estimate the effect of generator structure on turbine top head mass, and subsequently on tower, foundation and lifting cost and overall turbine cost of energy.
- To develop a thermal model to estimate the effect of temperature due to different losses and cooling cost to cool down the magnet and winding temperature.
- To develop a cooling model, showing costs and losses for variable cooling requirements

The generator structural models for both stator and rotor, linking deflections in the air-gap to structural masses are described in this chapter. A simple thermal model is then introduced to estimate the thermal effect due to power losses (copper, iron and magnet losses) in the generator. This modelling is verified using the FEMM heat flow analysis module. Next, the required cooling air flow, additional cost and energy consumption

incurred to cool down the magnet and winding temperature by forced air flow using fan and heat exchanger is modelled. The air flow control is controlled so that the fan energy consumption varies with variable wind speed. Subsequently characteristics of the wind turbine and the site wind resources and calculation of annual energy production is shown for different power ratings. The influence of generator mass on inertia (and hence turbine performance) and the effect of turbine top head masses on tower, foundation and lifting cost are also modelled in this chapter.

This chapter is an important step to answer secondary research questions *Q*2, *Q*3 and *Q*5, also supports answering *Q*4 and *Q*6 partially. The next chapter will describe the optimisation procedure that helps to answer some of the secondary research questions, hence the primary research questions for overall optimisation.

4.2 Generator structural model

In order to design lightweight and cost effective direct drive generators, the designer should include a structural model of the generator along with the active material model. McDonald [6] showed the structural models with different types of rotor and stator structures for direct drive generators. In this study a simple structure – where a cylinder is connected to the shaft by arms, in a so-called "spider" arrangement – has been used to represent both the generator rotor and stator. The work here in this chapter goes further than [6] as it finds minimum dimensions of the arms that will meet deflection requirements.

An example rotor and stator structure and different types of deflection with 6 arms is shown in Figure 4.2 and Figure 4.3. The cylinder includes the 'yoke' or back iron. For the flux-concentrating generators there is no steel rotor yoke; instead of steel, pole pieces are mounted on an aluminium cylinder. The rotor deflection is allowed to deflect radially into air-gap by 5% of the air-gap length, the permitted tangential deflection is 0.5% of the air-gap and the structure is allowed to deflect axially by 0.02% of the air-gap.

The electromagnetic and structural models are coupled and so if the air-gap flux density increases with a design change then the loads on the rotor and stator increase. This means that if the magnet MMF increases or if the air-gap clearance is reduced (and the air-gap reluctance drops) then the magnetic loading increases. In order to keep

the air-gap open, stiffer and heavier generator structures are needed, leading to a structural cost increase.

The major force that the rotor and stator structures must face is the normal component of Maxwell's stress. A mean normal radial stress, q_r is applied to the outside surface of the rotor and inner part of the stator – for an inner rotor machine,

$$q_r = \frac{{B_g}^2}{2\mu_0}\frac{w}{\tau_p} \tag{4.1}$$

where B_g is the air-gap flux density, $w = w_m$ for surface-mounted Nd-Fe-B generator and $w = w_p$ for flux-concentrating generators. In this study, the structural dimensions of the arms and yoke are varied to meet the deflection criteria. In the flux-concentrating generators case, additional aluminium cylinder thickness is added. Equation (4.1) shows that the loads on the structure are strongly dependent on the electromagnetic model.

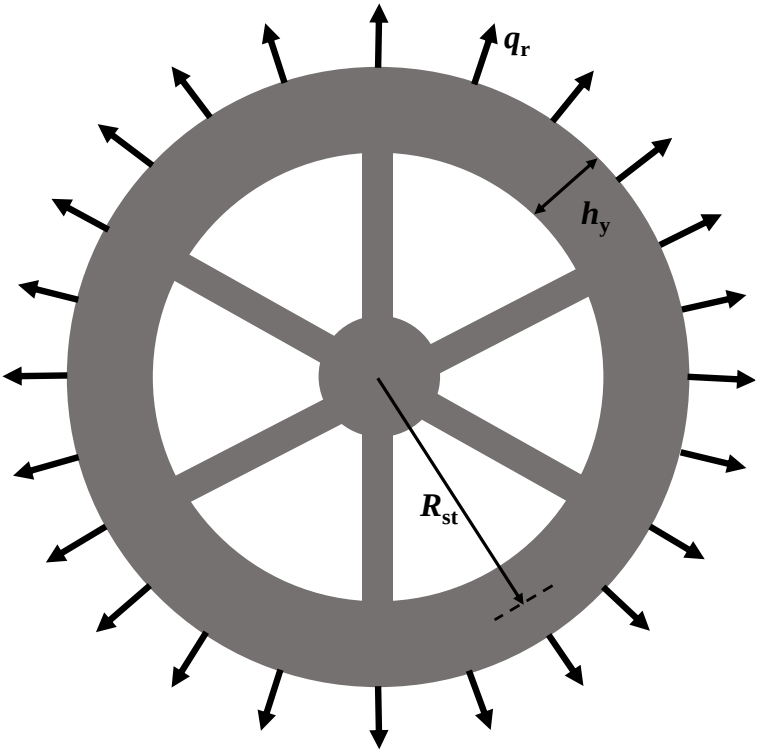

Figure 4.1: Rotor with arms

The radial deflection at the mid-point of the back iron between two arms – see Figure 4.1- is given in [6] and [12] as,

$$u = \frac{q_r {R_{st}}^2}{Y_{st} h_y}\left(1 + \frac{{R_{st}}^3}{I_r}\alpha\right) \tag{4.2}$$

where R_{st} is the radius of the structure, Y_{st} is the Young's Modulus of the structural material, h_y is the height of yoke, I_r is the second moment of area of the cross-section of yoke and α is a function of the number of arms and the dimensions of the rotor or stator structure [87].

In terms of the tangential or circumferential direction, the deflection z for the rotor or stator structure can be found as [87],

$$z = \frac{T_{max} {l_{ar}}^3}{12 Y_{st} I_z} \tag{4.3}$$

where T_{max} is the maximum torque of generator, l_{ar} is the radial length of the arms and I_z is the second moment of area of the structural arms in the circumferential direction.

The axial deflection of the generator rotor or stator due to gravity, y is given in [6] and [87] as

$$y = \frac{W {l_b}^3}{12 Y_{st} I_y} + \frac{w {l_{ar}}^4}{24 Y_{st} I_y} \tag{4.4}$$

where W is the weight component of the back iron (i.e. permanent magnet, copper, aluminium, iron or other materials in rotor or stator yoke), l_b is the radial length of the beam, w is the weight component of the arms and I_y is the second moment of area of the structural arms in the axial direction.

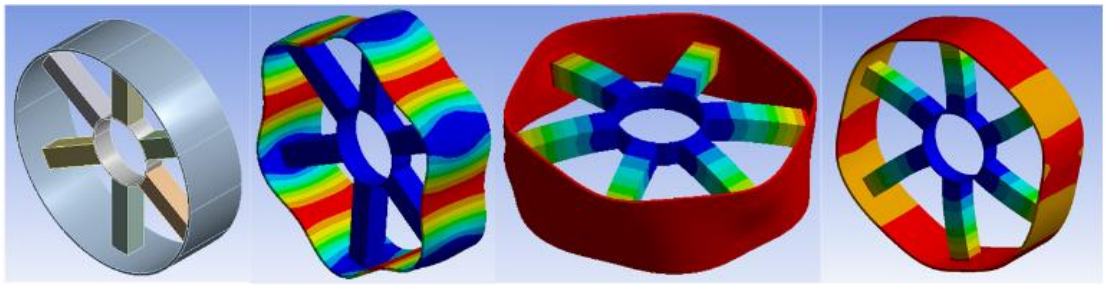

Figure 4.2: From left to right, (a) Structural model of rotor (b) Radial deflection (c) Axial deflection (d) Tangential deflection

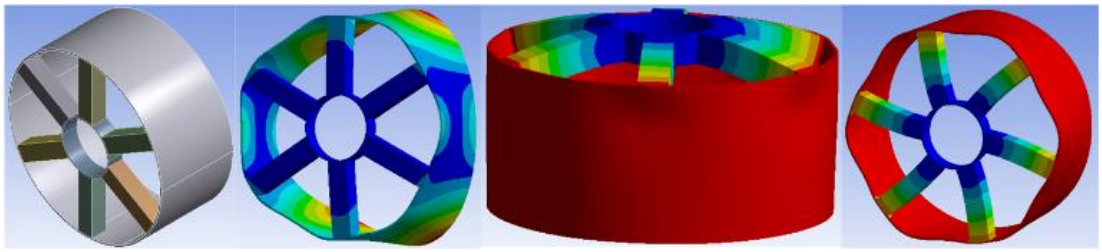

Figure 4.3: From left to right, (a) Structural model of stator (b) Radial deflection (c) Axial deflection (d) Tangential deflection

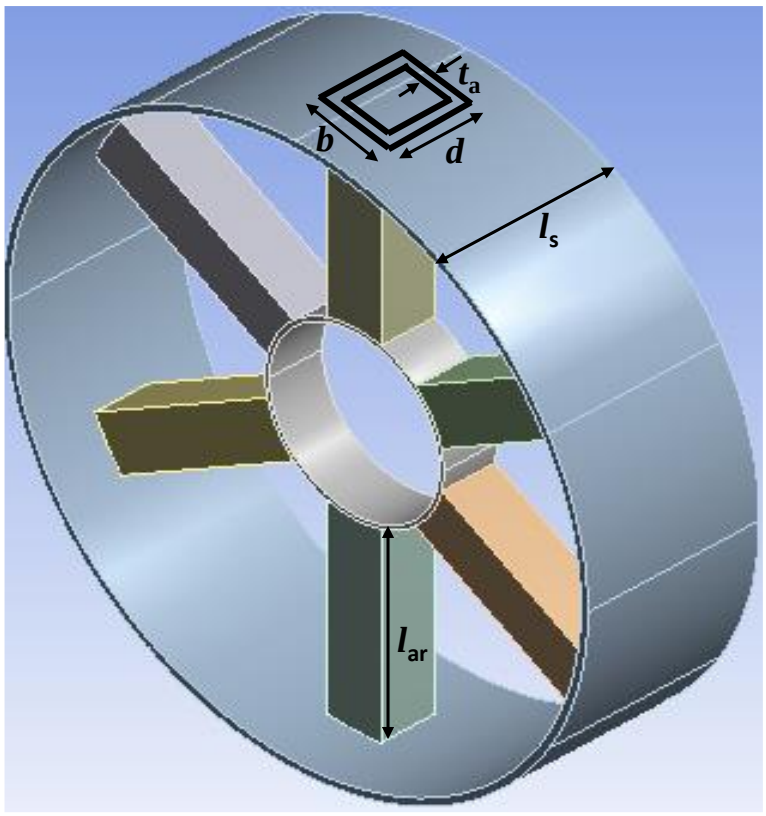

Figure 4.4: Rotor arms with dimensions

The structural mass of a generator can be found by the summation of the structural mass of rotor and the structural mass of stator. The structural mass of rotor or stator, m_{str} can be calculated as

$$m_{str} = \rho_{st}\left[2\pi R_{sto} h_{y0} l_s + n_{ar} l_{ar}\{bd - (b - 2t_a)(d - 2t_a)\}\right] \quad (4.5)$$

where ρ_{st} is the density of the material, R_{sto} is the outer radius of the structure, h_{y0} is the extra yoke height due to deflection, n_{ar} is the number of arms, b is the average beam width (circumferential), d is the average beam width (axial) and t_a is the wall thickness of beam.

4.3 Thermal model/cooling

It is important to understand the effect of operating temperature on Nd-Fe-B magnets. Typically, Nd-Fe-B magnets operate best at lower temperatures, i.e. their B_r and H_c are larger. Regular Nd-Fe-B magnets can work safely up to 80°C temperature but after this point, they begin to irreversibly lose their magnetism. On the other hand, grades with an "H" rating can operate in temperatures up to 120°C.

This study estimates the temperature effect due to power losses, the additional cost and energy consumption incurred to cool down the magnet temperature by forced air flow

using fan and heat exchanger. Different "H" grade Nd-Fe-B magnets (N35H –N52H) with operating temperature of 120˚C are used in the rotor of 6 MW SM Nd-Fe-B generator to estimate the temperature rise due to losses. After that a cooling system is introduced to cool down the magnet temperature from 120˚C to 80˚C. Subsequent to that, different regular grade magnets (N35-N52) with maximum operating temperature of 80˚C are used instead of "H" grade magnet to compare the effect of temperature and cost of energy. The process of controlling the cooling air flow for variable losses comes after that.

4.3.1 Temperature Effect on Resistance and Br

In the case of additional cooling, the winding temperature will be decreased. The resistivity of copper, ρ_{cu} depends on the winding temperature and so,

$$\rho_{\mathrm{cu}}(T) = \rho_0(1 + \alpha_{\mathrm{t}}\Delta T) \tag{4.6}$$

where ρ_0 is the resistivity at ambient temperature (20˚C) and α_{t} is the temperature coefficient of copper. This varying resistivity affects the winding resistance,

$$R_{\mathrm{s}} = \frac{\rho_{\mathrm{cu}}(T) l_{\mathrm{cu}}}{A_{\mathrm{cu}}} \tag{4.7}$$

where l_{cu} is the length of a winding and A_{cu} is the cross-section area of copper conductor. The copper losses of the generator vary due to temperature effect on resistance.

The magnet's remanence (B_{r}) and coercivity vary with temperature as given in [58]. Indeed, changing the temperature of a N40H magnet from 120°C to 80°C will increase its effective BH_{max} by more than 12%. This in turn affects the magnetomotive force, hence the flux density and power production will vary with temperature. The magnetic properties in different operating temperature can be found from Table 3.7.

4.3.2 Thermal Model

A detailed thermal model based on the work of Grauers [3] is used in this study. A lumped-parameter thermal network model is used to define the 6 MW SM Nd-Fe-B generator. A simplified thermal model for the complete generator given in Figure 4.5. The simplified model reduces thermal resistance from the detailed model using symmetry by connecting Q_{s} parallel models for a stator slot pitch, coil, 2 p parallel models for a rotor pole and the model for the internal air and the two end shields (where Q_{s} is the number of slots and p is the pole pair). The reason behind the simplification

is to assess only essential nodes to calculate the winding and magnet temperatures, where the simplified thermal resistance are the replacement of the series and parallel connected thermal resistances. This simplified model consists of twelve nodes and eighteen thermal resistances as shown in Figure 4.6.

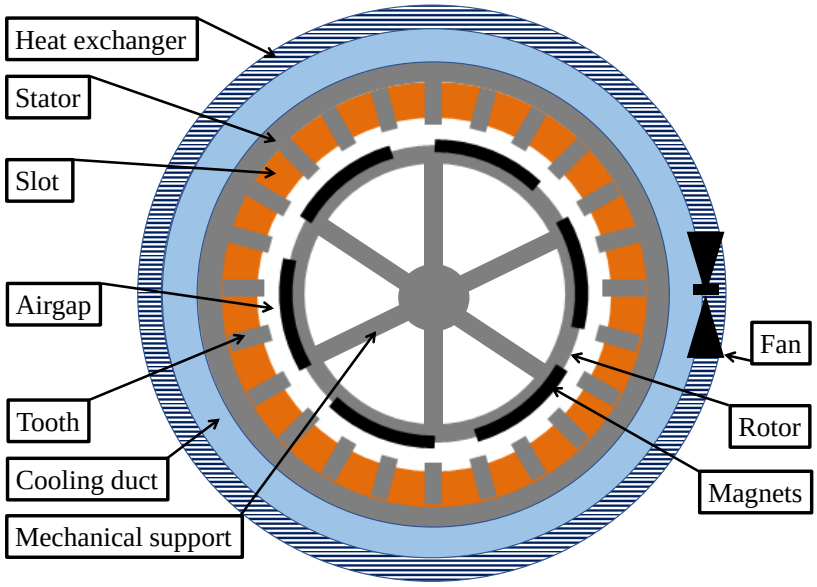

Figure 4.5: A simple direct-drive generator for wind turbine with active materials, mechanical support and cooling system

The temperature differences in the circumferential direction of the generator are neglected, i.e. losses are uniformly distributed from one tooth to the next, one slot to the next and one pole to the next. The two end windings of a coil are simplified as one because of symmetrical generator cooling in the axial direction.

The losses are assumed to be dominated by the copper losses coming from the stator winding, iron losses come from the stator teeth and yoke, eddy current losses come from the magnets and additional stray losses (core losses at rated load assumed to be about 20 % of the core losses at no load) [3]. It is assumed that, friction and windage losses do not affect the temperature rise of the winding or magnets, hence it is neglected. The copper losses are divided into losses in the end windings and in the top and bottom coil sides in the slots. The losses in the magnets are assumed to be spread equally, while supplementary losses are expected to be in the tooth tip.

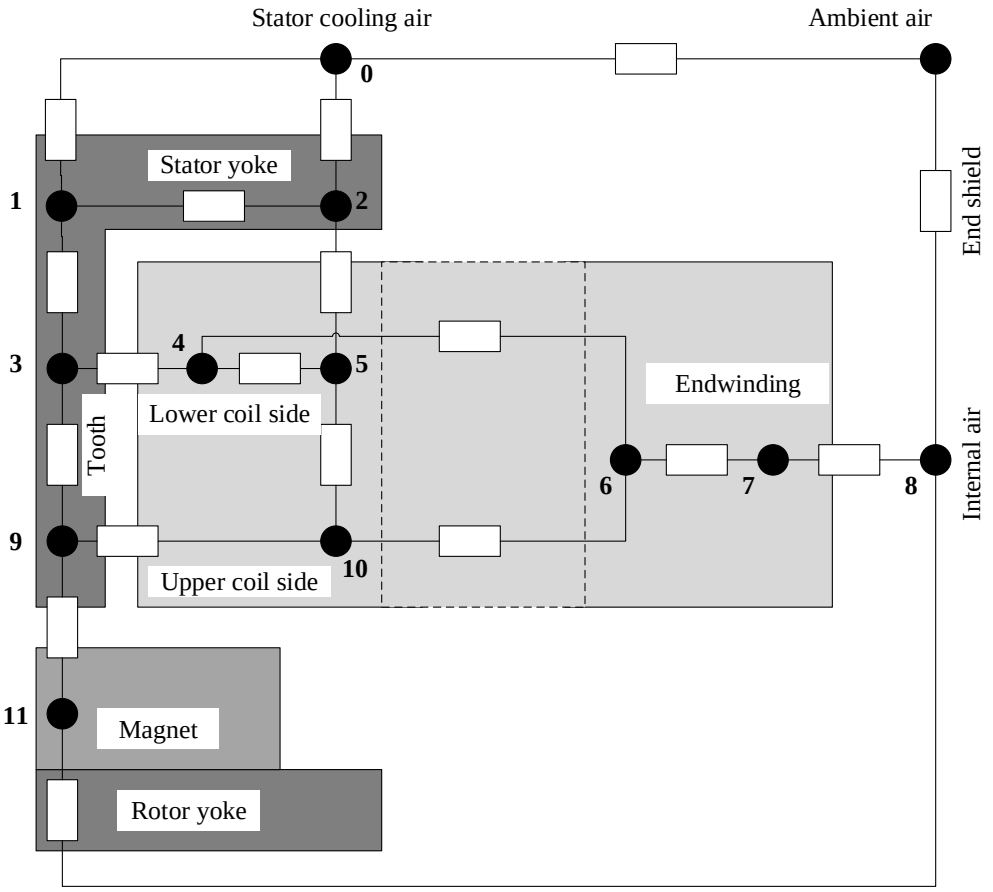

Figure 4.6: The simplified thermal model based on one slot pitch, one rotor pole, one coil, internal air and end shield [88]

Cooling air is passed through circumferential cooling channels to cool down the generator outer surface of the stator core. An equivalent thermal resistance is added in the model to represent the temperature increase in the cooling air. A matrix equation is used to formulate the temperature rise problem. The temperature difference, ΔT between the nodes across a given thermal resistance, R_{th} which results from power losses at specific node, P_{loss} (losses in different nodes and thermal resistance across the nodes can be calculated as Grauers [3]) can be given as,

$$P_{\text{loss}} = \frac{\Delta T}{R_{\text{th}}} = \Delta T K_{\text{th}} \tag{4.8}$$

where K_{th} is the thermal conductance. The temperature rises vector is calculated by multiplying the loss vector by the inverse of the thermal conductance matrix. Figure 4.7 shows the simplified thermal resistance network that has been developed in this thesis.

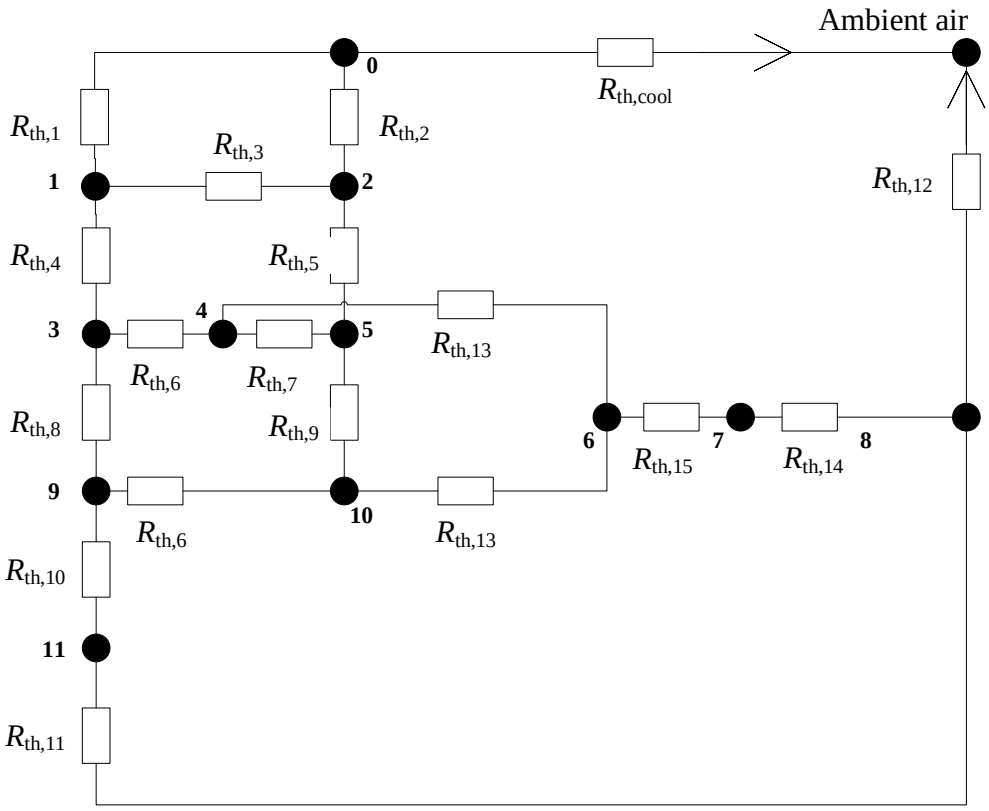

Figure 4.7: Simplified thermal resistance network of thermal model

4.3.3 Verification using FEMM heat flow software

The analytical results of thermal model are verified using 2D FEMM heat flow analysis [79]. Figure 4.8 shows the post processing of a thermal model of 6 MW SM Nd-Fe-B generator after FEMM heat flow analysis. The temperature of a node can be measured from this analysis.

Different materials in the generator including insulations are defined as input with specific heat capacity and thermal conductivity. The heat sources produced by generator losses (copper losses, iron losses, magnet losses) are also defined as input with volume heat generation (W/m^3). The convection boundary condition is applied on the regions having contact with ambient temperature. The convection boundary condition is also applied to the boundary between the stator yoke and cooling duct, rotor yoke and internal air. To achieve different node temperature near to analytical results, an iterative method is used in FEMM, where after every run the boundary properties between stator yoke and cooling duct, rotor yoke and internal air were varied.

The 3D components of the thermal model such as cooling channel are represented using equivalent conductivity. For the cooling channel, the equivalent conductivity can be calculated as,

$$\lambda_{\text{cool}} = \frac{h_{\text{FEMM}}}{2l_s R_{\text{th,cool}} \pi r_{\text{s,out}}} \tag{4.9}$$

where h_{FEMM} is the chosen height in FEMM for the cooling channel and $r_{\text{s,out}}$ is the outer radius of the stator.

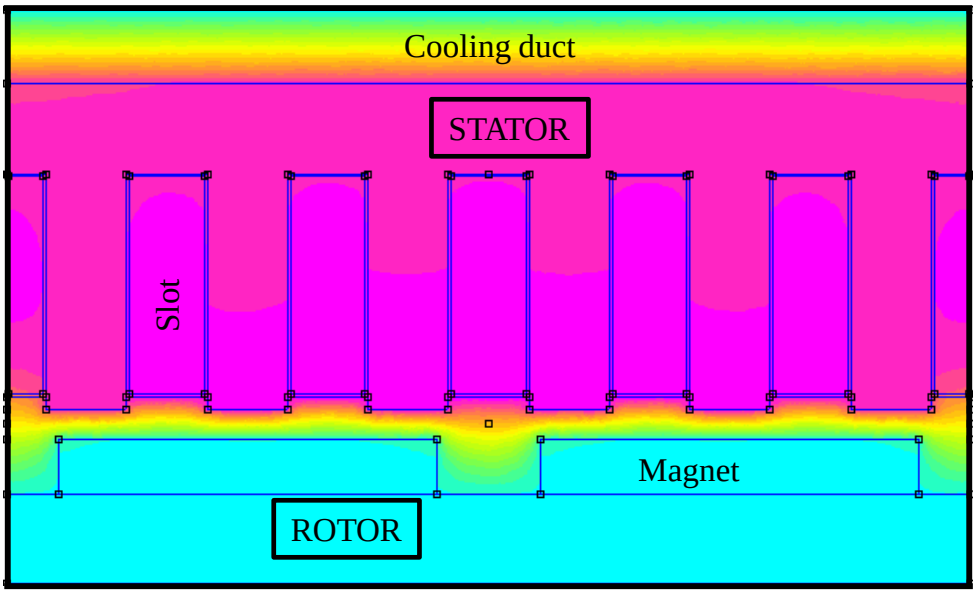

Figure 4.8: FEMM heat flow analysis

Table 4.1 shows some nodes temperature verified using finite element software for a 6 MW SM Nd-Fe-B optimised design.

Table 4.1: Analytical results vs FEMM heat flow analysis results

Nodes	**Analytical (°C)**	**FEMM (°C)**
Yoke above a tooth	134.2	133.8
Bottom coil side in a slot	145.2	144.9
Top coil side in a slot	150.1	149.7
Magnet	80.1	79.8

4.3.4 Air Flow

The volumetric cooling air flow is varied to determine the required air flow to cool down the magnet temperature from 120˚C to 80˚C. This varying cooling air flow, q_{vc} varies the temperature rise of the cooling duct, which can be represented as equivalent thermal resistance, $R_{\text{th,cool}}$ given in [3],

$$R_{\text{th,cool}} = \frac{1}{q_{\text{vc}} \rho k_{\text{thc}}} \tag{4.9}$$

where ρ is the density and k_{thc} is the specific heat capacity of the cooling air. Figure 6.25(c) shows the trend line of required cooling air flow for a 6 MW Nd-Fe-B generator using N40H magnet, cool down to different magnet temperature.

Typically, a wind turbine generator that is forced air-cooled has a closed loop system which transfers heat from the generator to heat exchangers mounted on the nacelle, where the heat is radiated to the outside air which is at ambient temperature. The flow rate in such a closed system is defined by the characteristics of the fan(s) and the characteristic of the loop. A given fan at a given speed and power input will produce a range of flow rates, depending resistance to flow. Its operating characteristic is given by a curve, showing that it has low flow rates when it works at higher pressure but higher flow rates when it works at lower pressures. The pressure that it has to work at is effectively determined by the "resistance" of the loop to air flow. The equation associates to pressure drop, P_{d} to volumetric cooling air flow and the system resistance to airflow, R_{sys} can be found by using the equation given as [89],

$$P_{\text{d}} = R_{\text{sys}} {q_{\text{vc}}}^2 \tag{4.10}$$

The flow path with all changes are presented by system flow resistance can be calculated as [89],

$$R_{\text{sys}} = \frac{k_{\text{f}} \rho}{2 {A_{\text{f}}}^2} \tag{4.11}$$

where k_{f} is the coefficient of related fluid resistance that depends on the nature of flow (obstruction, expansion, contraction, and so on). The k_{f} factors for all changes in the air flow path from fan to heat exchanger can be calculated from the formulation given in [89] and [90]. A_{f} is the flow section area.

4.3.5 Cooling Fan and Heat Exchanger

A number of fans are used and their combined pressure-airflow characteristics [91] can be modelled as a quadratic curve as shown in Figure 4.9. This figure also shows the system flow resistance curve, the heat exchangers' resistance curve [92] and the combination to give the total system resistance curve, also modelled as a quadratic function. The actual air flow (due to combination of fans and heat exchangers) can be found at the point where the fan curve and the system resistance curve cross. Table 4.2

gives the specification of a single fan at its maximum speed and the cost of fan and heat exchanger.

A number of fans are needed for the required cooling and these can be used in series and parallel combination. For the case of identical fan units in parallel, the volumetric airflow (at a given pressure) of one fan is multiplied by the number of fans in parallel.

Table 4. 2: Fan and heat exchanger specification [91], [92]

Maximum fan power (W)	430
Maximum fan current (A)	2
Maximum fan speed (r/min)	1500
Maximum fan pressure (Pa)	250
Maximum fan airflow (m^3/s)	0.53
Cost of single fan (€)	180
Cost of single heat exchanger (€)	673

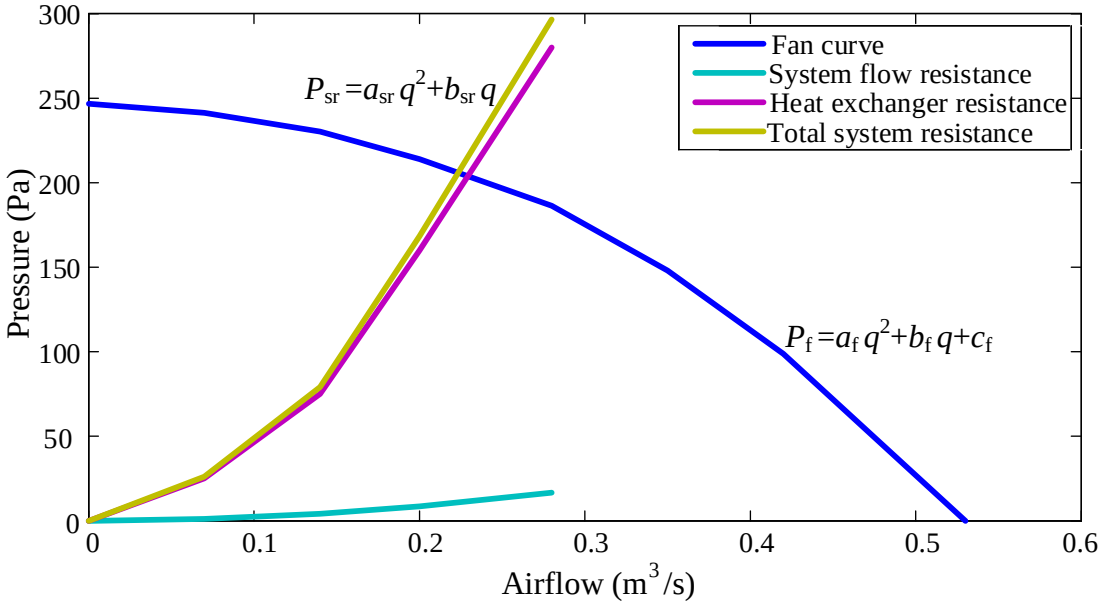

Figure 4.9: Fan, heat exchanger and system resistance curve

For the case of series fans, the pressure (at a given airflow) of one fan is multiplied by the number of fans in series. It is important to note that if the fans in combination are not identical, the weaker fan becomes an additional resistance on the system [90]. The combination of series and parallel fan gives a combined characteristic curve which crosses the total system resistance curve and hence the resultant volumetric air flow, q_{vc} at the intersecting point can be found as,

$$q_{vc}=\frac{-\left(\frac{b_f F_S}{F_P}-b_{sr}\right)-\sqrt{\left(\frac{b_f F_S}{F_P}-b_{sr}\right)^2-4\left(\frac{a_f F_S}{F_P{}^2}-a_{sr}\right)(c_f F_S-c_{sr})}}{2\left(\frac{a_f F_S}{F_P{}^2}-a_{sr}\right)} \quad (4.12)$$

where a_f, b_f and c_f represents the fan curve coefficients, a_{sr}, b_{sr} and c_{sr} represents the total system resistance curve coefficients, F_s is the number of fans in series and F_p is the number of fans in parallel.

Where fan curve can be found from Figure 4.9,

$$P_f = a_f q^2 + b_f q + c_f \tag{4.13}$$

And the total system resistance curve which is the combination of system flow resistance and heat exchanger resistance can be given as,

$$P_{sr} = a_{sr} q^2 + b_{sr} q \tag{4.14}$$

There is a cost implication of this cooling system, both from the capital cost of the fans and heat exchangers and from the energy that is needed to power them. The total cost of fan, C_{fan} used for cooling can be calculated as,

$$C_{fan} = C_{fmn} + C_{fen} \tag{4.15}$$

where C_{fmn} is the manufacturing cost of the total number fan and C_{fen} is the cost of electricity consumed by those fans, which can be calculated by using data from Table 4.2. The required heat exchangers are connected in parallel; hence the number of heat exchangers are proportional to the required cooling air flow. The cost of each heat exchanger can be found in Table 4.2. This would likely be fewer, when larger fans and heat exchangers are used.

4.3.6 Air flow control at variable wind speed

The wind turbine has variable power losses which depend on wind speed – that is until rated wind speed is reached. The required cooling air flow will also vary with wind speed and it is always less than the required cooling air flow at rated wind speed as shown in Fig. 4.10. After installation of fans (series and parallel) to achieve the maximum required cooling air flow at rated wind speed, the number of series fan can be varied by turning on/off (series fan multiply the pressure with the number of fans turning on) to control the air flow while the number of parallel fans remain fixed by using equation (4.12).

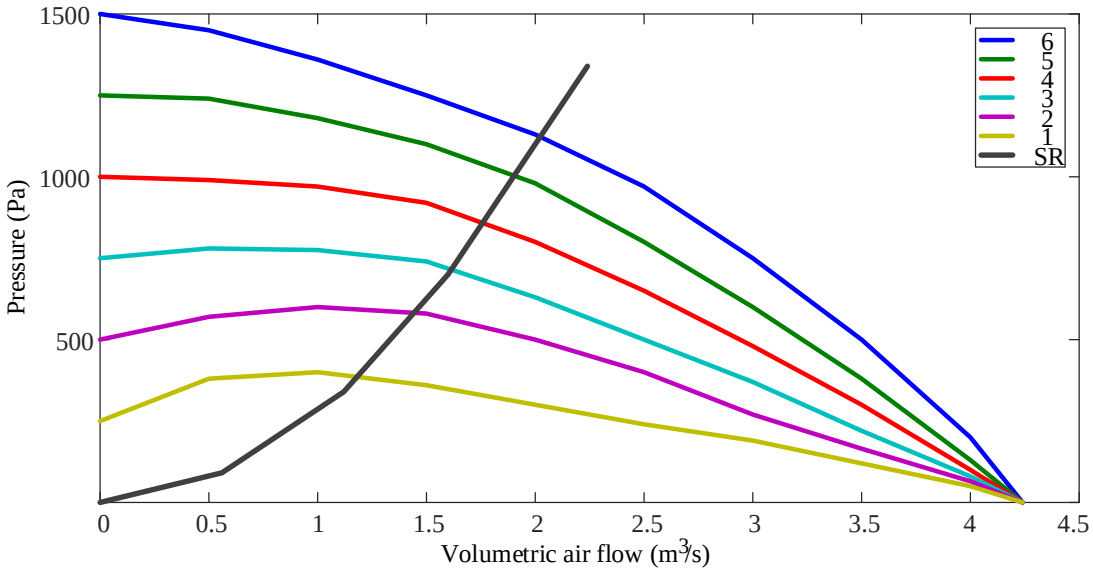

Figure 4.10: Fan curves for series fan (6 fan in series) intersects total system resistance curve where intersecting point is the achieved volumetric cooling air flow

4.4 Turbine

4.4.1 Turbine model and wind speed

In this study, a generic 3-bladed, pitch regulated variable speed wind turbine is modelled for an offshore application. The wind farm assumed in this study consist of 100 wind turbines. The major ratings and assumptions for three different rated powers are given in Table 4.3.

Table 4.3: Characteristics of the wind turbine and site wind resources

Rated wind speed (m/s)			11
Cut in wind speed (m/s)			3
Cut out wind speed (m/s)			25
Optimal tip speed ratio			8.3
Coefficient of performance at optimal tip speed ratio			0.48
Wind turbine availability (%) [93]			94
Site wind speed shape parameter			2.3
Site wind speed scale parameter (m/s)			10.8
Mean wind speed (m/s)			9.6
Turbine characteristics for different power ratings			
Rated grid power (MW)	6	8	10
Rotor diameter (m)	145	166	185
Rated rotational speed (rpm)	12	10.5	9.4
Hub height (m)	90	100	110
Fixed charge rate (FCR)	0.116	0.116	0.116
Wind firm turbine capital cost (exc. Generator, tower and foundation) (k€) [69]	16309	20564	24948
Operation and maintenance cost (k€) [10]	628	816	1005

It is assumed that the turbine rotor operates at its maximum power coefficient below the rated wind speed and hence has a rotational speed that varies in proportion to the wind speed. The blades are pitched and the rotor speed is limited once the turbine reaches the rated wind speed and power. The probability of a wind speed can be defined by using a Weibull distribution with shape and scale parameters given in Table 4.3, where the mean wind speed is 9.6m/s.

4.4.2 Annual energy production

The assumed wind turbine mechanical power curve for a 6 MW generator is shown in Figure 4.11. To calculate the baseline Annual Energy Production, first the Electrical Power, $P_{\text{electrical}}(v)$ at each wind speed, v is given by,

$$P_{\text{electrical}}(v) = P_{\text{mechanical}}(v)\eta(v) \tag{4.16}$$

where $\eta(v)$ is the electrical system efficiency.

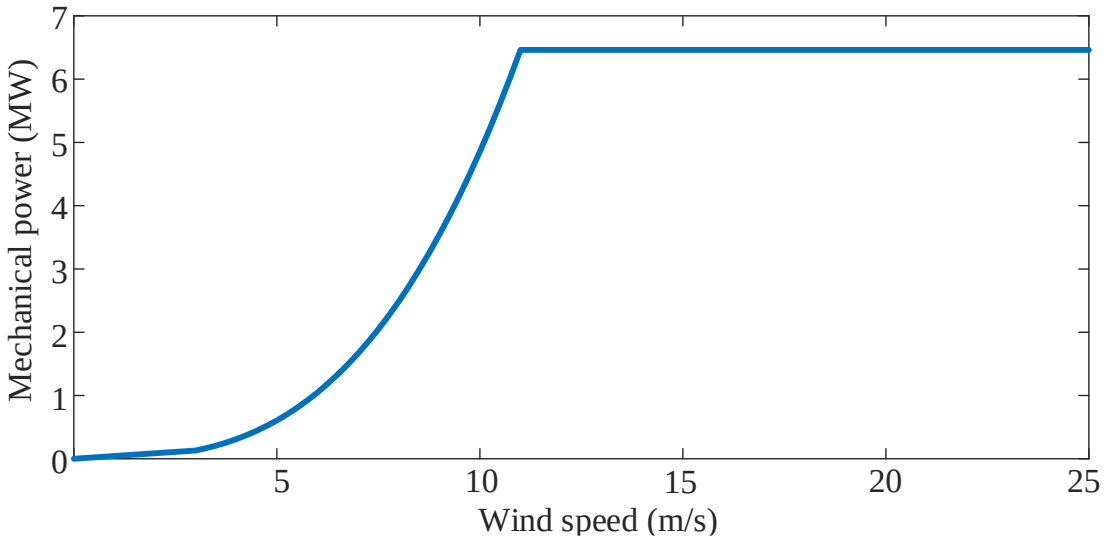

Figure 4.11: Mechanical power vs. wind speed for the assumed wind turbine

The assumed wind speed Weibull probability distribution is shown in Figure 4.12 (with an assumed shape parameter, k= 2.32 and a scale parameter, C = 10.8 m/s).

Equation (4.17) gives the probability, p_r of a given range of wind speeds$(A < v \leq B)$,

$$p_r(A < v \leq B) = Q(v > A) - Q(v > B) = e^{-(A/C)^k} - e^{-(B/C)^k} \tag{4.17}$$

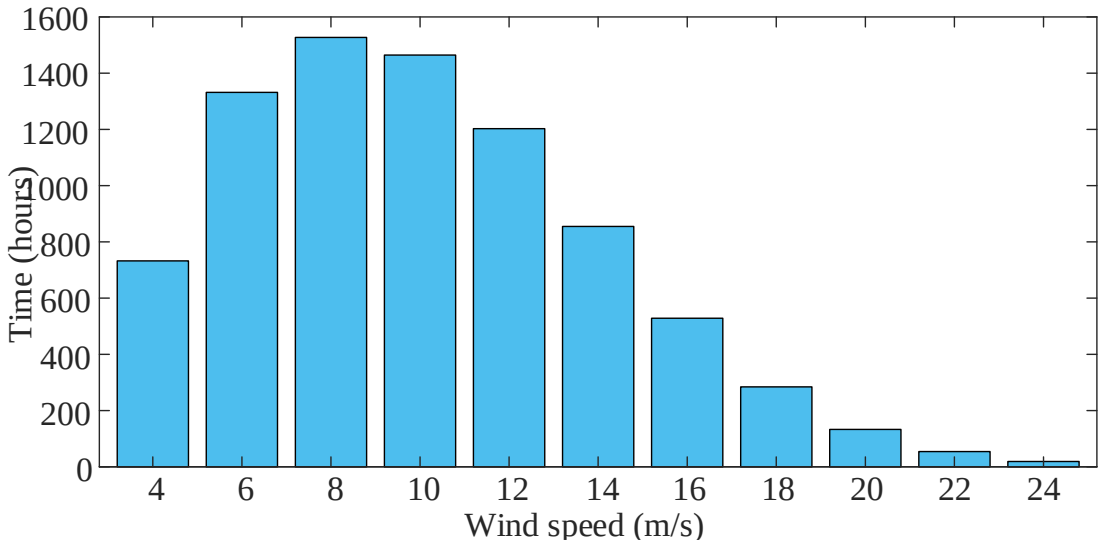

Figure 4.12: Weibull probability distribution

To calculate the Annual Energy Produced at each wind speed range in a year, equation (4.18) gives,

$$E_{\mathrm{y}}(A < v \leq B) \cong 365 \times 24 \times p_{\mathrm{r}}(A < v \leq B) P_{\mathrm{electrical}}(\bar{v} = x) \qquad (4.18)$$

where E_y is the Annual Energy Production for the range of wind speed and x is the average wind speed of that range.

Repeating this for a number of wind speed ranges between cut in and cut out wind speeds gives the Annual Yield curves. The integral of such a curve will give the Annual Energy Production, with units of Wh.

An availability of 94% is used, indicating that the wind project is ready to produce power between wind turbine cut-in and cut-out wind speeds 94% of the time [93]. The availability can be defined as [94],

$$Availability = \frac{Time\ that\ the\ turbine\ is\ available\ and\ ready\ to\ operate\ in\ a\ given\ time\ period}{Total\ time\ in\ that\ period} \qquad (4.19)$$

4.4.3 Estimating the influence of varying inertia

In order to assess the influence of varying generator rotor inertia, a number of power production simulations were carried out using Bladed [95]. Wind speed time series were created with turbulence at different average wind speeds. (Figure 4.13 shows one sample when the mean wind speed is 12m/s).

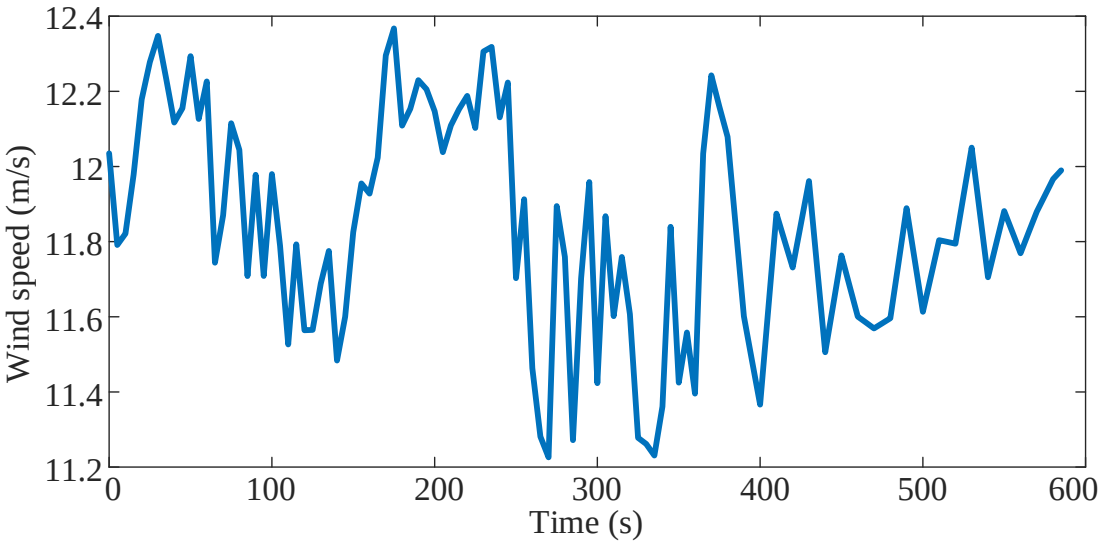

Figure 4.13: Sample wind speed time series, with $\bar{v}$ = 12m/s

Two wind turbine models were created, identical apart from the generator rotor inertia. Each wind speed time series was run to evaluate the different energy capture of these two turbine models. If the energy capture during the sample time series for the baseline wind turbine is $E_{\text{sample},1}(\bar{v} = x)$, then the energy capture for the turbine with the modified generator rotor for the same wind speed time series is $E_{\text{sample},2}(\bar{v} = x)$. This can be repeated for different average wind speeds. For this analysis, it is assumed that equation (4.20) holds and that,

$$\left(\frac{E_2}{E_1}\right)_{\bar{v}=x} = \frac{E_{\text{sample},2}(\bar{v}=x)}{E_{\text{sample},1}(\bar{v}=x)} \tag{4.20}$$

Equation (4.21) can be adapted for the new generator rotor inertia,

$$E_{\text{y}}(A < v \leq B) \cong 365 \times 24 \times p_{\text{r}}(A < v \leq B) P_{\text{electrical}}(\bar{v} = x) \left(\frac{E_2}{E_1}\right)_{\bar{v}=x} \tag{4.21}$$

and subsequently a new, modified Annual Energy Production can be calculated.

4.4.4 Power ratings

The rated power capacity of offshore wind turbines is increasing rapidly. In recent years, the turbine power generation capacities are moving from the 6 MW range to 10 MW and beyond. As a result, their size and mass, which grow rapidly with power capacity, is becoming a problem in terms of capital cost, logistics and assembly. Moreover, offshore wind turbines demand higher reliability, encouraging wind turbine manufacturers to integrate into their new designs inherently more reliable direct drive

permanent magnet synchronous generators. However, today's high-power direct drive generators are massive units that will need to become smaller to minimise costs.

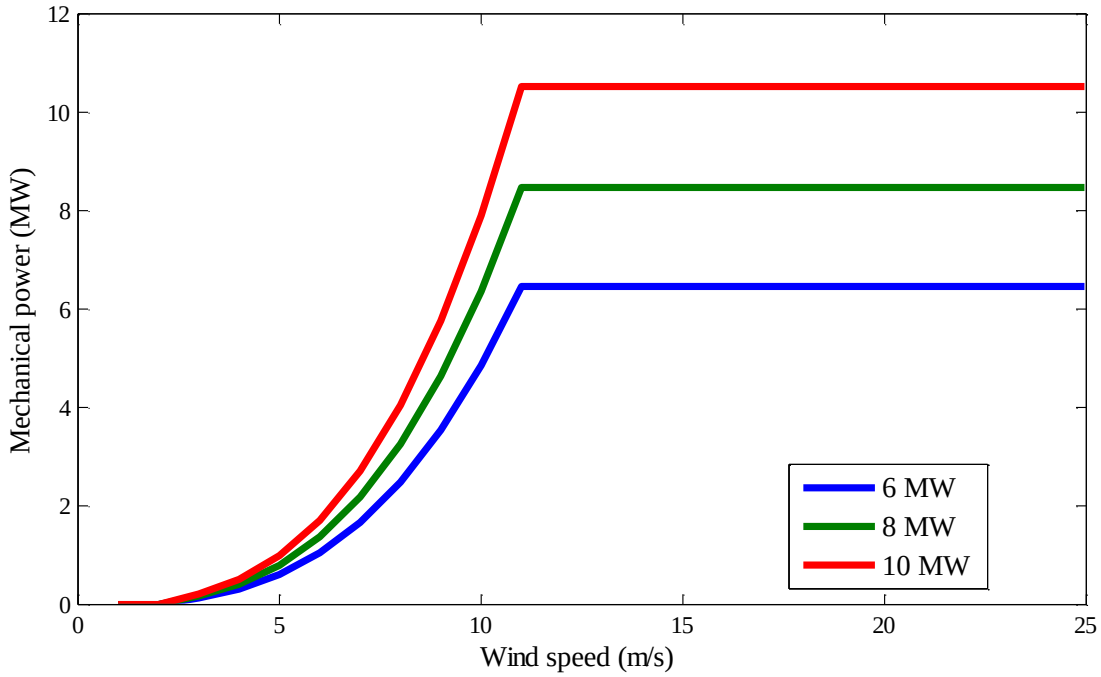

Figure 4.14: Mechanical power at each wind speed for the generators with different power ratings

In order to estimate and compare the size, masses, cost of energy and other variables, the generators with different power ratings (6 MW, 8 MW and 10 MW) are designed and optimised in this study. Turbine characteristics and capital cost for different power ratings are given in Table 4.3. Figure 4.14 shows the assumed mechanical power at each wind speed from the wind turbine rotor.

4.4.5 Tower and foundation

Tower mass depends on the top head mass (the combined mass of the wind turbine rotor and the equipment in the nacelle, including the generator) is shown in [96]. The tower mass, m_{tower} (kg) can also be estimated as [97],

$$m_{\text{tower}} = 0.4\pi \left(\frac{D_{\text{r}}}{2}\right)^2 h_{\text{hub}} - 1500 \qquad (4.22)$$

where D_{r} is the rotor diameter and h_{hub} is the hub height. The tower cost can be calculated by multiplying the tower mass with the structural steel cost from Table 4.4.

The foundation type is assumed to be a mono-pile in this study. For a water depth of 30m, the mono-pile mass, m_{mp} (kg) can be calculated for different turbine ratings and hub height (given in Table 4.3) as [97],

$$m_{\mathrm{mp}} = \frac{\left((1000T_{\mathrm{r}})^{1.5} + \frac{h_{\mathrm{hub}}{}^{3.7}}{10} + 2100 d_{\mathrm{w}}{}^{2.25} + (1000 m_{\mathrm{top}})^{1.13}\right)}{10} \tag{4.23}$$

where T_{r} is the turbine rating, d_{w} is the water depth and m_{top} is the top head mass of the turbine.

The top head mass is the sum of the generator mass and the rest of the turbine rotor and nacelle mass. This top head mass can be calculated as,

$$m_{\mathrm{top}} = m_{\mathrm{rtop}} + m_{\mathrm{act}} + m_{\mathrm{str}} \tag{4.24}$$

where m_{rtop} is the rest of the turbine top head mass excluding the generator mass m_{act} is the generator active material mass and m_{str} is the generator structural mass. The rest of the turbine top head mass is based on [98].

The substructure and foundation mass, m_{sf} can be found as,

$$m_{\mathrm{sf}} = m_{\mathrm{mp}} + m_{\mathrm{tpos}} \tag{4.25}$$

where m_{tpos} is the mass of monopole transition piece. The mono-pile cost and the mono-pile transition piece cost (assuming 60% pile and 40% transition piece and outfitting steel) is calculated using the steel cost from the Table 4.4.

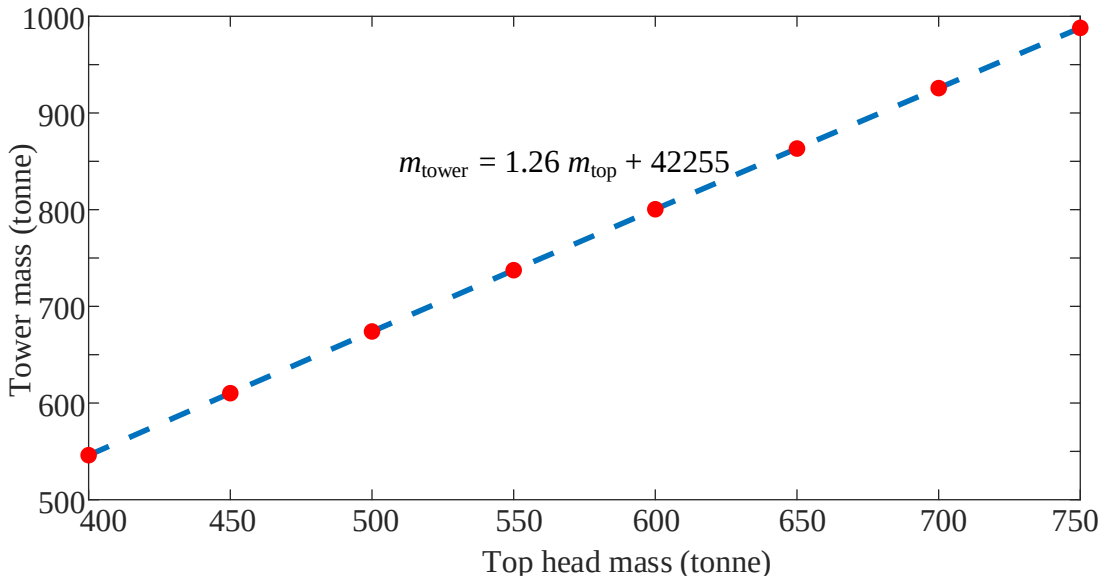

Figure 4.15: Tower mass for different turbine top head mass

Figure 4.15, 4.16, 4.17 and 4.18 shows the trend lines of tower mass, tower cost, Substructure and foundation mass, Substructure and foundation cost for different top head mass of a 6 MW wind turbine generator. These trend lines are applicable for all the generator topologies as the hub height and water depth for a 6 MW generator are assumed same.

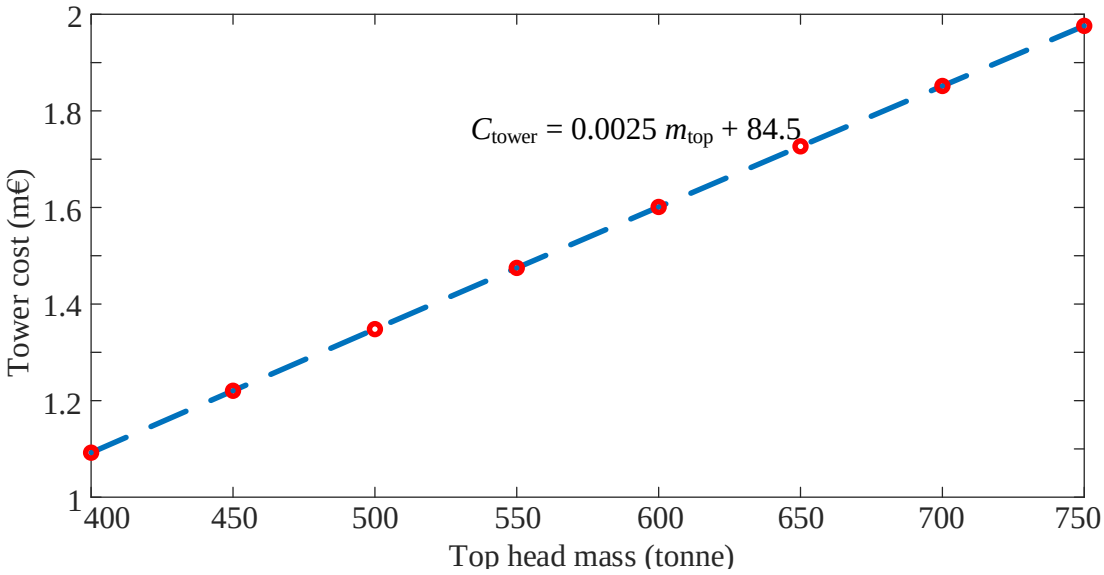

Figure 4.16: Tower cost for different turbine top head mass

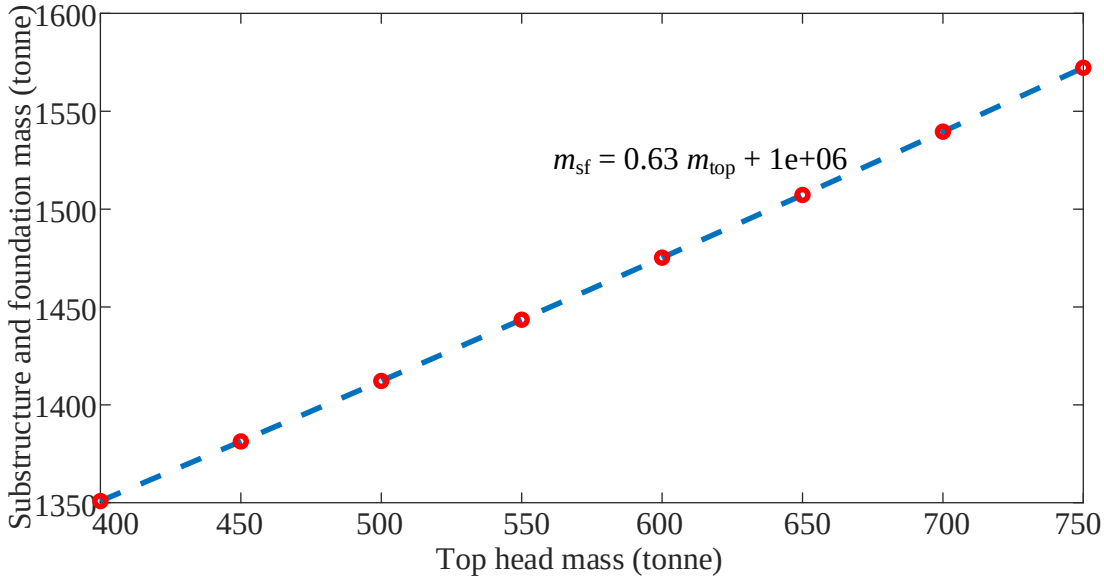

Figure 4.17: Substructure and foundation mass for different turbine top head mass

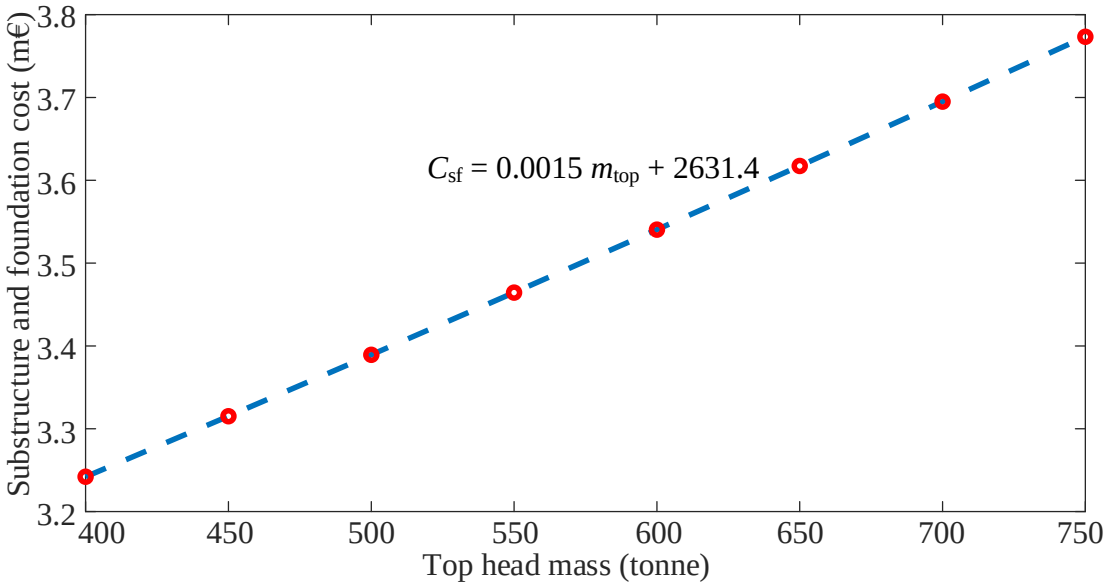

Figure 4.18: Substructure and foundation cost for different turbine top head mass

4.4.6 Lifting cost

For offshore wind turbines it was found that the lifting costs are not really dependent on the top head mass. The reason for this is, the vessels needed for all offshore projects are large heavy lift vessels with cranes attached and most of these ships have large cranes with ample ranges and typical lifting capacities of more than 1,500 tonnes. Thus they are capable of installing the turbines in this study as the top head mass of surface mounted Nd-Fe-B turbine is 450 tonnes and the maximum increased mass in flux concentrating ferrite turbine is 126 tonnes.

4.4.7 Turbine cost of energy

Turbine cost of energy can be calculated as,

$$CoE = \frac{(FCR \times ICC) + AOM}{E_y} \tag{4.26}$$

where *FCR* is the fixed charge rate given in Table 4.3, *ICC* is the initial capital cost of the turbine and *AOM* is the annual operation and maintenance cost.

The initial capital cost can be calculated as,

$$ICC = C_{\text{gact}} + C_{\text{gstr}} + C_{\text{tower}} + C_{\text{sf}} + C_{\text{fan}} + C_{\text{hex}} + C_{\text{rt}} \tag{4.27}$$

where C_{gact} is the generator active materials cost, C_{gstr} is the generator structural materials cost, C_{tower} is the tower cost, C_{sf} is the substructure and foundation cost, C_{hex}

is the cost of heat exchanger and C_{rt} is the rest of the turbine cost. The rest of the turbine cost for different rated power given in Table 4.3 are based on [69]. The annual operating and maintenance cost, *AOM*, is also given in Table 4.3. For the 6 MW turbine, the cost is taken from [99] and is scaled up for 8 MW and 10 MW according to [10], where costs are estimated on a \$0.027/kWh basis, the Annual Energy Productions are 30 GWh, 39 GWh and 48 GWh for the baseline design of 6 MW, 8 MW and 10 MW turbines respectively (assumed to be unaffected by the generator design) and \$1.29 = €1.

4.4.8 Cost modelling

Table 4.4 shows the cost modelling of different active and structural materials of the generator for the offshore wind turbine application. Where the lamination cost and copper costs are taken from [2]. Permanent magnet, ferrite magnet, rotor iron, aluminium and structural steel cost including marginal cost increases in going from raw material costs to manufacturing costs is drawn from the authors' experience.

Table 4.4: Generator cost modelling [2]

Cost Modeling	
Lamination cost (€/kg)	3
Copper cost (€/kg)	15
Permanent magnet cost (N40H magnet) (€/kg)	60
Ferrite magnet cost (€/kg)	3
Rotor iron cost (€/kg)	2
Aluminum cost (€/kg)	10
Structural steel cost (€/kg)	2
Price of kWh energy (€/kWh)	0.19

4.5 Baseline Design

The baseline design of structural and thermal model is for 6 MW generator, which is the extended part of electromagnetic baseline design given in section 3.2.

4.5.1 Structural model

Table 4.5 gives some results of the structural model for a 6 MW generator with different generator topologies. Structural costs are calculated using the cost modelling given in Table 4.4. Generator structural cost includes structural material costs and manufacturing costs. The structural costs in flux-concentrating machines are higher while the structural masses are lower in comparison to SM Nd-Fe-B machine. This is

because the flux-concentrating machines uses lightweight – but relatively expensive – aluminium in the rotor structure, in order to avoid high permeability paths which can encourage leakage flux.

Table 4.5: Baseline structural model results for different generator topologies

	SM Nd-Fe-B	**FC Nd-Fe-B**	**FC ferrite**
Generator structural mass (kg)	25352	20732	22084
Generator structural cost (k€)	101.4	116.2	119

4.5.2 Thermal model

Table 4.6 shows the temperature of different nodes of the thermal model for a 6 MW SM Nd-Fe-B generator baseline design without cooling. The magnet temperature of the baseline design is very high due to high power losses (mainly copper losses). The required cooling air-flow is also high to cool down the magnet temperature from 128.2^{o}C to 80^{o}C. The cooling requirements for the baseline design are given in Table 4.7. These results show the necessity of cooling this machine. Without additional cooling, the coil insulation would be damaged and the magnets would be subject to irreversible demagnetisation. Table 4.7, shows the additional cooling requirements to bring the magnet temperature to 80^{o}C.

Table 4.6: Baseline nodes temperature of thermal model before cooling for a 6 MW SM Nd-Fe-B generator

Nodes	**Analytical (°C)**
Yoke above a tooth	257.8
Bottom coil side in a slot	266.5
Top coil side in a slot	268.7
Magnet	128.2

Table 4.7: Cooling requirements for the baseline design of 6 MW SM Nd-Fe-B

Required cooling airflow at rated speed (m^3/s)	1.69
Number of parallel fans	6
Number of series fan	5
Number of heat exchanger	6

4.5.3 Tower and foundation

Machine mass does affect tower and foundation costs. The tower and foundation costs of the baseline designs are given in Table 4.8.

Table 4.8: Tower and foundation costs of the baseline design

	SM Nd-Fe-B	**FC Nd-Fe-B**	**FC ferrite**
Tower cost (k€)	1219.5	1216.2	1433.4
Foundation cost (k€)	3414.7	3413	3523.1

4.5.4 Annual energy production and cost of energy

The annual energy production E_y and cost of energy (*CoE*) for the baseline design of different generator topologies are given in Table 4.9.

Table 4.9: Annual energy production and cost of energy for baseline design

	SM Nd-Fe-B	**FC Nd-Fe-B**	**FC ferrite**
E_y (GWh)	28.8	29.5	29
CoE (€/MWh)	108.3	105.8	108.9

4.6 Discussions and conclusions

This chapter describes the method of structural modelling, thermal modelling, cooling system, turbine, cost modelling, the calculation of tower, substructure and foundation costs, annual energy production and overall cost of energy for offshore wind turbine. The analytical thermal model is verified using finite element software. The influence of varying inertia and turbine with different power ratings are also described in this chapter. The results for baseline design of structural and thermal model, tower, substructure and foundation, annual energy production and overall cost of energy are also shown in this chapter. The next chapter will describe the optimisation process, which will help to answer the primary research question.

Chapter 5

Optimisation

5.1 Introduction

The generator designer needs to deliver a number of performance characteristics including high efficiency, low power losses at part load, high availability, low machine mass, reduced volume and lower material and manufacturing costs. Normally the designers employ some element of optimisation to achieve the best balance of these aspects [18]. To achieve the best performance machine, the overall machine model (electromagnetic, structural and thermal model from chapter 3 and chapter 4) is optimised in this study.

The main purpose of this chapter is:

- To examine different objective functions for different generator topologies to test whether the recommendation of objective functions is independent of the machine type
- To investigate the effect on the optimisation of a number of factors that interest a typical designer: the inclusion of structural and thermal model along with the electromagnetic model in the objective functions, the choice of magnet grade, the inclusion of a cooling system, the inclusion of the impact of generator mass on the cost of turbine tower and foundation, the upper limit of generator diameter, the sensitivity results to magnet specific cost, turbine cost, operation and maintenance cost and the wind conditions
- To find the best way of optimisation and the factors or approaches that should be or shouldn't be included in the optimisation process

Design optimisation methods generally use an algorithm which takes independent variables as inputs and varies those inputs to evaluate modelled dependent variables and hence optimise an objective function (subject to predetermined constraints). In this chapter, the independent variables and constraints are described in the following section 5.2. The analytical models are used to evaluate a range of different dependent

variables, some of them contribute to the objective functions laid out in section 5.3. The process is driven by optimisation algorithm as described in section 5.4. The post processing and optimisation runs/investigations comes after that.

This chapter is an important step to answer secondary research questions $Q1$, $Q2$, $Q3$, $Q4$, $Q5$ and $Q6$. The following chapter (chapter 6) gives the results and discussions for each of the optimisation run in this chapter to find the best performance machine.

5.2 Independent variables and constraints

The chosen independent variables are based on other research papers and their output.

Table 5.1: Boundary limits for independent variables

Surface mounted Nd-Fe-B generator						
	6 MW		8 MW		10 MW	
Independent variables	LB	UB	LB	UB	LB	UB
Air-gap diameter, D (m)	6	15	6	16	6	17
Axial length, l_s (m)	0.7	1.8	0.7	2	0.7	2.2
Magnet width/pole pitch, w_m/τ_p	0.5	0.9	0.5	0.9	0.5	0.9
Magnet height, h_m (m)	0.01	0.06	0.01	0.08	0.01	0.1
Pole pairs, p (-)	60	100	60	100	60	100
Height of tooth, h_t (m)	0.04	0.09	0.04	0.1	0.04	0.11
Flux concentrating Nd-Fe-B generator						
Air-gap diameter, D (m)	6	15	6	16	6	17
Axial length, l_s (m)	0.7	1.8	0.7	2	0.7	2.2
Magnet width/pole pitch, w_m/τ_p	0.5	0.9	0.5	0.9	0.5	0.9
Magnet height, h_m (m)	0.01	0.08	0.01	0.12	0.01	0.15
Pole pairs, p (-)	60	100	60	100	60	100
Height of tooth, h_t (m)	0.04	0.09	0.04	0.1	0.04	0.11
Flux concentrating ferrite generator						
Air-gap diameter, D (m)	6	15	6	18	6	20
Axial length, l_s (m)	0.7	1.8	0.7	2.2	0.7	2.4
Magnet width/pole pitch, w_m/τ_p	0.6	0.9	0.6	0.9	0.6	0.9
Magnet height, h_m (m)	0.1	0.8	0.1	0.9	0.1	1.2
Pole pairs, p (-)	60	100	60	100	60	100
Height of tooth, h_t (m)	0.04	0.09	0.04	0.1	0.04	0.11

The independent variables used in this study are machine diameter, axial length, magnet height, the ratio of magnet width to pole pitch, number of pole pairs and tooth height.

The optimisation algorithm chooses these independent variables randomly from a given boundary limit. Boundaries are used to limit search space, time and remove unfeasible combinations. The boundaries for independent variables are initially chosen from the contour plot of baseline design in section 3.2 and then modified after primary optimisation runs and investigations given in section 5.6.1. The lower boundaries (LB) and the upper boundaries (UB) of independent variables for different generators are given in Table 5.1.

To simplify the optimisation, a number of assumptions and constraints are used, such as setting the air gap clearance to a fixed ratio of the machine diameter, maximum flux density (1.5 T) to avoid saturation in stator and rotor yoke and limiting rated electrical power to greater than or equal to 6, 8 or 10 MW depending on the required turbine ratings.

5.3 Objective Functions

The machine designer focuses on a number of performance characteristics including high efficiency, low power losses at part load, high availability, low machine mass, reduced volume and lower material and manufacturing costs. Normally the designers employ optimisation to achieve the best balance of these aspects. Different authors have approached the problem of formulating the objective function of such optimizations in different ways as shown in section 2.11. To achieve the best balance of machine performance, four different objective functions are used and compared for different performance characteristics in this study. The following subsections describe the objective functions.

5.3.1 Objective function 1

Reducing the use of rare-earth magnet is one of the most important issue for the machine designer. According to the aim of minimizing the use of rare-earth Nd-Fe-B magnets, the first objective function is rated generator torque T per magnet mass m_{PM}. This tries to minimize the amount of magnet material. In this case the objective function is,

$$F_1 = \frac{T}{m_{\mathrm{PM}}} \tag{5.1}$$

5.3.2 Objective function 2

Potgieter and Kamper discussed the importance of reducing the mass and cost of generator active materials [100]. The second objective function, F_2 seeks to minimize the cost of the electromagnetically active materials instead of only considering the magnet mass. The active materials cost includes the magnet cost C_{PM}, copper cost C_{Cu} and active iron cost C_{Fe}. This objective function is

$$F_2 = \frac{T}{C_{\mathrm{PM}} + C_{\mathrm{Cu}} + C_{\mathrm{Fe}}} \tag{5.2}$$

5.3.3 Objective function 3

The third objective function, F_3, presented in [7] seeks to minimise the cost of active material while maximizing the revenue produced from the wind turbine over a number of years, P_{y}. In this paper this objective function is assessed with P_{y} = 5, 10 and 15 years. This time period is multiplied by C_{E}, the revenue corresponding to 1 kWh of electrical energy and E_{y}, the annual energy yield of the turbine,

$$F_3 = C_{\mathrm{PM}} + C_{\mathrm{Cu}} + C_{\mathrm{Fe}} - P_{\mathrm{y}} C_{\mathrm{E}} E_{\mathrm{y}} \tag{5.3}$$

5.3.4 Objective function 4

The ultimate customer of the wind turbine manufacturer wants the lowest cost of energy and so the final objective function calculates this [11],

$$F_4 = CoE = \frac{(FCR \times ICC) + AOM}{E_{\mathrm{y}}} \tag{5.4}$$

The cost of energy, *CoE* is described in section 4.4.7

5.4 Optimisation process

There is a range of different optimisation approaches that can be used by the designers to find the best value of an objective function from some set of available alternatives. The Genetic Algorithm (GA) and Particle Swarm Optimization (PSO) are the most commonly used optimisation algorithm [8], [18], [101-103].

In this study, a hybrid Genetic and Pattern Search (PS) algorithm which has been developed in MATLAB is used as an optimisation procedure [104], [105]. Although GAs are good at searching global optima over an entire problem region, the speed of

convergence to the optimal point can be slow [106]. A GA can reach the region near an optimum point relatively quickly but it takes longer to achieve convergence. On the other hand, deterministic optimisation methods like the PS are very efficient for local searching [107]. To compensate for the weaknesses of these two methods, a hybrid algorithm combining both methods was proposed in [108]. The Genetic Algorithm (GA), the Pattern Search (PS) and the optimisation process using hybrid algorithm are described in following subsection.

5.4.1 Genetic Algorithm

The GA have been proved to be good and reliable methods of solving such problems. They are suitable for both constrained and unconstrained optimisation problems based on a natural selection process that mimics biological evolution. The algorithm repeatedly modifies a population of individual solutions. At each step, the GA selects individuals randomly from the current population and uses them as parents to produce the children for the next generation. Over consecutive generations, the population advances towards an optimal solution. It can solve the problems that are not suitable for standard optimisation algorithms, including problems in which the objective function is discontinuous, non-differentiable, stochastic, or highly nonlinear [104], [109].

5.4.2 Pattern Search

The PS is a direct search method for solving optimisation problems that does not require any information about the gradient of the objective function. The PS is good for local search which searches a set of points around the current point, looking for one where the value of the objective function is lower than the value at the current point. It can be used to solve problems for which the objective function is not differentiable, or is not even continuous. At each step, the algorithm searches a set of points around the current point (the point computed at the previous step of the algorithm), that called a mesh. The mesh is formed by adding the current point to a scalar multiple of a set of vectors called a pattern. If the PS finds a point in the mesh that improves the objective function at the current point, the new point becomes the current point for the next step of the algorithm [104]. In such method, the PS finds the local optimum result.

5.4.3 Optimisation process using hybrid algorithm

In the hybrid algorithm technique, a global search is carried out first using the GA for a small number of generations to get near to an optimum point. Then the solution from the GA is used as an initial point for the PS that is faster and more efficient for a local search. The solution from this Pattern Search is considered as the global optimal solution. In this case, the GA developed by [110] was used in MATLAB. The hybrid optimisation algorithm [104] runs in a way that takes the results of the Genetic Algorithm as an initial guess for the Pattern Search to get the global minimum for each of the objective functions.

Figure 5.1 shows the flow chart of the optimisation process. The GA starts by generating an initial population randomly from the boundary limit design space of independent variables given in Table 5.1. For this initial population, the GA evaluates the fitness of each candidate against a given objective function. The GA runs for a number of generations (until it reaches the maximum generation number set for this algorithm) and in each generation, a new population is created using selection, crossover and mutation. The best results after the maximum generations of GA (which are near to the global optimal result) are used as the initial point of the Pattern Search algorithm to make a further optimisation (local search near to global optimal point). At the next step, the PS constructs a pattern vector to create mesh point using the results of independent variables from the GA. After that, the PS evaluates the fitness of this initial mesh point for the given objective function. If there any improved results found at the mesh point, then the PS expands the mesh size and constructs a new pattern vector to create a new mesh point and evaluates the fitness of the new mesh point. If there is no improvement in results and no stopping criteria occurs, then the PS contracts the mesh size and evaluates the fitness of the new mesh point. If any stopping criteria occur, then the PS gives the final result of optimisation. Stopping criteria includes constraint, function and mesh tolerance.

The number of generations used for the GA is 4 (after 4 generations the GA gives results near to the global optimal solution in this study), the population size is 100, the maximum stall generation is 10 and the function tolerance is 1×10^{-3}. The mutation function chosen is adaptive feasible. For the Pattern Search algorithm, the mesh size expansion factor is 2 and the mesh size contraction factor is 0.5 [104].

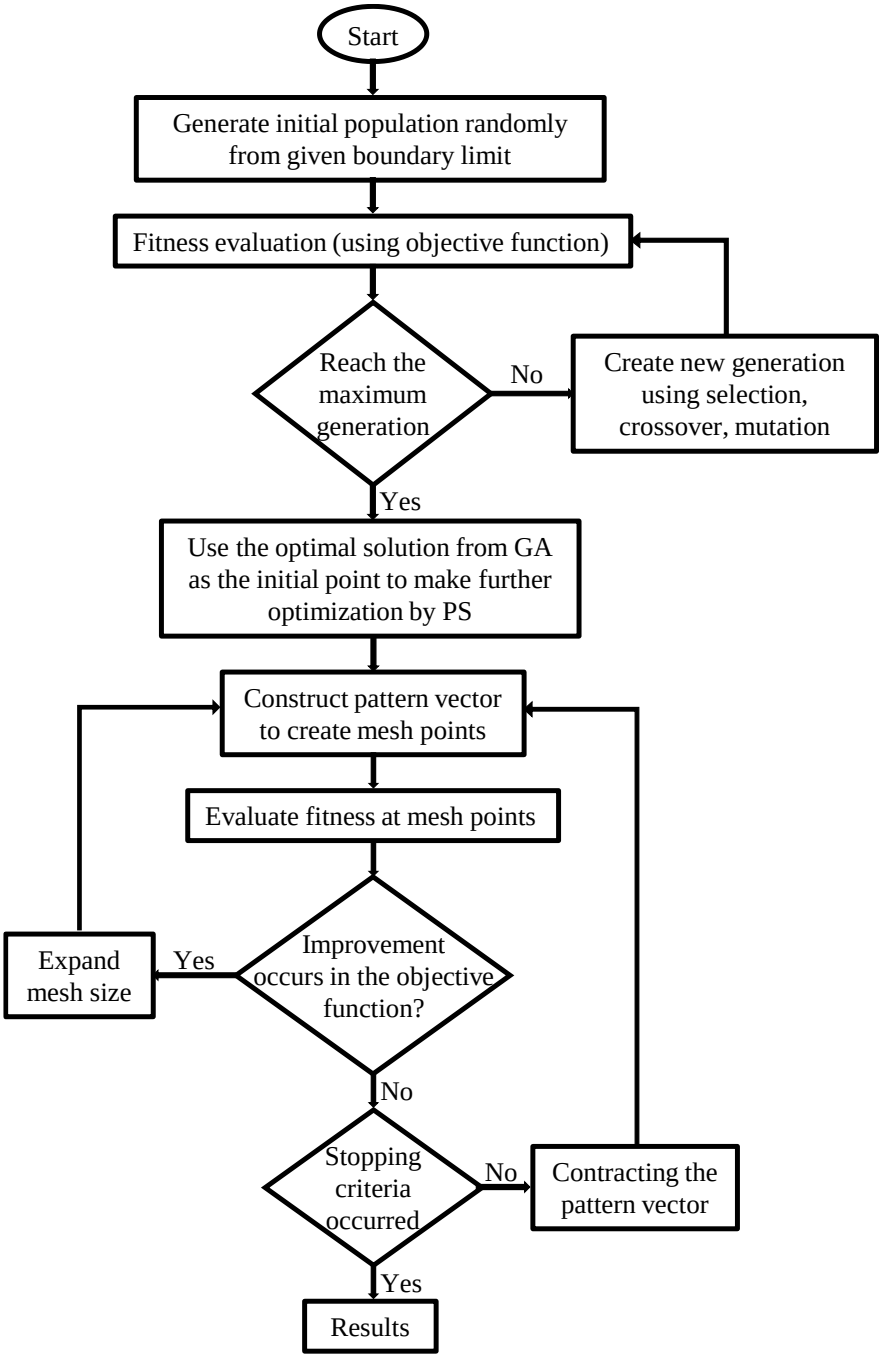

Figure 5.1: Flow chart for optimisation process

A typical optimisation run for a SM Nd-Fe-B generator takes 7 min in MATLAB 2014 on a 64 bit Windows 7 operating system on a PC with an Intel core i7 3.4GHz processor.

5.5 Post Processing

After the optimisation process is complete, the equations (5.1) to (5.4) are applied to all the optimised designs to compare the results of objective functions in each optimised design. Table 5.2 shows the format of results for equations (5.1) to (5.4) in

the left hand side of the table for each objective function (on the top of the table) after optimisation. The lowest value of each equation should be the result where the equation number and objective function is same. Dependent variables such as efficiency, annual energy production, losses, flux density, cost and masses of different active and structural materials are produced after optimisation.

Table 5.2: Format of post processing results for different objective functions

Equations	**Objective functions**			
	$\boldsymbol{F_1}$	$\boldsymbol{F_2}$	$\boldsymbol{F_3}$	$\boldsymbol{F_4}$
F_1 (N.m / kg)				
F_2 (N.m / €)				
F_3 (k€)				
F_4 (€ / MWh)				

5.6 Runs/Investigations

5.6.1 Choice of objective function

Initially the optimisation program was run for two generator types (SM Nd-Fe-B, and FC ferrite generators) for each of the four objective functions. Optimisation program runs from the analytical model coded in MATLAB for all the four objective functions and the fitness function for each objective function was set accordingly.

Table 5.3: Initial boundary limits for independent variables

Independent Variables	**SM Nd-Fe-B**		**FC ferrite**	
	LB	UB	LB	UB
Air gap diameter, D (m)	6	10	6	10
Axial length, l_s (m)	0.7	1.8	0.7	1.8
Magnet width/pole pitch, w_m/τ_p	0.5	0.9	0.6	0.9
Magnet height, h_m (m)	0.01	0.04	0.1	0.45
Pole pairs, p (-)	60	100	60	100
Height of tooth, h_t (m)	0.04	0.09	0.04	0.09

Independent variables and constraints are the same for all the objective functions. The boundaries for independent variables are initially chosen from the contour plot of baseline design. The rated power set for all the generator types was 6 MW. Table 5.3 shows the initial boundary limits for independent variables chosen from the contour plot of baseline design given in section 3.2.

Surface-mounted Nd-Fe-B Generator

Figure 5.2 shows the efficiency curves for different designs with surface-mounted Nd-Fe-B magnet. Table 5.4 gives the independent variables selected by the optimisation for the objective functions (where F_3(i), F_3(ii), F_3(iii) represents the third objective function when P_y is 5, 10 and 15 years respectively), some dependent variables, performance outputs and post-processed optimisation results using equations (5.1) - (5.4). The optimal result for each objective function is also highlighted in Table 5.4.

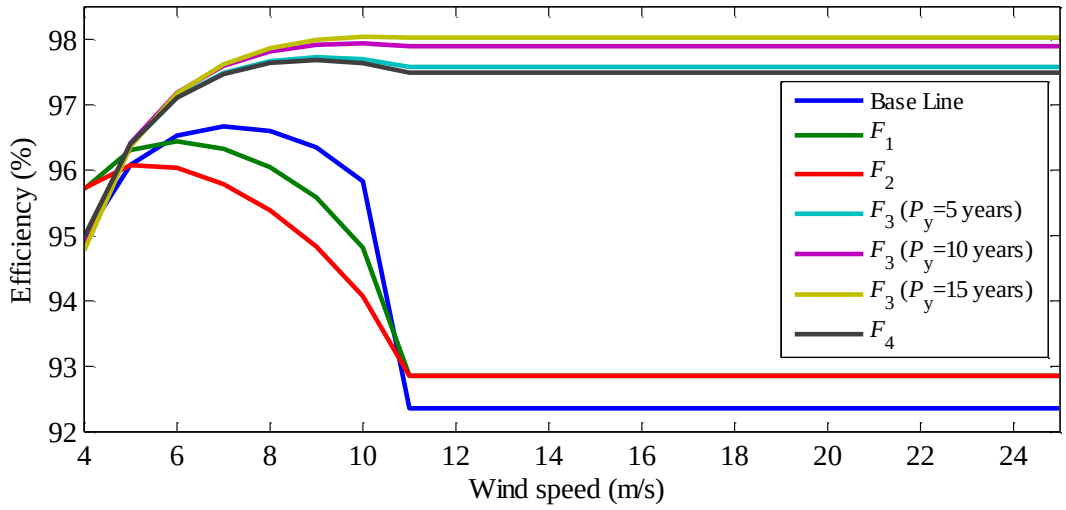

Figure 5.2: Baseline and optimised efficiency curves for different objective functions with 6 MW SM Nd-Fe-B generators

The objective function F_3 (with P_y=15 years) gives the highest efficiency at rated wind speed which is 98.0% and except the baseline, F_1 and F_2 give the lowest efficiency of 92.9%. F_3 and F_4 give similar efficiency at rated wind speed where F_3 is slightly higher than F_4; efficiency in F_3 increases with P_y.

Table 5.4: Optimisation results for a 6 MW SM Nd-Fe-B generator with different objective functions, where F_1, F_2 and F_4 represents first, second and fourth objective function *and* $F_3(i)$, $F_3(ii)$, $F_3(iii)$ represents the third objective function when number of years, P_y is 5, 10 and 15 years respectively

	F_1	F_2	F_3(i)	F_3(ii)	F_3(iii)	F_4
Air gap diameter, D (m)	9.03	8.36	9.99	9.99	9.99	9.92
Axial length, L (m)	1.62	1.17	1.19	1.33	1.41	1.17
Magnet width/pole pitch, w_m/τ_p	0.69	0.81	0.8	0.82	0.82	0.81
Magnet height, h_m (m)	0.012	0.018	0.021	0.023	0.025	0.021
Pole pairs, p (-)	100	100	98	79	72	100
Height of tooth, h_t (m)	0.053	0.045	0.09	0.09	0.09	0.09
Airgap flux density, B_g (T)	0.71	0.927	0.93	0.95	0.97	0.92
Height of rotor yoke, h_{ry} (m)	0.02	0.027	0.033	0.042	0.048	0.03
Height of stator yoke, h_{sy} (m)	0.02	0.027	0.033	0.042	0.048	0.03
Mass of magnet, m_{PM} (kg)	2980.8	3292.7	4807.5	6069.6	6966.6	4632.4
Mass of copper, m_{Cu} (kg)	7636.5	4536.3	11469	13100	14027	11192
Mass of active iron, m_{Fe} (kg)	24577	18476	32633	42759	48968	31465
Copper Losses (MWh)	1868.1	1969.7	529.6	437.12	392.95	556.36
Iron Losses (MWh)	164.15	139.95	264.66	269.24	278.01	261.08
AEP (GWh)	28.82	28.74	29.98	30.06	30.1	29.96
Cost of generator active materials, C_{gact} (k€)	367.1	321	558.4	688.9	775.3	540.2
F_1^{-1} (Nm/kg)	**1598.4**	1446.9	1041.2	833.3	714.3	1079.6
F_2^{-1} (Nm/€)	12.97	**14.84**	8.96	7.29	6.49	9.26
F_3(i) (m€)	-26.9	-26.87	**-27.79**	-27.76	-27.71	-27.78
F_3(ii) (m€)	-54.3	-54.18	-56.27	**-56.31**	-56.3	-56.25
F_3(iii) (m€)	-81.66	-81.48	-84.75	-84.87	**-84.89**	-84.71
F_4(€/MWh)	108	108.1	104.9	105	105.2	**104.8**

Flux-concentrating ferrite generator

Figure 5.3 shows the efficiency curves for different designs with FC ferrite magnet. Table 5.5 gives the independent variables selected by the optimisation for the objective functions, some dependent variables, performance outputs and post-processed optimisation results using equations (5.1) - (5.4). The optimal result for each objective function is also highlighted in the Table.

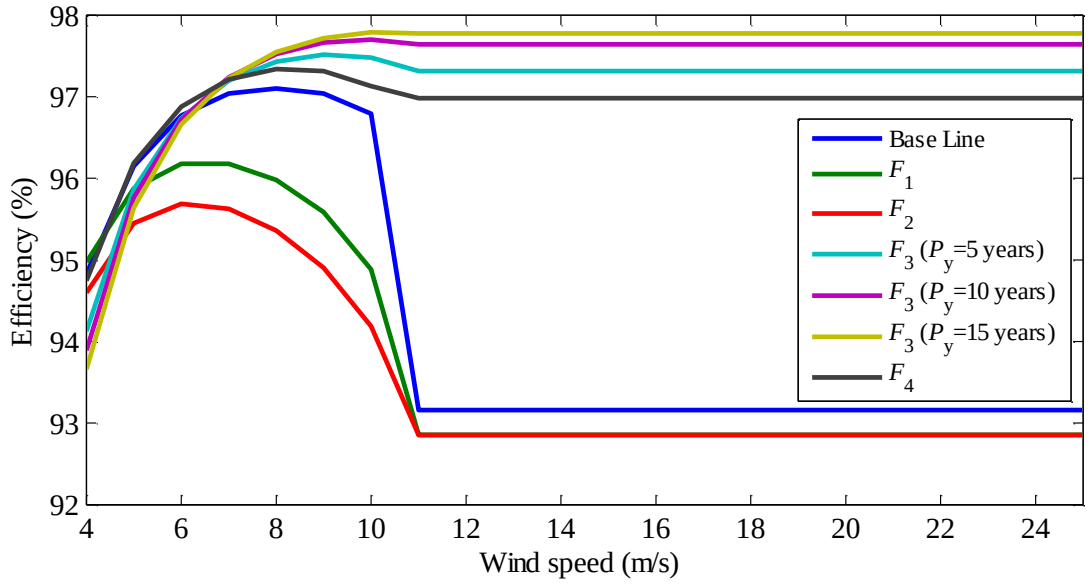

Figure 5.3: Baseline and optimised efficiency curves for different objective functions with 6 MW FC ferrite generators

The FC ferrite generators have similar efficiency to the SM Nd-Fe-B machines: F_3 gives maximum efficiency 97.8% at rated wind speed and F_1 and F_2 give a lower efficiency of 92.9%. F_3 and F_4 give similar efficiency where F_3 is slightly higher.

Table 5.5: Optimisation results for a 6 MW FC ferrite generator with different objective functions, where F_1, F_2 and F_4 represents first, second and fourth objective function and $F_3(i)$, $F_3(ii)$, $F_3(iii)$ represents the third objective function when number of years, P_y is 5, 10 and 15 years respectively

	F_1	F_2	F_3(i)	F_3(ii)	F_3(iii)	F_4
Air gap diameter, D (m)	9.24	9.14	9.99	9.99	9.99	9.9
Axial length, L (m)	1.64	1.51	1.45	1.48	1.63	1.29
Magnet width/pole pitch, w_m/τ_p	0.69	0.6	0.75	0.76	0.82	0.78
Magnet height, h_m (m)	0.23	0.28	0.38	0.45	0.45	0.39
Pole pairs, p (-)	88	100	73	64	60	74
Height of tooth, h_t (m)	0.052	0.041	0.089	0.09	0.09	0.089
Airgap flux density, B_g (T)	0.71	0.77	0.84	0.9	0.89	0.83
Height of stator yoke, h_{sy} (m)	0.024	0.021	0.038	0.047	0.05	0.038
Mass of magnet, m_{PM} (kg)	33700	40592	49782	59377	65094	42828
Mass of copper, m_{Cu} (kg)	7973.6	5671.1	14210	14978	16344	12825
Mass of active iron, m_{Fe} (kg)	54405	48302	89134	105480	118280	81260
Copper Losses (MWh)	1826.5	1895.9	571.9	469.8	417	708.2
Iron Losses (MWh)	209.8	215.7	307.9	324.7	343.1	264.9
AEP (GWh)	28.81	28.74	29.9	29.98	30.01	29.81
Cost of generator active materials, C_{gact} (k€)	383.9	351.7	629.9	719.2	795.3	564.6
F_1^{-1} (Nm/kg)	**140.8**	117.6	100	84	76.9	111.1
F_2^{-1} (Nm/€)	12.4	**13.6**	7.9	6.9	6.3	8.4
F_3(i) (m€)	-26.89	-26.78	**-27.7**	-27.6	-27.6	-27.6
F_3(ii) (m€)	-54.26	-54.09	-56	**-56.1**	-56.09	-55.9
F_3(iii) (m€)	-81.63	-81.39	-84.5	-84.57	**-84.62**	-84.3
F_4 (€/MWh)	108.4	108.8	105.9	106.1	106.2	**105.8**

Discussion on initial optimisation run

A number of different objective functions have been used in this study. It can be seen that each objective function produces a final design that gives the optimal value of that objective function highlighted in the table. For both generators, the objective functions F_1 and F_2 tend to produce lower efficiency machines than when energy yield in taken into account (as for F_3 and F_4). This is unsurprising as the formulations for F_3 and F_4 implicitly take losses into account.

Optimisation results in 1st objective function show the lowest magnet mass which makes highest torque per magnet mass and the 2nd objective function gives the lowest cost of generator active materials. The major difference is that F_1 achieves its goal at the expense of additional copper and iron mass. When the cost of energy is evaluated for the results of these optimisations, they give a high cost of energy. Even though the generator capital costs are the lowest, they sacrifice annual energy yield. This can be explained by the fact that the generator capital costs are a minority of the turbine capital costs, yet all of the turbine's energy in converted by the generator. This implies that generator efficiency is a higher priority than generator cost. The first and second objective functions are a poor choice when optimising wind turbine generators.

The major difference in losses between F_1/F_2 and F_3/F_4 is due to copper losses, with higher current density being used to reduce copper mass. More magnet is used in the 3rd and 4th objective functions which generally produces better air-gap flux density and helps to increase energy production. The balance of copper and iron losses are slightly different, with F_3/F_4 having slightly higher iron losses. It is because of lower mass and active iron that used in first two objective functions.

The resulting designs and cost of energy is very similar for F_3 and F_4. The third objective function does not include detailed turbine information and so is more general (Turbine cost of energy calculation is not the part of optimisation). The change in the number of years – for F_3 – does not make significant difference to the results. It may be that different turbine costs and designs may lead to a larger difference between F_3 and F_4.

It can be seen that, a designer can either chose F_3 or F_4 to produce an efficient machine design. Perhaps a designer might want to bias the results towards designs with higher efficiency could go for F_3 and lower cost of energy could go for F_4. It can also be seen

that the air-gap diameter in 3rd objective function always picks the highest limit of the boundary. So the upper boundary limits are modified according to the following section 5.6.2 and the modified boundary limits for independent variables are shown in Table 5.1.

5.6.2 Constraining diameter

Optimised results in 3rd objective function always tend to pick the maximum allowed diameter. This means the search for the optimal generator diameter; a typical problem that a machine designer needs to find. To see the highest possible diameter, the maximum allowed diameter is varied from 6m to 16m in upper boundary limit while the lower boundary limit remains same and runs the optimisation program for each diameter change for 3rd objective function.

5.6.3 Including structural materials

The optimisation program was run with both fixed and variable generator structural costs to see the effect on the cost of energy. For the fixed generator structural material model, a fixed cost is included with turbine initial capital cost and the structural mass is also fixed. For the variable generator structural materials, when the generator dimensions vary, structural mass is calculated and cost also varies. To investigate the effect of structural materials on turbine cost of energy, the 4th objective function was used in this study.

5.6.4 Variable generators top head mass

Top head mass of the turbine was varied by varying the generator mass to see the effect on tower and foundation cost and the cost of energy of the wind turbine. The 4th objective function was used to estimate the effect so that, it can optimise for minimum turbine cost of energy.

5.6.5 Variable power factor

Variable power factor was used to estimate the effect on the annual energy production and the cost of energy for a 6 MW SM Nd-Fe-B generator (It is assumed that the generators in this study run at unity power factor at all wind speeds except this variable power factor investigation). The 4th objective function was also used to estimate the effect for minimum cost of energy.

5.6.6 Choice of turbine power ratings

All the three generators are further optimised using different rated power (6, 8 and 10 MW) to compare the effect on over all turbine cost of energy and other variables. This was investigated using both 3rd and 4th objective functions.

5.6.7 Different magnet grade

The Nd-Fe-B magnet was varied from N35 to N52 (regular magnets) and N35H to N52H ("H" grade magnets) for a 6 MW SM Nd-Fe-B generator (baseline magnet grade in this study is N40H) using the 4th objective function to estimate the effect of different magnet grade on turbine cost of energy.

5.6.8 Including thermal model and cooling system

The thermal model is included in the optimisation program (using F_4) for a 6 MW Nd-Fe-B generator to calculate required cooling air flow to cool down the magnets temperature of generator from 120°C to 80°C. The optimisation was run using both "H" grade magnet and regular magnet with different magnet grades (N35 to N52). The effect on resistance and B_r is also included to calculate the cost of energy of the turbine with cooling.

5.6.9 Sensitivity analysis

Sensitivity analysis was performed for different magnet price, availability of the turbine, rest of the turbine cost, different wind condition and operation and maintenance cost to see the effect on cost of energy if each of these variables varies while other remains same.

5.7 Discussions and conclusions

In order to achieve best performance machine (best balance of performance characteristics including high efficiency, low power losses at part load, high availability, low machine mass, reduced volume and lower material and manufacturing costs, etc.), it is essential to optimise it. Optimisation result depends on the chosen objective function, constraints, independent variables and their limits. The selection of proper optimisation algorithm also important to achieve efficient optimised results in minimum time.

This chapter shows the optimisation process of different generators using different objective functions for large offshore wind turbine. The investigation was carried out to compare the optimisation results for different objective functions, generator

topologies, power ratings, magnet, temperature, cost of energy, annual energy production, losses and other variables to find the best performance machine and the best way of optimisation. It is found that the air-gap diameter in 3rd objective function always picks the highest limit of the boundary. So the upper boundary limits are modified for all the objective functions. The next chapter will present the optimisation results and detailed discussion to answer the primary research question.

Chapter 6

Results and Discussions

6.1 Introduction

A number of different optimisation runs and investigations are shown in previous chapter. This chapter presents the results of different optimisation runs and investigations given in section 5.6.

The main purpose of this chapter is:

- To present the results of different optimisation runs and investigations
- To compare and discuss the results in details

The performances of different generator topologies are presented in section 6.2.1. Next, the impact of generator air-gap diameter constraints, effect of generator and turbine structural models, effect of generator mass, effect of variable power factor, different turbine power ratings are presented in section 6.2.2 to 6.2.5. Effect of different magnet grades and effect of temperature and cooling cost are given in section 6.2.6 and 6.2.7. The sensitivity analysis results for different magnet price, availability of the turbine, rest of the turbine cost, different wind condition and operation and maintenance cost comes after that.

This chapter is an important step to answer secondary research questions $Q1$, $Q2$, $Q3$, $Q4$, $Q5$ and $Q6$ given in section 1.3. The following chapter (chapter 7) gives the overall conclusions for this study.

6.2 Results

6.2.1 Generator topologies

A number of different generator rotor topologies (Surface-mounted Nd-Fe-B generator, flux-concentrating Nd-Fe-B generator and flux-concentrating ferrite generator) are examined using Nd-Fe-B magnet and ferrite magnet to reduce the use of rare earth permanent magnet for offshore wind turbine. Four different objective

functions (F_1 to F_4 given in section 5.3) are used for optimisation to examine the effect on different generator topologies for a 6 MW offshore wind turbine.

6.2.1.1 Surface-mounted Nd-Fe-B generator

Table 6.1 shows the independent variables selected by the optimisation from Table 5.1 for the objective functions for a 6 MW SM Nd-Fe-B generator (where F_3 (i), F_3 (ii), F_3 (iii) represents the third objective function when P_y is 5, 10 and 15 years respectively). Figure 6.1 shows the efficiency curves for these different designs and Figure 6.2 shows the post-processed optimisation results using equation (5.1-5.4).

Table 6.1: Independent variables vs. objective functions, 6 MW SM Nd-Fe-B generators

Independent variables	F_1	F_2	F_3(i)	F_3(ii)	F_3(iii)	F_4
Air gap diameter, D (m)	8.4	8.4	10.3	11.4	11.9	10.2
Axial length, l_s (m)	1.27	1.29	1.24	1.45	1.38	1.2
Magnet width/pole pitch, w_m/τ_p	0.62	0.6	0.8	0.79	0.78	0.79
Magnet height, h_m (m)	0.02	0.022	0.019	0.017	0.02	0.02
Pole pairs, p (-)	100	100	99	89	82	100
Height of tooth, h_t (m)	0.059	0.048	0.089	0.089	0.089	0.083

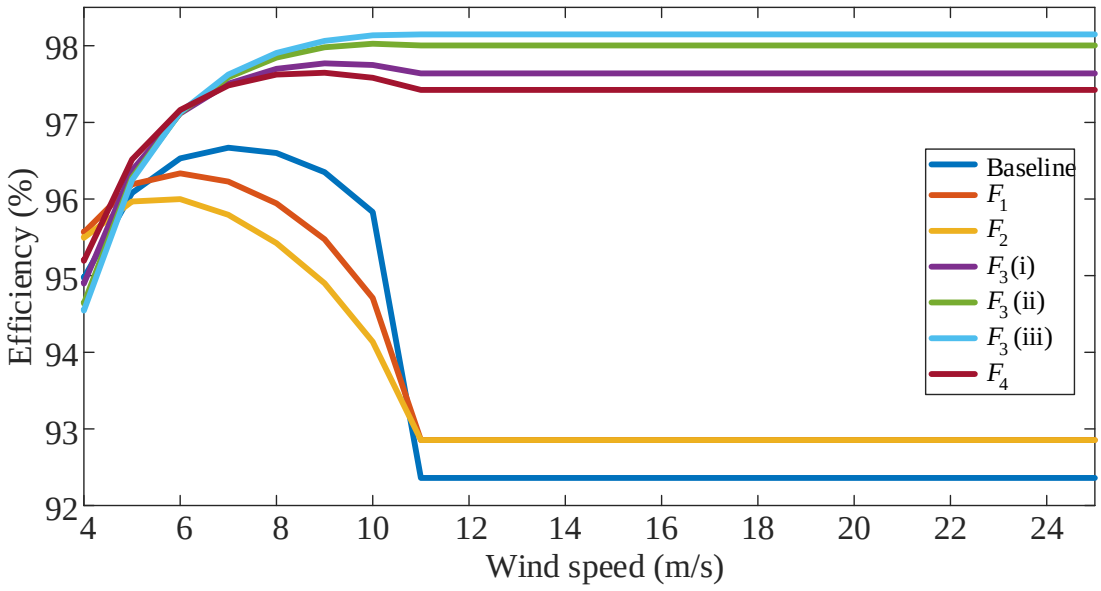

Figure 6.1: Baseline and optimised efficiency curves for different objective functions with 6 MW SM Nd-Fe-B generators

The objective function F_3 (iii) (with P_y=15 years) gives the highest efficiency at rated wind speed which is 98.15% and except the baseline, F_1 and F_2 give the lowest efficiency of 92.9%. F_3 and F_4 give similar efficiency at rated wind speed where F_3 is slightly higher than F_4; efficiency in F_3 increases with P_y.

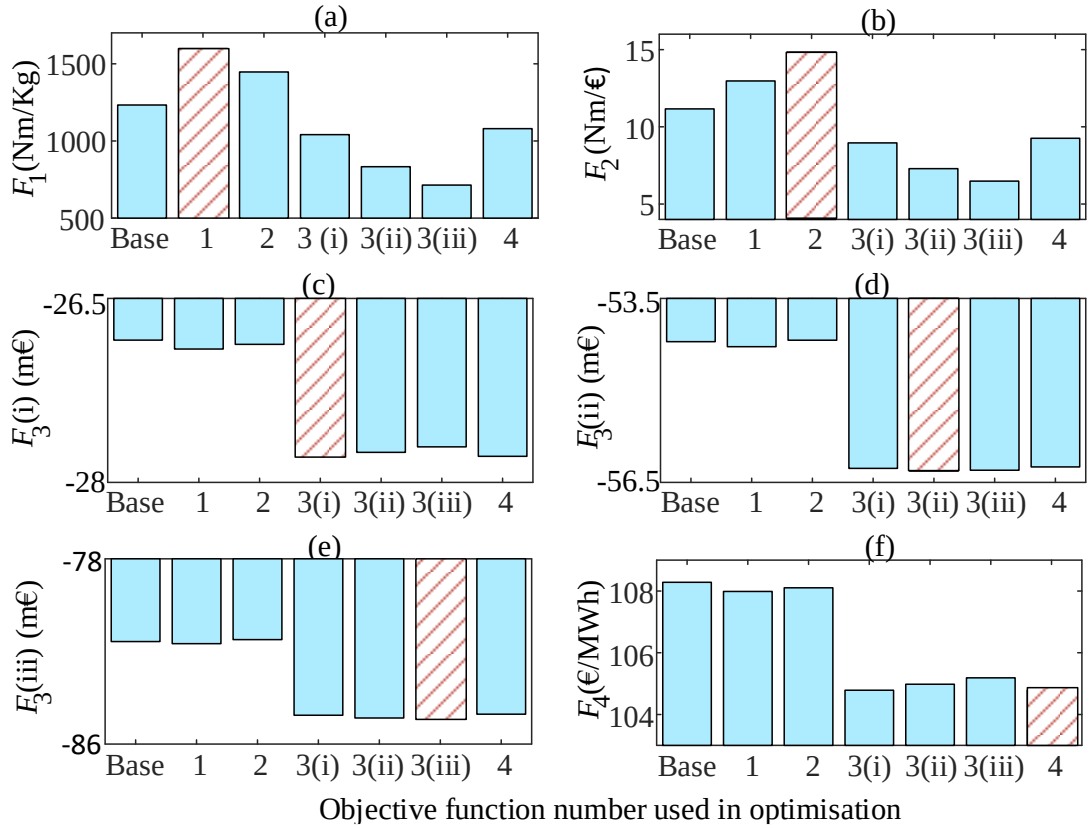

Figure 6.2: Optimisation results of different objective functions for the 6 MW SM Nd-Fe-B generators

The *y*-axis of Figure 6.2(a) shows the evaluated results of F_1 – equation (5.1) – for each of the different objective functions (as displayed on the *x*-axis) after post-processing. Similarly Figures 6.2(b)-(f) show the results for F_2-F_4. Each sub-figure has the optimal result highlighted, these values are 1479.8 Nm/kg, 14.1 Nm/€, -€27795k, -€56346k, -€84952k and €104.9/MWh.

F_1 gives highest torque per PM mass, where F_3 (iii) gives the lowest which is 43.7% less than F_1. In terms of torque per cost of active materials, F_2 gives the highest and F_3 (iii) gives the lowest which is 53.5% less than F_2. F_3 (i) closely match with F_4, moving from F_3 (i) to F_3 (iii) by increasing number of years P_y, both the torque per PM mass and torque per active materials cost decreases.

Table 6.2 shows some of the dependent variable results for different objective functions after optimisation. It can be seen that, F_4 closely match with F_3 (i) in terms

of turbine cost of energy. F_3 (ii) and F_3 (iii) produces better efficient machine design in terms of annual energy production and copper losses but gives higher turbine cost of energy.

Table 6.2: Some dependent variable results after optimisation, 6MW SM Nd-Fe-B

Dependent variables	F_1	F_2	F_3(i)	F_3(ii)	F_3(iii)	F_4
Air-gap flux density, B_g (T)	0.84	0.85	0.88	0.79	0.82	0.89
Mass of magnet, m_{PM} (kg)	3219.7	3409.4	4724.3	5403.2	6124.8	4502.4
Mass of copper, m_{Cu} (kg)	6409.5	5279.2	12280	16094	16516	10780
Mass of active iron, m_{Fe} (kg)	19489	18246	34598	47281	51100	31287
Structural mass, m_{str} (kg)	27770	28063	32560	28869	34490	32689
Copper losses (MWh)	1874.7	1947.8	508.6	389.4	343.1	593.2
Iron losses (MWh)	170.3	157.3	268.4	289.1	296.1	247.6
Cost of generator active materials, C_{gact} (k€)	347.8	338.5	571.4	707.4	768.5	525.7
Cost of generator structural materials, C_{gstr} (k€)	111.1	112.3	130.2	115.5	137.9	130.8
Annual energy production (GWh)	28.8	28.75	30	30.09	30.13	29.94
Cost of energy (€/MWh)	107.9	108.1	105	105.3	105.7	104.9

6.2.1.2 Flux-concentrating Nd-Fe-B generator

Table 6.3 shows the independent variables selected by the objective functions from Table 5.1 for the FC Nd-Fe-B generators. Figure 6.3 shows the efficiency curves for these different designs and Figure 6.4 shows the optimization results for the different objective functions after post-processing.

Table 6. 3: Independent variables vs. objective functions, 6 MW FC Nd-Fe-B generators

Independent variables	F_1	F_2	F_3(i)	F_3(ii)	F_3(iii)	F_4
Air gap diameter, D (m)	7.27	7.27	9.97	10.74	11.53	9.57
Axial length, l_s (m)	1.44	1.44	1.15	1.24	1.27	1.08
Magnet width/pole pitch, w_m/τ_p	0.79	0.79	0.76	0.78	0.79	0.75
Magnet height, h_m (m)	0.065	0.068	0.074	0.079	0.08	0.074
Pole pairs, p (-)	97	100	100	95	91	100
Height of tooth, h_t (m)	0.06	0.04	0.09	0.09	0.09	0.09

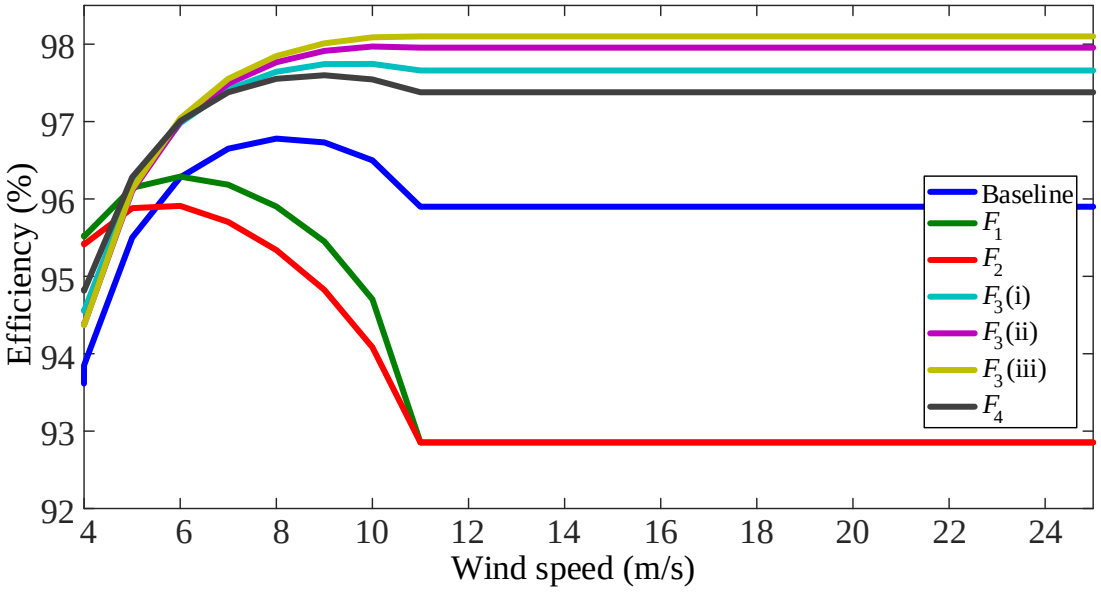

Figure 6.3: Baseline and optimised efficiency curves for different objective functions with 6 MW FC Nd-Fe-B generators

The FC Nd-Fe-B generators have similar efficiency to the SM Nd-Fe-B machines: F_3 (iii) gives maximum efficiency 98.1% at rated wind speed and F_1 and F_2 give a lower efficiency of 92.9%. F_3 and F_4 give similar efficiency where F_3 is slightly higher.

Figure 6.4 is laid out as Figure 6.2 is, with the evaluated results of F_1–F_4 for each of the different objective functions after post-processing. In each sub-figure the optimal result is highlighted, i.e. 1413.9 Nm/kg, 13.26 Nm/€, -€27813k, -€56345k, -€84932k and €104.8/MWh.

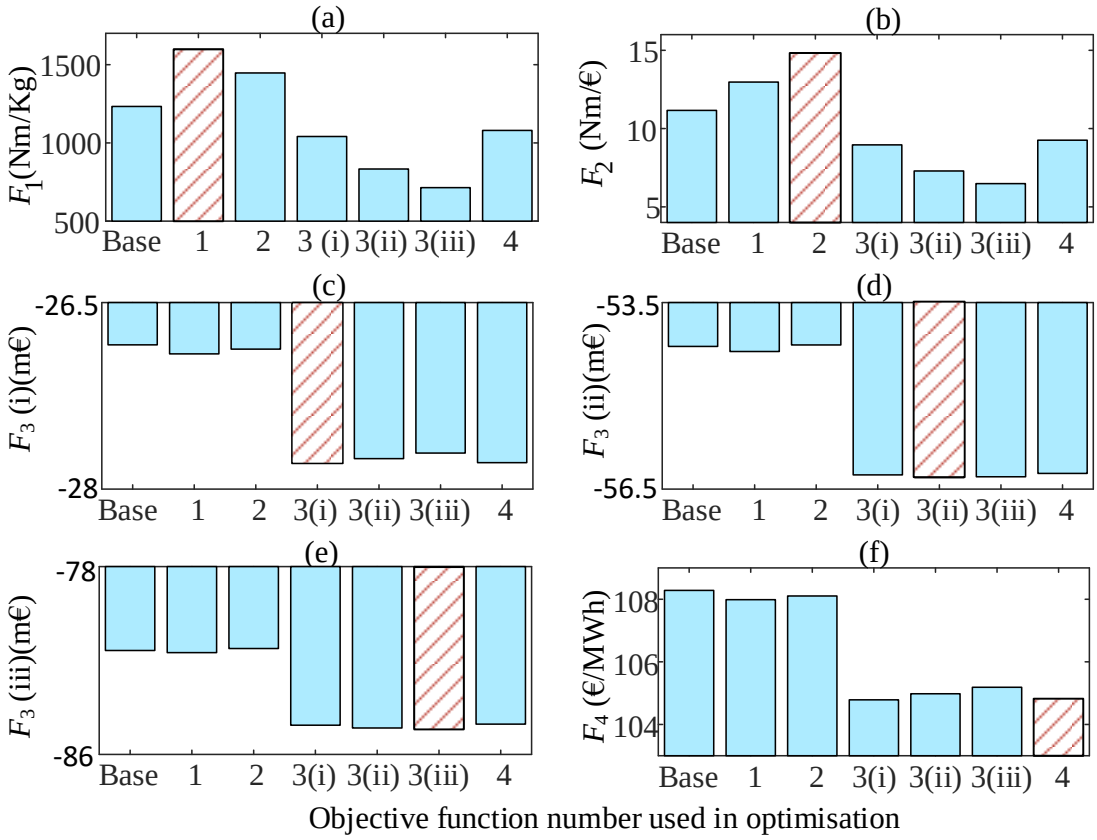

Figure 6.4: Optimisation results of different objective functions for the 6 MW FC Nd-Fe-B generators

For the FC Nd-Fe-B generator optimisation, F_1 gives highest torque per PM mass, where F_3 (iii) gives the lowest which is 41.1% less than F_1. In terms of torque per cost of active materials, F_2 gives the highest and F_3 (iii) gives the lowest which is 48.7% less than F_2. F_3 (i) closely match with F_4, moving from F_3 (i) to F_3 (iii) by increasing number of years P_y, both the torque per PM mass and torque per active materials cost decreases.

Table 6.4 shows some of the dependent variable results for different objective functions after optimisation. It can be seen that, for FC Nd-Fe-B generator also F_4 closely match with F_3 (i) in terms of turbine cost of energy. F_3 (ii) and F_3 (iii) produces better efficient machine design in terms of annual energy production and copper losses but gives higher turbine cost of energy.

Table 6.4: Some dependent variable results after optimisation, 6MW FC Nd-Fe-B

Dependent variables	F_1	F_2	F_3(i)	F_3(ii)	F_3(iii)	F_4
Air-gap flux density, B_g (T)	1	1.03	0.99	0.94	0.88	1.03
Mass of magnet, m_{PM} (kg)	3369.8	3544.8	4946	5544.4	5962.3	4469.5
Mass of copper, m_{Cu} (kg)	5593.3	4393.4	10859	12962	14619	9494.9
Mass of active iron, m_{Fe} (kg)	27813	26933	38986	47875	54367	34239
Structural mass, m_{str} (kg)	19112	19037	26138	29254	34629	25847
Copper losses (MWh)	1875.7	1953.5	487.9	392.6	349.1	582.1
Iron losses (MWh)	171.7	159.6	290.1	304.9	307.2	269.5
Cost of generator active materials, C_{gact} (k€)	369.5	359.4	576.6	670.7	740.1	520.5
Cost of generator structural materials, C_{gstr} (k€)	77.8	77.5	106.1	118.8	140.5	104.8
Annual energy production (GWh)	28.8	28.7	29.9	30.1	30.1	29.9
Cost of energy (€/MWh)	107.9	108	104.9	105.2	105.7	104.8

6.2.1.3 Flux-concentrating ferrite generator

Table 6.5 shows the independent variables selected by the objective functions from Table 5.1 for the FC ferrite generators. Figure 6.5 shows the efficiency curves for these different designs and Figure 6.6 shows the optimisation results for the different objective functions after post-processing.

Table 6.5: Independent variables vs. objective functions, 6 MW FC ferrite generators

Independent variables	F_1	F_2	F_3(i)	F_3(ii)	F_3(iii)	F_4
Air gap diameter, D (m)	12.03	8.25	11.89	11.77	11.8	12.09
Axial length, l_s (m)	1.41	1.59	1.5	1.52	1.51	1.5
Magnet width/pole pitch, w_m/τ_p	0.77	0.6	0.75	0.77	0.77	0.69
Magnet height, h_m (m)	0.2	0.33	0.28	0.33	0.38	0.23
Pole pairs, p (-)	100	94	95	79	71	100
Height of tooth, h_t (m)	0.05	0.05	0.08	0.09	0.09	0.07

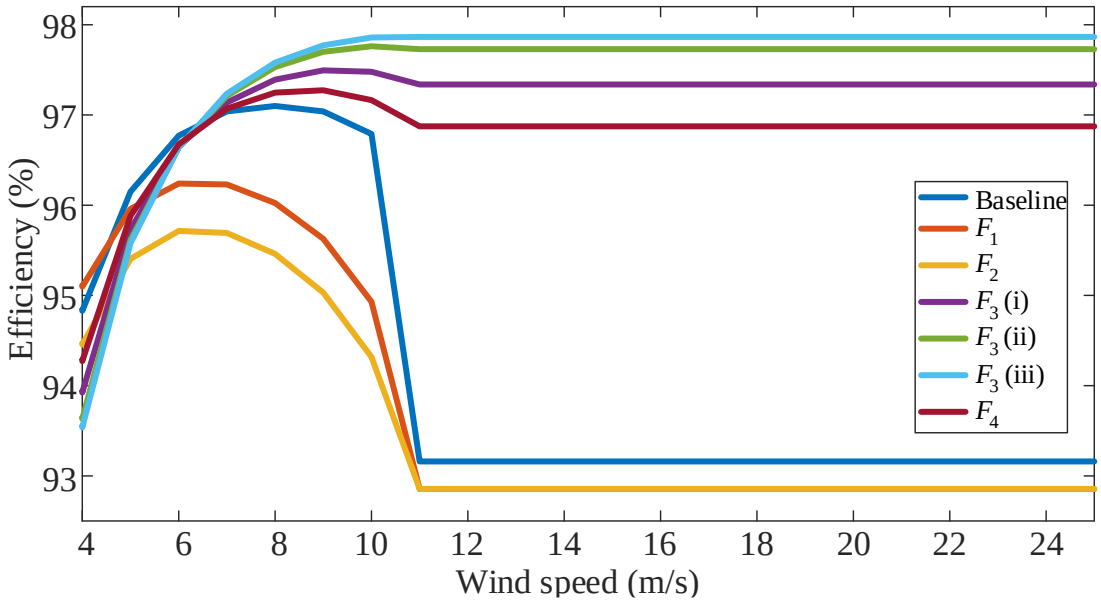

Figure 6.5:Baseline and optimised efficiency curves for different objective functions with 6 MW FC ferrite generators

The FC ferrite generators also have similar efficiency to the Nd-Fe-B machines: F_3 (iii) gives maximum efficiency 97.9% at rated wind speed and F_1 and F_2 give a lower efficiency of 92.9%. F_3 and F_4 give similar efficiency where F_3 is slightly higher.

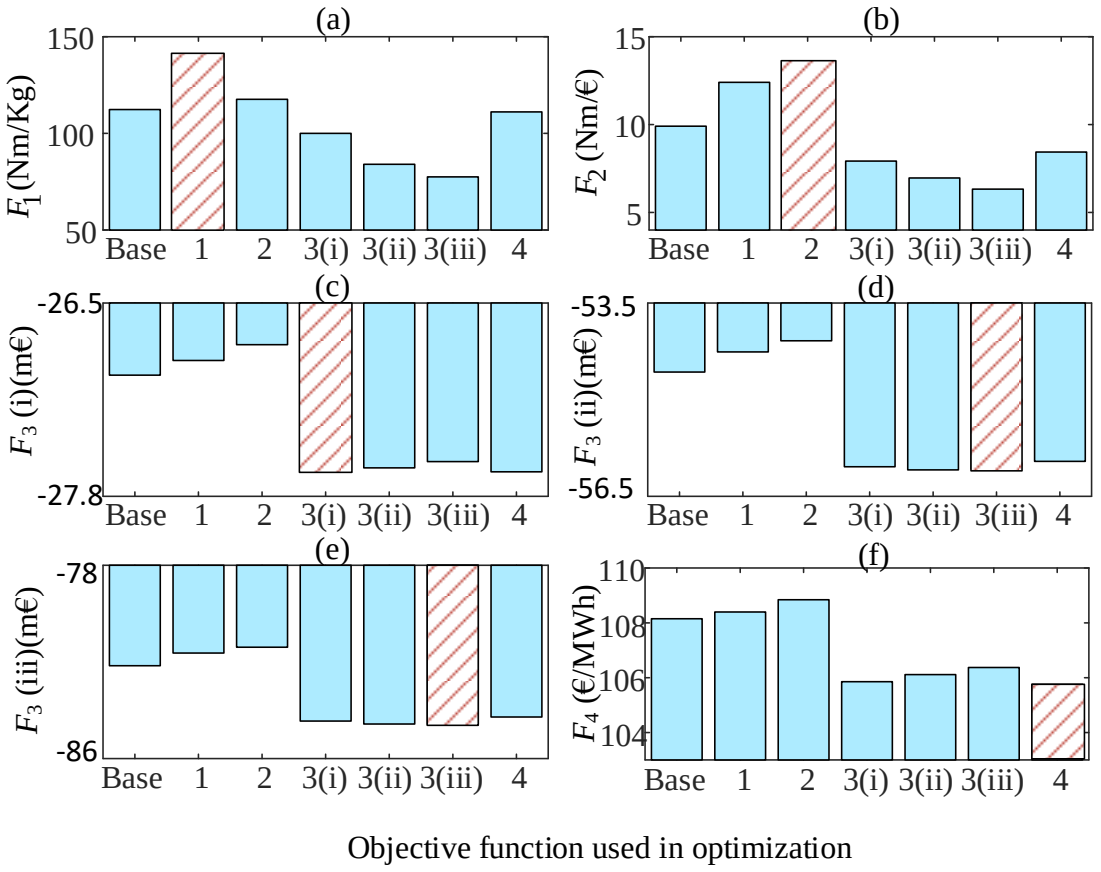

Figure 6.6: Optimisation results of different objective functions for the 6 MW FC ferrite generators

Figure 6.6 is also laid out as Figure 6.2 is, with the evaluated results of F_1–F_4 for each of the different objective functions after post-processing. In each sub-figure the optimal result is highlighted, i.e. 161.3 Nm/kg, 12.6 Nm/€, -€27670k, -€56133k, -€84648k and €106.5/MWh.

For the FC ferrite generator optimisation, F_1 gives highest torque per PM mass, where F_3 (iii) gives the lowest which is 47% less than F_1. In terms of torque per cost of active materials, F_2 gives the highest and F_3 (iii) gives the lowest which is 49.5% less than F_2. F_3 (i) closely match with F_4, moving from F_3 (i) to F_3 (iii) by increasing number of years P_y, both the torque per PM mass and torque per active materials cost decreases.

Table 6.6 shows some of the dependent variable results for different objective functions after optimisation. It can be seen that, for FC ferrite generator also F_4 closely match with F_3 (i) in terms of turbine cost of energy. F_3 (ii) and F_3 (iii) produces better efficient machine design in terms of annual energy production and copper losses but gives higher turbine cost of energy.

Table 6.6: Some dependent variable results after optimisation, 6MW FC ferrite

Dependent variables	F_1	F_2	F_3(i)	F_3(ii)	F_3(iii)	F_4
Air-gap flux density, B_g (T)	0.56	0.84	0.67	0.72	0.76	0.62
Mass of magnet, m_{PM} (kg)	29411	44338	44326	52365	58851	38838
Mass of copper, m_{Cu} (kg)	8436	5914.3	15289	17660	18176	13964
Mass of active iron, m_{Fe} (kg)	56893	51818	83915	101380	112950	68818
Structural mass, m_{str} (kg)	27422	27000	27319	28290	30002	27925
Copper losses (MWh)	1826.4	1871.5	554.4	429.1	386.9	702.4
Iron losses (MWh)	203.9	227.9	323.7	344.8	351	296.6
Cost of generator active materials, C_{gact} (k€)	385.5	377.2	614.1	726.1	788	532.4
Cost of generator structural materials, C_{gstr} (k€)	111.9	168.1	122.3	139.2	157.4	127.8
Annual energy production (GWh)	28.8	28.8	29.9	30	30	29.8
Cost of energy (€/MWh)	109	109.6	106.7	107.3	107.8	106.5

6.2.1.4 Comparison of generator topologies

Table 6.7 compares the 3 types of generators by best possible objective function F_1, F_2, F_3, F_4; independent variables (light grey); important dependent variables (dark grey). It shows the generator type and objective function that gives the best optimised result. Where 1, 2, 3 represents the SM Nd-Fe-b, FC Nd-Fe-B and FC ferrite generator respectively and L, H represents the lowest and the highest value after optimisation.

In terms of objective functions, it can be seen that the SM Nd-Fe-B gives best results for F_1, F_2, F_3 (ii), F_3 (iii) and the FC Nd-Fe-B gives best results for F_3 (i), F_4. In terms of independent variables, The SM Nd-Fe-B gives the best result for magnet height with objective function F_3 (ii), the FC Nd-Fe-B gives the best results for air-gap diameter with F_1, axial length with F_4 and the FC ferrite gives the best results for magnet width/pole pitch with F_2, pole pairs with F_3 (iii), height of tooth F_2. The generator type

and objective function that gives the best optimised result of some important dependent variables are also shown in Table 6.7.

Table 6.7: Generator type and objective function that gives the best optimised result (Where 1, 2, 3 represents the SM Nd-Fe-b, FC Nd-Fe-B and FC ferrite generator respectively and L, H represents the lowest and the highest value after optimisation)

	F_1	F_2	F_3(i)	F_3(ii)	F_3(iii)	F_4
F_1	1, H					
F_2		1, H				
F_3(i)			2, L			
F_3(ii)				1, L		
F_3(iii)					1, L	
F_4						2, L
Air-gap diameter, D (m)	2, L					
Axial length, l_s (m)						2, L
Magnet width/pole pitch, w_m/τ_p		3, L				
Magnet height, h_m (m)				1, L		
Pole pairs, p (-)					3, L	
Height of tooth, h_t (m)		3, L				
Air-gap flux density, B_g (T)						2, H
Mass of magnet, m_{PM} (kg)	1, L					
Mass of copper, m_{Cu} (kg)		2, L				
Mass of active iron, m_{Fe} (kg)		1, L				
Structural mass, m_{str} (kg)		2, L				
Copper losses (MWh)					1, L	
Iron losses (MWh)		1, L				
Cost of generator active materials, C_{gact} (k€)		1, L				
Cost of generator structural materials, C_{gstr} (k€)		2, L				
Annual energy production (GWh)					1, H	

The highest efficiency is at rated wind speed in the cases that the objective function F_3 (iii) is used. Figure 6.7 shows the comparison of highest efficiency curves for a 6 MW generator with different generator topologies. The SM Nd-Fe-B generator gives the highest efficiency which is 98.15%, the FC Nd-Fe-B generator gives 98.1% and the FC ferrite generator gives the lowest efficiency of 97.9%.

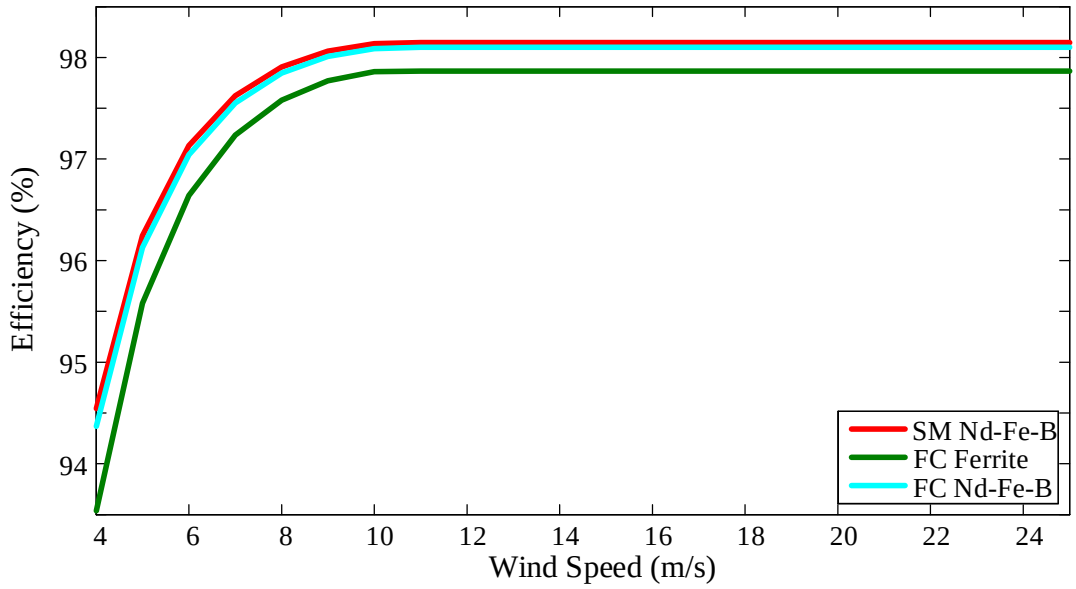

Figure 6.7: Efficiency of a 6 MW generator with different generator topologies after optimisation

6.2.2 Impact of generator air-gap diameter constraints

Figure 6.8 to Figure 6.13 shows the impact of the choice of upper limit of the generator air-gap diameter for a 6 MW SM Nd-Fe-B generator and a 6 MW FC ferrite generator. By varying the maximum allowed boundary for both generators diameter from 6m to 16m, it can be seen that, the optimal value for the SM Nd-Fe-B generator is near to 11.7m and for the FC ferrite generator, it is 12.6m. The optimised result for 3rd objective function varies from -€84004k to -€84952k for the SM Nd-Fe-B generator and -€83722k to -€84648k for the FC ferrite generator. The cost of energy in SM Nd-Fe-B generator varies from €106.2/MWh to €105.2/MWh and the cost of energy in flux-concentrating ferrite magnet generator varies from €107.1/MWh to €106.2/MWh. The largest drop in cost of energy occurs when extending the upper limit from 6m to 8m.

The total generator mass for the SM Nd-Fe-B generator varies from 75.6 tonnes to 105.5 tonnes and from 215.1 tonnes to 231.3 tonnes for the FC ferrite machine. To allow smooth optimisation, the upper boundary of FC ferrite generator is relaxed for magnet height with 6m and 8m air-gap diameter. This leads to the largest active material mass in the 8m air-gap diameter generator.

Active materials cost largely varies from 6m to 10m air-gap diameter for both type of generator, after that they are similar. The annual energy production (*AEP*) varies from 29.8 GWh to 30.12 GWh for the SM Nd-Fe-B generator and from 29.7 GWh to 30.03 GWh for the FC ferrite generator. The largest increase in *AEP* occurs when extending the upper limit from 6m to 8m.

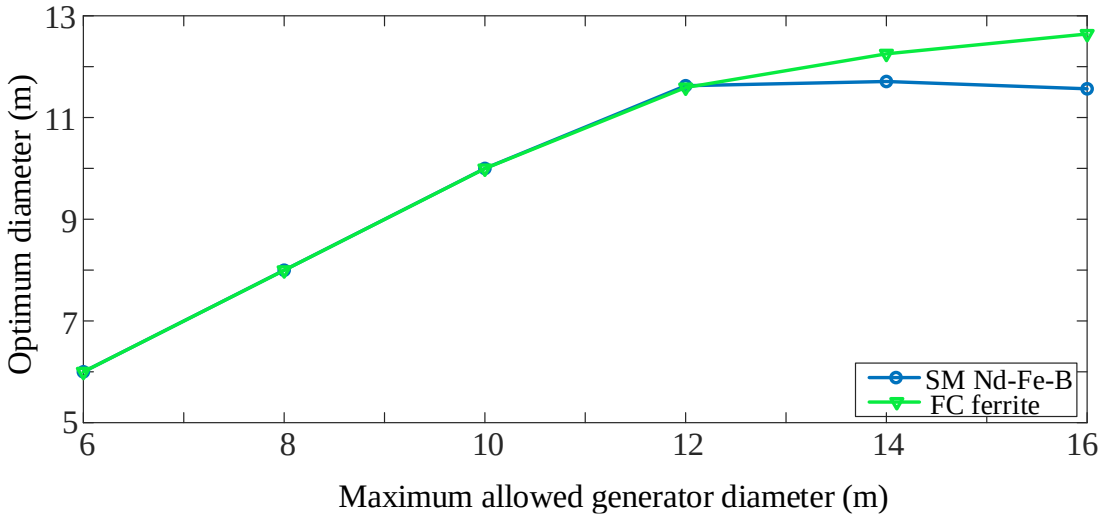

Figure 6.8: Impact of the choice of maximum allowed generator air-gap diameter: Maximum allowed generator diameter vs optimum diameter

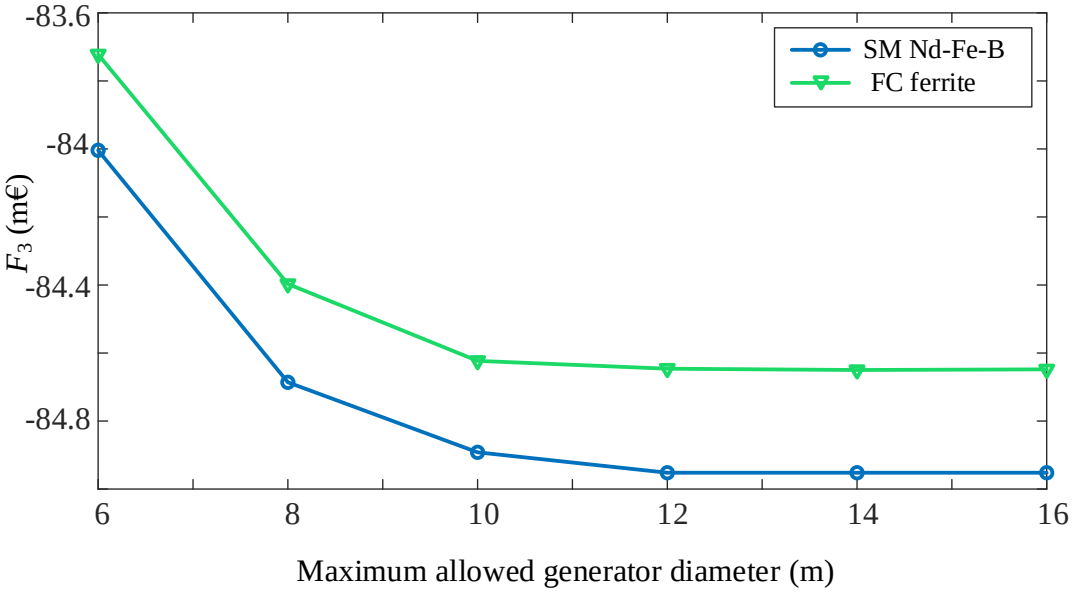

Figure 6.9: Impact of the choice of maximum allowed generator air-gap diameter: The optimised result for 3rd objective function

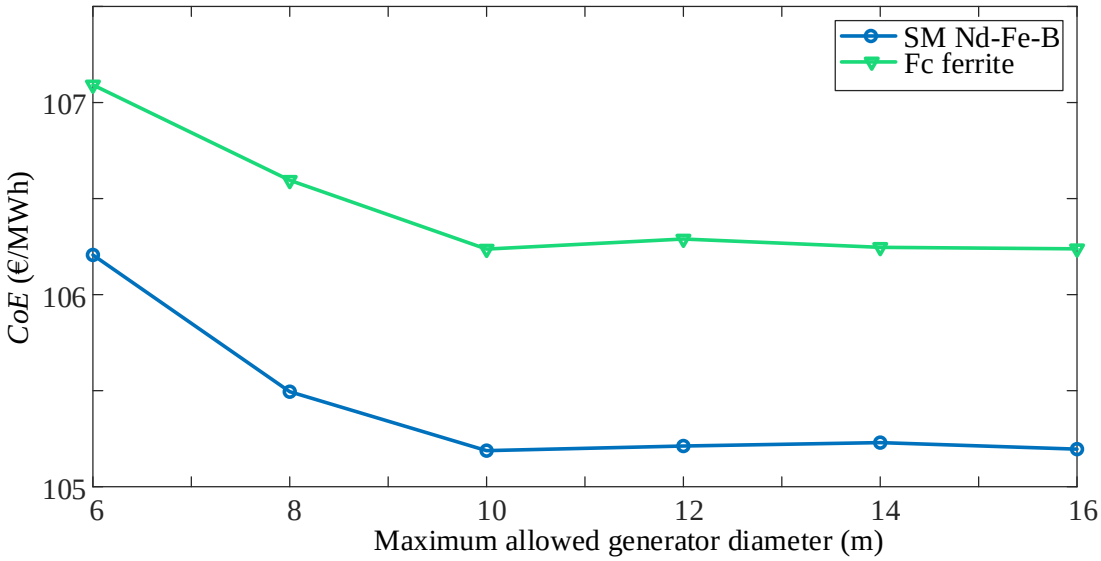

Figure 6.10: Impact of the choice of maximum allowed generator air-gap diameter: variation of cost of energy

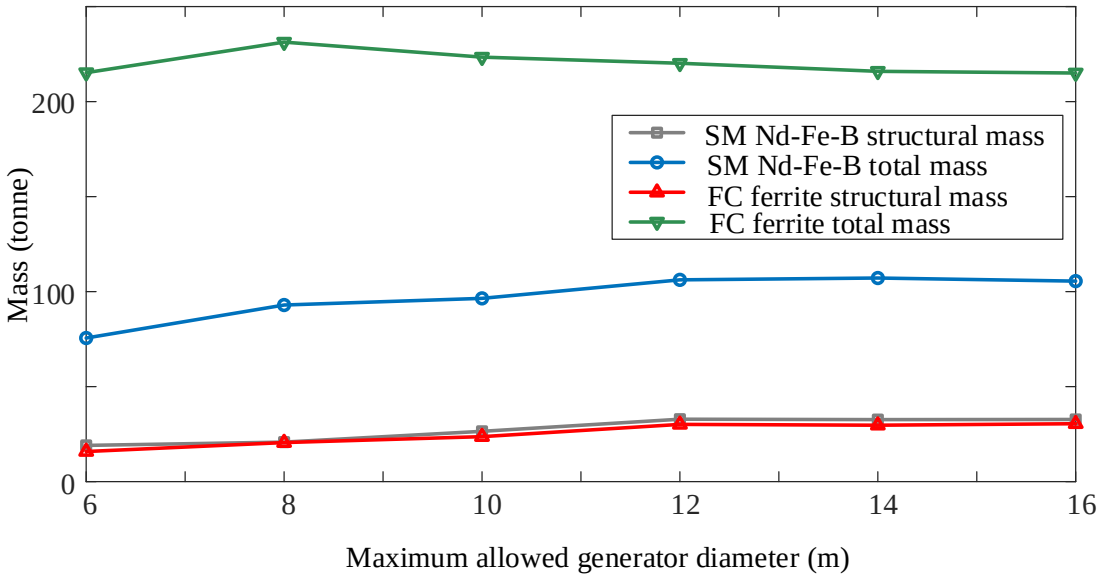

Figure 6.11: Impact of the choice of maximum allowed generator air-gap diameter: variation in generator masses

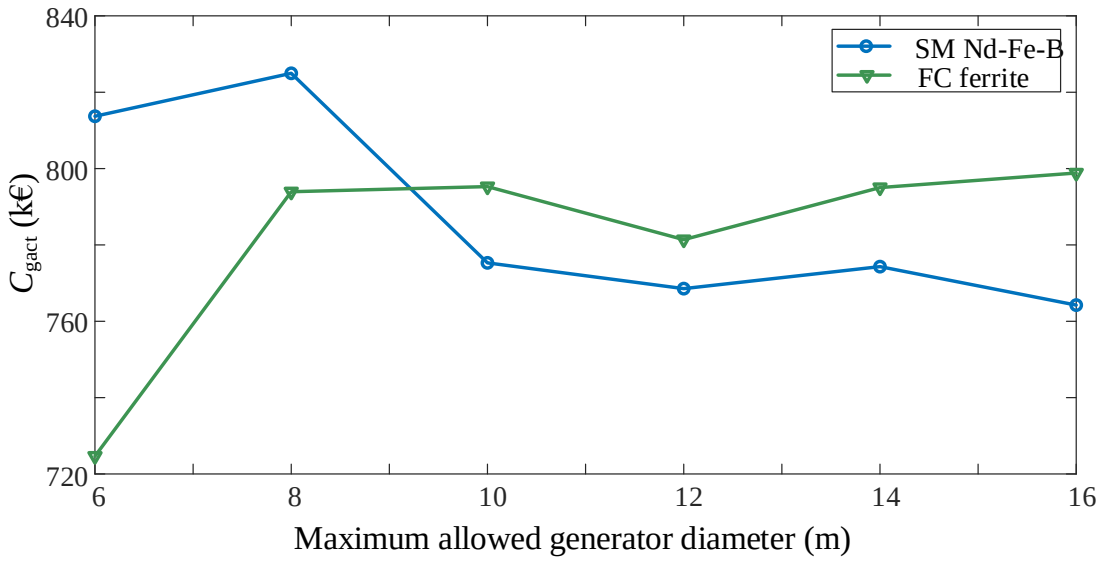

Figure 6.12: Impact of the choice of maximum allowed generator air-gap diameter: variation of generators active material cost

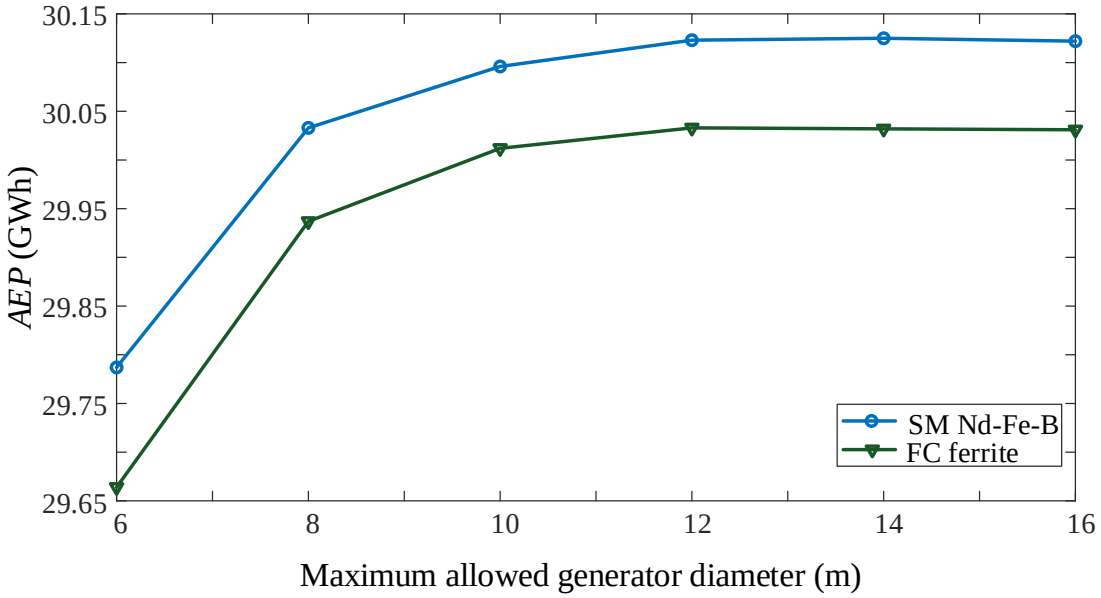

Figure 6.13: Impact of the choice of maximum allowed generator air-gap diameter: variation of annual energy production

6.2.3 Effect of generator and turbine structural models

When the generator structural model is included in the optimisation process (using the F_4 objective function to optimise the 6 MW SM Nd-Fe-B and FC ferrite generator) then the deflections are 0.5 mm in the radial direction, 0.44 mm in the tangential direction and 0.24 mm in the axial direction. Similar results are found for the flux-concentrating machines. The cost of energy increased by 0.26% in SM Nd-Fe-B generator and by 0.29% in FC ferrite magnet generator when the structural model and its limits are included.

If the radial deflection limit for the 6 MW SM Nd-Fe-B generators is relaxed from 5% to 7% and 10% of the air-gap clearance, the optimal fundamental air-gap flux density increases from 0.89 T to 0.97 T and 0.98 T, the optimal air-gap diameter decreases from 10.16 m to 9.69 m and 9.7 m, the generator active materials mass decreases from 46.6 tonne to 44.4 tonne and 44.2 tonne and the generator structural mass decreases from 32.7 tonne to 26.8 tonne and 26.4 tonne respectively.

When the turbine structural model is included then the tower cost increased by €2.54k for the addition of one tonne of generator mass; this is about 0.012% of the total wind turbine cost. The offshore substructure and foundation cost increased by €1.5k for every additional one tonne of generator mass, which is about 0.007% of the total wind turbine cost.

6.2.4 Effect of variable power factor

Figure 6.14 shows the efficiency curve of a 6 MW SM Nd-Fe-B generator with unity power factor and leading power factor (when θ=0.5δ). The independent variables selected randomly from Table 5.1 by the optimisation. It is found that, the power factor at rated wind speed is 0.94 for the SM Nd-Fe-B generator with variable power factor after optimization, where the power factor varies with load angle at below rated wind speed. The efficiency of SM Nd-Fe-B with variable power factor is slightly higher than the generator with unity power factor. Table 6.8 gives the comparison of some results after optimisation.

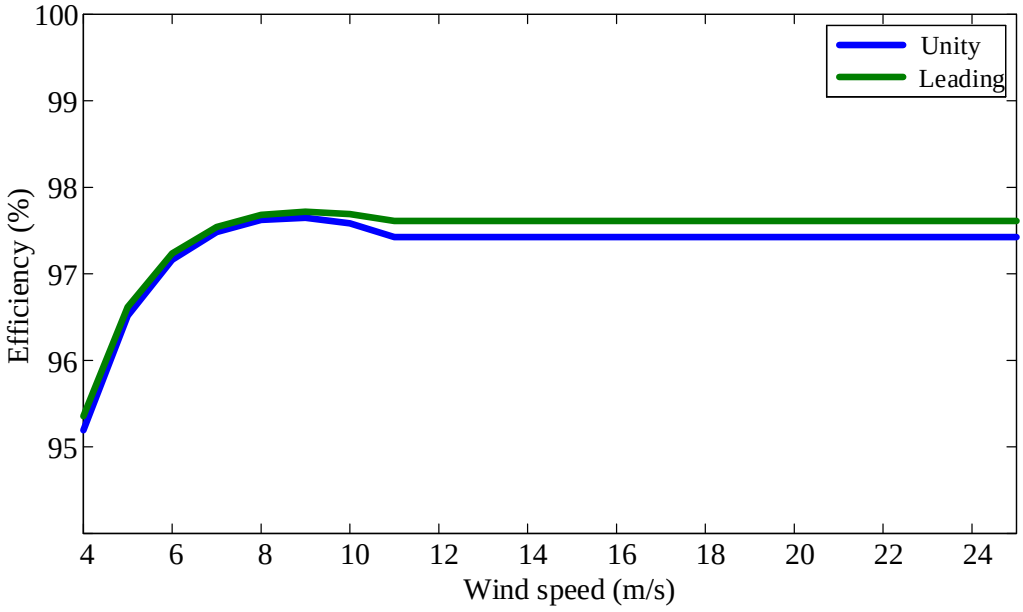

Figure 6.14: Efficiency curve of unity and leading power factor for a 6 MW Nd-Fe-B generator

Figure 6.15 compares optimisation results for some important dependent variables of 6 MW SM Nd-Fe-B, FC Nd-Fe-B and SM Nd-Fe-B generator with variable power factor. Where SM Nd-Fe-B generator with variable power factor gives minimum cost of energy of €104.6/MWh in Figure 6.15(a). Figure 6.15(b) shows the annual energy production of different generator design, where SM Nd-Fe-B generator with variable power factor gives maximum energy of 30 GWh. The FC Nd-fe-B generator gives minimum active material cost €520.5k, shown in Figure 6.15(c). Figure 6.15(d) shows the magnet mass of different generator designs, where SM Nd-Fe-B generator with variable power factor gives minimum magnet mass of 3.82 tonnes.

Table 6.8: Comparison of some results after optimisation with different power factor

Variables	**Unity power factor**	**Leading power factor (θ=0.5δ)**
Air gap diameter, D (m)	10.2	10.58
Axial length, l_s (m)	1.2	1.28
Magnet width/pole pitch, w_m/τ_p	0.79	0.79
Magnet height, h_m (m)	0.02	0.015
Pole pairs, p (-)	100	100
Height of tooth, h_t (m)	0.083	0.09
Air-gap flux density, B_g (T)	0.89	0.78
Mass of magnet, m_{PM} (kg)	4502.4	3820.2
Mass of copper, m_{Cu} (kg)	10780	12837
Mass of active iron, m_{Fe} (kg)	31287	33828
Structural mass, m_{str} (kg)	32689	29848
Copper losses (MWh)	593.2	547.8
Iron Losses (MWh)	247.6	236.4
Generator active materials cost (k€)	525.7	523.3
Generator structural materials cost (k€)	130.8	119.4
Converter cost (k€)	121.8	129.6
Annual energy production (GWh)	29.94	30
Cost of energy (€/MWh)	104.9	104.6

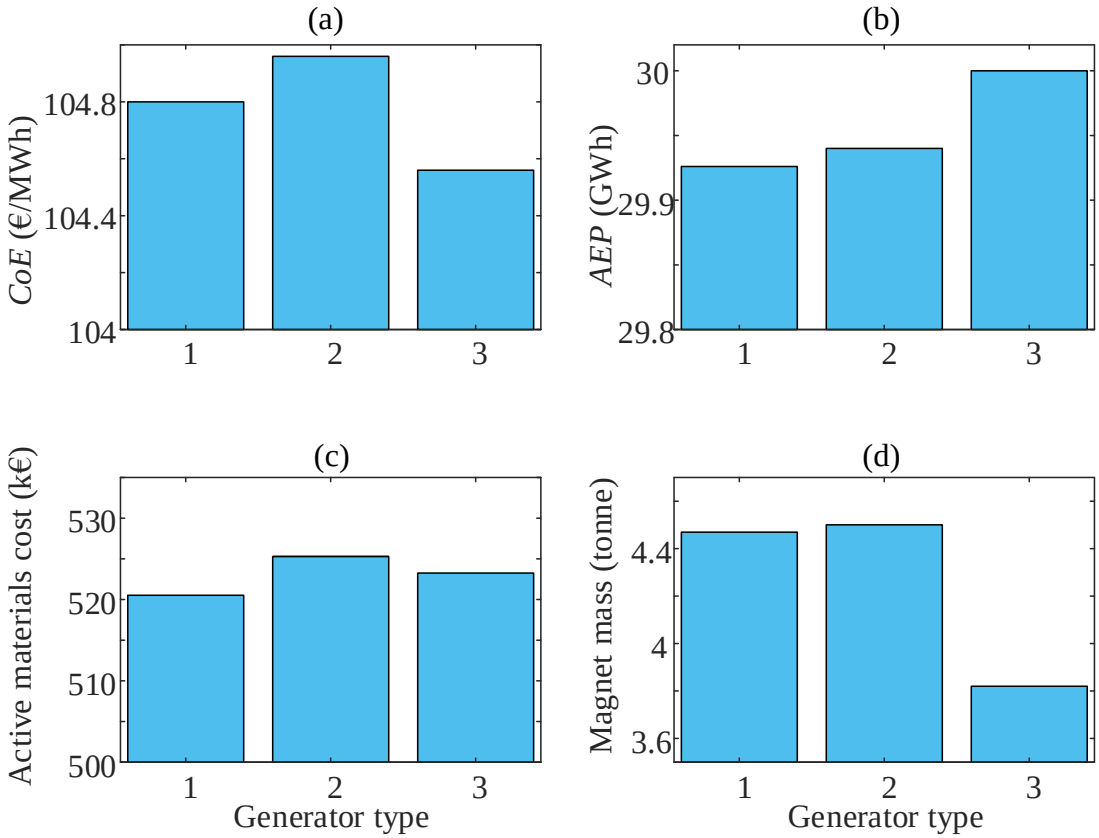

Figure 6.15: Comparison of optimisation results for some dependent variables, where in x-axis, 1,2 and 3 represents different generator type, FC Nd-Fe-B, SM Nd-Fe-B and SM Nd-Fe-B with variable power factor respectively

6.2.5 Different turbine power ratings

All the three generator topologies in this study are optimised for different power ratings (6 MW, 8 MW and 10 MW) using 3rd objective function, F_3 (P_y = 15 years) and 4th objective function, F_4. Table 6.9 shows the independent variables selected by the optimization for the both objective functions with different generator topologies and power ratings.

The highest efficiency is at rated wind speed in the cases that the objective function F_3 (iii) is used. This is the case across all power ratings, regardless of generator topology. Figure 6.16 shows the efficiency curves for the SM Nd-Fe-B generator with different power ratings. The generator with 10 MW power rating gives the highest efficiency which is 98.3%, 8 MW generator gives 98.2% and 6 MW generator gives the lowest efficiency of 98.15%. The FC Nd-Fe-B and FC ferrite generators also follow the same fashion where 10 MW generators give the highest efficiency and 6 MW generators give the lowest efficiency. Higher power means more expensive turbine, therefore need to try higher generator efficiency to minimise *CoE*.

Table 6.9: Independent variables vs. generator topology for different power ratings

Surface mounted Nd-Fe-B generator						
	6 MW		**8 MW**		**10 MW**	
Independent variables	F_3 (iii)	F_4	F_3 (iii)	F_4	F_3 (iii)	F_4
Air-gap diameter, D (m)	11.9	10.2	13.22	10.43	11.55	11.74
Axial length, l_s (m)	1.38	1.2	1.63	1.18	1.84	1.55
Magnet width/pole pitch, w_m/τ_p	0.78	0.79	0.8	0.67	0.86	0.77
Magnet height, h_m (m)	0.02	0.02	0.02	0.04	0.038	0.025
Pole pairs, p (-)	82	100	86	88	64	95
Height of tooth, h_t (m)	0.089	0.083	0.1	0.09	0.11	0.1
Flux concentrating Nd-Fe-B generator						
Air-gap diameter, D (m)	11.5	9.57	12.5	10.64	13.5	10.2
Axial length, l_s (m)	1.27	1.08	1.5	1.22	1.65	1.45
Magnet width/pole pitch, w_m/τ_p	0.79	0.75	0.79	0.76	0.78	0.72
Magnet height, h_m (m)	0.08	0.074	0.09	0.088	0.095	0.086
Pole pairs, p (-)	91	100	91	100	94	99
Height of tooth, h_t (m)	0.09	0.085	0.1	0.094	0.11	0.105
Flux concentrating ferrite generator						
Air-gap diameter, D (m)	11.8	12.09	13.2	13.78	15	14.13
Axial length, l_s (m)	1.51	1.5	1.7	1.74	2.09	1.85
Magnet width/pole pitch, w_m/τ_p	0.77	0.7	0.76	0.7	0.75	0.7
Magnet height, h_m (m)	0.38	0.23	0.42	0.24	0.36	0.3
Pole pairs, p (-)	71	100	74	100	73	100
Height of tooth, h_t (m)	0.089	0.073	0.1	0.076	0.11	0.09

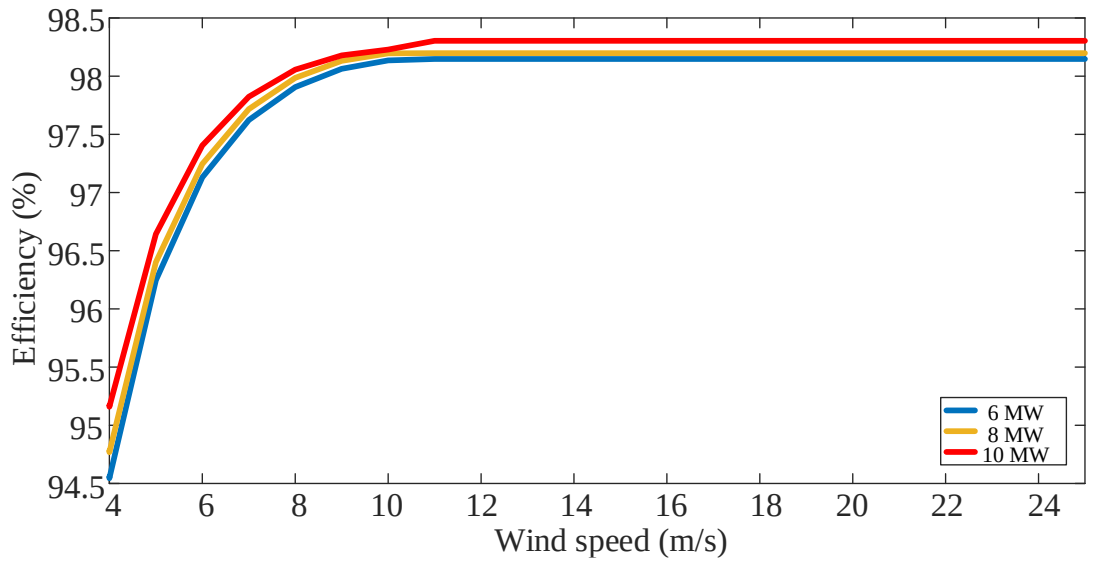

Figure 6.16: Efficiency curves for different power ratings

Figure 6.17 shows the post-processed optimisation results using F_3 (iii) with different generator topologies and power ratings. For all the power ratings, the SM Nd-Fe-B generator gives the highest revenue while minimizing active material costs with -€84952k for 6 MW, -€111320k for 8 MW and -€138230k for 10 MW.

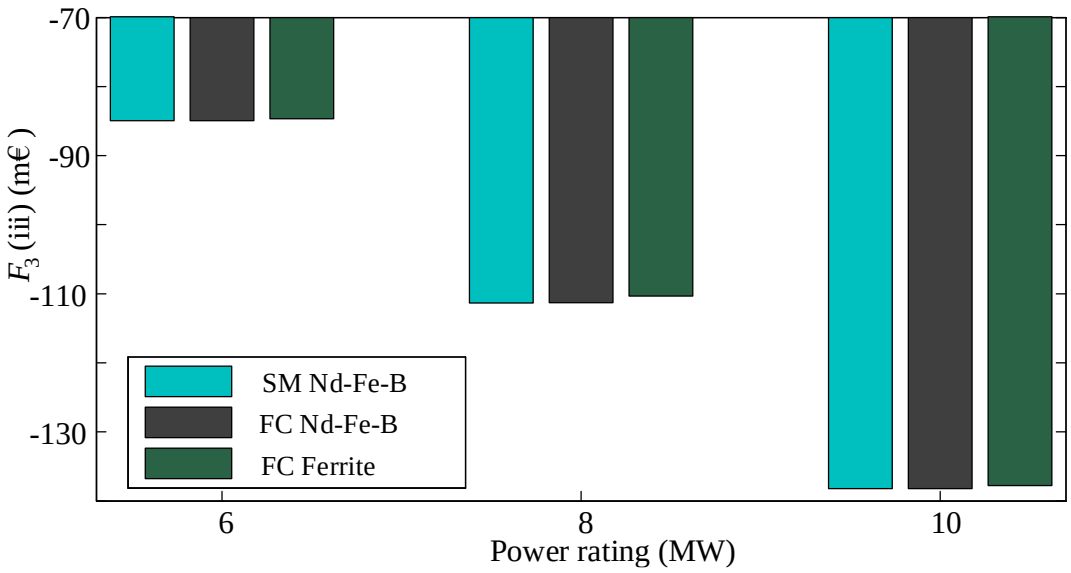

Figure 6.17: Optimisation results of F_3 (iii) with different generator topologies and power ratings

Figure 6.18 shows the post-processed optimisation results using F_4 with different generator topologies and power ratings. For all the power ratings, the FC Nd-Fe-B generator gives the lowest cost of energy with €104.8/MWh for 6 MW, €102.9/MWh for 8 MW and €102.6/MWh for 10 MW.

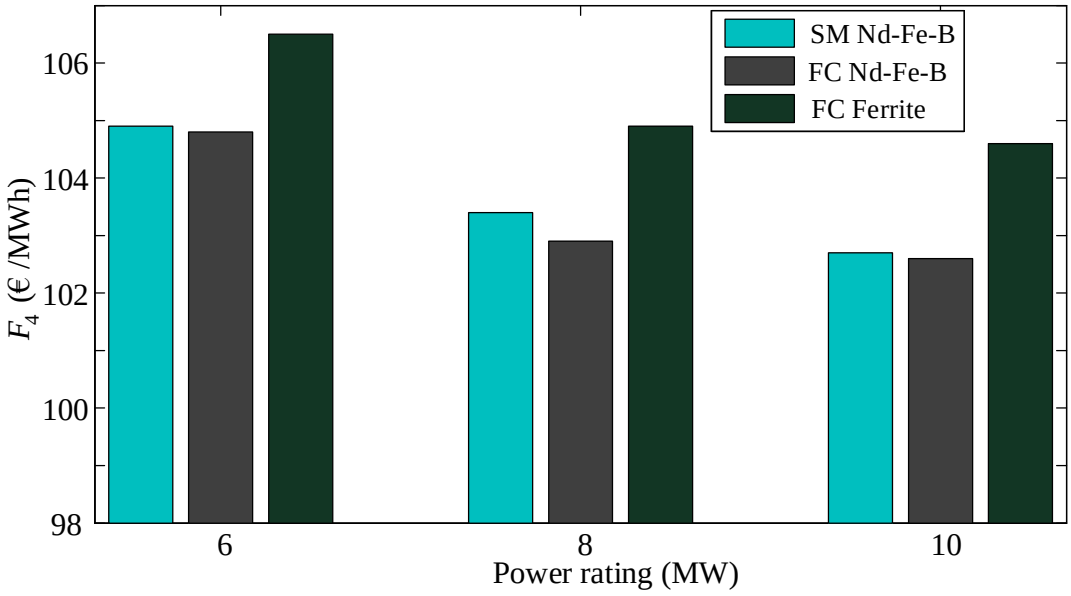

Figure 6.18: Optimisation results of F_4 with different generator topologies and power ratings

Figure 6.19 shows the cost of generator active materials for different generator topologies and power ratings (using F_4). For all three types of generator topology, the FC Nd-Fe-B generator gives lowest cost of generator active materials which is €520.5k for 6 MW, €735.6k for 8 MW and €913.4k for 10 MW generator. It can be expressed as €0.087/W for 6 MW, €0.092/W for 8 MW and €0.091/W for 10 MW generator. In

relation with torque, it is €0.105/Nm for 6 MW, €0.106/Nm for 8 MW and €0.098/Nm for 10 MW generator.

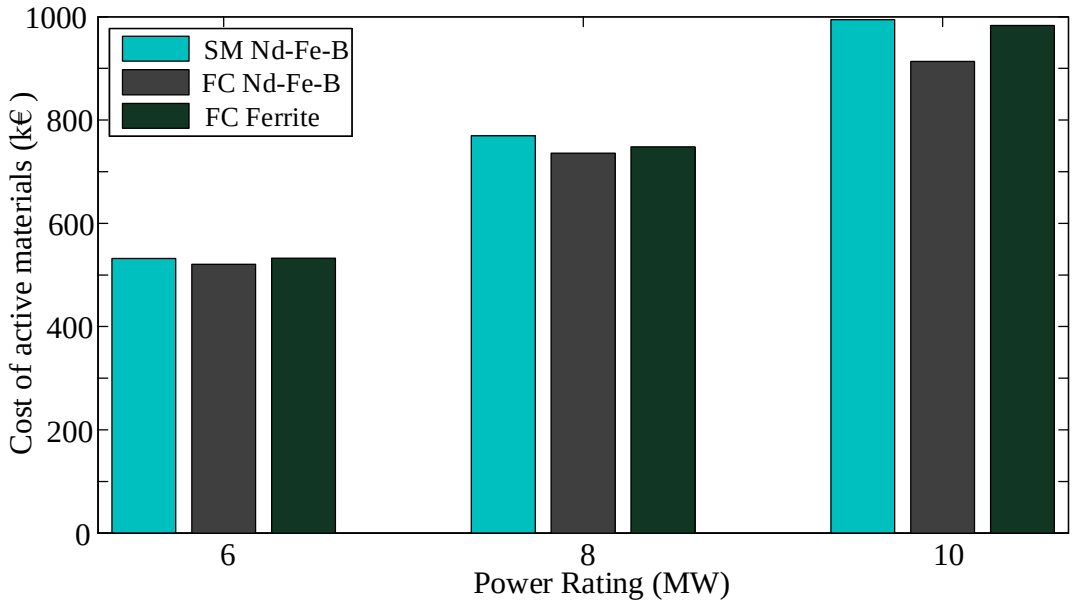

Figure 6.19: Cost of active materials for different generator topologies and power ratings

Figure 6.20 shows the magnet mass for different generator topologies and power ratings after optimisation (using F_4). The FC Nd-Fe-B generator gives the lowest magnet mass for all three types of generator and power ratings which is 4469.8 kg for 6 MW, 6484.7 kg for 8 MW and 8352.4 kg for 10 MW generator. It can be expressed as 0.00075 kg/W for 6 MW, 0.0008 kg/W for 8 MW and 0.00084 kg/W for 10 MW generator. In relation with torque, it is 0.00092 kg/Nm for 6 MW, 0.00087 kg/Nm for 8 MW and 0.0008 kg/Nm for 10 MW generator.

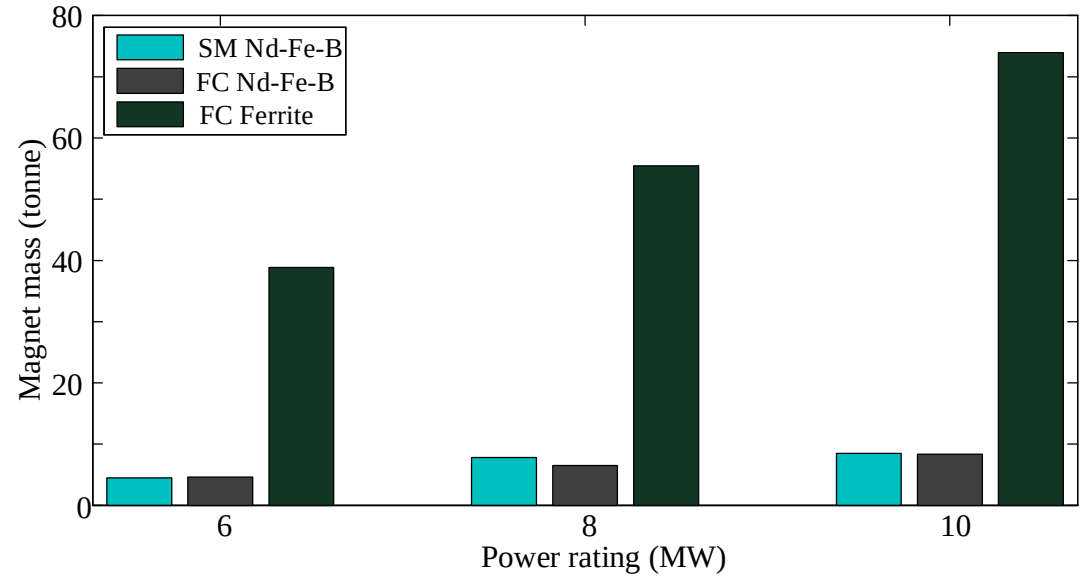

Figure 6.20: Magnet mass for different generator topologies and power ratings

Figure 6.21 shows the structural materials cost for different generator topologies and power ratings after optimisation (using F_4). The FC Nd-Fe-B generator gives the lowest structural materials cost for all three types of generator and power ratings which is €104.8k for 6 MW, €167.9k for 8 MW and €265.1k for 10 MW generator.

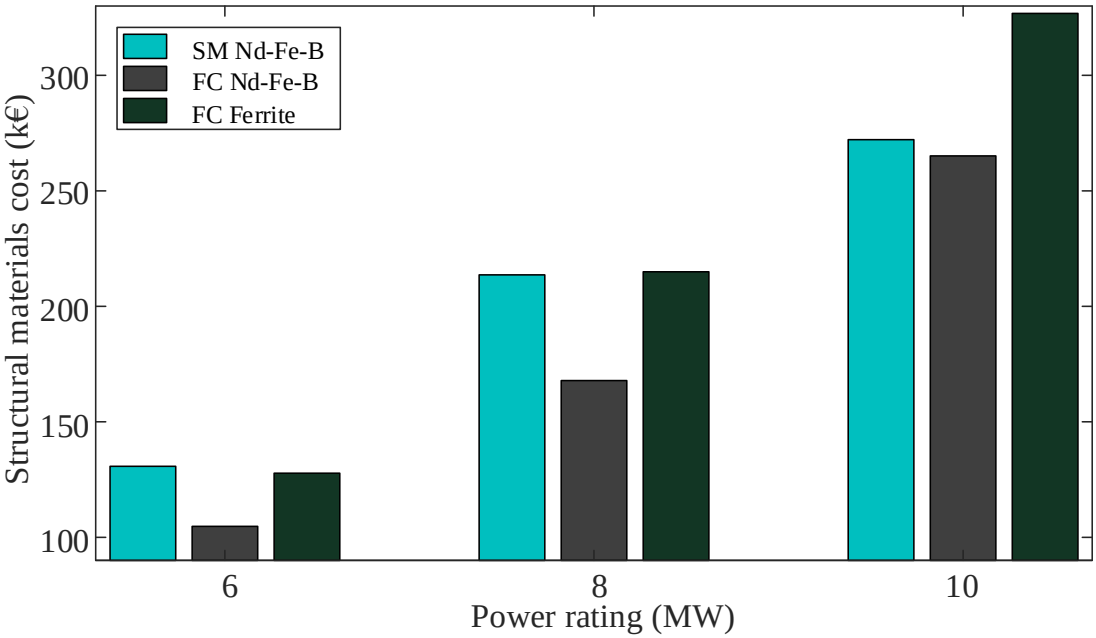

Figure 6.21: Structural materials cost for different generator topologies and power ratings

Figure 6.22 shows the annual energy production (*AEP*) for different generator topologies and power ratings after optimisation (using F_4). In terms of *AEP*, different generator topologies with same power rating give similar results. The SM Nd-Fe-B

generator gives slightly better *AEP* for the 6 MW and 10 MW generator with 29.94 GWh and 48.8 GWh respectively. The FC Nd-Fe-B gives highest *AEP* for 8 MW generator with 39.25 GWh.

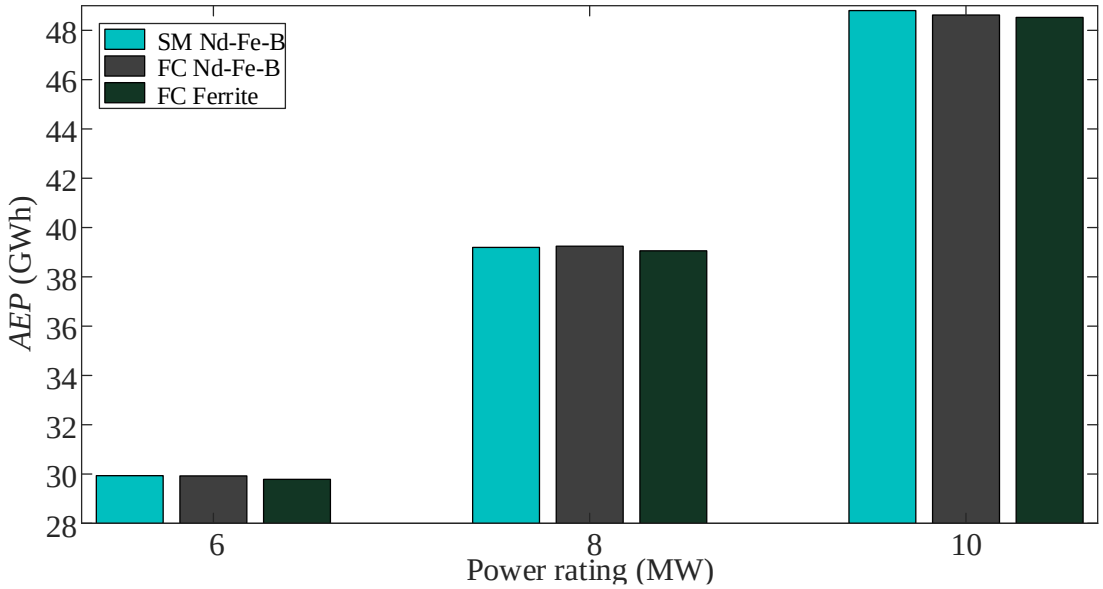

Figure 6.22: Annual energy production (AEP) for different generator topologies and power ratings

Table 6.10 shows the difference of cost and energy production per MW for a SM Nd-Fe-B generator, upgrading from 6 MW to 8 MW and 10 MW (using F_4). It can be seen that, upgrading from 6 MW to 8 MW and 10 MW increase the active materials cost, structural material cost, substructure and foundation cost and decrease the tower cost wind farm rest of the turbine capital cost, *AEP* per MW.

Table 6.10: Difference of cost and energy production per MW when upgrading from 6 MW to 8 MW and 10 MW

	8 MW	**10 MW**
Active materials cost	8.6% increased	12.2% increased
Structural material cost	24.2% increased	26.6% increased
Tower cost	2.2% decreased	3.2% decreased
Substructure and foundation cost	2.1% increased	9.5% increased
Wind farm rest of the turbine capital cost	5.4% decreased	8.2% decreased
Annual energy production	1.8% decreased	2.2% decreased

6.2.6 Effect of different magnet grades

Figure 6.23 shows the effect of different magnet grades on the cost of energy for a 6 MW SM Nd-Fe-B generator. The results are shown for “H” grade magnet at 120°C as well as regular and “H” grade magnet at 80°C (cooled down from 120°C).

By varying the magnet grade from N35 to N52, the cost of energy using "H" grade magnet decreases until N48 and then increases for N50 and N52; the cost of energy using regular magnets (at 80°C) decreases from N35 to N50 and then slightly increases for N52.

Figure 6.24 shows the effect of different magnet grades on the magnet mass for a 6 MW SM Nd-Fe-B generator. By varying the magnet grade from N35 to N52, the magnet mass using "H" grade magnet at 120°C varies from 5 tonnes to 3.4 tonnes. Others also follow the same decreasing trends.

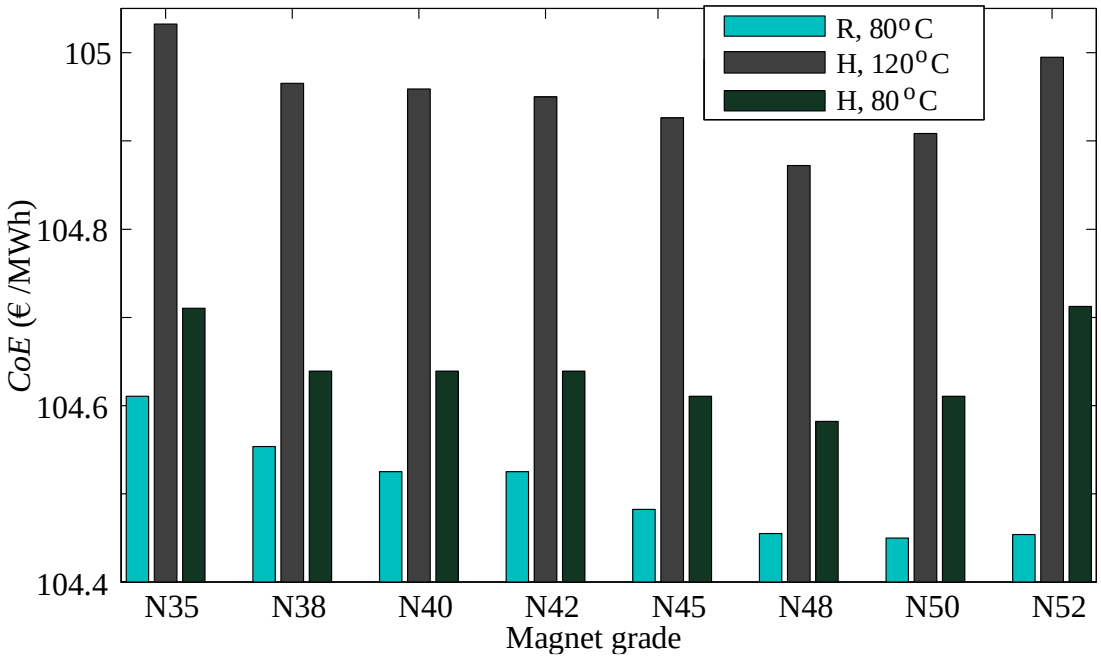

Figure 6.23: Effect of different magnet grade on cost of energy

It is found that for a 6 MW SM Nd-Fe-B generator using N40H magnet, a +5% tolerance in magnet's remanence, B_r decrease the turbine cost of energy by 0.03% and a -5% tolerance increase the turbine cost of energy by 0.05%. Also +2 MGOe tolerance in maximum energy product reduce the cost of energy by 0.006% and -2 MGOe tolerance increase the cost of energy by 0.003%.

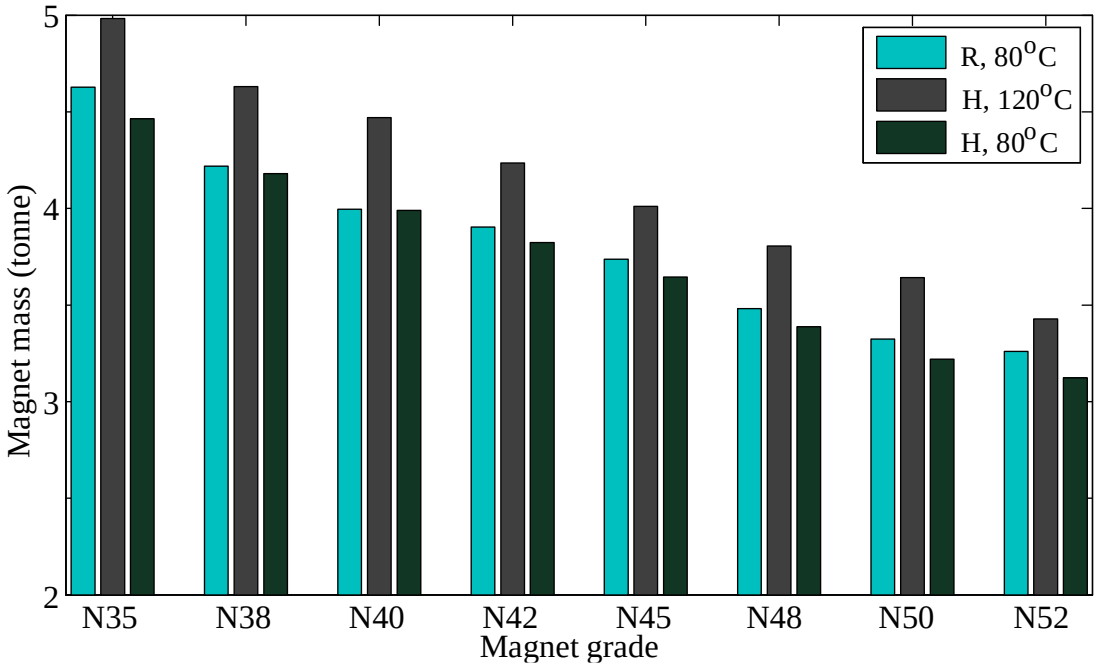

Figure 6.24: Effect of different magnet grade on magnet mass

6.2.7 Effect of temperature and cooling cost

Figure 6.25 shows the effect of temperature for a 6 MW SM Nd-Fe-B generator using N40H magnet: (a) shows the power losses at 80°C and 120°C temperatures, (b) shows the required volumetric cooling airflow to cool down the magnet temperature of the generator from 120°C to 80°C. It can be seen that the power losses below rated wind speed are variable and hence the required volumetric cooling airflow also varies, (c) shows the trend line of the required cooling air flow for different magnet temperature (d) shows the number of series fan required (5 series fan, where each of the fan curves denotes the number of series fan) the generator to achieve the required volumetric cooling airflow (1.38 m^3/s in this case) to cool down the temperature from 120°C to 80°C while the number of parallel fans are fixed (4 parallel fan). It can be seen that the maximum air flow at rated power can be achieved by using the maximum number of series fans and this is reduced by subsequently turning off some of the series fans.

In order to reduce the magnet temperature from 120˚C to 80˚C for a 6 MW SM Nd-Fe-B generator using N40 magnet, the required cooling airflow at rated speed is 1.38 m^3/s, the number of parallel fans is 4, the number of series fans is 5 and the number of heat exchangers is 5.

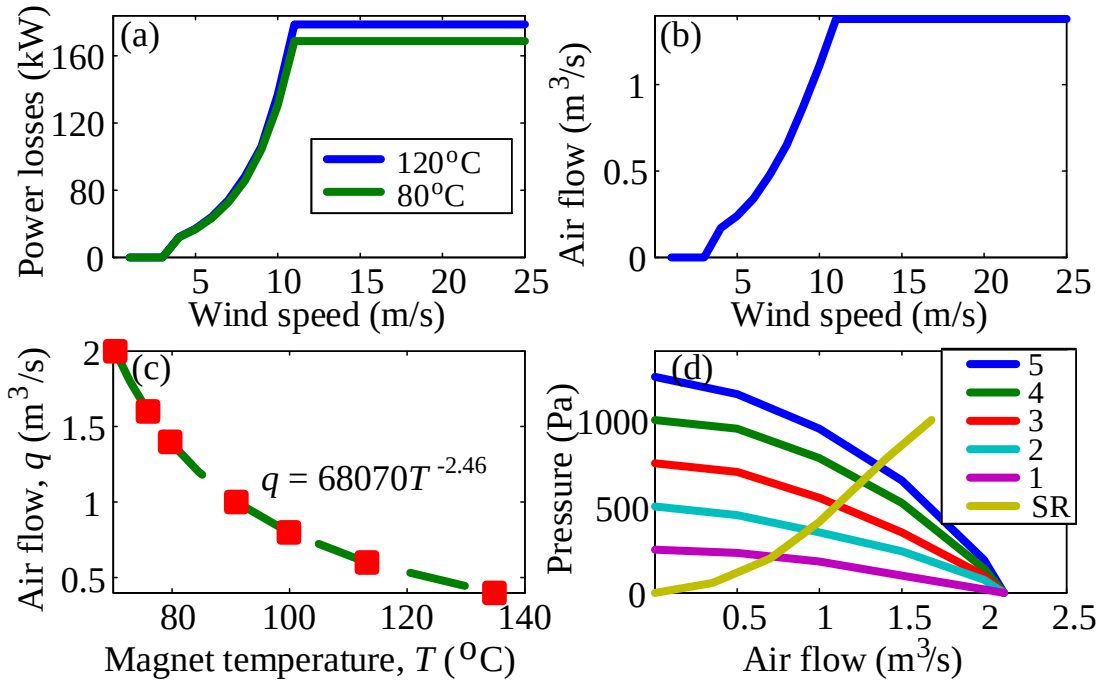

Figure 6.25: Effect of Temperature and cooling (a) Power losses at 80°C and 120°C (b) Required volumetric cooling airflow to cool down the magnet temperature from 120˚C to 80˚C (c) Trend line of cooling air flow required for different magnet temperature (d) Fan curves for series fan intersects total system resistance curve (SR) where intersecting point is the volumetric cooling airflow achieved (4 parallel fan and 5 series fan)

The cost of energy for a 6 MW SM Nd-Fe-B generator including cooling system is given in Figure 6.23, and this shows that the cost of energy using "H" grade magnet at 80˚C (using cooling system) is less than the cost of energy at 120˚C without cooling system. The regular magnet at 80˚C (using cooling system) gives the better cost of energy compared to the "H" grade magnet.

6.2.8 Sensitivity analysis

Figure 6.26 shows the sensitivity of turbine cost of energy for a 6 MW SM Nd-Fe-B generator when cost of Nd-Fe-B magnet per kg varies and other turbine parameters are assumed to be constant in the optimisation process. It can be seen that, if the Nd-Fe-B cost increase to €120/kg, the cost of energy would rise to €105.9/MWh. However, if the magnet costs fall to €40/kg, the cost of energy will fall back to €104.4/MWh.

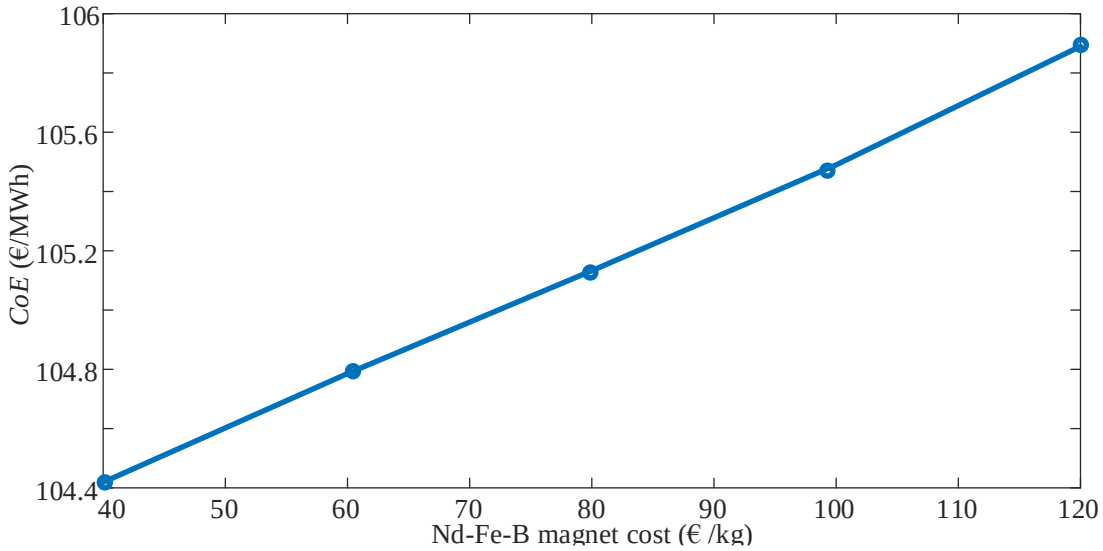

Figure 6.26: Sensitivity of turbine cost of energy for cost of a kg Nd-Fe-B

Figure 6.27 presents availability varying from 90% to 96% (other turbine parameters are assumed to be constant in the optimisation process) and the cost of energy in 6 MW SM Nd-Fe-B generator varies from €109.4/MWh to €102.6/MWh, where the cost of energy in 6 MW FC ferrite generator varies from €110.5/MWh to €103.6/MWh.

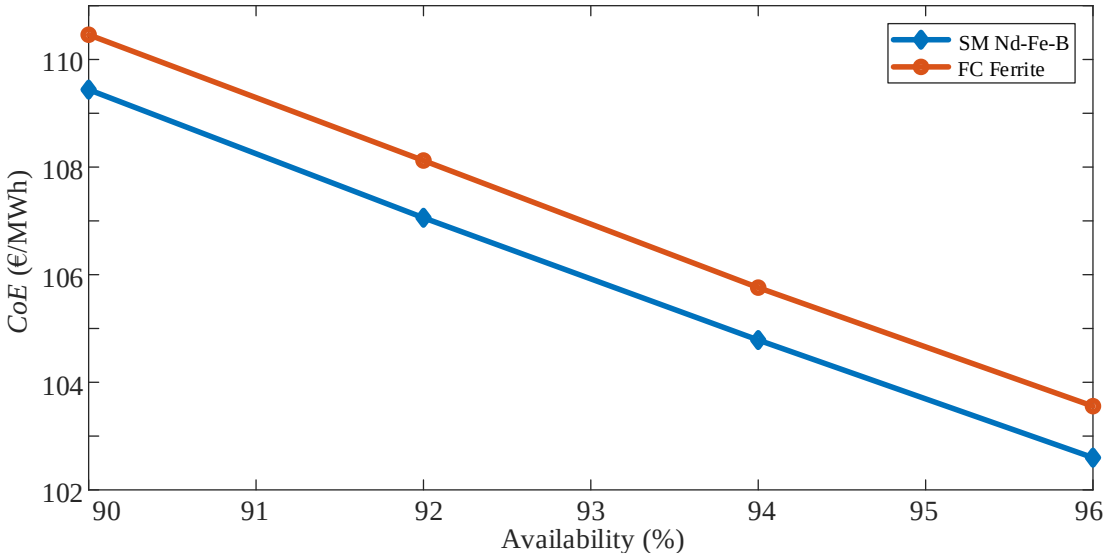

Figure 6.27: Sensitivity of turbine cost of energy for availability

If the rest of the turbine cost for a 6 MW generator (except generator active materials cost, generator structural cost and foundation cost) varies from €16m to €18m as shown in Figure 6.28, the cost of energy of the SM Nd-Fe-B generator varies from €98.9/MWh to €106.6/MWh and the cost of energy of the FC ferrite magnet generator varies from €99.8/MWh to €107.6/MWh.

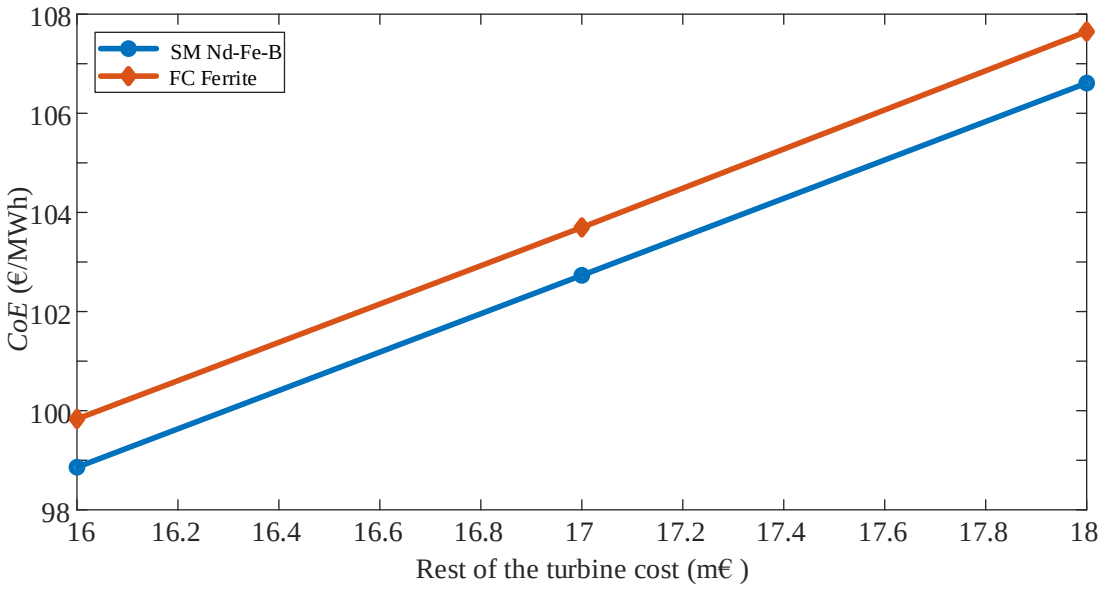

Figure 6.28: Sensitivity of turbine cost of energy for rest of the turbine capital cost

If the annual operation and maintenance cost for a 6 MW generator varies from €500k to €700k as shown in Figure 6.29, the cost of energy of the SM Nd-Fe-B generator varies from €100.5/MWh to €107.2/MWh while the cost of energy of the FC ferrite magnet generator varies from €101.5/MWh to €108.2/MWh.

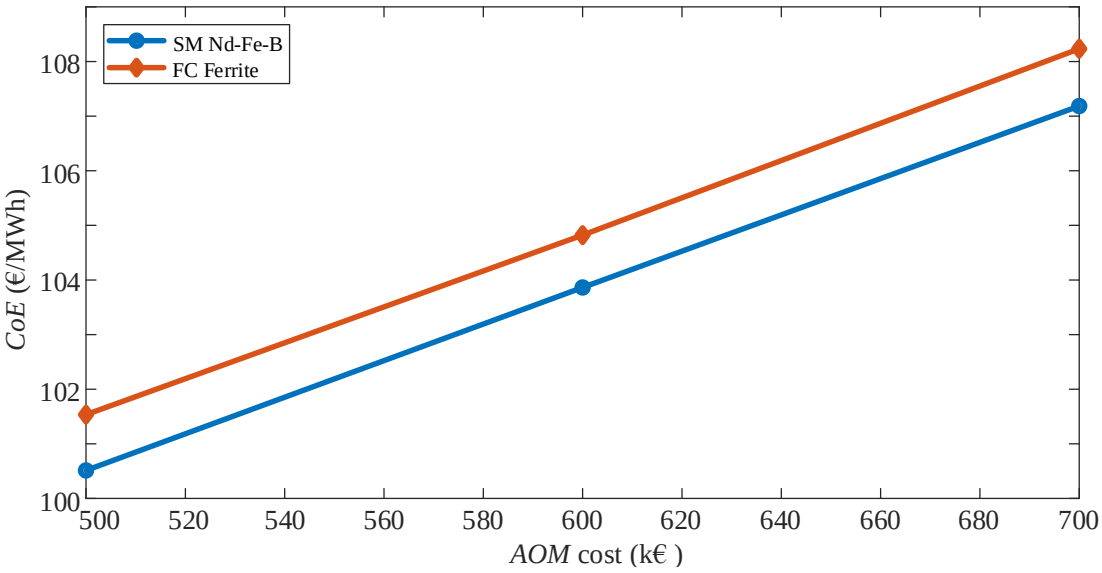

Figure 6.29: Sensitivity of turbine cost of energy for annual operation and maintenance cost

Figure 6.30(a) and Figure 6.30(c) shows the effect on cost of energy and annual energy production for a 6 MW SM Nd-Fe-B generator by varying the wind speed scale parameter from 9.5 m/s to 11.3 m/s with fixed shape parameter 2. Figure 6.30(b) and Figure 6.30(d) shows the effect on cost of energy and annual energy production for a 6 MW SM Nd-Fe-B generator by varying the mean wind speed from 8.4 m/s to 10

m/s. The FC Nd-Fe-B and FC ferrite generator also gives the similar results when the wind speed scale parameter and the mean wind speed are varied.

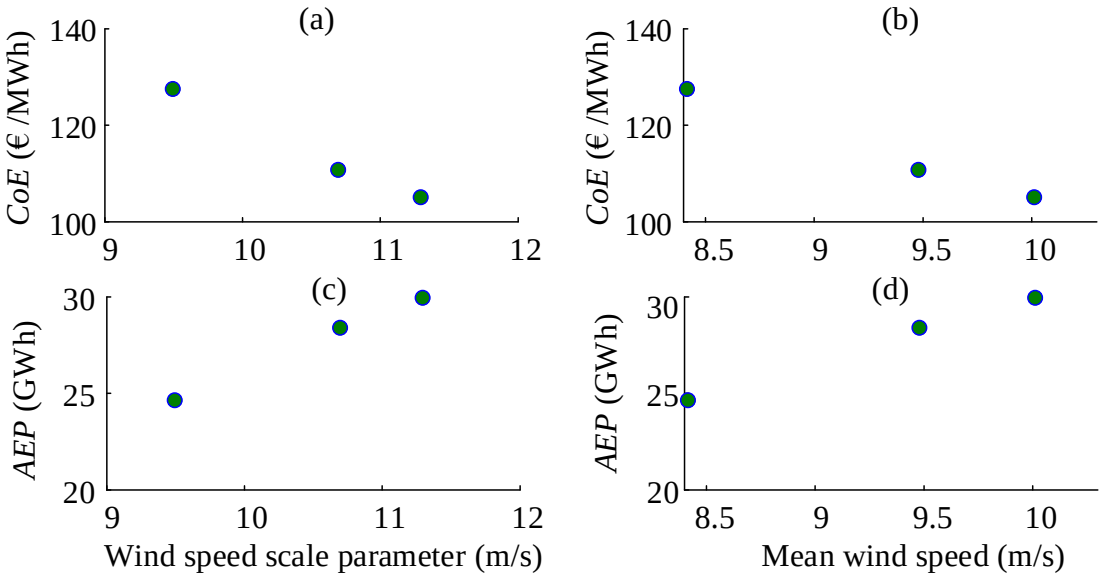

Figure 6.30: Effect of different wind condition

6.3 Discussions

This section gives an overall discussion on the investigations performed and the results achieved that will help to answer the secondary research questions given in section 1.3 as well as primary research question given in section 1.2. A number of different investigations includes: different objective functions, different generator topologies, constraining generator diameter, including structural materials, different power factor, different power ratings, different magnet grades, thermal effects and cooling. The following sub-sections will give an overall discussion on the results that has been achieved after each investigation.

6.3.1 On the choice of objective function

Four different objective functions are used in this study to optimise different generator types for wind energy: (a) Torque per magnet mass (objective function 1, F_1), (b) Torque per generator active material cost (objective function 2, F_2), (c) the difference between generator active material costs and the wind turbine revenue for 5, 10 and 15 years period of operation (objective function 3, F_3) and (d) the wind turbine cost of energy (objective function 4, F_4).It can be seen that, the objective functions F_3 and F_4 produce higher efficiency designs for all the types of generators than the objective functions F_1 and F_2. This is unsurprising as the formulation for F_3 and F_4 explicitly includes annual energy yield. The major difference in losses between F_1 & F_2 and F_3

& F_4 is due to the copper losses. Higher current density is used to increase electrical loading in F_1 & F_2, which implies higher copper losses. For F_1 this allows reduced magnetic loading and hence a reduction in magnet mass; for F_2 the higher electrical loading leads to a reduction in both magnet and copper mass. The balance of copper and iron losses are slightly different with F_3 & F_4 having slightly higher iron losses. In machine design it is often the case that lower losses are found when contributions from copper and iron losses are more closely balanced.

In terms of the application, a balance of high efficiency and low cost is attractive. The designs resulting from the 1st and 2nd objective functions give a high cost of energy when evaluated post-optimisation. F_1 and F_2 reduce the volume of active material (magnet mass in the case of F_1 and all the active material, weighted by their specific costs in the case of F_2) for the rated torque at the expense of higher losses. Although their generator capital costs are lowest, they achieve this by sacrificing annual energy yield. In reality, the generator capital cost is only a modest contributor to the total turbine capital cost and yet generator inefficiency affects all of the turbine power output. So, the 1st and 2nd objective functions are a poor choice in terms of cost of energy for the optimisation of wind turbine generators.

The optimised design parameters and the ultimate cost of energy are very similar for F_3 and F_4. Different turbine costs and parameters could lead to a larger difference between F_3 and F_4 (it can be seen that the difference of cost of energy between F_3 (i) and F_4 is 3.6% for a 6 MW turbine whereas 9.7% for a 10 MW turbine), however it appears that F_3 is quite a good proxy for F_4. The change in the number of years for F_3 makes a slight difference in the cost of energy. The higher the number of years used (i.e. 10 and 15 years rather than 5 years) produces more efficient designs, but also increases the cost of energy for this case study. For larger, more capitally expensive offshore wind turbines (e.g. those in deeper waters) it may be useful to opt for 10 or 15 years when using F_3. One of the benefits of the 3rd objective function is that it does not need detailed turbine information and so is more general in comparison to 4th objective function.

6.3.2 On the choice of generator topology

The optimal surface-mounted Nd-Fe-B (SM Nd-Fe-B) and the flux-concentrating Nd-Fe-B (FC Nd-Fe-B) designs give similar efficiency and slightly better efficiency than the optimal flux-concentrating ferrite (FC ferrite) generator. The efficiency is the

primary driver for differences in the cost of energy: both the Nd-Fe-B designs are better than the FC ferrite generator. Of secondary importance is the active material cost: the FC Nd-Fe-B generator gives slightly better cost of energy than the SM Nd-Fe-B generator; but the lower active material cost of the FC ferrite generator does not make up for its lower efficiency.

The SM Nd-Fe-B generator uses slightly less magnet than the FC Nd-Fe-B generator (in most of the optimisation except F_3 (iii) and F_4). That shows the flux-concentrating nature of FC Nd-Fe-B doesn't help that much to increase air-gap flux density and the FC ferrite generator needs a very large amount of magnet and iron which makes a large difference in generator mass in comparison to the other generators.

In this study, the FC Nd-Fe-B always gives lowest structural mass. It generally has a similar generator diameter to the SM Nd-Fe-B generator, but the additional radial height of flux-concentrating poles effectively fulfils a structural role meaning the rotor structure has a smaller radius than that for the SM Nd-Fe-B machine. The FC ferrite generator also gives lower structural mass in comparison to the SM Nd-Fe-B generator but the structural cost in the FC ferrite generator is higher (in most of the optimisations). This higher cost is due to the amount of aluminium in the rotor structure of flux-concentrating machine in order to avoid high permeability paths which can encourage leakage flux, which is significant in the ferrite machine (as it has a large diameter). Also note, industrial experience has shown that mixing steel and aluminium structures can be challenging. ABB made a prototype for Zephyros/Harakosan which had air-gap closure problems due to different coefficients of thermal expansion. So there may be more cost involved in dealing with different coefficients of thermal expansion, but this is not captured in the model.

The active material cost in the flux-concentrating ferrite magnet generators is slightly higher and the generator mass is higher because of a large difference in magnet mass and rotor iron mass (the mass of pole pieces exceeds that of the rotor yoke in the other machine). Torque per magnet mass in the Nd-Fe-B machines are unsurprisingly very high because of the magnet mass difference.

6.3.3 On the impact of air-gap diameter constraints

Constraining the diameter of the generator is often necessary for onshore wind turbines as there are limits to what can be transported by road; for offshore turbines this is not

necessarily the case. Allowing the upper limit of diameter to increase to 10m reduces the turbine cost of energy by about 1%; further increases in air-gap diameter yields only small marginal gains and these are unlikely to be worth the extra effort involved in the manufacturing processes and cost of larger manufacturing tooling and facilities. The cost and mass of the generator structure increases with increasing the diameter for all the generator types. In smaller diameter generators, the cost of generator active materials is slightly higher in the Nd-Fe-B generators. Annual energy production generated by lower diameter generators is slightly lower for all the generator types. It is known that, smaller air-gap diameter produces higher shear stress which means higher electrical loading also high copper losses. This high loss needs more cooling requirement and cost which increase the overall turbine cost of energy.

6.3.4 On the effect of including structural materials

Including generator structural materials can affect the generator mass and hence the tower and foundation cost. It is found that when the generator structural materials were included in the optimisation model, the cost of energy increased by 0.26% for the SM Nd-Fe-B generators and by 0.29% for the FC ferrite magnet generators. While they have similar structural masses, the increase in cost of energy is higher for the ferrite magnet machine because aluminium – which is relatively expensive – is used in its rotor structure. It is also found that, the structural materials cost increases when the air-gap diameter increase and the structural materials cost decreases when the air-gap flux density increase. The cooling requirement increases when the structural cost decreases.

6.3.5 On the impact of generator mass

The active material mass in the ferrite magnet generator is about 200% more than for the Nd-Fe-B generators. More inertia (due to the extra mass on the generator rotor) might affect energy capture, as the optimal tip speed ratio implies changing wind speed should be matched by changing rotational speed. More inertia means slower $d\Omega/dt$ and hence less time at optimal tip speed ratio and hence C_{pmax}. The additional rotational inertia does not make a significant change to the energy capture of the turbine. Although the rotational inertia of the generator rotor increases a lot, the total rotational inertia i.e. including the turbine rotor, only changes by a small fraction. The bigger the turbine, the smaller is the change in overall inertia. There may be some impacts for smaller turbines (e.g. less than 1MW) and/or multi-rotor turbines.

The increased top head mass – due to a heavier generator – can affect the tower costs and foundation costs. Typically for the 6 MW turbine, the ferrite magnet generators are about 100 tonnes heavier (including structural mass), implying that the tower costs would be €254k more expensive and the substructure and foundation costs would be €150k more expensive than the equivalent Nd-Fe-B generator. It can be seen that, the tower cost increased by €2.54k for the addition of one tonne of generator mass; this is about 0.012% of the total wind turbine cost. The offshore substructure and foundation cost increased by €1.5k for every additional one tonne of generator mass, which is about 0.007% of the total wind turbine cost. These figures can be higher depending on the water depth. In terms of different power ratings, the cost ratio will be different due to different rotor diameter and hub height.

6.3.6 On the effect of variable power factor

Assuming unity power factor at all wind speed instead of variable power factor tends to overestimate the generator losses and material costs and underestimate the power converter rating and cost. Varying the load angle so that the phase current is between the induced emf and terminal voltage produces better annual energy and lower cost of energy. It is found that, for a 6 MW SM Nd-Fe-B generator, the optimal design with leading power factor gives 0.002% better efficiency than unity power factor. It can be seen that, the peak torque is achieved with 0.15% less generator active material cost, at a power factor of 0.94, but that means that the power converter cost is increased by 0.06% (because of the higher apparent power).

6.3.7 On the choice of turbine power ratings

The cost of energy marginally decreases when moving from 6 to 8 to 10 MW rated power. Although the per MW cost of the generator's active and structural materials, substructure and foundation cost are increasing with turbine size, this is mitigated by the rest of the turbine cost. The 6 MW turbine gives slightly better revenue per MW over the first 15 years of life than the turbines with higher rated power turbine, but the difference is small. It is found that, the efficiency of the machine increases with the power ratings.

6.3.8 On the effect of magnet grade

The cost of energy of the turbine and the magnet mass slightly decreases by using magnet grades with higher maximum energy product, BH_{max}. Although the magnet price increases for the higher magnet grade, the higher BH_{max} produces higher air-gap

flux density and ultimately improves the energy conversion efficiency with lower magnet mass. That implies, moving to higher grade magnet, meaning B_r increases, magnet specific cost increases, flux density increases (for same dimensions), shear stress increases, so either dimensions can be reduced or electrical loading can be reduced. As long as the relative improvement in flux density per increase in cost is better, then it makes sense to move to a higher magnet grade. However, when selecting an Nd-Fe-B grade, the designer should keep in mind that the higher grade magnets can be more brittle.

6.3.9 On the effect of temperature and including cooling system

The generators that use regular temperature grade Nd-Fe-B magnets generally give lower cost of energy but with slightly higher magnet mass than using "H" grade Nd-Fe-B magnets. The main downside of the regular magnet is the maximum operating temperature which is 80°C whereas for the "H" grade magnet it is 120°C. When selecting the working temperature, one needs to make sure that the maximum operating temperature of the magnet is not exceeded, otherwise the magnet can be irreversibly demagnetized. If the rated power and losses of a machine leads to a magnet temperature of 120°C, then an additional cooling system (or additional levels of cooling) can be implemented to bring it down to 80°C, allowing the regular temperature grade magnets to be used. This additional cooling system cost and energy consumption accounts for about 0.3% of cost of energy.

In variable wind speeds at below rated power, the generator losses also vary. The required cooling air flow is variable – this can be controlled by varying the number of series fan while number of parallel fans are fixed. The cooling regime can be optimised for minimizing the cost of energy.

As well as facilitating the use of the cheaper, regular temperature grade of magnets, the additional cooling gives two benefits regardless of the temperature grade used in the generators. The cooling helps to reduce the stator winding temperatures, the resistance and hence the copper losses. The lower magnet temperatures also increase the effective remanent flux density due to the negative temperature coefficient of remanence.

When comparing the magnet temperature grades, the regular magnets provide lowest cost of energy. Using the high temperature magnets near to their maximum working

temperature (120°C) leads to higher copper losses and a reduction in remanent flux density. This can be reduced by cooling these machines down to 80°C. The difference between regular and high temperature magnets at 80°C is small, and the use of high temperature magnets may be safer as the magnets will not demagnetize if the cooling system fails.

6.3.10 Sensitivity

If the specific cost of Nd-Fe-B magnets were to increase by a large enough margin (while the ferrite magnet material cost remained constant) then the FC ferrite machine would become more attractive from a cost of energy perspective. However, in this study even if the specific magnet cost doubled (from €60/kg to €120/kg) the cost of energy is still lower for the generator using Nd-Fe-B magnets than for the FC ferrite machine. The cost of energy sensitivity to specific magnet cost might be more significant for onshore turbines, as the rest of the turbine has lower capital costs. However, when varying the rest of the turbine cost, the gap between the cost of energy for the two generators did not change significantly.

The availability results show that a generator's availability is a very important factor to minimize the cost of energy; however, there is not likely to be a large availability differential in the generator types considered here. The generator types are unlikely to have different effects on the annual operation and maintenance costs. The important factor could be differences in failure rates, corrosion of different magnet types (probably climate controlled), demagnetisation likelihood and any other in terms of failure rates probably not going to make a big difference. The cooling system size and converter size, perhaps, more parts the bigger they get, hence bigger failure rate. If there anything going to change are repair costs and repair rates. Bigger generator will be heavier and larger – will probably need same type of repair vessel type/capability but may need more people or take longer to replace.

It can be seen that higher wind speed scale parameter tries to make a more efficient generator which is less expensive. The higher mean wind speed also parameter tries to make a more efficient generator which is less expensive.

6.4 Summary discussion

The results of different investigations and discussions on that are presented in this chapter. A number of different investigations includes: different objective functions,

different generator topologies, constraining generator diameter, including structural materials, different power factor, different power ratings, different magnet grades, thermal effects and cooling. It has been shown that, choice of objective function is very important to get an efficient optimal machine design. Generator topologies, air-gap diameter, including structural materials along with generator active materials also has impact on turbine cost of energy and efficient machine design. A designer can further improve their design by choosing a magnet grade that could survive at higher working temperature (for safety) but operate it at lower temperature (using cooling system) to improve magnetic loading, efficiency and energy yield. The next chapter gives the overall conclusion of this study.

Chapter 7

Conclusion and future work

This thesis focuses on the optimisation of the generator and the important factors that can affect the optimisation process for offshore wind energy application. This chapter gives a summary of all the chapters in this study and the overall conclusion. Some potential future research is also given.

7.1 Chapter summaries

Chapter 2 investigate the previous works related to research questions given in section 1.2 and 1.3, that includes: wind energy, drivetrain, different generator topologies, magnet, power converter, optimisation process and real time wind turbine.

The electromagnetic models of three different direct drive generator topologies for offshore wind turbine are described in chapter 3, that includes: electromagnetic modelling of different generator topology, verification of electromagnetic model using finite element software FEMM, different strategies to reduce rare earth permanent magnet, magnet grades, power factor, losses and active material mass for different generator topologies.

The generator structural models for both stator and rotor, linking deflections in the air-gap to structural masses are described in chapter 4. A thermal model is then introduced to estimate the thermal effect due to power losses in the generator and verified using the FEMM heat flow analysis module. The required cooling air flow, additional cost and energy consumption incurred to cool down the magnet and winding temperature by forced air flow using fan and heat exchanger is also modelled in this chapter. Subsequently characteristics of the wind turbine and the site wind resources and calculation of annual energy production is shown for different power ratings. The influence of generator mass on inertia (and hence turbine performance) and the effect of turbine top head masses on tower, foundation and lifting cost are also modelled in chapter 4.

Chapter 5 describe the optimisation process, different objective functions for different generator topologies and investigate the effect on the optimisation of a number of factors that interest a typical designer: the inclusion of structural and thermal model along with the electromagnetic model in the objective functions, the choice of magnet grade, the inclusion of a cooling system, the inclusion of the impact of generator mass on the cost of turbine tower and foundation, the upper limit of generator diameter, the sensitivity results to magnet specific cost, turbine cost, operation and maintenance cost and the wind conditions.

Chapter 6 present the results of different optimisation run and investigations and also gives a detailed discussion on that.

7.2 Key findings

1) The first and second objective functions are a poor choice when optimising wind turbine generators. The major difference in losses between F_1/F_2 and F_3/F_4 is due to copper losses, with higher current density being used to reduce copper mass. More magnet is used in the 3rd and 4th objective functions which generally produces better air-gap flux density and helps to increase energy production. The balance of copper and iron losses are slightly different, with F_3/F_4 having slightly higher iron losses. It is because of lower mass and active iron that used in first two objective functions. a designer can either chose F_3 or F_4 to produce an efficient machine design. Perhaps a designer might want to bias the results towards designs with higher efficiency could go for F_3 and lower cost of energy could go for F_4.
2) It is found that the air-gap diameter in 3rd objective function always picks the highest limit of the boundary. After varying the upper boundary limits the optimum diameter for a 6 MW generator found is close to 12 m.
3) Out of three generator rotor topologies, FC Nd-Fe-B is the best in terms of cost of energy.
4) Out of two magnet materials, neodymium is optimum in terms of cost of energy and efficiency.
5) Rotor Inertia is not important. The additional rotational inertia does not make a significant change to the energy capture of the turbine.
6) The cost of energy of the turbine and the magnet mass decreases by using higher magnet grades. Although the magnet price increases for the higher

magnet grade, the higher *BH*max produces higher air-gap flux density and ultimately improves the energy conversion efficiency with lower magnet mass.

7) The difference between regular and high temperature magnets at 80°C is small, and the use of high temperature magnets may be safer as the magnets will not demagnetize if the cooling system fails.
8) The cost of energy marginally decreases when moving from 6 to 8 to 10 MW rated power. The efficiency of the machine also increases with the power ratings.

7.3 Answer to research question

The primary research question given in section 1.2 is:

"What is the best approach to optimise a generator for offshore wind turbine?"

From this study it can be seen that, the best approach to optimise a generator for offshore wind turbine is to link the electromagnetic, thermal and mechanical model, using either F_3 or F_4 as an objective function and including magnet specification, cost and temperature effects in the model. To answer this primary research question, a number of other smaller secondary research questions given in section 1.3 are answered throughout each chapter of this thesis. The answers found for each of the research question are concluded here:

Q1) Can different magnet materials and rotor topologies be used to reduce Nd-Fe-B content in offshore wind turbines?

Three different rotor topologies and two magnet types are used in this study. It is found that, the optimal SM Nd-Fe-B generator uses slightly less magnet than the FC Nd-Fe-B generator (in most of the optimisation except F_3 (iii) and F_4). That shows the flux-concentrating nature of FC Nd-Fe-B doesn't help that much to increase air-gap flux density but depending on objective function the result can vary. The FC ferrite generator needs a very large amount of magnet which makes a large difference in generator mass in comparison to the other generators. If the specific cost of Nd-Fe-B magnets were to increase by a large enough margin (while the ferrite magnet material cost remained constant) then the FC ferrite machine would become more attractive from a cost of energy perspective.

Q2) Should the generators structural model, tower, substructure and foundation be included with active materials in optimisation of generators for offshore direct drive wind turbines?

It has been demonstrated that it is important to include structural modelling and materials when optimizing direct drive wind turbine generators for three reasons: (a) it impacts on the generator cost estimation by more than 0.26%, which is €0.28/MWh for 6 MW SM Nd-Fe-B generator (b) the added top head mass affects the tower and foundation costs estimation by about €0.4m and (c) it allows the maximum allowed diameter to be varied. In the latter case, the largest drop in cost of energy is when the air-gap diameter upper limit is increased from 6m to 8m. The drop in cost of energy is about 0.9% for both generator types which is about €0.7/MWh for 6 MW SM Nd-Fe-B generator.

Typically for the 6 MW turbine, the ferrite magnet generators are about 100 tonnes heavier (including structural mass), implying that the tower cost increased by €2.54k for the addition of one tonne of generator mass; this is about 0.012% of the total wind turbine cost. The offshore substructure and foundation cost increased by €1.5k for every additional one tonne of generator mass, which is about 0.007% of the total wind turbine cost. These figures can be higher depending on the water depth. In terms of different power ratings, the cost ratio will be different due to different rotor diameter and hub height.

Q3) Are these findings dependent on turbine power ratings? If so, to what degree?

In this study, the findings for 6 MW generators are also valid for other power ratings and the variation of overall cost per MW is small. The cost of energy marginally decreases when moving for higher rated power. Although the increase of per MW cost of the generator's active and structural materials are high, this is mitigated by the rest of the turbine cost. Although the cost of energy of 6 MW turbine is similar for F_3 (i) and F_4, the difference between these objective functions increases by increasing the turbine power rating. It is found that, the efficiency of the machine increases with the power ratings but the difference is small.

Q4) How does the choice of magnet grade affect the resulting optimal design?

The choice of magnet grade affects the resulting optimal design. The cost of energy of the turbine and the magnet mass slightly decreases by using magnet grades with higher maximum energy product, BH_{max}. That implies, moving to higher grade magnet, meaning B_r increases, magnet specific cost increases, flux density increases (for same dimensions), shear stress increases, so either dimensions can be reduced or electrical loading can be reduced. A higher grade magnet can be chosen, as long as the relative improvement in flux density per increase in cost is better than the lower grade magnet.

Q5) How does the thermal model, cooling circuit and machine temperature affect the optimal design?

Thermal model is important to measure the machine temperature due to losses. If the working temperature exceed the maximum operating temperature, the magnet can be irreversibly demagnetized. For safety, it can be operated at lower temperature by using cooling system to improve magnetic loading, efficiency and energy yield.

As well as facilitating the use of the cheaper, lower temperature grade of magnets, the additional cooling gives two benefits regardless of the temperature grade used in the generators. The cooling helps to reduce the stator winding temperatures, the resistance and hence the copper losses. The lower magnet temperatures also increase the effective remanent flux density due to the negative temperature coefficient of remanence.

In variable wind speeds at below rated power, the generator losses also vary. The required cooling air flow is variable – this can be controlled by varying the number of series fan while number of parallel fans are fixed. The cooling regime can be optimised for minimizing the cost of energy.

Q6) How does the choice of objective function affect the resulting optimal design?

The optimal design varies depending on objective function. In this study, four different objective functions (F_1-F_4) are used to optimise different generator types for wind energy. It is found that, the objective functions F_3 and F_4 produce higher efficiency designs with lower cost of energy for all the types of generators than the objective functions F_1 and F_2. This is due to objective function. The designs resulting from the F_1 and F_2 objective functions give a high cost of energy although reduces the volume of active material (magnet mass in the case of F_1 and all the active material, weighted

by their specific costs in the case of F_2) for the rated torque at the expense of higher losses. In terms of the application, a balance of high efficiency and low cost is attractive. So, the 1st and 2nd objective functions are a poor choice in terms of cost of energy and efficiency for the optimisation of wind turbine generators. Despite being quicker to formulate and needing only limited information about the turbine, F_3 is a close proxy for F_4; the latter explicitly models the cost of energy and so it is able to find a marginally better cost of energy.

7.4 Future work

A number of areas have been stated throughout this thesis in which improvement could be made with further work. The following paragraphs will outline the further work that could be carried out to improve the work on this thesis.

In this thesis three different type of generator topologies are used for optimisation runs and investigations. Other generator topology such as synchronous reluctance machine, permanent magnet assisted synchronous reluctance machine, Halbach array machine, hybrid excited machine and other generator topology could be used to optimise and compare with the generator topologies that is used in this study to achieve the best performance machine topology.

This research could be further extended with different objective function, different magnet material, cost vs temperature and *BH*max for other magnet materials, different cooling system, different cooling fluid such as liquid, hybrid rotor using different magnet materials, different structural design and different tower and foundation types.

The things neglected in this study but should look at: other loss mechanisms, power converter interface losses might vary with turbine design, voltage level and hence insulation, reliability for different generator topologies studied here, demagnetisation, corrosion and reliability of cooling systems.

References

[1] S. Eriksson, H. Bernhoff, “Rotor design for PM generators reflecting the unstable neodymium price,” in *Proc. XXth Int. Conf. Elect. Mach.,* Marseille, France, 2012, pp.1419-1423.

[2] H. Polinder, F. F. A. van der Pijl, G. J. de Vilder, and P. J. Tavner, "Comparison of direct-drive and geared generator concepts for wind turbines," *Energy Conversion, IEEE Transactions on,* vol. 21, pp. 725-733, 2006.

[3] A. Grauers, “Design of direct-driven permanent-magnet generators for wind turbines,” Ph.D. dissertation, Chalmers Univ. Technol., Goteborg, Sweden, 1996.

[4] T. Bazzo, J. F. Kolzer, R. Carlson, F. Wurtz, and L. Gerbaud, “Optimum design of a high-efficiency direct-drive PMSG,” in *2015 IEEE Energy Convers. Congr. and Exposition,* Montreal, QC, 2015, pp. 1856-1863.

[5] A. Zavvos, A. McDonald, and M. Mueller, “Optimisation tools for large permanent magnet generators for direct drive wind turbines,” *IET Renew. Power Generation,* vol. 7, no. 2, pp. 163-171, Mar. 2013.

[6] A. S. Mcdonald, "Structural analysis of low speed, high torque electrical generators for direct drive renewable energy converters," PhD Thesis, University of Edinburgh, Edinburgh, Scotland 2008.

[7] H. Polinder, “Principles of electrical design of permanent magnet generators for direct drive renewable energy systems,” in *Electrical Drives for Direct Drive Renewable Energy Systems,* Woodhead Publishing, 2013, ch. 2, pp. 43.

[8] H. Li, Z. Chen, and H. Polinder, “Optimization of multibrid permanent-magnet wind generator systems,” *IEEE Trans. Energy Convers.,* vol. 24, no. 1, pp. 82–92, Mar. 2009.

[9] C. Hurst, “China’s Rare Earth Elements Industry: What Can the West Learn?,” Institute for the analysis of global security (IAGS), Washington, USA, Tech. Rep. [Online]. Available at: http://www.iags.org/rareearth0310hurst.pdf, Accessed on: Feb. 20, 2018.

[10] L. Fingersh, M. Hand, A. Laxson, “Wind turbine design cost and scaling model,” Nat. Renew. Energy Lab., Golden, CO, USA, Tech. Rep. NREL/TP-500-40566, Dec. 2006.

[11] C. Moné, A. Smith, B. Maples, and M. Hand, “2014 Cost of Wind Energy Review,” Nat. Renew. Energy Lab., Golden, CO, USA, Tech. Rep. NREL/TP-6A20-64281, Oct. 2015.

[12] A. S. McDonald, M.A. Mueller and H. Polinder, “Structural mass in direct-drive permanent magnet electrical generators,” *IET Renew. Power Generation*, vol. 2, no. 1, pp. 3-15, Mar. 2008.

[13] R. S. Semken, M. Polikarpova, P. Roytta, J. Alexandrova, J. Pyrhonen, J. Nerg, A. Mikkola and J. Backman, “Direct-drive permanent magnet generators for high-power wind turbines: benefits and limiting factors,” *IET Renew. Power Generation*, vol. 6, no. 1, pp. 1-8, Jan. 2012.

[14] M. A. Mueller, A. S. McDonald, D. E. Macpherson, “Structural analysis of low-speed axial-flux permanent-magnet machines,” *IEE Proc*. –Electr. Power Appl., vol. 152, no. 6, pp. 1417–1426, Nov. 2005.

[15] Arnold Magnetic Technologies, Rochester, NY, USA. Neodymium Iron Boron Magnets. (2016) [Online]. Available at: http://www.arnoldmagnetics.com/en-us/Products/Neodymium-Magnets, Accessed on: Oct. 10, 2016.

[16] M. Polikarpova, P. Ponomarev, P. Roytts, S. Semken, Y. Alexandrova and J. Pyrhonen, “Direct liquid cooling for an outer-rotor direct-drive permanent-magnet synchronous generator for wind farm applications,” *lET Electric Power App*., vol. 9, no. 8, pp. 523-532, Sep. 2015.

[17] M. Polikarpova, P. Ponomarev, P. Lindh, I. Petrov, W. Jara, V. Naumanen, J. A. Tapia and J. Pyrhonen, “Hybrid Cooling Method of Axial-Flux Permanent-Magnet Machines for Vehicle Applications,” *IEEE Trans. Ind. Electron*., vol. 62, no. 12, pp. 7382–7390, Dec. 2015.

[18] D. C. Aliprantis, S. D. Sudhoff and B. T. Kuhn, “Genetic algorithm-based parameter identification of a hysteretic brushless exciter model*,” IEEE Trans. Energy Convers.*, vol. 21, no. 1, pp. 148-154, Mar. 2006.

[19] T. Burton, D. Sharpe, N. Jenkins, E. Bossanyi and M Graham *Wind Energy Handbook*, 3rd ed.: John Wiley & Sons, Ltd, 2021.

[20] P. Gipe and E. Möllerström, "An overview of the history of wind turbine development: Part I—The early wind turbines until the 1960s." *Wind Eng*. vol.46, no. 6, pp. 1973–2004, Aug. 2022.

[21] P. Gipe and E. Möllerström, "An overview of the history of wind turbine development: Part II—The 1970s onward," *Wind Eng*., vol. 47, no. 1, pp. 220–248, Feb. 2023.

[22] R. Green and N. Vasilakos, "The economics of offshore wind," *Energy Policy*, vol. 39, no. 2, pp. 496–502, Feb. 2011.

[23] K. S. R. Murthy and O. P. Rahi, "A comprehensive review of wind resource assessment," *Renewable Sustain. Energy Rev*., vol. 72, pp. 1320–1342, May 2017.

[24] E. Hau, "The wind resource," in *Wind Turbines*. Berlin, Germany: Springer, 2013, pp. 505–547.

[25] O. Anaya-Lara, N. Jenkins, J. Ekanayake, P. Cartwright, and M. Hughes, *Wind Energy Generation Modelling and Control*, 1st ed.: John Wiley and Sons, Ltd, 2009.

[26] E. W. Golding, *The Generation of Electricity from Wind Power*. London: E&F Spon Ltd., 1976.

[27] T.-H. Yeh and L. Wang, "A study on generator capacity for wind turbines under various tower heights and rated wind speeds using Weibull distribution," *IEEE Trans. Energy Convers.*, vol. 23, no. 2, pp. 592–602, Jun. 2008.

[28] Sunny Panels [Online]. Available: http://sunnypanels.com/wind-energy-generator/home-wind-turbine-generator/, Accessed on: Mar. 28, 2016

[29] A. R. Jha, *Wind turbine technology*, 1st ed.: CRC Press Inc, 2010.

[30] A. R. David, *Wind turbine operations, maintenance, diagnosis, and repair*. Burlington, MA: Burlington, MA: Jones & Bartlett Learning, 2013.

[31] M. Iulian, *Optimal control of wind energy systems: towards a global approach*. London: Springer, 2008.

[32] P. Tavner, *Offshore wind turbines: reliability, availability and maintenance*. London, U.K.: London, U.K.: Institution of Engineering and Technology, 2012.

[33] Renewable Energy World [Online]. Available: http://www.renewableenergyworld.com/rea/news/article/2010/06/wind-turbine-gearbox-reliability , Accessed on: Feb. 28, 2015.

[34] Inspections of Wind Turbine Gearboxes [Online]. Available: http://www.olympus-ims.com/en/applications/rvi-wind-turbine/, Accessed on: Jun. 11, 2018

[35] L. Dingguo, G. Xiang, and Q. Wei, "Current-based diagnosis for gear tooth breaks in wind turbine gearboxes," in *IEEE Energy Conversion Congress and Exposition*, Sept. 2012, pp. 3780-3786.

[36] J. Carroll, “Cost of energy modelling and reduction opportunities for offshore wind turbines,” Ph.D. dissertation, Elect. Elec. Eng., Univ. Strathclyde, Glasgow, U.K., 2016.

[37] H. Siegfried, *Grid integration of wind energy conversion systems*. Chichester, England; Hoboken, NJ: Wiley, 2006.

[38] A. McDonald and G. Jimmy, “Parallel wind turbine powertrains and their design for high availability,” *IEEE Trans. Sustain. Energy*, vol. 8, no. 2, pp. 880–890, Apr. 2017.

[39] W. Shepherd, *Electricity generation using wind power*. Singapore; London: World Scientific, 2011.

[40] J. F. Manwell, *Wind energy explained: theory, design and application*. Chichester, New York: Wiley, 2002.

[41] G. McPherson, *An introduction to electrical machines and transformers*. New York: Wiley, 1990.

[42] T. Ackermann, *Wind Power in Power System*, 1st ed. Chichester, England: John Wiley & Sons, Ltd, 2005.

[43] G. Wright, O. C. Duffy, S. A. Heard, *Fundamentals of mobile heavy equipment*. Jones & Bartlett Learning, 2017.

[44] E. J. Bueno, S. Cóbreces, F. J. Rodríguez, A. Hernández, and F. Espinosa, "Design of a back-to-back NPC converter interface for wind turbines with squirrel-cage induction generator," *IEEE Trans. Energy Convers*., vol. 23, no. 3, pp. 932–945, Sep. 2008.

[45] Y. Lei, A. Mullane, G. Lightbody, and R. Yacamini, "Modeling of the wind turbine with a doubly fed induction generator for grid integration studies," *IEEE Trans. Energy Convers.*, vol. 21, no. 1, pp. 257–264, Mar. 2006.

[46] F. G. Jacek, *Permanent magnet motor technology: design and applications*. Boca Raton: CRC Press, 2010.

[47] S. Sinisa, C. Neil, and H. Alan, *Urban wind energy*. London; Sterling, VA: Earthscan, 2009.

[48] Goldwind supplies 51 MW of wind turbines for Cuba wind farm [Online]. Available: http://santamarta-florez.blogspot.co.uk/2013/12/goldwind-supplies-51-mw-of-wind.html, Accessed on: Jun. 13, 2018

[49] New Electric Motor is 50% Smaller but has 2x More Torque (!) [Online]. Available: http://www.treehugger.com/cars/new-electric-motor-is-50-smaller-but-has-2x-more-torque.html, Accessed on: Jun. 14, 2018.

[50] W. M. Arshad, P. Thelin, T. Backstrom, and C. Sadarangani, "Use of transverse-flux machines in a free-piston generator," *IEEE Trans. Ind. Appl*., vol. 40, no. 4, pp. 1092–1100, Jul.–Aug. 2004.

[51] R. Kumar et al., "A review on transverse flux permanent magnet machines for wind power applications," *IEEE Access*, vol. 8, pp. 216543–216565, 2020.

[52] T. Husain, I. Hasan, Y. Sozer, I. Husain, and E. Muljadi, "Design considerations of a transverse flux machine for direct-drive wind turbine applications," *IEEE Trans. Ind. Appl.*, vol. 54, no. 4, pp. 3604–3615, Jul./Aug. 2018.

[53] R. Nasiri-Zarandi, A. M. Ajamloo, and K. Abbaszadeh, "Design optimization of a transverse flux Halbach-array PM generator for direct drive wind turbines," *IEEE Trans. Energy Convers.*, vol. 35, no. 3, pp. 1485–1493, Feb. 2020.

[54] H. Raich and P. Blumler, "Design and construction of a dipolar Halbach array with a homogeneous field from identical bar magnets: NMR Mandhalas," *Concepts in*

Magnetic Resonance Part B-Magnetic Resonance Engineering, vol. 23, pp. 16-25, 2004.

[55] B. Merritt, R. Post, G. Dreifuerst, and D. Bender, "Halbach array motor/generators: A novel generalized electric machine," Lawrence Livermore National Lab., CA, United States, 1994.

[56] C. Steve. The Magnetic Material Challenge [Online]. Available: http://www.arnoldmagnetics.com/workarea/downloadasset.aspx?id=5325, Accessed on: Mar. 14, 2015

[57] Permanent Magnet Selection and Design Handbook [Online]. Available: http://www.rare-earth-magnets.com/content/pdf/Permanent-Magnet-Selection-and-Design-Handbook.pdf, Accessed on: Mar. 15, 2015

[58] Arnold Magnetic Technologies, Rochester, NY, USA. Neodymium Iron Boron Magnets. (2016) [Online]. Available at: http://www.arnoldmagnetics.com/en-us/Products/Neodymium-Magnets, Accessed on: Oct. 10, 2016.

[59] F. P. Scalcon, G. Fang, C. J. V. Filho, H. A. Grundling, R. P. Vieira, and B. Nahid-Mobarakeh, ‘‘A review on switched reluctance generators in wind power applications: Fundamentals, control and future trends,’’ *IEEE Access*, vol. 10, pp. 69412–69427, 2022.

[60] P. Roshanfekr, S. Lundmark, T. Thiringer, and M. Alatalo, "A synchronous reluctance generator for a wind application-compared with an interior mounted permanent magnet synchronous generator," in Proc. 7th IET Int. Conf. Power Electron., Mach. Drives, Manchester, UK, 2014, pp. 1-5.

[61] M. R. Islam, Y. Guo, and J. Zhu, "Power converters for wind turbines: current and future development," *Materials and processes for energy: communicating current research and technological developments. Energy Book Series-2013 edn. Spain*, pp. 559-571, 2013.

[62] P. Badoni and P. J. Kumar, "Study of Power Converter Topology used for Renewable Energy Resources using Wind," *International Journal of Emerging Research in Management and Technology*, vol. 2, pp. 26-33.

[63] F. Blaabjerg, M. Liserre, and K. Ma, "Power electronics converters for wind turbine systems," in *Energy Conversion Congress and Exposition (ECCE), 2011 IEEE*, 2011, pp. 281-290.

[64] Wind Turbine Product Platform [Online]. Available: https://www.siemensgamesa.com/en-int/products-and-services , Accessed on: Jun. 19, 2018.

[65] Wind Turbines Overview [Online]. Available: https://www.ge.com/renewableenergy/wind-energy/turbines , Accessed on: Jun. 19, 2018.

[66] Wind Turbines [Online]. Available: http://www.enercon.de/en-en/Windenergieanlagen.htm, Accessed on: Jun. 19, 2018.

[67] Z. Y. Wu, R. H. Qu, J. Li, H. Y. Fang, and Z. S. Fu, "Structure optimization of rotor supporting of permanent magnet direct drive synchronous generators for large wind turbine based on genetic algorithm and finite element method," in *2015 IEEE Int. Elect. Mach. & Drives Conf.*, Coeur d'Alene, ID, 2015, pp. 1755-1760.

[68] Y. Duan and D. Ionel, "Nonlinear scaling rules for brushless pm synchronous machines based on optimal design studies for a wide range of power ratings," *IEEE Trans. Ind. Appl.*, vol. 50, no. 2, pp. 1044–1052, Mar. 2014.

[69] J. Carroll, A. McDonald, D. McMillan, T. Stehly, C. Mone, and B. Maples, *"*Cost of energy for offshore wind turbines with different drive train types*,"* presented at Eur. Wind Energy Assoc. Annu. Conf., Paris, France, Nov. 17-20, 2015.

[70] A. Fasolo, L. Alberti, and N. Bianchi, "Performance comparison between switching-flux and IPM machine with rare earth and ferrite PMs," *in Proc. 20th ICEM*, Sep. 2–5, 2012, pp. 731-737.

[71] S. J. Galioto, P. B. Reddy, and A. M. EL-Refaie, "Effect of magnet types on performance of high speed spoke interior permanent magnet machines designed for traction applications," *in Proc. IEEE ECCE*, Sep. 2014, pp. 4513–4522.

[72] O. Gutfleisch, M. A. Willard, E. Brück, C. H. Chen, S. G. Sankar, and J. P. Liu, "Magnetic materials and devices for the 21st century: stronger, lighter, and more energy efficient," *Adv. Mater.*, vol. 23, pp. 821–842, 2011.

[73] Y. Alexandrova, R. S. Semken, and J. Pyrhonen, “Permanent magnet synchronous generator design solution for large direct-drive wind turbines: Thermal behavior of the LC DD-PMSG,” *Appl. Therm. Eng*., vol. 65, nos. 1–2, pp. 554–563, 2014.

[74] A. Boglietti, A. Cavagnino, M. Pastorelli, D. Staton, and A. Vagati, “Thermal analysis of induction and synchronous reluctance motors,” *IEEE Trans. Ind. Appl*., vol. 42, no. 3, pp. 675–680, May/Jun. 2006.

[75] C. Kral, A. Haumer and T. Bauml, “Thermal Model and Behavior of a Totally-Enclosed-Water-Cooled Squirrel-Cage Induction Machine for Traction Applications, *IEEE Trans. Ind. Electron*.”, vol. 55, no. 10, pp. 3555-3565, Oct. 2008.

[76] Introduction to NdFeB magnets. [Online]. Available at: http://www.ndfeb-info.com/, Accessed on: Nov. 15, 2016.

[77] J. Pyrhonen, T. Jokinen, V. Hrabovcova, Design of Rotating Electrical Machines. Chichester, UK: Wiley, 2009, pp 230-249, 527-529

[78] S. Eriksson, “Inherent Difference in Saliency for Generators with Different PM Materials,” J. Renew. Energy, vol. 2014, Nov. 2014, Art. ID. 567896

[79] *Finite Element Method Magnetics* v4.2. (2016) [Online] Available at: http://www.femm.info/wiki/HomePage

[80] Create a Macro [Online]. Available: http://www.excel-easy.com/vba/create-a-macro.html

[81] N. A. Bhuiyan and A. McDonald, “Assessment of the Suitability of Ferrite Magnet Excited Synchronous Generators for Offshore Wind Turbines,” presented at Eur. Wind Energy Assoc. Offshore Conf., Copenhagen, Denmark, Mar. 10-12, 2015.

[82] N. A. Bhuiyan and A. McDonald, “Optimisation and comparison of flux-concentrating Nd-Fe-B generator considering variable power factor and wind conditions for a 6MW offshore wind turbine,” at 53rd Int. Universities Power Engineering Conf. (UPEC), Glasgow, UK, Sept. 4-7, 2018.

[83] O. Gutfleisch, “Controlling the properties of high energy density permanent magnetic materials by different processing routes,” J. Phys. D, Appl. Phys., vol. 33, p. R157, 2000.

[84] J. J. Becker, “Rare-Earth-Compound Permanent Magnets,” J. Appl. Phys., vol. 41, no. 3, pp. 1055-1064, 1970.

[85] Magnet Expert Ltd, Tuxford, Nottinghamshire, UK. Neodymium Magnets. (2016) [Online]. Available at: https://www. magnetexpert.com/technical-advice-i685/materials- information-i682, Accessed on: Nov. 15, 2016.

[86] Ningbo ZhaoBao Magnet Co., Ltd, Ningbo, Zhenhai, China. Neodymium Magnets. (2016) [Online]. Available at: http://www.zhaobaomagnet.com/, Accessed on: Nov. 15, 2016.

[87] W. C. Young and R. G. Budynas, Roark's Formulas for Stress and Strain. 7th ed. New York, NY, USA: McGraw-Hill, 2002, pp. 189-192.

[88] N. A. Bhuiyan and A. McDonald, "Optimization of offshore direct drive wind turbine generators with consideration of permanent magnet grade and temperature," *IEEE Trans. Energy Convers.*, vol. 34, no. 2, pp. 1105–1114, Jun. 2019.

[89] D. Staton and A. Cavagnino, "Convection heat transfer and flow calculations suitable for electric machines thermal models," *IEEE Trans. Ind. Electron.*, vol. 55, no. 10, pp. 3509–3516, Oct. 2008.

[90] *Woods Practical Guide to Fan Engineering*, Woods Colchester Ltd., Colchester, U.K., Jun. 1960.

[91] Torin-Sifan, Swindon, Wiltshire, UK. Fan deck DPN160-222 EC. (2016) [Online]. Available at: http://www.torin-sifan.com/display.asp?product=78, Accessed on: Oct. 25, 2016.

[92] Vent-Axia, Crawley, Sussex, UK. HR500EP/IP Passive HR Unit. (2016) [Online]. Available at: https://www.vent-axia.com/ sites/default/files/mvhr_-_hr500ep_ip.pdf, Accessed on: Oct. 30, 2016.

[93] J. Carroll, A. McDonald, I. Dinwoodie, D. McMillan, M. Revie, and I. Lazakis, "Availability, operation and maintenance costs of offshore wind turbines with different drive train configurations," Wind Energ., Jul. 2016, [Online]. Available at: http//dx.doi.org/10.1002/we.2011.

[94] Graves et al. *Understanding Availability Trends of Operating Wind Farms*. Houston. AWEA 2008.

[95] *Bladed Wind turbine simulation tool* [Online]. Available: https://www.dnvgl.com/services/bladed-3775.

[96] A. McDonald and N. A. Bhuiyan, "On the Optimization of Generators for Offshore Direct Drive Wind Turbines," *IEEE Trans. Energy Convers*., vol. 32, no. 1, pp. 348-358, Mar. 2017.

[97] M. Maness, B. Maples, and A. Smith, "NREL Offshore Balance-of-System Model," Nat. Renew. Energy Lab., Golden, CO, USA, Tech. Rep. NREL/TP-6A20-66874, Jan. 2017.

[98] P. Jamieson, "*Upscaling of Wind Turbine System*" in Innovation in Wind Turbine Design, 1st ed. Chichester, UK: Wiley, 2011, ch 4, pp 90-94.

[99] K. Hart, A. McDonald, H. Polinder, E. Corr, and J. Carroll, "Improved cost of energy comparison of permanent magnet generators for large offshore wind turbines," presented at the Eur. Wind Energy Conf., Barcelona, Spain, Mar. 10–13, 2014.

[100] J. H. J. Potgieter and M. J. Kamper, "Optimum Design and Comparison of Slip Permanent-Magnet Couplings with Wind Energy as Case Study Application*," IEEE Trans. Ind. appl.*, vol. 50, no. 5, pp. 3223–3234, Sept. 2014.

[101] H. Vansompel, P. Sergeant, and L. Dupré, "Optimized design considering the mass influence of an axial flux permanent-magnet synchronous generator with concentrated pole windings," *IEEE Trans. Magn*., vol. 46, no. 12, pp. 4101–4107, Dec. 2010.

[102] T. Wang and Q. Wang, "Optimization design of a permanent magnet synchronous generator for a potential energy recovery system," *IEEE Trans. Energy Convers*., vol. 27, no. 4, pp. 856–863, Dec. 2012.

[103] J. Aubry, H. B. Ahmed, and B. Multon, "Sizing optimization methodology of a surface permanent magnet machine-converter system over a torquespeed operating profile: Application to a wave energy converter," *IEEE Trans. Ind. Electron*., vol. 59, no. 5, pp. 2116–2125, May 2012.

[104] MathWorks, Natick, MA, USA. Global Optimization Toolbox User's guide. (2016) [Online]. Available at: http://in.mathworks.com /help/pdf_doc/gads/gads_tb.pdf, Accessed on: Mar. 28, 2016.

[105] N. A. Bhuiyan and A. McDonald, "Optimisation and comparison of generators with different magnet materials for a 6MW offshore direct drive wind turbine," in

Proc. 8th IET Int. Conf. Power Electron., Mach. Drives (PEMD), Glasgow, UK, 2016, pp. 1-6.

[106] K. Choi, D. H. Jang, S. I. Kang, J. H. Lee, T. K. Chung and H. S. Kim, "Hybrid Algorithm Combing Genetic Algorithm with Evolution Strategy for Antenna Design," *IEEE Trans. Magn.*, vol. 52, no. 3, pp. 1-4, Mar. 2016.

[107] J.-K. Kim, D.-H. Cho, H.-K. Jung, and C.-G. Le, "Niching genetic algorithm adopting restricted competition selection combined with pattern search method," IEEE Trans. Magn., vol. 38, no. 2, pp. 1001–1004, Mar. 2002.

[108] Y. Tai, Z. Liu, H. Yu, and J. Liu, "Efficiency optimization of induction motors using genetic algorithm and Hybrid Genetic Algorithm," in Proc. Int. Conf. Elect. Mach. and Syst., Beijing, China, 2011, pp. 1-4.

[109] J. McCall, "Genetic algorithms for modelling and optimisation*," Journal of Computational and Applied Mathematics*, vol.184, no. 1, pp. 205-222, Dec. 2005.

[110] A. Chipperfield, P. Fleming, H. Pohlheim, C. Fonseca, Genetic Algorithm Toolbox for use with MATLAB. (1994) [Online]. Available at: http://codem.group.shef.ac.uk/index.php/ga-toolbox .